The development and application of ICP-MS for the determination of plutonium and neptunium in the marine environment

Kate Elizabeth Sampson

presented as a thesis for the degree of
Doctor of Philosophy
University of Glasgow

Scottish Universities Research and Reactor Centre
September 1994

ProQuest LLC.
789 East Eisenhower Parkway
P.O. Box 1346
Ann Arbor, MI 48106 – 1346

ABSTRACT

Inductively coupled plasma-mass spectrometry (ICP-MS) is a rapid and sensitive technique which enables the determination of pg ml^{-1} concentrations of ^{237}Np, ^{239}Pu and ^{240}Pu from a single sample. It is a versatile technique with the capability of analysing gaseous, liquid or solid samples by the utilisation of different sample introduction techniques. In this study, liquid nebulisation and electrothermal vaporisation were investigated. Liquid nebulisation was found to be the most reliable technique with a typical detection limit for the actinides of 5 pg ml^{-1}, using a minimum sample volume of 3 ml. Inconsistent results were obtained using electrothermal vaporisation, but under optimum conditions, a detection limit of 0.3 pg ml^{-1} was obtained, using only a 50 μl sample. More typically, the detection limit for the actinides was of the order of 1 pg ml^{-1}. It was shown that ICP-MS offers certain advantages over α-spectrometric techniques, such as the determination of $^{240}Pu/^{239}Pu$ atom ratios and ^{237}Np concentrations from the same sample within a matter of minutes. In addition, ICP-MS is more tolerant of sample impurities, reducing the need for lengthy, time consuming sample preparation procedures such as those required for α-spectrometry.

Application of ICP-MS to the analysis of environmental samples required consideration of a number of additional factors. The introduction of liquid samples into the plasma restricted the dissolved solids content to less than 0.2% (w/v), to prevent the blocking of the nebuliser and overloading of the plasma. This restriction, coupled with the low concentrations of actinides in environmental media, made the separation of the actinides from the bulk matrix necessary. In addition, the high concentrations of ^{238}U in environmental matrices resulted in formation of significant levels of $^{238}UH^+$ in the plasma which, in turn, caused an isobaric interference on the ^{239}Pu peak. This was overcome by removing uranium from the samples until the final ^{238}U concentration was less than 100 ng ml^{-1} and the $^{238}UH^+$ contribution to the 239 peak was below the detection limit, enabling accurate determination of $^{240}Pu/^{239}Pu$ atom ratios.

An analytical procedure was developed to isolate nuclides of Pu and Np from the bulk matrix and uranium using a combination of anion exchange and solvent extraction. This procedure was validated by the analysis of a Ravenglass silt sample which had been analysed by independent techniques. It was then applied to the analysis of intertidal surface sediment and core samples from the eastern shores of the Irish Sea. Good

agreement was found (with linear correlation coefficients of > 0.95) between $^{239+240}Pu$ specific activities obtained by ICP-MS and independent data obtained by α-spectrometry. A systematic difference was found between the results when different yield tracers were used. For some samples, $^{240}Pu/^{239}Pu$ atom ratio data obtained by Thermal ionisation mass spectrometry (TIMS) were also available. These showed excellent agreement with ICP-MS data, although the precision of TIMS was much greater. To some extent this could be accounted for by the limited sample size (1-5 g) available for ICP-MS analysis. Although TIMS is a more sensitive technique than ICP-MS for the detection of actinides, like α-spectrometry, it requires lengthy sample preparation procedures and the sample throughput is less than half that of ICP-MS.

Sediment core samples obtained from areas of accumulating sediments at Maryport and the Solway Firth, provided a temporal record of the environmental signature of Sellafield discharges. $^{240}Pu/^{239}Pu$ atom ratio profiles in these cores indicated that sediment material deposited at the time of the early discharges from Sellafield had low $^{240}Pu/^{239}Pu$ atom ratios (< 0.10), characteristic of low burn-up material. With time, the $^{240}Pu/^{239}Pu$ atom ratios in the sediments increased until they attained a value typical of the average burn-up in a nuclear power station (approximately 0.2). Low $^{240}Pu/^{239}Pu$ atom ratios were also observed in the surface samples of the Maryport core and from some other sites close to Sellafield. Although these could be caused by the incursion of significant quantities of 'older' material, it was concluded that they were more likely to be representative of $^{240}Pu/^{239}Pu$ atom ratios in the discharges from Sellafield in the late 1980s. Confirmation of this could not be obtained as no information is available on the relative quantities of plutonium isotopes in the discharges, or the average burn-up of material reprocessed at any given time. The ^{237}Np specific activity profile was obtained for the Maryport core. The profile showed some correlation with the available Sellafield discharge data. $^{237}Np/^{239+240}Pu$ activity ratios in the core samples highlighted the different behaviour of these nuclides in the environment, the average K_d value for Np being an order of magnitude lower than that for Pu. Disparities between the expected and observed $^{237}Np/^{239+240}Pu$ activity ratios near the surface of the core suggested a relative remobilisation of Np compared to Pu.

Although the marine system is highly complex and dynamic, several attempts have been made to describe the system in terms of a simple model. To match the radionuclide discharge data with sediment core profiles, two models were investigated. The first related the core profiles directly to the annual Sellafield discharge data [Kershaw et al.,

1990], and the second related the core data to the time-integrated Sellafield discharges, including a correction term to account for dilution and dispersion of the contaminated sediments [MacKenzie et al., 1994]. When applying these to the $^{239+240}$Pu specific activity profiles of the Maryport and Solway cores, it was found that both models were inadequate. Comparison of the model predictions with the radionuclide profiles suggested that the fine structure of the core profiles closely followed the annual discharge data, while the underlying profile matched the time-integrated discharge profile. Empirical observations found that the sediment profiles could be described by the addition of a fraction of both the annual and integrated discharge profiles, the relative proportions of each varying according to the location of the sample site. At Maryport, close to Sellafield, the $^{239+240}$Pu specific activities were described by the addition of a greater proportion of the annual discharge profile to a smaller fraction of the integrated discharge profile, but the reverse was found in the Solway. These observations were insufficient to provide a method of deconvoluting the radionuclide core profiles.

In the long-term, assessment of the potential sources and sinks of radiological significant radionuclides, such as Pu and Np, is required. ICP-MS offers the opportunity to determine environmental levels of these radionuclides and provides information on the ^{240}Pu/^{239}Pu atom ratios. It is hoped that such techniques will be applied in the future to observe the change in the environmental inventory of Pu and Np and to address the omissions in the Sellafield discharge data.

Acknowledgements

I would like to thank Roger Scott and Gus MacKenzie for all their help and encouragement during the preparation of this thesis. Thanks also to Murdoch Baxter for his early supervision, Marian Scott for inspiration and help with the statistics, and Keith McKay for his patience and good humour in showing me the secrets of ICP-MS analysis. I would also like to acknowledge staff and students at SURRC, in particular, Margaret and Irene for their patience during the last few frantic weeks.

In addition, numerous people have helped to keep me sane during the long incubation time of this thesis. In particular thanks to my drinking partners, Joel, Sarah, Fiona and Anne; Bruce and Gawen for mad frenzies into the snow; Phil for excursions into the woods; and Martin for the constant supply of chocolate! Thanks also to my family and Sarah who provided much support even from the other end of the phone.

Financial support for this research project was provided by the Natural Environment Research Council. Lastly thanks to Robert Hutton and VG Elemental who provided additional support for travel and conferences.

Declaration

Except where specific reference is made to other sources, the work presented in this thesis is the original work of the author. It has not been submitted, in part or in whole for any other degree. Certain of the results have been published elsewhere.

Kate E Sampson

CONTENTS LIST

PAGE NO

CHAPTER 1 INTRODUCTION 1

1.1 OVERVIEW 1
1.2 THE SOLUTION CHEMISTRY OF THE ACTINIDES 2

1.2.1 Electronic configuration and oxidation states 3
1.2.2 Hydrolysis 4
1.2.3 Complex formation 5

1.3 ACTINIDES AND THE NUCLEAR FUEL CYCLE 5

1.3.1 Production in nuclear reactors 5
1.3.2 Nuclear fuel reprocessing 10

1.4 SOURCES OF PLUTONIUM AND NEPTUNIUM IN THE MARINE ENVIRONMENT 14

1.4.1 Natural production 14
1.4.2 Nuclear weapons testing 16
1.4.3 Controlled discharges from nuclear installations 18

1.5 BEHAVIOUR OF ACTINIDES IN THE MARINE SYSTEM 22

1.5.1 The Irish Sea 24
1.5.2 Behaviour of actinides in sea water 27
1.5.3 Association with sediments 31
1.5.4 Remobilisation of actinides from the sea-bed 33
1.5.5 The environmental record of the Sellafield discharges 37

1.6 EXPOSURE OF THE HUMAN POPULATION TO ACTINIDES 38

1.6.1 Sea-to-land transfer 38
1.6.2 Exposure through the consumption of marine biota 39
1.6.3 Radiological significance of the long-term disposal of radioactive wastes 41

1.7 DETECTION METHODS 43

1.7.1 Overview 43
1.7.2 Radiometric methods 43

1.7.2.1 Alpha Spectrometry 45
1.7.2.2 Gamma spectrometry 48
1.7.2.3 Neutron activation 48

1.7.3 Mass based techniques 49

CONTENTS LIST

PAGE NO

1.7.3.1 Inductively coupled plasma-mass spectrometry (ICP-MS) 49
1.7.3.2 Thermal ionisation mass spectrometry (TIMS) 51
1.7.3.3 Resonance ionisation mass spectrometry (RIMS) . . . 52

1.7.4 Counting versus mass-based techniques 52

1.8 AIMS OF RESEARCH 53

CHAPTER 2 INDUCTIVELY COUPLED PLASMA-MASS SPECTROMETRY 54

2.1 INDUCTIVELY COUPLED PLASMA-MASS SPECTROMETRY 54

2.1.1 Historical development 54
2.1.2 Instrumentation Overview 56
2.1.3 Sample introduction 56

2.1.3.1 Liquid Nebulisation 58
2.1.3.2 Electrothermal Vaporisation 58

2.1.4 The Inductively Coupled Plasma 60

2.1.4.1 Plasma Generation 62
2.1.4.2 Fundamental Properties of the ICP 64
2.1.4.3 Ionisation and distribution of ions in the Plasma 64

2.1.5 The Sample Interface 68

2.1.5.1 Ion Extraction 68
2.1.5.2 Ion Focusing 71
2.1.5.3 Space charge effects 72

2.1.6 Ion Selection and Detection 74

2.1.6.1 The quadrupole mass filter 74
2.1.6.2 Ion detection 76
2.1.6.3 Data collection 78

2.2 ANALYTICAL PERFORMANCE 79

2.2.1 Optimisation 79

2.2.1.1 Lens settings and sampling position 80
2.2.1.2 Nebuliser flow rate and RF power 80
2.2.1.3 Resolution 81
2.2.1.4 Data collection and sample throughput 84

CONTENTS LIST

PAGE NO

2.2.2 ETV Optimisation 85

2.2.2.1 Temperature profile 86
2.2.2.2 Freon flow rate 89
2.2.2.3 Data Collection 89

2.2.3 Signal response, stability and reliability 92

2.2.3.1 Response across the mass range 94
2.2.3.2 Long term signal response 94
2.2.3.3 Short term signal response and signal stability 94
2.2.3.4 Reliability 95

2.2.4 Validation 95

2.2.4.1 Calibration and sampling protocol 95
2.2.4.2 Accuracy and precision 98

2.2.5 Detection limits 103
2.2.6 Summary 106

2.3 LIMITATIONS FOR THE ANALYSIS OF 'REAL' SAMPLES 108

2.3.1 Spectroscopic Interferences 108

2.3.1.1 Polyatomic and Oxide Interferences 108
2.3.1.2 Isobaric interferences 111

2.3.2 Non-spectroscopic interferences 111

2.4 SAMPLE REQUISITES SUMMARY 114

CHAPTER 3 DEVELOPMENT AND VALIDATION OF A METHOD FOR ANALYSIS OF SEDIMENT SAMPLES 117

3.1 INTRODUCTION 117
3.2 CHEMICAL SEPARATION TECHNIQUES FOR THE ACTINIDES 117

3.2.1 Co-precipitation 118
3.2.2 Liquid-liquid extraction 119

3.2.2.1 Anionic extractants 119
3.2.2.2 Neutral extractants 120

3.2.3 Ion exchange 121

3.3 METHOD DEVELOPMENT 124

CONTENTS LIST

PAGE NO

3.3.1 Radiochemical yield tracers 126
3.3.2 Spiked sediment sample 127
3.3.3 Initial sample preparation and dissolution 127
3.3.4 Anionic exchange 129
3.3.5 TTA solvent extraction 132
3.3.6 Determination of ^{237}Np recoveries 134

3.4 APPLICATION TO IRISH SEA SEDIMENT SAMPLES 135

3.4.1 Sample site locations 135

3.4.1.1 Intertidal surface sediments 135
3.4.1.2 Sediment core samples 139

3.5 VALIDATION OF RESULTS 140

3.5.1 $^{239+240}Pu$ results 140
3.5.2 $^{240}Pu/^{239}Pu$ results 142

CHAPTER 4 AN ENVIRONMENTAL APPLICATION 146

4.1 INTRODUCTION 146
4.2 RESULTS FOR INTERTIDAL SURFACE SEDIMENTS FROM THE IRISH SEA 147

4.2.1 $^{239+240}Pu$ specific activity 148
4.2.2 $^{240}Pu/^{239}Pu$ atom ratios 148

4.3 SEDIMENT CORE DATA 153

4.3.1 $^{240}Pu/^{239}Pu$ atom ratios 158

4.3.1.1 The Maryport core 158
4.3.1.2 The Solway core (SC1) 161

4.3.2 ^{237}Np specific activity in the Maryport core 165
4.3.3 Matching core profiles with Sellafield discharge data 169

4.3.3.1 The Maryport core 172
4.3.3.2 The Solway Core 185
4.3.3.3 Establishing core chronologies 191

4.4 CONCLUSIONS 196

REFERENCES 197

CHAPTER 1
INTRODUCTION

1.1 OVERVIEW

Over the last few decades there has been a growing awareness of the detrimental affects of contaminating the environment with toxic substances. Of particular concern has been the release of long-lived artificial radionuclides from nuclear installations; concern which has been justified by the increasing evidence that low-level exposure to radiation can result in significant health effects [Bertell, 1985]. This has led to the continuous monitoring and assessment of the environmental impact of released radionuclides [MAFF, 1969-1993; BNFL 1979-1993]. In the last 40 years the environmental inventories of man-made radionuclides have steadily increased as a result of continuous discharges from the nuclear industry, the testing of nuclear devices and in situ production from the decay of discharged parent atoms. In this study, attention is focused on alpha emitting isotopes of plutonium and neptunium. These nuclides dominate in long-term hazard assessment of radionuclides released to the environment from the nuclear industry, both in terms of their toxicity, and their potential to cause severe damage if they decay within the body.

Many investigations have studied the behaviour of radionuclides in the environment and obtained information on processes such as their transport, accumulation or dispersion and potential for post-deposition remobilisation. This has required the development of sensitive analytical techniques to determine the low concentrations of radionuclides in environmental media. Traditional methods have been based on detecting the products of radioactive decay and although such techniques can be both sensitive and specific, they are often laborious, requiring lengthy chemical pretreatments and long analysis times. This is particularly the case when alpha-spectrometry is used to determine environmental concentrations of Pu and Np, as the problems are exacerbated by the low specific activities of the nuclides and the requirement for thin, clean sources. In this study, a mass-based technique, ICP-MS has been investigated, and methods developed to determine the concentrations of the long-lived isotopes of Pu and Np in environmental samples. ICP-MS offers

certain advantages over alpha-spectrometry: it is rapid, more tolerant of sample impurities and can resolve ^{239}Pu and ^{240}Pu, enabling the determination of $^{240}Pu/^{239}Pu$ atom ratios which cannot easily be obtained by α-spectrometry. This technique has been used to determine the distribution of ^{237}Np and variation of $^{240}Pu/^{239}Pu$ ratios in marine sediments from the Irish Sea. Interpretation of the results requires an understanding of the behaviour of these radionuclides in the marine environment, their transport to the sediments and the potential mixing and remobilisation processes which may occur within the sediments. The unravelling of the environmental record of these radionuclides can potentially provide information on the source which may not be available in the records of discharges.

1.2 THE SOLUTION CHEMISTRY OF THE ACTINIDES

The actinides are the transition series from actinium (atomic number, Z = 89) to lawrencium (Z = 103), resulting from successive filling of the 5f electron shell. Katz *et al.* [1986a] have extensively detailed the chemical behaviour of the individual actinide elements as well as the trends of the series as a whole. A full account of this subject is beyond the scope of this thesis, but some of the pertinent features are summarised below, with particular reference to neptunium (Np), plutonium (Pu), uranium (U) and americium (Am).

Reviews are available for the individual solution chemistry of U [Weigel, 1986], Np [Fahey, 1986; Patil *et al.*, 1978; Hursthouse, 1990], Pu [Weigel *et al.*, 1986; Choppin, 1983; Cleveland, 1970] and Am [Schulz and Penneman, 1986]. Some of the general aspects of actinide solution chemistry are discussed below. In the environment, the concentrations of the actinides in solution are extremely small, for example, ^{234}Th in equilibrium with ^{238}U has a typical concentration of approximately 10^{-22} M. In these circumstances, the uptake of particle-reactive species on to particulate surfaces can be the dominant factor in controlling actinide solubility. More detail on this and the behaviour of actinides in the environment is discussed in section 1.4 and the specific chemical procedures required for the extraction of actinides from environmental matrices is outlined in chapter 3.

Table 1.1: Electronic configuration of some actinide atoms and ions [Katz *et al.*, 1986b]

Element	Gaseous atom	$M^+(g)$	$M^{2+}(g)$	$M^{3+}(g)$	$M^{4+}(g)$
U	$5f^36d7s^2$	$5f^37s^2$	$5f^36d?$	$5f^3$	$5f^2$
Np	$5f^46d7s^2$	$5f^57s?$	$5f^5?$	$5f^4$	$5f^3$
Pu	$5f^67s^2$	$5f^67s$	$5f^6$	$5f^5$	$5f^4$
Am	$5f^77s^2$	$5f^77s$	$5f^7$	$5f^6$	$5f^5$

1.2.1 Electronic configuration and oxidation states

To a large extent, the solution chemistry of the actinides is determined by the 5f valence electrons and by the oxidation states of the actinide ions. Table 1.1 shows the most likely outer electron configurations of the ground-state gas-phase neutral atoms of U, Np, Pu and Am, as well as those for the singly, doubly and triply charged gaseous atoms [Katz *et al.*, 1986b]. In general, due to shielding of the nucleus, the energy difference of electrons in the 5f, 6d and 7s orbitals is small [Greenwood and Earnshaw, 1984]. As a consequence, actinide ions can be present in multiple oxidation states, making their chemical behaviour complex.

The observed oxidation states in solution, including the most stable state and form, are shown in Table 1.2. M(III) and M(IV) states show a strong tendency to solvation, hydrolysis and polymerisation due to their high charge. MO_2^+ and MO_2^{2+} (the form of the M(V) and M(VI) state respectively) are stable configurations and tend to stay as a unit through chemical transformations [Katz *et al.*, 1986b]. Rapid oxidation and reduction reactions occur when transitions do not involve cleavage of the metal-oxygen bond, i.e. between the M^{4+}/M^{3+} and the MO_2^+/MO_2^{2+} couples. Other transitions, between MO_2^+/M^{3+}, MO_2^+/M^{4+} and MO_2^{2+}/M^{4+}, are not reversible and tend to occur slowly [Katz *et al.*, 1986b]. The dominant oxidation states are U(IV), Np(IV), Pu(III,IV) and Am(III) under reducing conditions and U(VI), Np(V), Pu(IV,V) and Am(III) under oxic conditions [Allard *et al.*, 1984]. In general,

actinides in the same oxidation state display similar behaviour although there are marked differences between the various oxidation states.

Table 1.2: The oxidation states of some actinide elements [Katz *et al.*, 1986b]

Element	U	Np	Pu	Am	Stable form
Oxidation states	3	3	3	**3**	M^{3+}
	4	4	**4**	4	M^{4+}
	5	**5**	5	5	MO_2^{+}
	6	6	6	6	MO_2^{2+}
		7	(7)	7?	MO_5^{3-}

Bold type = most stable; ( ) = unstable; ? = claimed but not substantiated.

1.2.2 Hydrolysis

All actinide ions have a strong tendency to interact with water molecules, forming aquo cations. The extent of hydrolysis is dependent on the charge to ion size ratio, the interaction decreasing in the order $M^{4+} > MO_2^{2+} > M^{3+} > MO_2^{+}$ [Katz *et al.*, 1986b]. Aquo cations, particularly M^{4+} and M^{3+}, tend to act as acids in solution:

$$M(OH_2)_x^{n+} = M(OH_2)_{x-1}(OH)^{(n-1)+} + H^+$$

However, when considering the extent of hydrolysis for ions of the same charge, factors other than the charge/size ratio must be involved. For example, the order of acidity for the 4+ ion is: $U^{4+} \approx Pu^{4+} > Np^{4+}$ [Katz *et al.*, 1986b]. In addition, the degree of hydrolysis for the M(V) and M(VI) ions follows the reverse order to that expected, with hydrolysis decreasing with increasing atomic number. The additional factors which influence the interactions of actinide ions with water have yet to be determined.

Aquo cations, particularly actinide (IV) ions, can form polymeric species through

hydroxo (M-OH-M) or oxo (M-O-M) bridges. Polymers of U(IV) and Np(IV) have been observed in aqueous solution [Weigel, 1986; Fahey, 1986; Burney and Harbour, 1974], but more extensive study has been directed to the polymerisation of Pu(IV) [Hursthouse, 1990]. Pu(IV) shows a particularly tendency to form stable polymers, especially when solutions are diluted with water [Coleman, 1965]. Although such reactions are unlikely to occur at environmental concentrations, they can cause severe difficulties in nuclear fuel reprocessing as Pu(IV) is the most common oxidation state used for chemical separations.

1.2.3 Complex formation

Strong complexes are formed with the actinide ions where ligands exchange with water molecules in the hydrated shell [Ahrland, 1986]. Such inner-sphere complexes generally occur with oxygen-containing ligands (oxides, hydroxides, phosphates, carbonates and sulphates) and fluoride. For singly charged anions, the actinide ions complexing power is in the order fluoride > nitrate > chloride > perchlorate, and for doubly charged anions carbonate > oxalate > sulphate [Katz *et al.*, 1986b]. The complex strength increases with the effective charge of the acceptor ion (ie, M(V) < M(III) <= M(VI) < M(IV)) [Ahrland, 1986]. Once again (as with hydrolysis) there are discontinuities when considering the stability of the complexes of ions with the same charge, but generally the stability increases with increase in charge/size ratio.

Outer-sphere complexes can also be formed where the ligand attaches to the water molecules of the hydrated shell. Weak complexes are often an equilibrium between the inner- and outer-sphere complexes although these have been little investigated [Ahrland, 1986].

1.3 ACTINIDES AND THE NUCLEAR FUEL CYCLE

1.3.1 Production in nuclear reactors

Figure 1.1 shows the main actinide production and decay processes that occur in the fuel elements of a nuclear reactor. The picture is fairly complex, with the

Figure 1.1 The main actinide production and decay processes that occur in the fuel elements of a nuclear reactor [Choppin and Rydberg, 1980]. Figures along the lines are half-lives or effective reaction cross-sections (barns) for a standard power LWR, with thermal (0.024eV) cross-sections within parentheses.

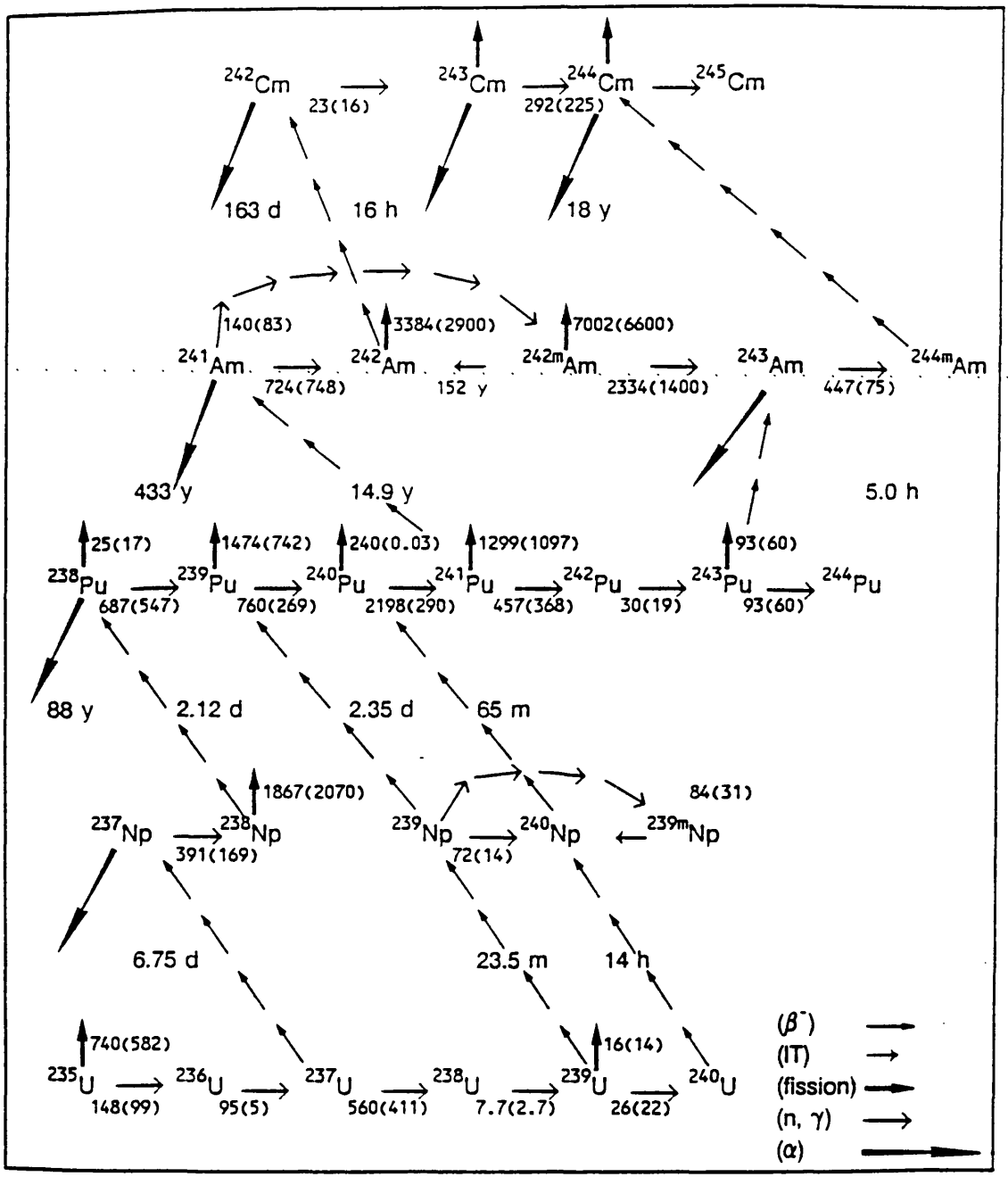

significance of any one pathway for the production of the heavier radionuclides being dependent on the initial fuel composition and the degree of burn-up.

^{239}Pu is produced via neutron capture by ^{238}U:

$$^{238}U + n \rightarrow {}^{239}U \xrightarrow[t_{1/2}\ 23.5\text{min}]{} {}^{239}Np + \beta^- \xrightarrow[t_{1/2}\ 2.35d]{} {}^{239}Pu + \beta^-$$

The higher plutonium isotopes are then formed by successive neutron capture:

^{239}Pu (n,γ) ^{240}Pu (n,γ) ^{241}Pu (n,γ)...etc

The isotopic composition of plutonium in a fuel element of a nuclear reactor varies according to how long the plutonium formed is kept in the neutron flux [Weigel *et al.*, 1986]. Figure 1.2 shows the build up of heavier plutonium isotopes with irradiation of Magnox fuel, the main type of fuel reprocessed at Sellafield (see section 1.3.2). For all fuel types the ^{240}Pu/^{239}Pu ratio increases with burn-up, as shown in Figure 1.3.

^{239}Pu and ^{241}Pu produced in nuclear reactors contribute to energy production through fission. As fission products accumulate, the fuel elements become increasingly inefficient due to loss of neutrons through neutron capture. After an average burn-up of 3000 MWdt^{-1} for Magnox fuels [Allardice *et al.*, 1983], the used fuel elements are replaced and, following an initial cooling period of up to 2 years, are sent to Sellafield for storage and reprocessing (see section 1.3.2).

Plutonium can also be specifically produced for use in nuclear weapons. Weapons grade plutonium consists of fairly pure ^{239}Pu (> 95%) [Choppin and Rydberg, 1980]. For maximum energy release and efficiency, neutron multiplication within a nuclear device should start only after the critical size has been well exceeded. As a consequence, the concentration of ^{240}Pu in weapons grade plutonium is kept as low as practicable as it causes the early release of neutrons through spontaneous fission. The production of weapons grade plutonium therefore requires low burn-up

Figure 1.2 The change in isotopic composition with irradiation for Magnox fuel [Tyror, 1971]

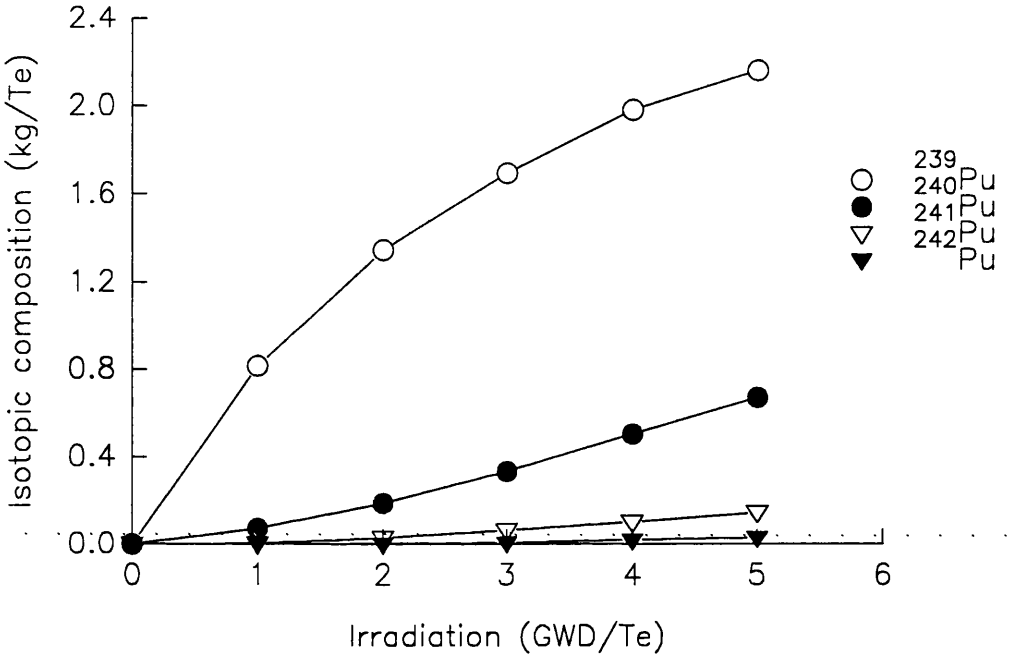

Figure 1.3 $^{240}Pu/^{239}Pu$ atom ratios as a function of irradiation of fuel from Magnox, S.G.H.W.R. and HTR reactors [from Tyror, 1971]

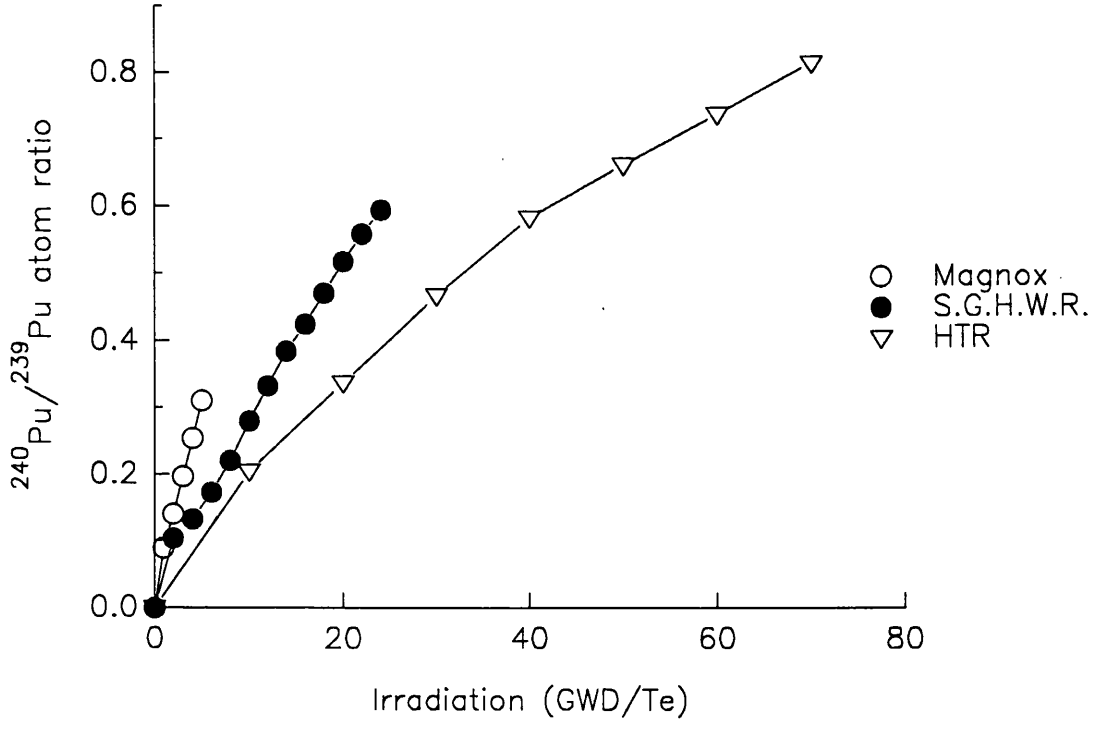

(<2000 $MWdt^{-1}$) [Choppin and Rydberg, 1980]. This corresponds to a characteristic $^{240}Pu/^{239}Pu$ atom ratio of less than 0.14 (see Figure 1.3).

^{237}Np is produced in a nuclear reactor fuel element via several reactions [Fahey, 1986], approximately 70% via

$$^{238}U(n,2n)^{237}U \xrightarrow[t_{1/2} = 6.8 days]{} {}^{237}Np + \beta^-$$

and 30% from two processes:

$$^{235}U(n,\gamma)^{236}U(n,\gamma)^{237}U \xrightarrow[t_{1/2} = 6.8\ days]{} {}^{237}Np + \beta^-$$

and

$$^{241}Pu \xrightarrow[t_{1/2} = 14\ years]{} {}^{241}Am + \beta^- \xrightarrow[t_{1/2} = 433\ years]{} {}^{237}Np + \alpha$$

Again, the significance of any one pathway for the production of ^{237}Np will depend on the initial fuel composition and the degree of fuel burn-up. Once ^{237}Np has been produced, neutron capture leads to the production of ^{238}Pu via

$$^{237}Np(n,\gamma)^{238}Np \xrightarrow[t_{1/2} = 2.1\ days]{} {}^{238}Pu + \beta^-$$

More detailed discussions of the physics of burn-up and the design and operation of nuclear reactors are given by Tyror (1971), Choppin and Rydberg (1980), Flowers (1983) and Askew *et al.* (1983).

1.3.2 Nuclear fuel reprocessing

Since 1952, over 35,000 tonnes of Magnox fuel have been reprocessed at Sellafield (formally Windscale), Cumbria [BNFL, 1992b]. In addition, a mixture of highly irradiated oxide fuels from experimental UK WAGR (Windscale advanced gas-cooled reactor), SGHWR (sodium-cooled graphite moderated heavy-water reactor) and foreign LWR (light water reactors) were reprocessed from 1969 until 1973, when the specialised plant was closed after an incident involving the release of radioactivity [Allardice *et al.*, 1983]. Spent oxide fuel elements have since been stored in cooling ponds at Sellafield, awaiting the commissioning of the Thermal Oxide Reprocessing Plant (THORP) [BNFL, 1992b].

Originally, the purpose of reprocessing was to recover uranium and plutonium for use in fast reactors, maximising the energy yield from the fuel [BNFL, 1992b]. However, funding for the fast reactor programme was cut, so now the recovered uranium and plutonium is stored or used to produce mixed oxide fuel for thermal reactors.

Figure 1.4 shows the main steps involved in the reprocessing of Magnox fuels at Sellafield. Spent nuclear fuel elements are highly radioactive and hot due to the absorbtion of the released radiation in the fuel and surrounding shielding material [Choppin and Rydberg, 1980]. To reduce the radioactivity, the fuel elements are stored in cooling ponds which remove heat and allow time for some of the fission products to decay. The initial military programmes used 180 day cooling programs. Due to the lack of reprocessing facilities, the average cooling time for commercial fuel elements has been up to 7 - 10 years [Choppin and Rydberg, 1980]. The cooling ponds are constantly purged with water, the waste water originally being discharged directly into the Irish Sea via a pipeline [BNFL, 1978]. However, it was found that the magnesium or aluminium alloys used to can the Magnox fuel elements corroded, releasing actinides and fission products into the effluent. As an interim measure to reduce the radioactivity of the discharges, zeolite skips were introduced into the cooling ponds in 1976 [Handyside *et al.*, 1982]. Since 1985, the Magnox pond waste water has been passed through a Site Ion Exchange Effluent Treatment Plant (SIXEP) which removes suspended particulates (which

Figure 1.4 Basic steps involved in the reprocessing of magnox fuels at Sellafield [BNFL, 1986b]

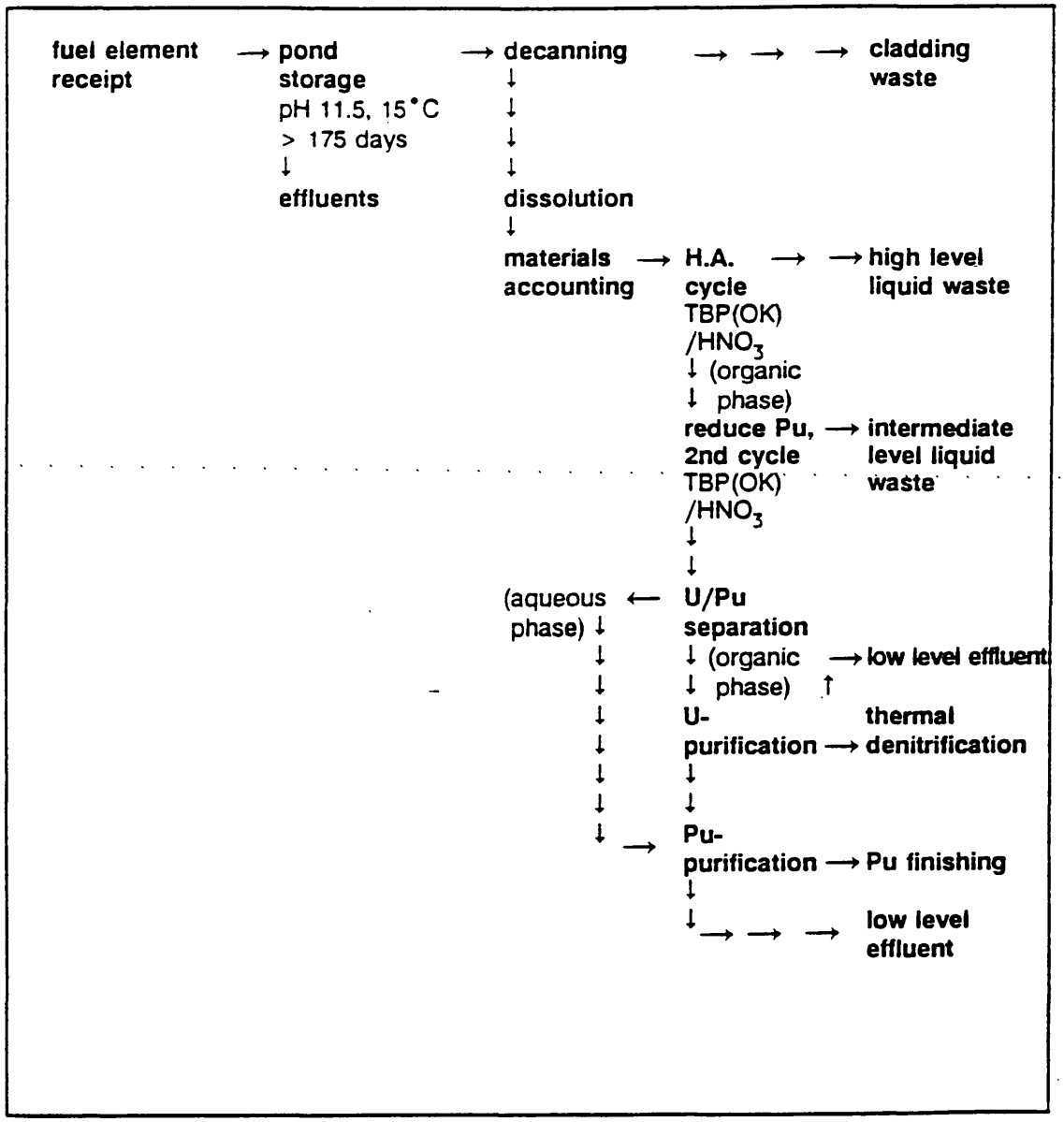

Table 1.3: The pre-reprocessing levels of ^{237}Np generated in fuel from different reactors for 1 GW(e)-year of electricity. [Rees and Ship, 1981]

Reactor	Rating (MW/t)	Amount of ^{237}Np		% ^{237}Np due to:		
		(Bq)	(kg)	^{237}Np	^{241}Am	^{241}Pu
Magnox	3.16	2.9×10^{11}	7.7	23	26	51
AGR	14.66	1.3×10^{11}	5.1	16	21	63
LWR	38.3	2.1×10^{11}	8.1	18	20	62

often contain actinides) and reduces the activity of strontium and caesium released into the Irish Sea [BNFL, 1985-1992]. Water from oxide fuel cooling ponds is still discharged directly to sea as the Zircaloy clad fuel elements are more resistant and can be stored for decades without the risk of leakage [BNFL, 1988]. Table 1.3 shows the amount of neptunium present in spent fuel from a number of different reactors. Once the fuel is removed from the reactor, ^{237}Np continues to accumulate from the decay of ^{241}Pu and ^{241}Am. The contribution to the final ^{237}Np levels, after a 5 year cooling time, are $> 50\%$ due to ^{241}Pu, and $< 26\%$ due to ^{241}Am [Rees and Ship, 1983]. By contrast, the levels of ^{239}Pu and ^{240}Pu in spent nuclear fuel elements decrease by radioactive decay which is insignificant in terms of the cooling time scales. $^{240}Pu/^{239}Pu$ atom ratios in the discharges are therefore related to the degree of burn-up of the reprocessed fuel elements.

In the first stage of reprocessing, the fuel is stripped from its cladding (or sheared into small sections) and dissolved in boiling nitric acid [Allardice *et al.*, 1983]. Low level liquid wastes from the decanning plant are past through SIXEP and combined with effluent from the Magnox cooling ponds to form one of the main discharge streams from Sellafield into the Irish Sea (see section 1.4.3).

The separation of uranium and plutonium is based on solvent extraction. Initially, the BUTEX process was used (with dibutoxy-diethylether solvent), but this was replace in 1964 by the cheaper and more efficient PUREX system, using tri-n-

butlyphosphate (TBP-OK) [BNFL, 1992b]. The feed solution from the decanning plant is conditioned with nitrite to convert virtually all the plutonium into the extractable Pu(IV) states [Drake, 1987]. Under such conditions neptunium exists mainly in the V and VI state [Drake, 1987; Rees and Shipp, 1983]. The exact ratio of the oxidation states of neptunium is difficult to predict as it is dependent on the concentration of nitrous acid, which is formed from the radiolysis of nitric acid and is therefore dependent on the radioactivity of the feed solution [Rees and Shipp, 1983]. This in turn makes the prediction of the destination of neptunium throughout the extraction process difficult, as each oxidation state behaves differently. At the nitric acid concentrations used, Np(VI) is highly extractable by TBP, Np(IV) moderately extractable, and Np(V) virtually unextractable [Drake, 1987]. This leads to a division of the neptunium in the initial extraction process, 20-50% following the high level waste, the rest remaining in the plutonium and uranium stream [Rees and Shipp, 1983]. Virtually none of the ^{241}Am present in the feed solution is extracted into TBP, the Am remaining with unextracted Np in the high level waste. Approximately 99.9% of the uranium and 99.98% of the plutonium is extracted into the solvent phase, leaving 99.5% of the fission products in the aqueous raffinate [Allardice *et al.*, 1983].

To separate the plutonium from the uranium, ferrous sulphamate is added to reduce the plutonium to unextractable Pu(III), uranium remaining in the solvent phase as U(VI) [BNFL, 1992]. Under such conditions, Np(VI) is rapidly reduced to Np(V) with 32-72% of the original ^{237}Np following the Pu into the aqueous phase, about 0.1% remaining in the uranium fraction [Drake, 1987]. Once the separate uranium and plutonium streams have been further purified, uranyl nitrate is concentrated and thermally denitrated to give UO_3. The plutonium is precipitated as oxalate and then thermally degraded to PuO_2 [BNFL, 1992b]. Low level liquid effluents from the U and Pu purification stages which contain a variable amount of Pu and Np are placed in sea tanks [Hursthouse, 1990]. The effluent is then neutralised with ammonia solution, resulting in the precipitation of ferric hydroxide, prior to discharge into the Irish Sea [Kershaw *et al.*, 1992].

There have been no extensive studies on the chemical form of the discharge although some data exist for 1982 [Pentreath *et al.*, 1984]. It was found that

some 99% of the Pu(α) and ^{241}Am, and 60% of the ^{237}Np, in the sea tanks were associated with particulate (>0.22 μm) material. The pond waters were mildly oxidising, so lower proportions of the transuranics (89-99% of Pu and Am, and 12% of Np) were particle-associated. Considering the relative contributions from each source, it was concluded that only 1% of the Pu and 50% of the Np would be discharged in the oxidised (V and VI) form [Pentreath, 1984]. Am, on the other hand, was only present in the III state [Kershaw *et al.*, 1992].

The effluents have also been found to contain 'hot-particles' which are small clusters of α-emitters [Hamilton and Clifton, 1981]. These have been found to persist in the environment for several months [Hamilton, 1981; Kershaw *et al.*, 1986] although its not certain what proportion they are of the discharged plutonium. There have been some suggestions that these hot-particles are fragments of the Magnox fuel elements such particles are now removed from the effluent by the Site Ion Exchange Plant (SIXEP).

1.4 SOURCES OF PLUTONIUM AND NEPTUNIUM IN THE MARINE ENVIRONMENT

Plutonium and neptunium have been released into the environment both on a global scale, through the testing of nuclear weapons, and on a more local level, for example through controlled discharges from nuclear reprocessing plants. This has led to the contamination of the natural environment with artificial radionuclides. The sources and their contribution to environmental radioactivity are discussed below.

1.4.1 Natural production

Table 1.4 lists the long lived (>100 years) isotopes of Np, Pu, U and Am along with their respective half lives. With the exception of ^{235}U, and ^{238}U, the half lives are too short for them to exist today as primordial elements. Plutonium, neptunium and americium isotopes can be produced naturally from neutron reactions in uranium. Both ^{237}Np and ^{239}Pu have been detected in pitchblende [Peppard *et al*, 1952, Myres and Linder, 1971]. In a sample containing 40.72% U, 5.45 x 10^9

Table 1.4: Nuclear properties of some of the long-lived actinides [Katz *et al.*, 1986].

Element	Mass no.	Half-life (y)	Mode of decay	Main radiations (MeV)	Method of production
U	233	1.59×10^5 1.2×10^{17}	α SF	α4.824 (83%) 4.783 (15%)	^{233}Pa daughter
	234	2.45×10^5 2×10^{16}	α SF	α4.777 (72%) 4.723 (28%)	nature
	235	7.04×10^8 3.5×10^{17}	α SF	α4.397 (57%) 4.367 (18%)	nature
	236	2.34×10^7 2×10^{16}	α SF	α4.494 (74%) 4.445 (26%)	^{235}U(n,γ)
	238	4.47×10^9 8.2×10^{15}	α SF	α4.196 (77%) 4.149 (23%)	nature
Np	236[a]	1.55×10^5	EC87% β^-13%	γ 0.163	^{235}U(d,n)
	237	2.14×10^6 $> 1 \times 10^{18}$	α SF	α4.788 (51%) 4.770 (19%)	^{237}U, ^{241}Am daughter
Pu	236	2.85 3.5×10^9	α SF	α5.768 (68%) 5.721 (32%)	^{235}U(α,3n) ^{236}Np daughter
	238	87.74 4.8×10^{10}	α SF	α5.499 (71%) 5.457 (29%)	^{242}Cm,^{238}Np daughter
	239	2.41×10^4 5.5×10^{15}	α SF	α5.155 (74%) 5.143 (15%) γ 0.129	^{239}Np daughter, n capture
	240	6.56×10^3 1.3×10^{11}	α SF	α5.168 (73%) 5.123 (27%)	multiple n capture
	241	14.4	$\beta^- > 99\%$ $\alpha 10^{-3}\%$	β^- 0.021 γ 0.149	multiple n capture
	242	3.76×10^5 6.8×10^{10}	α SF	α4.901 (74%) 4.857 (26%)	multiple n capture
	244	8.26×10^7 6.6×10^{10}	α SF	α4.589 (81%) 4.546 (19%)	multiple n capture
Am	241	432.7 1.2×10^{14}	α SF	α5.486 (84%) 5.443 (13%) γ 0.059 (35.7%)	^{241}Pu daughter, multiple n capture
	243	7.38×10^3 2.0×10^{14}	α SF	α5.277 (88%) 5.234 (11%)	multiple n capture

[a] Not known whether ground-state nuclide or isomer

^{237}Np atoms g^{-1} U and 7.84 x 10^9 ^{239}Pu atoms g^{-1} U were determined by isotope dilution mass spectrometry and α-spectrometry respectively [Myres and Linder, 1971]. ^{244}Pu has also been detected in Precambrian bastnasite [Hoffman *et al*, 1971], but again the levels found were extremely small, only 2 x 10^7 atoms being detected from 85 kg of ore. In general, the natural occurrences of Pu, Np and Am isotopes are insignificant and any such nuclides observed in the environment can be considered to be the result of anthropogenic activities.

Uranium, however, is a relatively common element in the earth's crust, the typical concentration in igneous rocks being 1-10 $\mu g\ g^{-1}$ [Katz *et al.*, 1986b]. Uranium concentrations in natural waters typically range from 0.01-10 $\mu g\ l^{-1}$, the variation being a function of salinity. In open sea water, with a salinity of 35‰, the uranium concentration is 3.3 $\pm$ 0.2 $\mu g\ l^{-1}$ [Pentreath, 1984], but in particularly saline waters the uranium content can be as high as 500 $\mu g\ l^{-1}$ [Allard *et al.*, 1984].

1.4.2 Nuclear weapons testing

The testing of nuclear weapons and devices has led to the global deposition of artificial radionuclides. Since the first nuclear detonation in 1945, over 800 events have been publically recorded, with peak periods during 1955-1958 and 1961-1962 [Pentreath, 1988]. These have been listed by Carter and Moghissi [1977] and Carter [1979] along with approximate explosive yields for each event.

The destination and composition of the fall-out resulting from atmospheric nuclear explosions depends on the size of the device, detonation location (height and latitude) and prevailing climatic conditions [Carter and Moghissi, 1977; Perkins and Thomas, 1980]. Radioactive fallout consists of fission products arising from the fissile material used in the explosive device and neutron activation products from activation of the device components and the surrounding medium. Within a few seconds of the explosion the gaseous components start to condense into small particles. Micro-particles of aluminium and iron also form, often entraining radionuclides and oxides [Pentreath, 1988]. The heavier particles fall back to earth, within a few hundred km from the site of the explosion. Particles entering the

troposphere result in far-field contamination, deposition occurring up to several months after the event and mainly at the same latitude as the explosion [Pentreath, 1988]. High-yield thermonuclear devices can inject particles into the stratosphere. With mean residence times of a few months up to 2 years (depending on the season and latitude), with subsequent deposition of particles from the stratosphere resulting in world-wide distribution of the long-lived radionuclides.

The global inventory of $^{239+240}Pu$ fallout has been estimated to be between 1.2 x 10^4 TBq and 1.6 x 10^4 TBq [Hardy *et al.*, 1973; Efurd *et al.*, 1984; Pentreath, 1988]. To establish the global distribution of fallout plutonium, Hardy *et al.* (1973) analysed soil samples, to a depth of 30cm. At a latitude of 60-50 °N, corresponding to the British Isles, the $^{239+240}Pu$ fallout was on average 48 ± 7 Bq m^{-2}. A later UK soil survey established the average $^{239+240}Pu$ fallout depositions for grassland and woodland as 63 Bq m^{-2} and 59 Bq m^{-2} respectively [Cawse and Beedham, 1979]. After correcting for the average rainfall, the fallout deposit in Cumbrian soils was calculated to be 48 Bq m^{-2} $^{239+240}Pu$ [Cambray and Eakins, 1980]. Assuming that the $^{239+240}Pu$ from fallout is uniformly distributed in the top 10cm of sediment, this would correspond to 0.5 Bq kg^{-1} dry [Aarkrog, 1988]. Hardy *et al.* (1973) also measured the ^{238}Pu activity in global soil samples. Fallout ^{238}Pu has two contributions, that from weapons testing and fallout from the stratospheric burn up of the SNAP-9A satellite in 1964 [Pentreath, 1988]. In the UK the ^{238}Pu contributions were calculated to be 1.1 ± 0.1 Bq m^{-2} from weapons fallout and 0.48 ± 0.15 Bq m^{-2} from SNAP-9A [Hardy *et al.*, 1973].

The isotopic composition of the fallout from a nuclear explosion depends on the neutron flux which increases with the size of the device, resulting in an increase in the production of the heavier radionuclides. Since the majority of the nuclear tests occurred between latitudes 30° N and 30° S, the fallout in the UK is dominated by stratospheric fallout, corresponding to high yield devices. The mean plutonium isotopic composition in soils taken from Wantage in the UK were $^{240}Pu/^{239}Pu$ = 0.1860 ± 2.7%, $^{241}Pu/^{239}Pu$ = 0.0091 ± 9.4% and $^{242}Pu/^{239}Pu$ = 0.0043 ± 2.3% [Krey *et al.*, 1976].

Estimates of the amount of ^{237}Np released from nuclear weapons have also been

made [Holm, 1981; Efurd *et al.*, 1982; 1984]. ^{237}Np is expected to be present in similar concentrations by mass to ^{239}Pu since the (n, 2n)/(n, γ) reaction ratio for ^{238}U in a thermonuclear device ranges from 0.5 to 1 [Holm, 1981]. This was confirmed by Efurd *et al.* (1984), who found the $^{237}Np/^{239}Pu$ mass ratio (determined by isotope dilution TIMS) to be 0.7 ± 0.2 in soil samples representative of global fallout. This led to the estimation that approximately 3,000 kg of ^{237}Np have been released from nuclear weapons testing. Another source of neptunium in the environment is from the decay of ^{241}Pu and ^{241}Am. The activity of ^{241}Pu produced by weapons testing has been estimated to be 1.7×10^5 TBq [Pentreath, 1988], resulting in the production of 5.5×10^3 TBq of ^{241}Am, with the maximum ^{241}Am activity occurring in 2037. This secondary supply of ^{237}Np was calculated to account for 0.05% of ^{237}Np fallout in 1981 [Holm, 1981].

Measurements of fallout concentrations of ^{237}Np in the environment are scarce [Hursthouse, 1990]. Soil representative of the average global fallout was found to contain 2.26×10^{-3} Bq kg^{-1} ^{237}Np [Efurd *et al.*, 1982; 1984]. ^{237}Np concentrations have also been determined in water and sediment samples collected close to detonation sites in the Pacific [Noshkin, 1980; Sakanoue, 1987; 1988], where open ocean water was found to contain 0.48 ± 0.11 μBq l^{-1} [Noshkin, 1980].

1.4.3 Controlled discharges from nuclear installations

Around the world, a number of laboratories and nuclear installations routinely discharge radionuclides into the environment. Figure 1.5 shows the main sources of artificial radionuclides to the aquatic environment of the UK. Discharges are dominated by the British Nuclear Fuels plc reprocessing plant at Sellafield in Cumbria [Kershaw *et al.*, 1992]. Between 1952 and 1992, the authorised releases from Sellafield into the Irish Sea have included over 1.3 GBq of alpha emitting radionuclides, of which more than 54% was plutonium [BNFL, 1977-1992; Cambray, 1982]. The $^{239+240}Pu$ discharges from Sellafield are estimated to be equivalent to 45% of the inventory in the North Atlantic due to global fallout [UNSCEAR, 1982]. Although plutonium originating from Sellafield has been detected as far as 2500 miles from the discharge point [Holm *et al.*, 1986], over 78% of the plutonium discharged can be found in the sediments and seawater of

Figure 1.5 Main UK sources of artificial radionuclides [Kershaw *et al.* 1992]

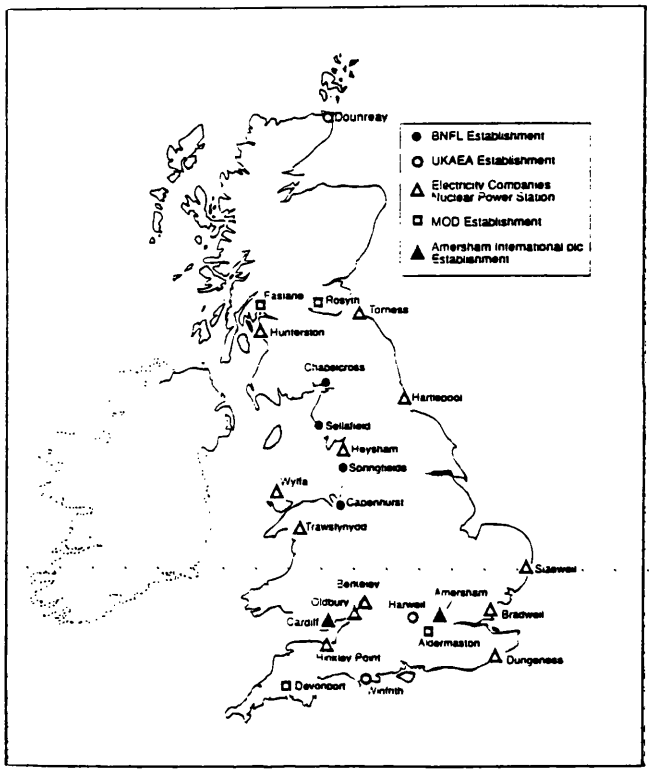

Figure 1.6 $^{239+240}$Pu marine discharges from Sellafield [BNFL, 1977-1992; Cambray, 1982]

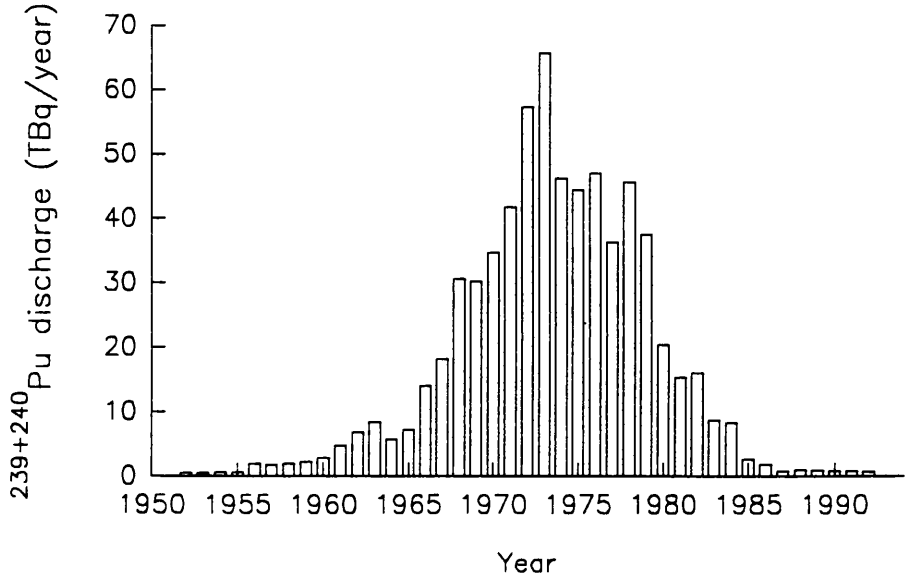

Notes: only Pu (alpha) discharges were recorded between 1952 and 1977, when all the Pu(alpha) was assumed to be $^{239+240}$Pu, and after 1985, when contributions from ^{238}Pu were accounted for, assuming a $^{239+240}$Pu/^{238}Pu ratio of 3.25

the Irish Sea, making Sellafield by far the dominant source of artificial radionuclides in the study area [Pentreath, 1988; 1985; Camplin and Aarkrog, 1989].

Effluents from Sellafield are a by-product of the storage and reprocessing of spent nuclear fuel elements (see section 1.2.2). Details have been published of the major components of the marine discharges since 1952, the fullest accounts occurring after 1978 [Cambray, 1982; BNFL 1971-1993]. In general, discharges into the Irish Sea increased from 1952 to maximum values in the mid1970s, dropping off to a fairly constant level in the last 7 years. No data are available for the individual ^{239}Pu and ^{240}Pu isotopes, however the $^{239+240}Pu$ marine discharges have been measured by α-spectrometry (see Figure 1.6). ^{237}Np has only been determined since 1978, probably after the discharges reached their maximum value. Predictions of the total amount of Np discharged are difficult to make as the levels bear no relation to other published nuclide data [Hursthouse, 1990; and section 1.3.2 for factors determining ^{237}Np concentrations in discharge]. Another consideration is the in situ ingrowth of ^{237}Np from the decay of discharged ^{241}Pu and ^{241}Am. Day and Cross (1981) calculated the accumulation of ^{241}Am in the Irish Sea sediments from the decay of ^{241}Pu. Assuming steady-state conditions, it was estimated that the ingrowth of ^{241}Am would level off at approximately 48 TBq yr^{-1} by 2059. From similar calculations, it was estimated that the ingrowth of ^{237}Np, resulting from the decay of ^{241}Am, will reach its maximum in 7296 [Hursthouse, 1990]. Figure 1.7 shows the recorded Sellafield discharge data for ^{241}Pu, ^{241}Am and ^{237}Np along with the decay corrected integrated discharges, including contributions from ingrowth.

Medium-level radioactive wastes have been stored on site at Sellafield, awaiting the commissioning of the Enhanced Actinide Removal Plant (EARP), which took place in March, 1994. The greater efficiency of EARP will remove a higher proportion of the plutonium and americium [BNFL, 1992b], however the increased volume of material reprocessed may result in an increase in the discharge levels. Increases in discharges of ^{99}Tc, ^{129}I, ^{60}Co and ^{14}C will be far greater due to EARP's inefficiency at removing these 'less radiologically significant' radionuclides.

Figure 1.7 Recorded and decay corrected integrated marine discharges from Sellafield, including contributions from ingrowth, for (a) ^{241}Pu, (b) ^{241}Am, and (c) ^{237}Np [BNFL, 1977-1992; Day and Cross, 1981]

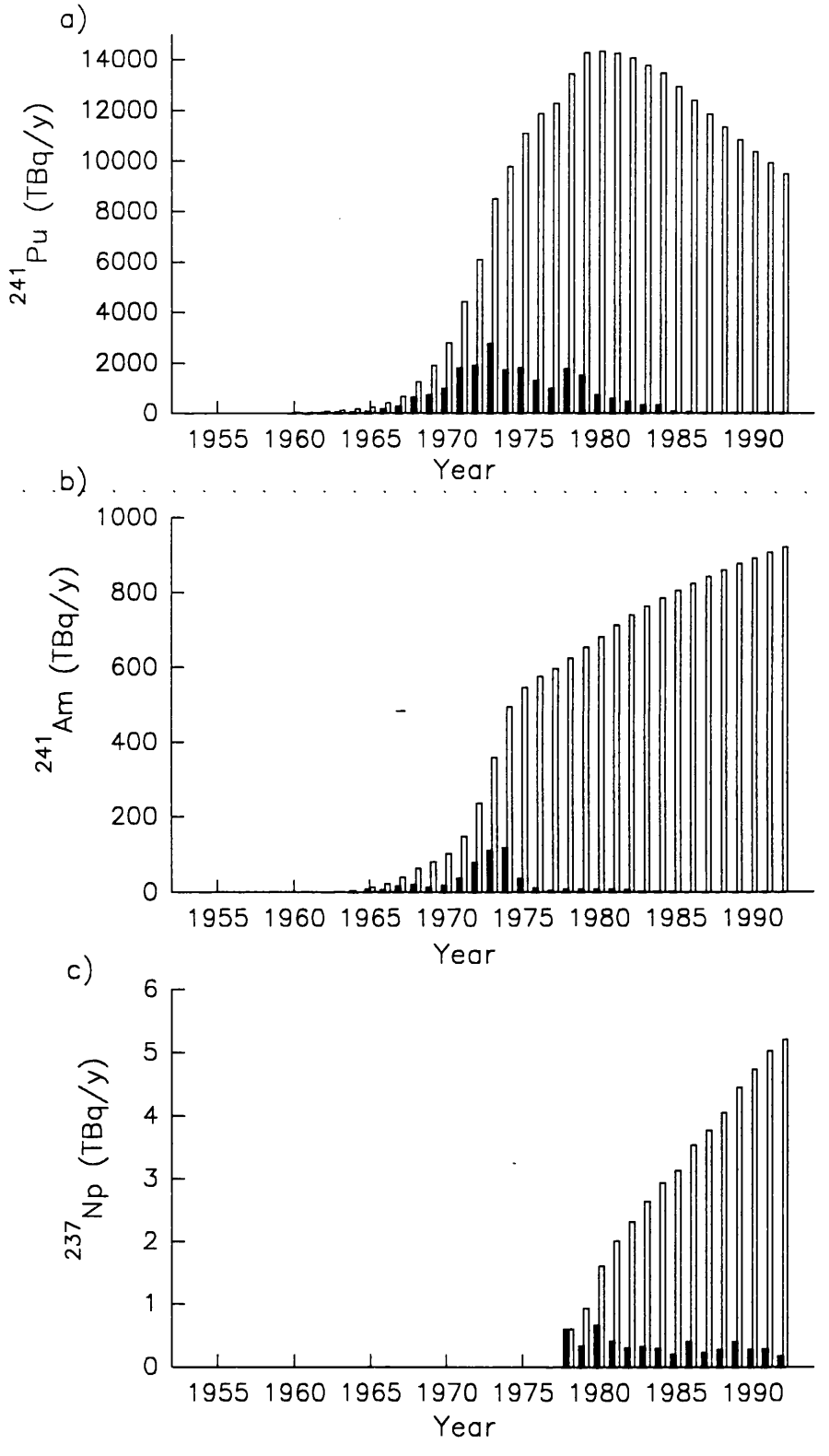

Since 1966, the Cap de la Hague reprocessing plant near Cherbourg, France has routinely discharged radionuclides into the English Channel [Pentreath, 1988]. Guegueniat *et al.* (1981) and Calmet and Guegueniat (1985), presented $^{239+240}Pu$, ^{238}Pu and ^{241}Am discharge data for La Hague and local environmental data for sediment and biota samples. The total Pu(α) discharge from La Hague has been insignificant compared to that from Sellafield, corresponding to only 0.4% of the Sellafield discharges [Kershaw *et al.*, 1994]. No discharge data are available for ^{237}Np. Pentreath *et al.* (1986a) measured ^{237}Np concentrations in filtered seawater samples around Britain, and found that the levels increased from less than 5×10^{-6} Bq l^{-1} at each end of the English channel, to $(1.0 - 1.4) \times 10^{-5}$ Bq l^{-1} opposite the Cherbourg peninsula. This is insignificant compared to a level of 4 mBq l^{-1} found in the Irish Sea [Pentreath *et al.*, 1986b].

1.5 BEHAVIOUR OF ACTINIDES IN THE MARINE SYSTEM

Predicting the behaviour of radionuclides released into the marine environment is difficult, not only because of the complex chemistry of the individual nuclides, but also because of the dynamic nature and variability of the marine system itself. The main biogeochemical processes which occur in the marine environment are summarised in Figure 1.8. Concern over the accumulation of artificial radionuclides in the environment, and their potential use as tracers of environmental processes, has led to a huge research effort to determine the behaviour of radionuclides in the environment. A number of reviews are available detailing the physical and chemical factors affecting the movement and distribution of radionuclides in the marine system [e.g. Santschi and Honeyman, 1989; Santschi, 1988; Dyer, 1986]. A recent review [Kershaw *et al.*, 1992] summarises the literature relating to the Irish Sea. Considerable effort has been directed towards investigations of the behaviour of plutonium and americium [e.g. Sholkovitz, 1983; Pentreath *et al.*, 1984; Nelson and Lovett, 1978; Hetherington, 1975; Aston *et al.*, 1983; McKay and Walker, 1990]. By comparison, neptunium has been neglected [Thompson, 1982].

In addition to environmental-based studies, a number of laboratory studies have been performed to attempt to elucidate the mechanisms involved in influencing the behaviour of transuranium radionuclides [e.g. Mudge *et al.*, 1988; Choppin and

Figure 1.8 The main biogeochemical processes occurring in the marine environment

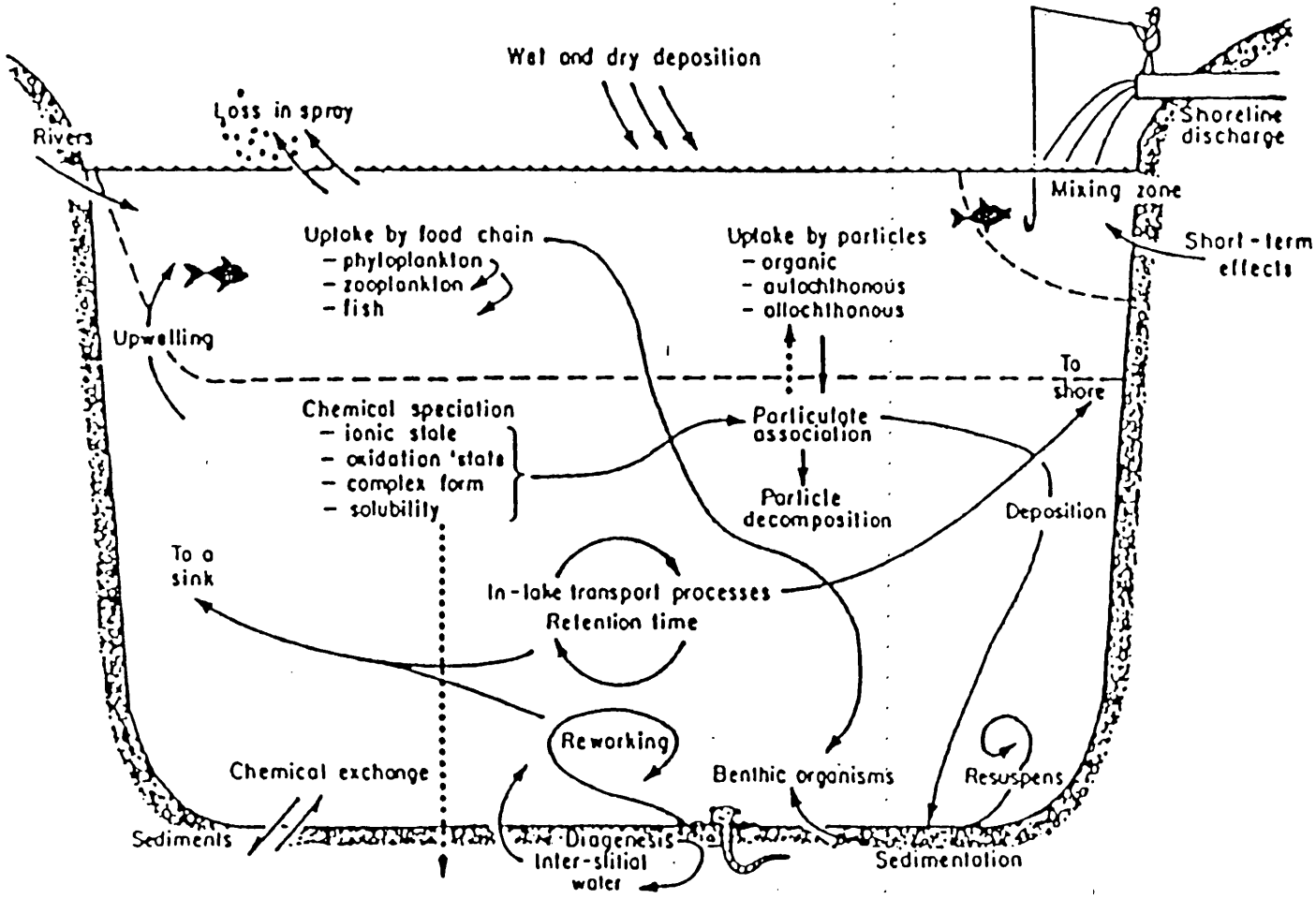

Figure 1.9 The Irish Sea

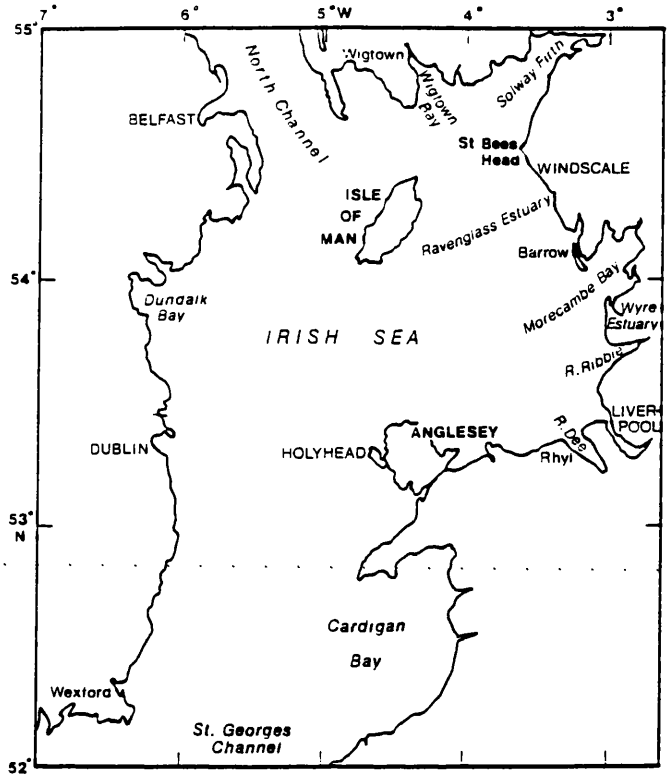

Morse, 1987; Aston *et al.*, 1983; Shen *et al.*, 1983]. However, the relevance of such experiments to the 'real' environment has often been brought into question [Onishi *et al.*, 1981; Choppin and Morse, 1987].

1.5.1 The Irish Sea

The Irish Sea is a semi-enclosed body of water, connected with the Atlantic Ocean in the south by the St George's Channel, and in the north by the narrower NorthChannel, Clyde Sea and Malin Shelf Sea (see Figure 1.9). It is a highly complex coastal shelf system, divided naturally into two sections, east and west of the Isle of Man. The western section contains a central deep channel (> 100 m) which runs parallel to the Irish coast. In contrast, the eastern section consists of a flat shelf with depths rarely exceeding 50 m, and reaching only 30 m between Sellafield and the Isle of Man [Kershaw *et al.*, 1992].

The dynamics of the Irish Sea are principally controlled by tides, propagated from the Atlantic Ocean through both the St George's Channel and the North Channel.

The tidal range is large with high tidal velocities [Dickson and Boelens, 1988]. In most areas, the tides are sufficiently energetic to create a vertically homogeneous water column, although some stratification can occur in winter and spring as a result of fresh-water input [Jones and Folkard, 1971]. The time averaged circulation of the Irish Sea is relatively weak, but the dominant flow is northwards with a persistent southward drift off St Bees Head and the northern Irish coast [Dickson, 1987]. The region is subject to frequent storms [Davies and Jones, 1992], leading to particle resuspension, mixing and transport. The prevailing wind also affects the currents, particularly in the near-shore region. Howarth [1984] concluded that water off Sellafield tended to oscillate, flowing southeast during periods of weak winds, and north-west during storms.

The geological structure of the area has been summarised by Dobson [1977a;b]. It consists of several sedimentary basins containing Carboniferous and Permo-Triassic rocks which have been deeply eroded by successive glacial advances and subsequently overlain by tills and boulder clays [Kershaw *et al.*, 1992]. There has been much discussion on the sedimentation history and the fate of fine-grained sediments in the Irish Sea, the most comprehensive account being given by Pantin [1977,1978]. The distribution of the fine-grained sediments is shown in Figure 1.10. There are two main areas of muddy sediments, a belt running parallel to the Cumbrian coast, extending from Liverpool Bay in the south to Wigtown Bay in the north, and a deep basin between the Isle of Man and the coast of Ireland. These areas correspond to regions with weak tidal currents [Howarth, 1984]. Regions north and south of the Isle of Man have the strongest tidal currents and are associated with the coarser sands and gravels. There is conflicting evidence as to whether the areas of muddy sediments are regions of active sedimentation. Hydrological and sedimentological evidence for sedimentation [Belderson and Stride, 1969; Pantin, 1977; 1978; Mauchline, 1980] was challenged by Kirby *et al.* [1983], who concluded that the evidence for present-day accretion was circumstantial and suggested that there are not enough sources of fine sediment to support continued sedimentation. ^{14}C dating of shells in the Irish Sea sediments suggests a low rate of accumulation in some areas over the last 100 years (approx. 0.1 mm y^{-1}) [Kershaw *et al.*, 1988], although additional contamination of the shells with ^{14}C discharged from Sellafield was not taken into account [Begg, 1992].

Figure 1.10 The distribution of fine-grained sediments in the surface sediments of the Irish Sea [Kershaw *et al.*, 1992]

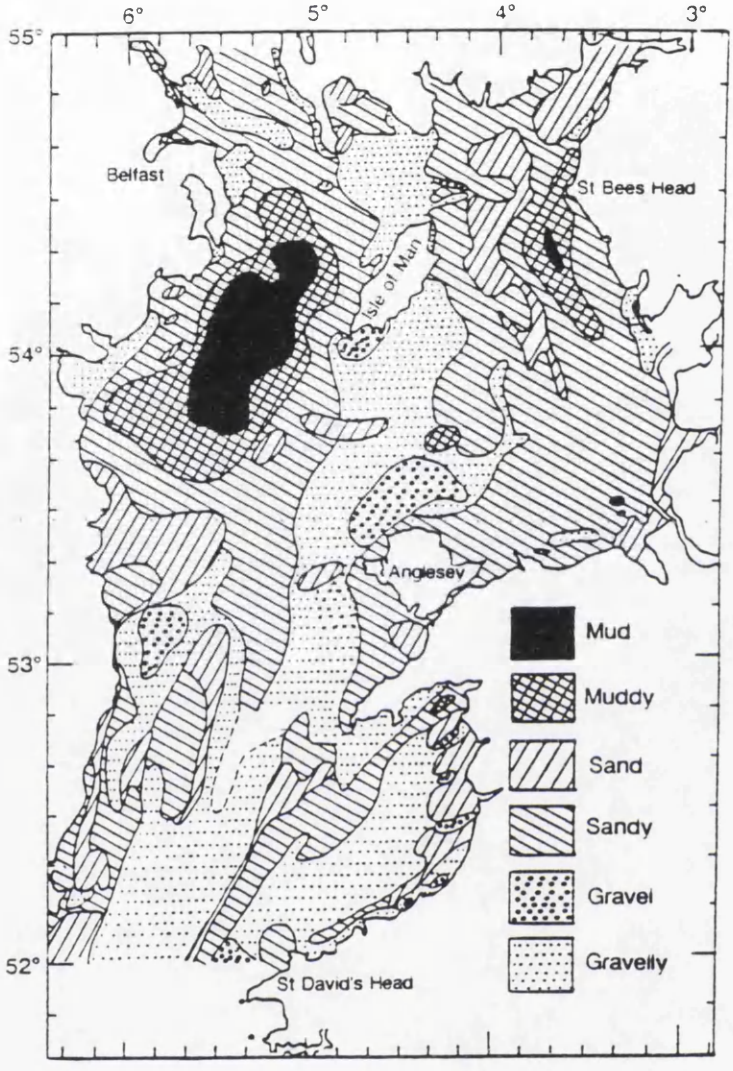

Dating of the bulk sediment carbonate fraction, down to a depth of over 1.6 m, revealed a well mixed sediment with an essentially constant age of 12,500 ± 1,000 years B.P. [Kershaw *et al.*, 1988].

1.5.2 Behaviour of actinides in sea water

Within the Sellafield effluent, almost all the plutonium and americium and over 60% of the neptunium discharged is thought to be associated with particulate material, and in particular, with iron precipitates (see section 1.3.2). Immediately after discharge, the effluent remains stratified for up to 3 to 4 days, moving to and fro with the tidal plug [Hetherington *et al.*, 1975]. Diffusion and advection cause dispersion, the soluble components following the main circulation system of the Irish Sea. There is some evidence that on contact with sea water, some of the plutonium and americium associated with the iron floc dissolves [Pentreath, 1987]. Calculations of the total environmental inventories of Pu(α) discharged from Sellafield to date suggest that 71% is associated with subtidal and intertidal sediments, 7% with sea water, leaving 22% unaccounted for [Pentreath, 1987].

Theoretical calculations predict that the dominant actinide species in environmental solutions are highly insoluble hydroxide complexes, which are likely to become incorporated in iron and manganese hydroxide-oxide phases [Aston *et al.*, 1985], soluble carbonate complexes and, to a lesser extent, organic complexes [Allard *et al.*, 1984]. Extensive studies of the chemical form of plutonium and americium in the waters of the Great Lakes found that the actinides were present in solution as simple anionic species [Edgington, 1981]. Since the actinides do not form strong complexes with halide ions [Sillen and Martell, 1964], it is likely that they are also present in the same form in sea water. Recent ultrafiltration techniques suggest that a significant proportion of Pu 'in solution' is associated with colloids, although further work is required to assess the precise nature of the colloids and their associations with Pu [Orlandini *et al.*, 1990].

Actinides are therefore present in sea water both in solution and associated with suspended particulate material. The distribution coefficient, K_d, defined as

$$K_d = \frac{\textit{concentration per unit mass of particulate}}{\textit{concentration per unit mass of filtrate}}$$

is widely used to describe the partitioning of radionuclides between the solid and solution phases, the particulate/solution cut-off being operationally-defined, usually at 0.22 or 0.45 μm. Strictly speaking, this assumes that the system is in equilibrium and that solid-solution reactions are reversible. However, these criteria may not be valid or be demonstrated, which has led to criticism of the extensive use of K_ds [Sholkovitz, 1983]. Recent studies have used K_d simply to describe the partitioning of the solid and solution phases, and not to indicate the state of a reaction [e.g. Hamilton-Taylor *et al.*, 1993].

Typical values for the bulk K_ds for Np, Pu and Am measured in situ in the Irish Sea are of the order of 10^4, 10^5, and 10^6 respectively, the degree of particle association decreasing in the order Am > Pu > Np [Pentreath, 1985]. The fraction of the total activity associated with the solution phase for a given K_d depends on the sediment load [Pentreath, 1987]. For Np and Pu, the activity in the solution phase dominates in regions away from the coast, where suspended loads are less than 10 mg l^{-1}. Close to the coast, the suspended loads can be more than 50 mg l^{-1}. Coastal surveys reveal little change in the K_d for Pu and Am with distance from the coast, implying that in inshore regions, a greater fraction of the total activity is associated with particulate material [McKay and Walker, 1990; McKay and Pattenden, 1989; Pentreath, 1987]. In complex estuarine environments the K_ds for Pu and Am have been found to vary by over an order of magnitude [Hamilton-Taylor *et al.*, 1993]. The average K_d values for ^{237}Np were found to decrease with distance from Sellafield. Although this can be attributed to a change in the oxidation state from Np(IV) to Np(V) (see below), other factors also have to be considered which could affect the K_d, such as the grain-size distribution and the composition of the suspended sediments [Edgington and Nelson, 1984].

The difference in K_d values for Pu and Np suggests that Np should be more mobile in the environment relative to Pu. This is supported by ^{237}Np/$^{239+240}$Pu data presented by Duniec *et al.* [1984] which indicate relative enrichment of ^{237}Np in the solution phase with increasing distance from Sellafield. Assessing the relative

mobility of ^{241}Am is complicated by the ingrowth of ^{241}Am from the decay of ^{241}Pu.

For plutonium and neptunium, the bulk K_d represents an average value, with contributions from different oxidation states. The K_d values for the reduced (III and IV) and oxidised (V and VI) forms of plutonium are of the order of 10^6 and 5×10^3 respectively [Nelson and Lovett, 1978]. Limited data exist for neptunium, but Harvey (1981) estimated a K_d of about 5×10^3 for the oxidised forms. From experiments conducted on sea water collected from the Irish Sea, Nelson and Lovett (1978) showed that 71 to 92% of the dissolved plutonium was oxidised, with Pu(V) expected to be the dominant species [Orlandini *et al.*, 1986; Bondietti and Trabalka, 1980]. Similarly, Np is predicted to be present in sea water mainly in the oxidised Np(V) state [Pentreath and Harvey, 1981]. In contrast, americium is considered to be present almost entirely as Am(III), although there have been suggestions that Am(V) species may be present [Pentreath *et al.*, 1985]. The difference in the K_d values for the individual oxidation states of the actinides emphasises the importance of the form of the nuclides in the environment, the oxidised state being more likely to be in solution and therefore more mobile. Dissolved species of plutonium originating from Sellafield have been detected in the North Sea [Kautsky and Eicke, 1982, Murray *et al.*, 1978], and as far north as the Barents and Greenland Seas [Holm *et al.*, 1986].

The distribution of plutonium and americium [Pentreath *et al.*, 1984; Mitchell *et al.*, 1991; McKay and Pattenden, 1993] and neptunium [Pentreath and Harvey, 1981] in filtered sea water from the Irish Sea reveals an exponential reduction in concentration with distance from the discharge point (see Figure 1.11). This would be expected from a combination of dilution of contaminated sea water and scavenging of dissolved species by suspended particulate material. Evidence of the removal of Pu by particle scavenging was shown by surveys in the North and South Atlantic, which found a reduction in the $^{239+240}Pu$ concentration in sea water by a factor of 4-5 between 1972 and 1988/89 [Holm *et al.*, 1991]. However, studies on the Pu concentration in the lagoon waters of the Enewetak and Bikini atolls (bomb test sites) suggest that dissolved Pu can be released from contaminated sediments [Noshkin and Wong, 1980]. The evidence for the remobilisation of actinides from the sediments in the Irish Sea is discussed in section 1.5.4.

Figure 1.11 Concentration of (a) $^{239+240}Pu$ and (b) ^{241}Am (mBq l^{-1}) in filtrate surface waters of the Irish Sea in April 1979 [Kershaw *et al.* 1992]

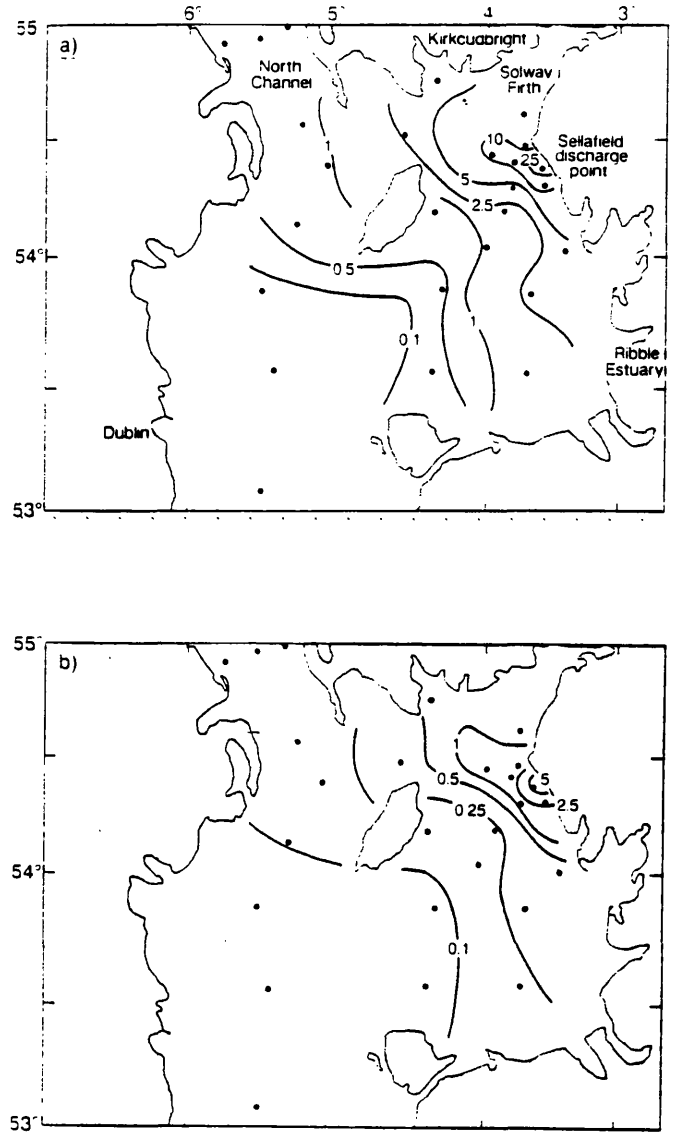

1.5.3 Association with sediments

The overwhelming evidence is that actinides discharged from Sellafield become rapidly associated with particulate material which is then incorporated into the sediments [Hetherington, 1978; Nelson and Lovett, 1978; Pentreath *et al.*, 1985; Sholkovitz, 1983; Aston *et al.*, 1985]. Particulate transport and the processes that occur in the sediments are therefore fundamental in understanding the behaviour of the actinides in the Irish Sea. Pentreath *et al.* [1986b] estimated that only 7% of the annual discharge of plutonium is transported out of the Irish Sea by seawater movement. As a consequence, the sedimentary inventory of plutonium (and by similar arguments, Am and Np) in the Irish Sea has been increasing since Sellafield discharges began.

Adsorption of radionuclides onto particulates can take place in several ways: by electrostatic attraction, by chemical bonding to specific sites on the solid surface, or by simple physical adsorption [Allard *et al.*, 1984]. Apart from the latter, these processes are dependent not only on the form of the species in solution, but also on the composition of the solid surface and the concentration of competing ions in solution. In the marine environment, available adsorption surfaces include sediment particles, (a mixture of sand, silt and clay), metal hydroxides and organic material. In addition actinides can be actively adsorbed to, and taken up by, biogenic material [Pentreath, 1985].

The dominant oxidation states of the transuranics in particulates and sediments are Pu(IV), Np(IV) and Am(III) [Edgington and Nelson, 1984; Harvey and Kershaw, 1984]. The sediment/porewater system is relatively reducing. For example, Malcolm *et al.* [1990] found that greater than 96% of Pu and greater than 99% of Am was in the reduced form at all depths within several sediment cores, except for the top 2 cm, where 27-67% of the Pu was in the oxidised form.

Pu and Am particulate concentrations in sediment have been found to be highly dependent on the grain size, the concentration increasing with decreasing size (see

Figure 1.12 $^{239+240}$Pu activities (Bq Kg^{-1} dry), normalised to 100% silt, in the surface sediments of the Irish Sea, 1988 [McCartney *et al.*, 1994]

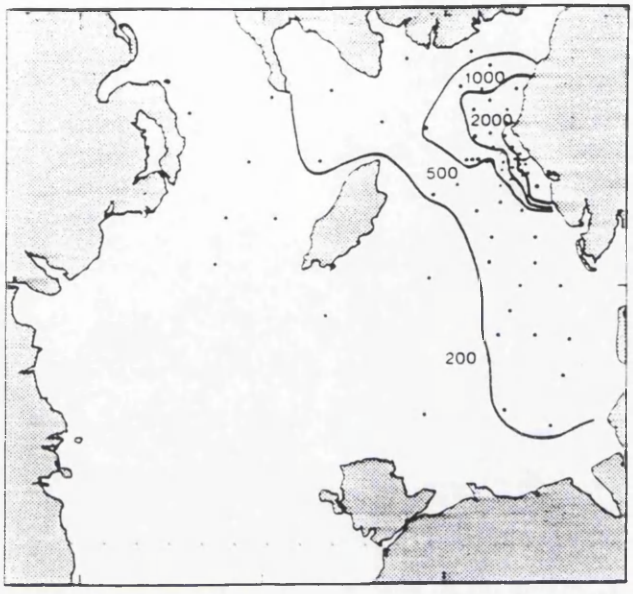

Table 1.5) [Hetherington, 1978; Aston *et al.*, 1985; Eakins *et al.*, 1990]. This suggests that physical adsorption is the dominant process of removal of plutonium from solution. The distribution of Pu and Am in the sediments of the Irish Sea closely follows that of the fine-grained sediments [Woodhead, 1988; Aston *et al.*, 1985; Eakins *et al.*, 1990]. From the limited data available, Np also appears to follow the same trend [Assinder *et al.*, 1991]. Correcting the surface sediment $^{239+240}$Pu activities for the grain-size effect, reveals a distribution dominated by the water circulation pattern (see Figure 1.12), but with a distinct northwards bias in the Sellafield inshore area [McCartney *et al.*, 1994]. The northward dispersal of plutonium is thought to be caused by two effects. Firstly, the Sellafield sea-tank discharges, which contain the largest proportion of discharged plutonium, are released on or around the high tide, when the tide ebbs to the north [Pentreath *et al*, 1984]. In addition, a predominant northward drift of particulate matter has been suggested both from observations of the relative radionuclide concentrations in the sediments [Jones *et al.*, 1988] and from hydrological model predictions [Davies and Jones, 1992].

Table 1.5: Distribution of plutonium nuclides as a function of particle size in a sample of surface sediment [Hetherington, 1978].

Size fraction, μm	$^{239+240}$Pu concentration, Bq kg^{-1} (dry)
< 2	11,900 ± 1,600
2 - 5.5	12,540 ± 700
5.5 - 15	11,100 ± 630
15 - 31	3,920 ± 260
31 - 46	1,630 ± 190
46 - 63	1,036 ± 74
> 63	592 ± 48

1.5.4 Remobilisation of actinides from the sea-bed

It is evident from the discussion above that the Irish Sea sediments initially act as a sink for the actinides discharged from Sellafield. However, the potential for remobilisation of the actinides from the sea-bed also has to be accounted for if the long term implications of the Sellafield discharges are to be assessed.

Remobilisation of actinides from the sediments requires two processes: chemical changes to produce more mobile forms in the interstitial water (for example, conversion of highly immobile Pu(IV) to more mobile Pu(V) or the complexation of Pu(IV) within the water), followed by physical transport of the mobile forms by processes such as diffusion and advection [Aston *et al.*, 1985]. In addition, direct loss of actinides from surface sediments or from resuspended particles could occur due to the operation of the law of mass action [Nelson and Lovett, 1981; MacKenzie and Scott, 1984]. Hunt and Kershaw [1990] estimated that 8 TBq (5.4% of discharges) of Pu(α) and 2.5 TBq (3.9% of discharges) of ^{241}Am have been remobilised from the sea-bed from 1979-87 and 1976-87 respectively. Their calculations were based on the differences observed between measured concentrations in seawater and the concentrations expected on the basis of extrapolation from the conditions of steadier discharge rates experienced in the past.

Measurement of the composition and the physico-chemical conditions in interstitial waters provide a direct and sensitive way of determining mechanisms and kinetics of chemical reactions in the sediments [Sholkovitz, 1983]. The microbial oxidation of organic matter within the sediment system causes variations in the redox potential with depth, influencing the distribution of redox-sensitive elements such as Fe and Mn [Kershaw *et al.*, 1992]. This may also effect the oxidation states of Pu and Np, emphasising the importance of measuring parameters such as Eh, pH, Mn^{2+}, Mn^{4+}, Fe^{2+}, Fe^{3+}, NO^{-}_{3}/NO^{-}_{2} and phosphate concentrations [Harvey, 1981]. Another suggestion is that dissolved organic carbon (DOC) could be responsible for complexing actinides in the interstitial water [Nelson *et al.*, 1985]. Difficulties are encountered in analysing interstitial water (or pore-water), as it is essential that the measurements reflect the in situ conditions. Any exposure to air during the collection and handling of the sediment or during pore-water extraction would result in the immediate precipitation of dissolved ferrous Fe, so all operations have to be performed in an inert atmosphere [Pentreath, 1987]. In addition, hundreds of ml of interstitial water are required to determine the oxidation states of Pu in the Irish Sea, litres being required from sediments contaminated with fallout. The low concentrations of Np, even in the Irish Sea, imply that even larger volumes (10-20 l) are required for accurate determination of Np oxidation states [Harvey, 1981].

Nelson and Lovett [1981] have presented data for Pu and its oxidation state distribution in interstitial water of sediments from the Irish Sea. They found that the concentration of oxidised Pu species generally decreased with depth (however some of these data may be suspect as they did not take precautions against exposure of the sediment to air during sampling). From profiles of the reduced Pu concentrations in the solid and liquid phase, the authors concluded that the K_d values for the reduced Pu remained constant with depth. This has since been disputed by Sholkovitz [1983], who suggested that their data display significant changes in K_d values implying that diagenetic reactions may be occurring to increase the pore-water concentration of the reduced form of Pu. Malcolm *et al.* [1990] also found small but systematic changes in the K_d values with depth for reduced Pu and Am within sediments from the same area. This suggests that the solid and liquid phases are not in equilibrium and that some Pu and Am may be released from the sediments [Malcolm *et al.*, 1990; Sholkovitz, 1983]. However,

Figure 1.13 The distribution of ^{237}Np in the solid phase and interstitial water of an Irish Sea sediment [Harvey and Kershaw, 1984]

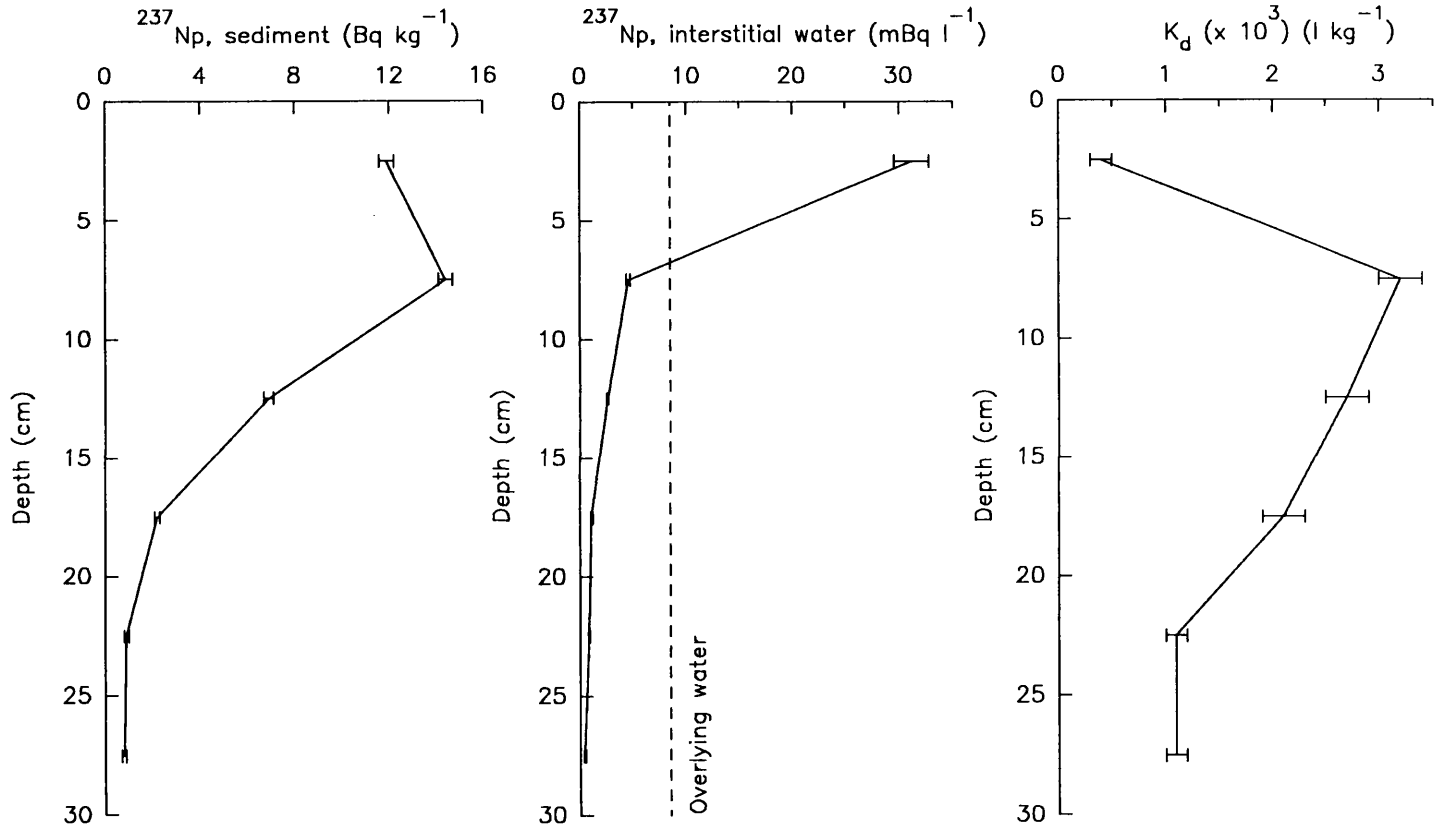

the interstitial profiles of reduced $^{239+240}Pu$ and ^{241}Am bore no relation to the indicators of diagenesis (NO^-_3, PO^{3-}_4, Fe^{2+}, Mn^{2+}, DOC, $Si(OH)_4$) with depth, but did display a qualitative relationship with the solid phase $^{239+240}Pu$ and ^{241}Am profiles [Malcolm *et al.*, 1990]. The distribution of Np in the solid phase and interstitial water of an Irish Sea sediment is shown in Figure 1.13 [Harvey and Kershaw, 1984]. Again, the K_d values show small variations with depth, but unfortunately no ancillary data were collected which could elucidate the mechanisms involved in releasing Np from the solid phase.

Once the actinides have been released from the solid phase, the rate of diffusion within the interstitial water, calculated from measured concentration gradients, would be extremely slow (e.g. $^{239+240}Pu$ would move less than 0.1 cm in 10 years for a 10% concentration front) [Nelson and Lovett, 1981; Buesseler and Sholkovitz, 1987a]. Nelson and Lovett [1981] also calculated that the advective movement of Pu would only be significant if the flow rate through the sediments was $> 10^3$ m yr^{-1}.

The evidence above suggests that there is potential for post-depositional remobilisation of Pu, Np and Am, but more work is required to determine the precise mechanisms involved. In the short term, such effects are insignificant in the Irish Sea compared to the continued input of actinides from Sellafield and their subsequent uptake by sediments from the water column [Sholkovitz, 1983].

Comparatively, the effects of physical mixing of sediments by wave action and bioturbation are significant. McCartney *et al.* [1994] observed that the distribution and concentration of $^{239+240}Pu$ in surface sediments has changed little between 1974 and 1988, despite the increase in the cumulative sedimentary inventory during this time. This was attributed to the mixing of sediments by benthic fauna. Bioturbation was first suggested as a mechanism to explain the 'irregular' shape of radionuclide concentration and ratio profiles in sea-bed cores, the profiles bearing no relation to the Sellafield discharge pattern. Several studies have since evaluated and described the process [Kirby *et al.*, 1983; Kershaw *et al.*, 1984; 1983; Swift and Kershaw, 1986; Woodhead, 1988; Hamilton *et al.*, 1991].

The degree and extent of the biological mixing of sediments is hard to quantify due to the large variations observed even in one area [Kirby *et al.*, 1983; Pentreath, 1987]. Examples of two species active in bioturbation below 5 cm are the Echiuran worm *Maxmülleria lankesteri* and the Thalassinid shrimp *Callinassa subterranea* [Kershaw *et al.*, 1984; Swift and Kershaw, 1986]. These species can be found to depths of 30 and 150 cm respectively. *M. lankesteri* feeds on surface sediment particles which are subsequently defecated within the burrow, later to become incorporated into the burrow lining. This results in enhanced concentrations of $^{239+240}$Pu and ^{241}Am, and 'recent' $^{239+240}$Pu/^{238}Pu activity ratios at depth [Kershaw *et al.*, 1984]. *C. subterranea* excavates a complex network of burrows, resulting in the transport of uncontaminated sediment to the surface, and the burying of fresh particulate deposits [Kershaw *et al.*, 1992]. Bioturbation is site specific so interpretation is required on an individual core basis [Gurbutt and Kershaw, 1987]. For example, in certain cores close to the Sellafield pipeline, unusual quantities of oxidised Pu (~60%) were found in the interstitial water, within the upper 2-5cm of sediment [Kershaw *et al.*, 1992; Malcolm *et al.*, 1990]. This was attributed to a large population of a burrowing Opiuroid species which effectively irrigated the sediment with the oxygenated overlying water [Kershaw *et al.*, 1992].

1.5.5 The environmental record of the Sellafield discharges

The sediments of the Irish Sea act as a major repository for particle reactive radionuclides, such as plutonium and neptunium, which are discharged from Sellafield. In areas of sediment accumulation, it might be expected that the sediments provide a record of the discharges from Sellafield [Kershaw *et al.*, 1990]. Indeed, several attempts have been made to match sediment core profiles with Sellafield discharge data [Hetherington, 1978; Aston and Stanners, 1982a; Stanners and Aston, 1981]. Many studies have relied on $^{239+240}$Pu/^{238}Pu activity ratios to establish the rate of sedimentation [Kershaw *et al.*, 1992]. Such techniques have been criticised due to the lack of ^{238}Pu discharge data prior to 1978, and the subsequent over reliance on yearly surface sediment data to establish the previous $^{239+240}$Pu/^{238}Pu ratios [Sholkovitz, 1983]. There is also evidence that bioturbation and chemical conditions within the sediments can affect the sediment profiles, in effect mixing sediments contaminated with 'older'

discharges with those associated with more recent releases (see section 1.5.4). Subsequently, sediment core profiles have been interpreted using a wider range of discharged radionuclides [Stanners and Aston, 1984; Kershaw *et al.*, 1990]. The most comprehensive studies stress the importance of understanding and assessing the dynamics and variability of the whole system in order to interpret any environmental data properly [Clifton and Hamilton, 1982; Hamilton, 1983; Hamilton and Clarke, 1984]. In addition, a recent publication presents evidence that the sediments do not preserve a year by year account of Sellafield discharges, but provide a history of the integrated discharges [MacKenzie *et al.*, 1994].

1.6 EXPOSURE OF THE HUMAN POPULATION TO ACTINIDES

One of the main considerations in assessing the long term implications of discharges from Sellafield is the resulting exposure of the public. This has led to a considerable research effort to determine the potential pathways by which radionuclides may return to the human population. Exposure can occur internally through the ingestion of sea food and inhalation of resuspended soil, silt, or sea spray and externally through exposure to contaminated sediments and beach material.

1.6.1 Sea-to-land transfer

Soil transects, taken inland from the West Cumbrian coast, showed an excess of plutonium, ^{241}Am and ^{137}Cs (above the weapons fallout contribution), which decreased with distance from the coast and correlated with Na deposits [Cambray and Eakins, 1982]. The activity ratios of these samples were characteristic of marine particulate material contaminated with discharges from Sellafield, indicating that radionuclides had been transferred from the sea on to the land. Since then, much work has been done on the mechanisms of sea-to-land transfer. These include deposition of seaborne sediment by tidal action and inundation [Horrill, 1984; Curtis *et al.*, 1991; McDonald *et al.*, 1992], and deposition of air borne material [Eakins and Lally, 1984; McKay and Pattenden, 1990].

Studies have found that particle associated radionuclides become enriched in sea

spray compared to the activities found in the seawater itself [Cambray and Eakins, 1982; Eakins and Lally, 1984; Pattenden *et al.*, 1989]. Bubbles rising to the surface are thought to scavenge particulates, producing aerosol droplets on bursting at the surface which have enrichment factors for the actinides of the order of 10 for the surf zone, and of the order of 100 further out to sea [McKay and Pattenden, 1990; McKay *et al.*, 1993].

In Cumbria, the sea-to-land transfer of radionuclides, and in particular Pu and ^{241}Am, results in exposure of the population through inhalation and through consumption of local produce. For an average person living in Seascale, 4 km from Sellafield, this exposure is calculated to have resulted in a peak dose of 24 μSvy^{-1} in 1973, falling to 4 μSvy^{-1} by 1987 with a further reduction to 2 μSvy^{-1} predicted for the year 2000 [Howorth and Eggleton, 1988]. The figures are higher for members of the 'critical group' in Seascale, whose exposure due to sea-to-land transfer in 1987 was calculated to be 8% of the dose received through the consumption of seafood [McKay and Pattenden, 1990]. The radiological significance of the sea-to-land transfer is small (< 5% of the ICRP principal limit of 1 mSvy^{-1}), but, it results in the exposure of the population to actinides, and is likely to persist through the continued presence and accumulation of actinides in surface sediments and suspended particulate material [McKay and Pattenden, 1990].

1.6.2 Exposure through the consumption of marine biota

To assess the radiation exposure of the public as a result of discharges from Sellafield, the Ministry of Agriculture, Fisheries and Foods (MAFF) has carried out annual monitoring and surveillance programmes in the Sellafield area and elsewhere in the UK coastal environment [MAFF, 1967-1993]. A major part of these programmes has been the determination of radionuclide concentrations in marine biota which form one of the main pathways of exposure of the human population. Figure 1.14 shows $^{239+240}$Pu concentrations measured by MAFF in a variety of marine samples. ^{237}Np has only been determined in a limited number of samples, since 1984 (Figure 1.15). Between 1967 and 1993, there have been three main pathways of exposure; the consumption of Porphyra, external exposure and the

Figure 1.14 $^{239+240}$Pu concentrations (Bq kg^{-1}, wet) in marine biota from the Irish Sea from 1969 to 1992 [MAFF, 1970-1993]

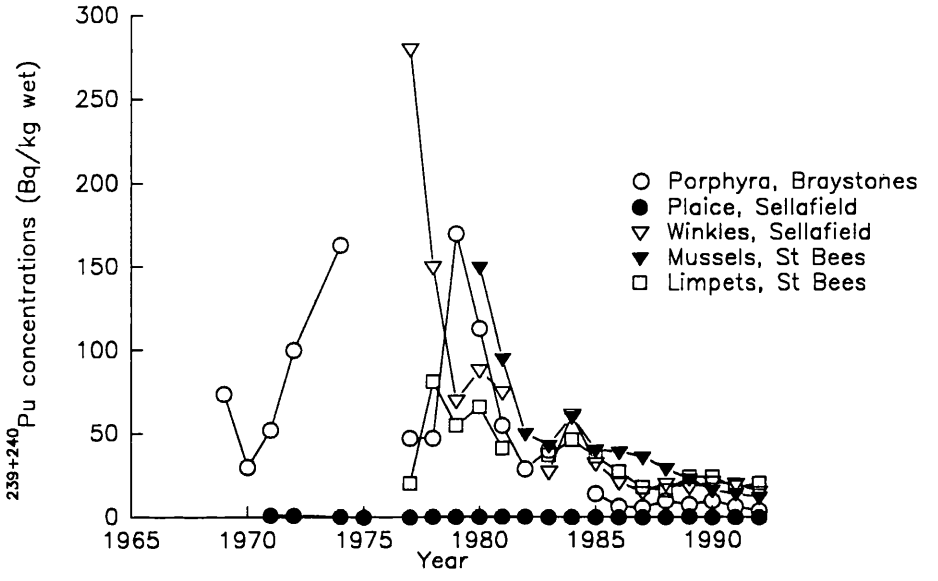

Figure 1.15 ^{237}Np concentrations (Bq kg^{-1}, wet) in marine biota from the Irish Sea from 1984-1992 [MAFF 1985-1993]

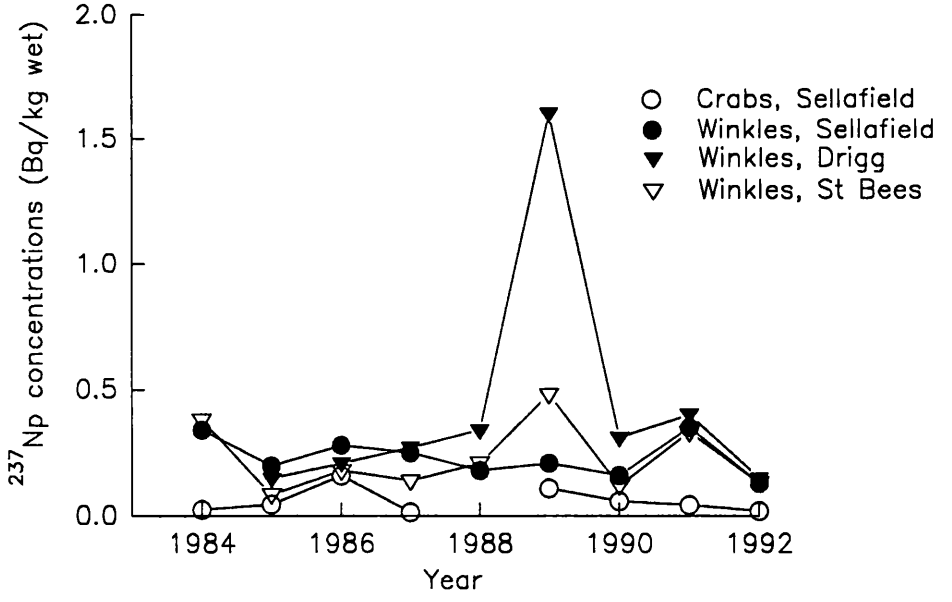

consumption of seafood including fish and shellfish (Figure 1.16).

Initial concern was directed towards the consumption of laverbread, produced from the alga Porphyra which was harvested from the coast near Sellafield. This was the dominant pathway of human radiation exposure between 1967 and 1972, resulting in a dose to individuals of the critical group of 4 to 7 $mSvy^{-1}$ [Preston and Jefferies, 1969]. After 1972, harvesting of Porphyra from the Cumbrian coast ceased, and external exposure to individual workers in the Esk Estuary became the dominant pathway, until 1974, when the critical group changed to shellfish and fish consumers [Kershaw *et al.*, 1992].

From early studies it was evident that transuranium nuclides were not highly accumulated by fish such as plaice [Pentreath and Lovett, 1976, 1977, 1978; Leonard and Pentreath, 1981], but were concentrated in edible shellfish [Hamilton and Clifton, 1980; Clifton *et al.*, 1983]. However, the initial dose received by shellfish consumers was predominantly caused by exposure to Cs nuclides, with $^{239+240}Pu$ and ^{241}Am accounting for less than 0.13 $mSvy^{-1}$ in 1974. By the 1980s the relative importance of the transuranium radionuclides increased, due to reductions in the levels of ^{137}Cs discharged and through revisions to the estimates of the gut absorbtion factors for Pu at low concentrations [Kershaw *et al.*, 1992]. In 1980, $^{239+240}Pu$ were the predominant nuclides, accounting for 9.5% of the effective dose equivalent of 1.95 $mSvy^{-1}$, but in 1981 changes to the critical group to include voracious mollusc eaters (45 g day^{-1}), made ^{241}Am the dominant nuclide, contributing 20% to the effective dose equivalent. Since the 1980s, the dose received by the shellfish consumers has declined as a result of the decrease in discharges and subsequent decrease in shellfish concentrations (see Figure 1.16), and since the late 1980s the critical pathway has been again through external exposure [Kershaw *et al.*, 1992].

1.6.3 Radiological significance of the long-term disposal of radioactive wastes

The expansion of the nuclear power industry since the late 1950s and nuclear fuel reprocessing, has led to substantial quantities of intermediate and high-level radioactive waste. Under government authorisation, UK Nirex Ltd are to build an

Figure 1.16 Exposure (mSv y^{-1}) of the public as a result of porphyra consumption, external exposure and fish and shellfish consumption [MAFF, 1970-1992]

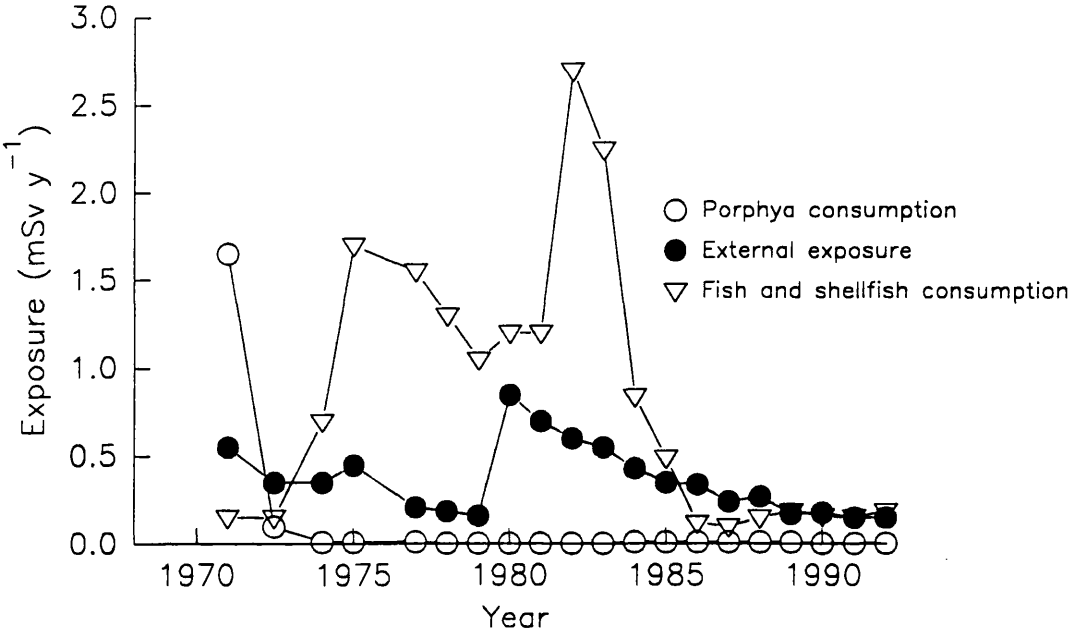

Figure 1.17 Cancer doses per Gwe-y in high level waste with time after reprocessing. The right hand scale indicates the number of cancer deaths/y per Gwe-y assuming a 10^{-12}/y transfer rate from rock into human stomachs [Cohen, 1982].

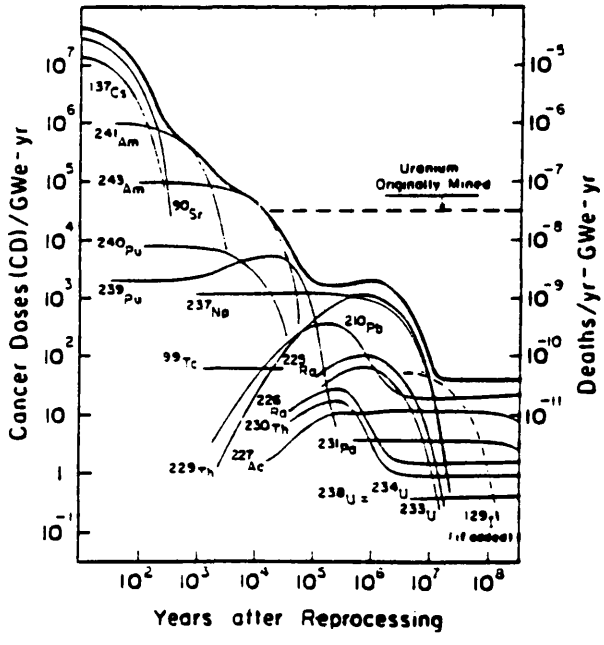

underground repository at Sellafield, designed for the long-term storage of intermediate waste. This repository will probably be located under the Irish Sea bed, so it is likely that eventually some radionuclides will escape from the repository into the marine system.

The assessment of the risks involved in the long-term disposal of high-level radioactive wastes has led to the calculation of hazard indices. These assess the implications of release of radionuclides from repositories into the biosphere and include considerations such as the composition of the waste, the behaviour of the radionuclides in the environment, the potential pathways to the food chain and the human population, and the radiotoxicity of the individual nuclides [Kirchner, 1990]. Such calculations reveal that ^{239}Pu and ^{240}Pu are significant components of high-level waste up to 10^5 years after reprocessing, after which ^{237}Np becomes more significant (see Figure 1.17) [Cohen, 1982; Cohen, 1983; Kirchner, 1990].

1.7 DETECTION METHODS

1.7.1 Overview

The concentrations of anthropogenic radionuclides in environmental media vary spatially and with time, depending on factors such as the source term, the chemical behaviour of the individual nuclides and the parameters of the environmental system into which they are introduced. Table 1.6 shows the typical ranges of concentrations of $^{239+240}Pu$ and ^{237}Np found in biota and sediments from the Irish Sea in the last 40 years. Although actinides in these samples are relatively enhanced, the concentrations are still at a trace or ultra-trace level, and their determination requires selective and sensitive techniques. Table 1.7 lists the main techniques used for the determination of the levels of ^{237}Np and isotopes of plutonium in environmental samples. The characteristics, advantages and limitations of some of these techniques are discussed below.

1.7.2 Radiometric methods

Conventional techniques used for determining radionuclide concentrations, are

Table 1.6: Typical ^{237}Np and plutonium isotope concentrations in samples from the Irish Sea [MAFF, 1969-1992; [a]Assinder et al., 1991; [b]Pentreath and Harvey, 1981; [c]Pentreath et al., 1984].

Nuclide	Sample type	Concentration range, Bq kg^{-1} (mBq l^{-1}, for seawater samples)
^{237}Np	[a]sediment	0.012 - 13.3
	[b]seawater	0.01 - 3.8
	fish	0.00015 - 0.016
	shellfish	0.0015 - 1.6
$^{239+240}Pu$	sediment	18 - 4,200
	[c]seawater	0.1 - 25
	fish	0.00046 - 0.37
	shellfish	0.012 - 280
	seaweed	0.2 - 170
^{238}Pu	sediment	3.9 - 1,100
	fish	0.00001 - 0.089
	shellfish	0.0032 - 30
	seaweed	1 - 43
^{241}Pu	sediment	1,200 - 61,000
	fish	0.25 - 2.5
	shellfish	1.3 - 3,000

based on the detection of decay products. Table 1.4 lists the decay modes of the long-lived radionuclides of Pu, Np, U, and Am. The majority of the actinides are α-emitters. Alpha particles and gamma rays emitted during the process of radioactive decay have characteristic energies which are specific to each transition and detection is based on measuring the energy distribution of the emitted radiation. However, detectors have finite energy resolution, depending on the type of the detector and the quality of the electronics, which limits the separation of the resulting signals and the distinction between transitions which have similar energies. In most circumstances, this can be overcome by radiochemical separation of the analytes prior to analysis. The low specific activity of the long-lived radionuclides (for example, ^{237}Np with a half-life of 2.14×10^6 years has a specific activity of 2.6×10^7 Bq g^{-1}) and the low concentrations of actinides in environmental samples often mean that some sample preconcentration is also required.

Table 1.7: Comparison of techniques used to measure environmental concentrations of ^{237}Np and plutonium isotopes [Cross and Hooper, 1987; and references in text].

Method	Detection limit	Comments
α-spectrometry	10^{-4} Bq (3.8×10^{-12} g ^{237}Np, 3.1×10^{-14} g $^{239+240}Pu$, based on fallout activity ratio)	detection limit based on 10^6 s count, low background, chemical separation required, counting times > 24 hours
neutron activation analysis	10^{-4} - 10^{-5} Bq ^{237}Np (3.8 - 0.38) $\times 10^{-12}$ g	detection limits dependent on neutron flux, some chemical separation required
alpha track counting	10^{-3} - 10^{-4} Bq	non-specific technique, determines total α- activity
laser induced photoacoustic spectrometry	approx. 10^{-8}M, (0.062 Bq ml^{-1} ^{237}Np, 5.5 Bq ml^{-1} ^{239}Pu)	not sensitive enough for low-level environmental samples
ICP-MS	10×10^{-12} g ml^{-1} (2.6×10^{-4} Bq ml^{-1} ^{237}Np, 0.023 Bq ml^{-1} ^{239}Pu, 0.084 Bq ml^{-1} ^{240}Pu)	advantages for long-lived nuclides, some chemical separation required, fast
TIMS	4.3×10^{-15} g ^{239}Pu (1.7×10^{-5} Bq $^{239+240}Pu$)	sensitive enough to determine fallout concentrations, chemical separation required
SID-TIMS	1×10^5 atoms, 1×10^{-9} Bq ^{237}Np, 9×10^{-8} Bq ^{239}Pu	

1.7.2.1 Alpha Spectrometry

The most widely used technique for measuring low-level activities of α-emitters is alpha spectrometry as it provides both an extremely low background and sufficient energy resolution to distinguish between different α-emitting actinides.

Alpha-particles are commonly detected using silicon surface barrier (SSB) detectors [Lally and Phillips, 1984]. These consist of a thin wafer of silicon, containing a p-n junction. N-type silicon is oxidised in air to produce the p-type contact. A layer of gold is evaporated on to one side to act as the positive contact, with aluminium being deposited on the reverse side as the negative contact. Full details of the

principles of semi-conductor devices are given by Knoll [1979]. Sources for high resolution α-spectrometry need to be uniform and very thin, to avoid self adsorption and are usually prepared by electrodeposition onto polished stainless steel discs. Separation of the actinides from the bulk matrix is required to remove all traces of iron and other metals from the sample which could 'plate out' with the actinides during electrodeposition, resulting in 'thick' sources.

For α-energies of 4 to 7 MeV, the typical energy resolution of SSB detectors is of the order of 10 to 20 keV (Full Width at Half Maximum, FWHM) and approximately 20 to 30% of the emitted α-particles are detected, depending on the solid angle of the detector. Even with an energy resolution of 10 keV, several of the actinides have α-particle energies which overlap. The potential interferences in the analysis of ^{237}Np and Pu isotopes in environmental samples are highlighted in Figure 1.18. For ^{237}Np analysis, α-particles resulting from the decay of ^{234}U cause major interference, especially considering that ^{234}U/^{237}Np activity ratios can be as high as 5×10^5 in certain environmental samples. Chemical separation of Np from U is therefore required prior to analysis. Corrections for any ^{234}U remaining in a separated sample can be made by calculating the concentration of uranium in the sample from detection of ^{238}U. Some separation of ^{237}Np from Pu is also required to reduce the contribution to the ^{237}Np peak from the tailing of the $^{239+240}$Pu α-peak. As a result, radiochemical separation procedures for determination of ^{237}Np by α-spectrometry are often long and laborious. Typical procedures are detailed by Holm and Nilson [1981] and Germain et al. [1987]. Plutonium isotopes are relatively free from interference, although counts from ^{210}Po may tail into the $^{239+240}$Pu peak if it is present in large concentrations. Unfortunately, SSB detectors cannot resolve ^{239}Pu and ^{240}Pu α-particles, so no information can be gained on the ^{240}Pu/^{239}Pu activity ratio from alpha spectrometry. Although there are fewer interferences involved in Pu analysis, radiochemical separation of Pu from the bulk sample is still required to produce thin, clean sources suitable for α-spectrometry.

Background count rates are essentially zero in alpha spectrometry, so detection is limited by the efficiency of the detector, the time available for counting each sample, and counting statistics. Counting times for low-level samples are long, often requiring over 24 hours. For a 10^8 second count, a source of approximately

Figure 1.18 Typical α-particle spectra obtained during the analysis of (a) plutonium and (b) ^{237}Np samples, showing nuclides which may cause interference

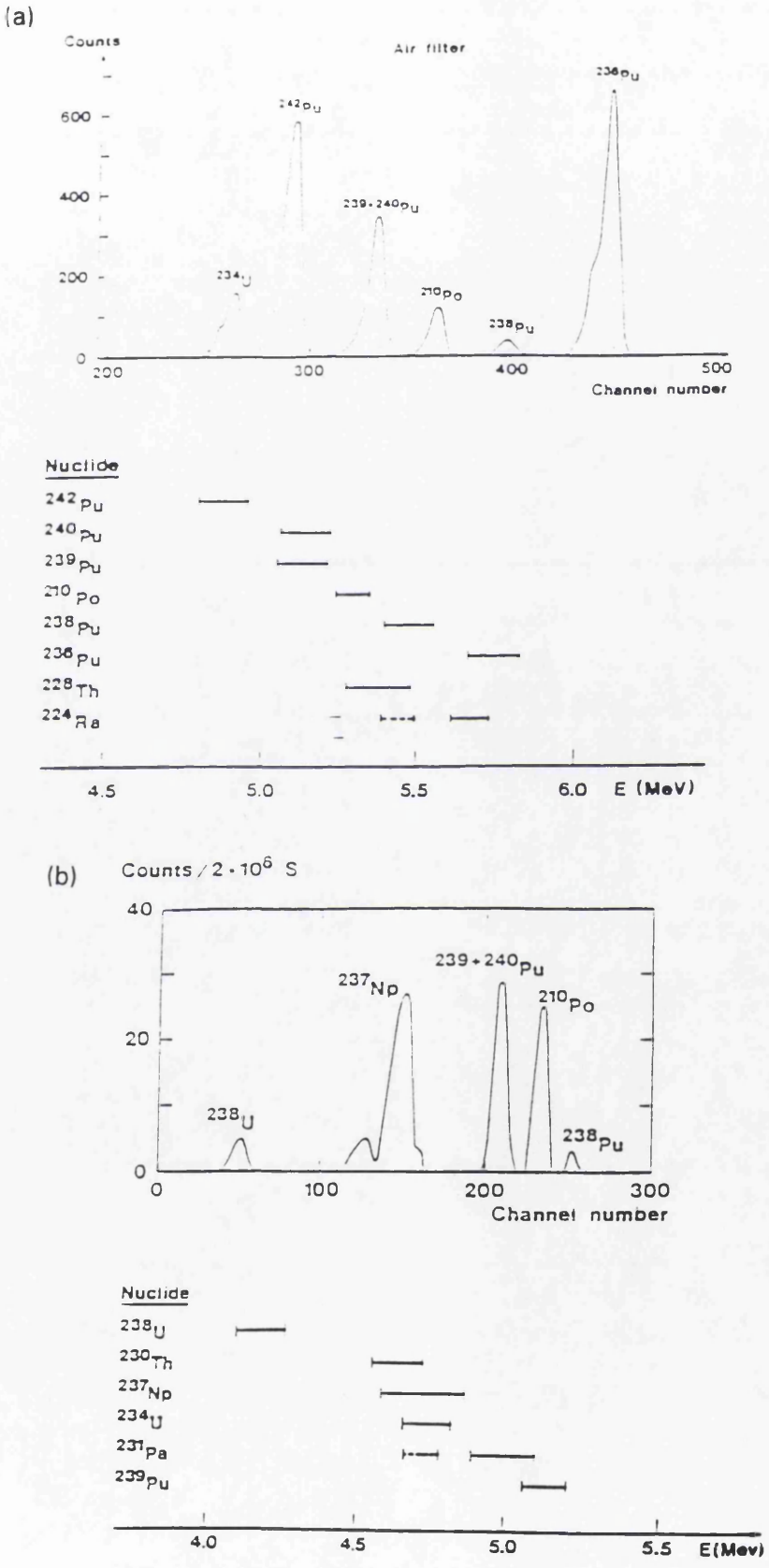

10^{-4} Bq would produce a peak of 10,000 counts, resulting in a standard deviation of ± 1% [Cross and Hooper, 1987; Hislop et al., 1987].

1.7.2.2 Gamma spectrometry

A number of the actinides are both α and low energy gamma emitters (see Table 1.4). However, gamma detectors have a high background count so determination of low levels of these nuclides is impossible [Cross and Hooper, 1987]. In the case of ^{237}Np, the low abundance of its γ emissions (87 keV, 13.1% and 29 keV, 9.8%) limits the sensitivity of the technique. ^{241}Am, however, can be determined to reasonably low levels, using the 60 keV emission. Cross and Hooper [1987] found that the detection limit for ^{241}Am from a 1 ml sample was approximately 0.05 Bq ml^{-1}, after 8 hours counting, but this was increased to 0.001 Bq ml^{-1} by counting a sample volume of 200 ml. The main advantage of γ-spectrometry is that aqueous samples can be analysed directly without the need for complex sample preparation.

1.7.2.3 Neutron activation

^{237}Np can been determined in environmental samples by neutron activation, based on the nuclear reaction ^{237}Np(n,γ)^{238}Np [May and Pinte, 1986; Germain et al., 1987; Byrne, 1986]. ^{238}Np is both a β^- and γ emitter with a 2.11 day half life, and quantification is achieved by detecting the intense γ-rays (1030 and 1027 keV at 100%, and 943 keV at 83%) which are free from interference.

The analysis of ^{237}Np by neutron activation is complicated by interferences which occur as a result of the irradiation of the sample. For example, additional ^{237}Np is produced from the decay of ^{237}U resulting from neutron reactions with both ^{238}U and ^{235}U [Germain et al., 1987]. Neutron activation of ^{238}U also results in the production of ^{239}U, whose decay product, ^{239}Np, is often used as a chemical yield tracer. Activation of environmental samples, particularly marine samples which have high levels of sodium, chlorine and bromine, generates highly radioactive samples which make sample handling difficult. To overcome this, and to reduce the interferences from the activation of uranium, pre and post irradiation chemical separations are required [May and Pinte, 1984; Byrne, 1986]. To some extent this

negates the advantage of neutron activation which, in combination with γ spectrometry, (for other samples) requires virtually no sample preparation compared to α-spectrometry.

The sensitivity of the technique is dependent on the neutron flux, with detection limits of the order of 5×10^{-4} to 1.3×10^{-5} Bq [Byrne, 1986; Germain et al., 1987].

1.7.3 Mass based techniques

An entirely different approach from using radiometric techniques to assay long-lived radionuclides is to determine their mass abundance. Low level samples with activities of 10^{-2} to 10^{-3} Bq ml^{-1} contain very low concentrations of the actinides (for example 10^{-2} Bq ml^{-1} corresponds to 4.4×10^{-12} g ml^{-1} for ^{239}Pu). Although these concentrations are below the detection limits of most methods normally used for trace metal analyses, there are a number of different mass spectrometric devices which can be used to determine the suitably long-lived nuclides [Koppenaal, 1988]. Some of these techniques are outlined below.

For mass spectrometry, interferences occur when more than one chemical species or nuclides have the same mass (isobars). Peaks may also overlap by peak tailing, the extent of which is determined by the resolution of the device. ^{237}Np, ^{239}Pu, ^{240}Pu and ^{242}Pu are all free from isobaric interferences, but ^{241}Am interferes with ^{241}Pu. ^{241}Pu is a relatively short lived radionuclide ($t_{1/2}$ = 14.4 years) and concentrations of 10^{-12} g ml^{-1} correspond to an activity of 3.8 Bq ml^{-1}, but, if it is present at these concentrations, ^{241}Pu can be determined by removing ^{241}Am prior to analysis. In the mass spectrometric determination of ^{237}Np and ^{239}Pu there is potential interference from the tailing of the ^{238}U peak, due to its high natural abundance. An advantage of the mass-based techniques is that the $^{240}Pu/^{239}Pu$ atom ratio can easily be determined.

1.7.3.1 Inductively coupled plasma-mass spectrometry (ICP-MS)

ICP-MS involves the coupling of an inductively coupled plasma to a quadrupole mass spectrometer. Full details of the technique are given in section 2.1. One of

the main advantages of ICP-MS is that sample preparation procedures are much simpler than the rigorous separation procedures required by α-spectrometry. The criterion used for ICP-MS is that analytes should be removed from the bulk matrix and presented to the instrument in a 2-5 ml solution with a total salt content of 0.2% or less. ICP-MS also has some advantages in sensitivity over radiometric techniques for the long-lived radionuclides. Figure 1.19 shows the ICP-MS detection limit in Bq against half-life, assuming a detection limit (apart from ^{129}I and ^{99}Tc which have isobaric interferences) of 10^{-11} g ml^{-1}, with a 1 ml sample required for analysis [Hislop et al., 1987]. This shows the advantage of ICP-MS for radionuclides with half-lives of over 10^6 years. ICP-MS also has the advantage of being a rapid technique, with the capability of routinely analysing over 20 samples in a day.

Figure 1.19 Effect of Half-Life on detection limit for ICP-MS vrs α-spectrometry [Hislop *et al.*, 1987]

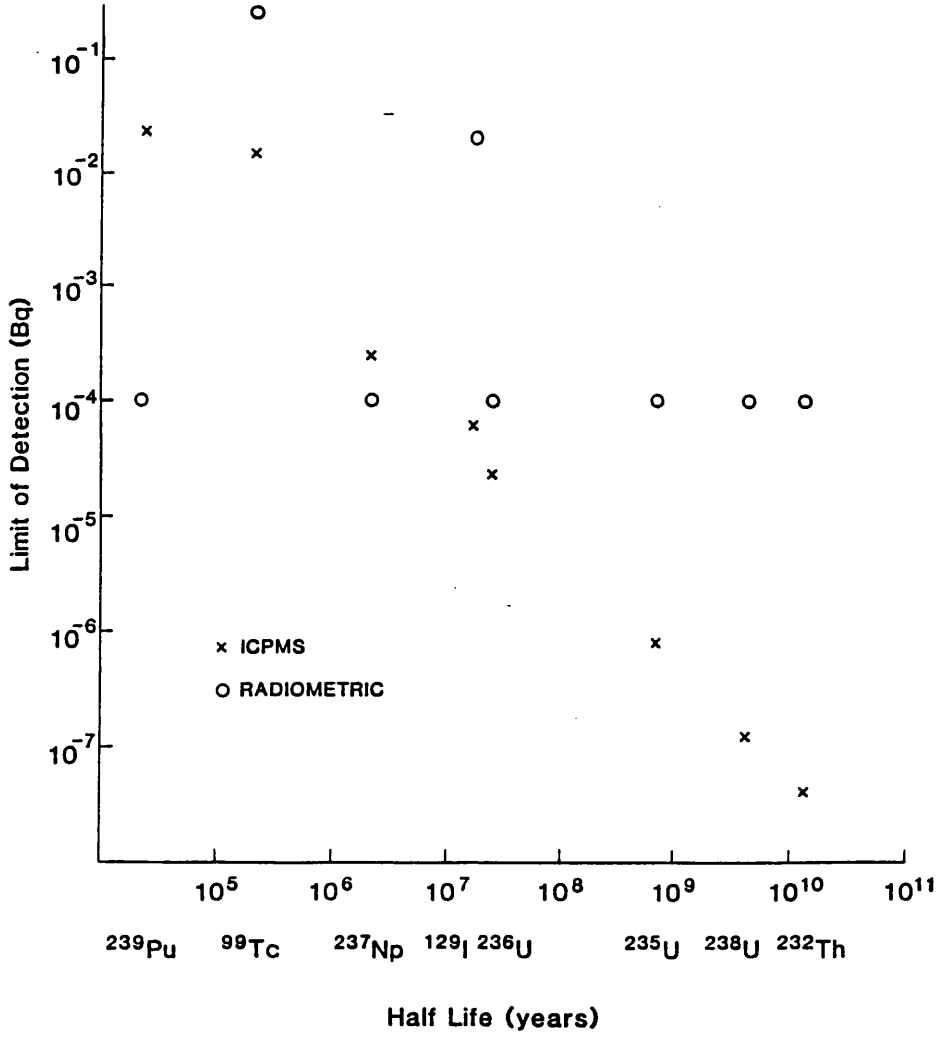

The initial applications of ICP-MS to radionuclide assay were for the determination of Th and U in geological samples [e.g. Gray and Date, 1983; Riddel et al., 1988; Russ, 1989]. Since the assessment of the technique for the analysis of long-lived radionuclides [Hislop et al., 1987; Brown et al., 1987] there has been a small, but increasing number of applications, including the determination of Sellafield-derived ^{237}Np in soils [Hursthouse et al., 1991] and intertidal sediments [Assinder et al., 1991].

1.7.3.2 Thermal ionisation mass spectrometry (TIMS)

TIMS is a standard technique in which samples are vaporised from a source filament (usually Re or Ta) and analysed by a mass spectrometer which can scan a number of individual mass units. The preparation of the source filament requires chemical purification procedures of similar complexity to those required for α-spectrometry [Buesseler and Halverson, 1987]. TIMS is a very sensitive technique with lower detection limits than both ICP-MS and α-spectrometry, even for isotopes of plutonium (1.7×10^{-5} Bq for $^{239+240}Pu$ or 4.3×10^{-15} g ^{239}Pu) [Buesseler and Halverson, 1987]. The detection limit of the system can be further improved by a surface ionisation-diffusion-type (SID) ionisation source, the preparation of which is described for ^{237}Np analysis by Effurd et al. [1986] and for Pu analysis by Perrin et al. [1984]. Detection limits were quoted as 1×10^{5} atoms (3.9×10^{-8} ng, or 1×10^{-9} Bq ^{237}Np and 9×10^{-8} Bq ^{239}Pu) with a precision of 0.15% (2σ). TIMS analysis takes longer than ICP-MS, approximately 8 samples requiring 8 hours analysis time [Buesseler and Halverson, 1987].

The sensitivity of this technique means that it can be applied to the analysis of plutonium and neptunium in samples representative of global fallout. For example, $^{240}Pu/^{239}Pu$ atom ratios have been determined in sediments from the North Atlantic [Buesseler and Sholkovitz, 1987a] and the Gulf of Mexico [Scott et al., 1983], as well as in the Arctic and Antarctic ice sheets [Koide et al., 1985]. Effurd et al. [1984] have also determined the $^{237}Np/^{239}Pu$ atom ratio in fallout soil and in lung and liver tissue of individuals exposed to global fallout. Soil and intertidal sediment samples contaminated by the Sellafield discharges have also been analysed by

TIMS, to obtain the $^{240}Pu/^{239}Pu$ and $^{241}Pu/^{239}Pu$ atom ratios [McCarthy and Nicholls, 1990].

1.7.3.3 Resonance ionisation mass spectrometry (RIMS)

RIMS consists of the combination of laser resonant photo-ionisation with mass spectrometry (magnetic sector, quadrupole or time-of-fight). The full details of the technique are described by Baxter et al. [1987]. The technique is highly selective as it involves the detection of atoms or molecules which have been ionised after having been excited to a particular state which is unique to the element of interest, and therefore requires little sample preparation. The potential of the technique for the analysis of actinides in the environment has yet to be realised, although some initial measurements have been made by Rimke et al. [1987], who quoted detection limits of less than 10^7 atoms of ^{239}Pu.

1.7.4 Counting versus mass-based techniques

To conclude, the conventional radiometric technique for determining the activity of actinides in environmental samples, α-spectrometry, is sensitive and selective but requires laborious and lengthy sample preparation procedures. By comparison, mass-based techniques can offer lower detection limits for long lived radionuclides and, in the case of ICP-MS and TIMS, much faster sample analysis. In addition, the sample requirements for ICP-MS are met by simplified sample preparation procedures. $^{240}Pu/^{239}Pu$ atom ratios can be determined by ICP-MS and TIMS, although TIMS has lower detection limits and greater precision. The main disadvantage of the mass-based techniques is that they are more expensive.

1.8 AIMS OF RESEARCH

There were 5 main aims of this project:

1. To investigate and characterise ICP-MS for the analysis of ^{237}Np and isotopes of plutonium.

2. To develop an analytical technique for ICP-MS to determine ^{237}Np, ^{239}Pu, and ^{240}Pu concentrations in sediment samples.

3. To investigate the variations in $^{240}Pu/^{239}Pu$ atom ratios in intertidal sediments contaminated with Sellafield-derived plutonium.

4. To investigate the sediment record of Pu and Np discharges from Sellafield by the analysis of sediment cores from intertidal regions of the Irish Sea.

5. To assess the potential for deconvolution of the sediment record to provide information on the source term.

CHAPTER 2
INDUCTIVELY COUPLED PLASMA-MASS SPECTROMETRY

2.1 INDUCTIVELY COUPLED PLASMA-MASS SPECTROMETRY

ICP-MS is a relatively new technique which combines the ability of inductively coupled plasmas to atomise and ionise samples with the selectivity and sensitivity of mass spectrometry [Houk and Thompson, 1988]. Excellent reviews are available detailing the principles of the technique [Jarvis *et al.*, 1992] and its applications [Date and Gray, 1989].

2.1.1 Historical development

Initially, inductively coupled plasmas were investigated as an excitation source to be used in combination with atomic emission spectrometry (AES) for trace metal determinations [Greenfield *et al.*, 1964; Wendt and Fassel, 1965]. It was shown that ICPs improved AES, giving detection limits of 0.1- 10 ng ml^{-1} for a range of elements; two or more orders of magnitude better than previous results [Dickinson and Fassel, 1969]. However, problems were found in the analysis of rock samples whose matrix elements, such as Ca, Al and Fe, caused severe spectral interferences, making it difficult to find free spectral lines for trace analysis. A technique was required that would analyse solid mineral samples and provide multi-element analyses at levels down to 10 ng g^{-1} in an analysis time of a few minutes [Gray, 1986a].

Of the spectrometric techniques available, mass spectrometry offered low detection limits across a wide elemental range and the ability to analyse trace elements from a complex matrix, along with simple spectra and high sample throughput. A technique was required to volatilise and dissociate the sample and provide a source of ions for the mass spectrometer. Spark source mass spectrometry, the main technique first used for multi-element mass spectrometry, required solid sample compacts whose preparation limited the sample throughput. Chemical flames were considered but they were not hot enough to ionise many elements, so attention was turned to atmospheric DC and RF plasmas which had already proved good

sources of ions for ICP-AES. The problem was then how to extract representative ions from the plasma at atmospheric pressure to the ion detector at high vacuum. Following the work on flame mass spectrometry analysis by Sugden [1965] and Knewstub and Hayhurst [1974], a feasibility study was set up by Moruzzi using a small capillary DC arc source with a small quadrupole mass analyser and a channeltron ion detector. The tailflame impinged on an aperture of 0.07 mm mounted in the wall of the first vacuum stage. This first system showed promise, with high sensitivity and essentially zero background [Gray,1992]. However, the discharge consisted of a single high temperature channel which resulted in poor sample introduction and a poorer degree of ionisation than expected so that elements with ionisation potentials above 8 eV had very low sensitivities. It was concluded that a hotter plasma such as the ICP was required [Gray, 1978].

By the late 1970s, three groups (at Surrey in the UK, Toronto in Canada, and the Ames laboratory in Iowa) were working on the problem of using an ICP as an ion source with its high temperature and RF fields. A detailed history of their developments can be found in the literature [Houk *et al.*, 1980; Date and Gray, 1981; Douglas *et al.*, 1983; Gray, 1985; 1986; 1989]. The main problem was the extraction of representative ions from the plasma into the mass analyser. Initially small apertures of 0.05-0.07 mm were used, similar to the capillary arc source, but these were found to be too small, as a cool boundary layer formed at the tip of the aperture. Larger apertures caused difficulty in removing the thermal flux, resulting in melting and enlargement of the tips. After achieving good thermal contact to the larger apertures (0.4mm), it was found that too much gas was extracted, causing the pumping system to stall. The solution was to have a two stage vacuum system with a preliminary, high-pressure stage of about 2 mbar, achieved using a rotary pump. 1981 saw the first demonstration of ion extraction from the bulk ICP plasma [Gray, 1982]. By 1983 two commercial instruments were launched, the VG PlasmaQuad, based on the Surrey system, and the Sciex Elan, based on the Toronto system. The principle of the two systems is the same, although there are differences in the grounding of the RF coil (and as a consequence the potential of the plasma) and in the arrangement of the ion optics. By 1984 the first instruments were installed in laboratories and since then their use for trace element analysis has rapidly expanded with applications in geological, environmental and

medical science and over 450 instruments around the world.

2.1.2 Instrumentation Overview

The ICP-MS used in this study was a VG PlasmaQuad PQ1, purchased in 1988. A schematic diagram of the overall system is shown in Figure 2.1. The system can be divided into four main sections; sample uptake and introduction into the plasma, the plasma, the sample interface, and ion selection and detection. Each of these sections is described below.

A variety of techniques can be used to introduce samples into the plasma, dependent on the sample composition and form. Once in the plasma the sample is volatilised, dissociated and the component atoms ionised. Representative ions are then extracted from the plasma into the first stage of the vacuum system via a sampling cone, a supersonic jet forming behind the cone as a result of the pressure difference. A skimmer cone is placed within the mach disc enabling ions to enter the second, high vacuum stage. The ions are then focused into the quadrupole mass analyser, whose parameters allow only ions with a narrow band of mass to charge ratios to pass through and be detected by the electron-multiplier. Scanning the quadrupole parameters allows ions to be detected sequentially in order of their mass to charge ratio.

2.1.3 Sample introduction

Samples can be introduced into the ICP as a gas, vapour or aerosol of fine droplets or solid particles of 10 μm or less in diameter. This enables rapid desolvation, volatilisation and atomisation to take place without disrupting the plasma. A wide variety of sample introduction techniques has been used with ICP, including pneumatic or ultrasonic nebulisation of liquid samples, electrothermal vaporisation of μl samples, laser or spark ablation from a solid, and direct introduction of volatile hydrides or oxides from a reaction vessel. A full account of sample introduction techniques is given by Williams [1992]. In the present study, both liquid nebulisation and electrothermal vaporisation were used as described below.

Figure 2.1 A schematic diagram of the VG PlasmaQuad ICP-MS system (PQ1) used in this study [VG Isotopes, 1988].

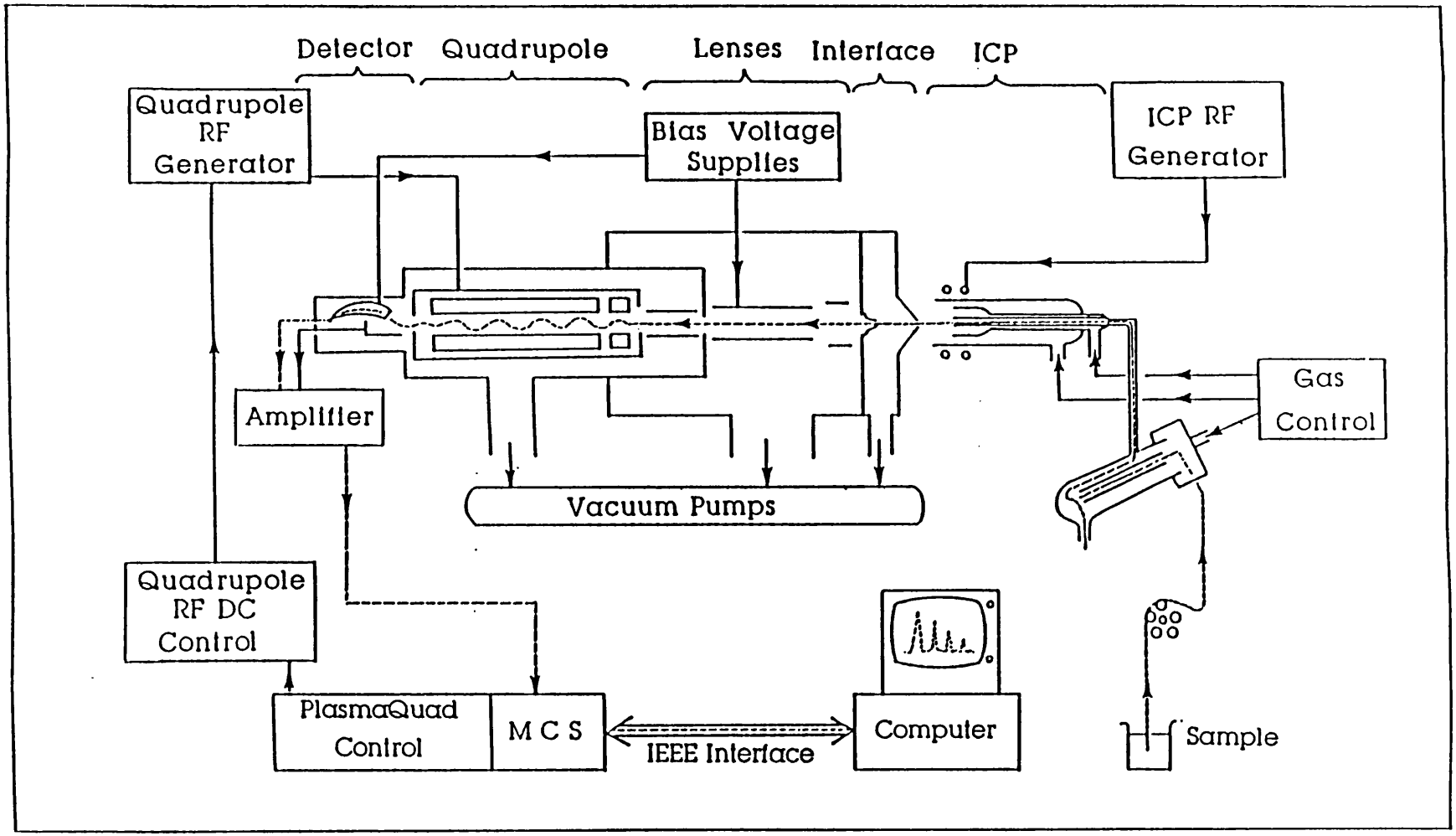

2.1.3.1 Liquid Nebulisation

The most commonly used sample introduction technique in ICP-MS is pneumatic nebulisation of liquid samples. A high velocity gas stream produces a fine droplet dispersion of the analyte solution with a broad distribution of droplet diameters up to 100 μm. To remove the larger droplets which would disrupt the plasma, the aerosol is passed through a spray chamber. This allows droplets of only 8 μm or less to enter the plasma [Montaser and Golightly, 1987]. The use of pneumatic nebulisation is widespread because it is a simple technique, enabling rapid sample throughput with good stability at low cost. However, it is a highly inefficient process with only 1-2% of the sample reaching the plasma [Thompson and Houk, 1987]. In addition, pneumatic nebulisation presents several problems when used with the ICP. Deposition of matrix elements can cause nebuliser blockage so samples are restricted to < 0.2 % (m/v) dissolved solid content. The presence of hydrogen, oxygen and matrix elements in the plasma also causes the formation of interfering polyatomic species and matrix-induced effects on the ion signal during ion transport between the source and the detector. Liquid nebulisation also requires a sample volume of 3-10 $\bar{m}$l. Ultrasonic nebulisers offer higher sampling efficiencies, but they are more complicated, expensive and can be unreliable [Boumans and De Boer, 1976].

The liquid nebulisation work in the present study used a Meinhard glass concentric nebuliser [Meinhard, 1976] and a Scott double pass spray chamber [Scott *et al.*, 1974] (Figure 2.2) with a Gilson peristaltic pump to meter the solution to the nebuliser. The sample uptake rate was kept between 0.7 and 1.0 ml min^{-1}.

2.1.3.2 Electrothermal Vaporisation

Electrothermal vaporisation (ETV) devices have been used for sample introduction in AES since 1974 [Nixon *et al.*, 1974]. The first use of ETV for sample introduction into an ICP-MS was in 1983 [Gray and Date, 1983]. Since then its use, for small samples and samples which cause severe matrix interference when liquid nebulisation is used, has been widespread [Williams, 1992].

Figure 2.2 Schematic diagram showing (a) a Meinhard nebuliser and

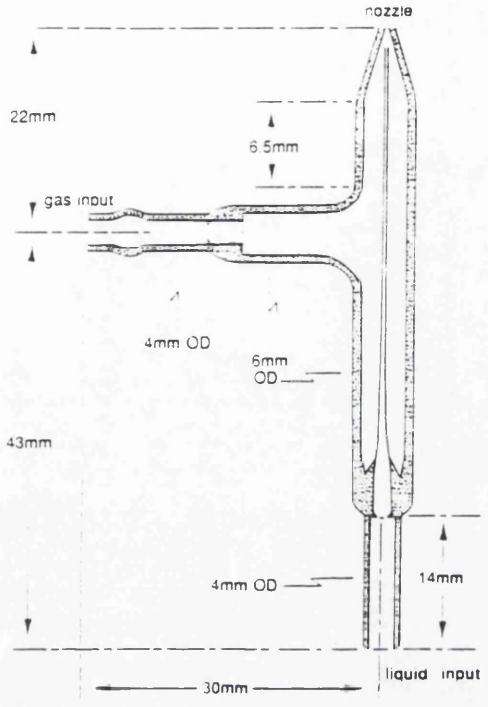

(b) a Scott double pass spray chamber used in the PQ1 system [Jarvis *et al*, 1992]

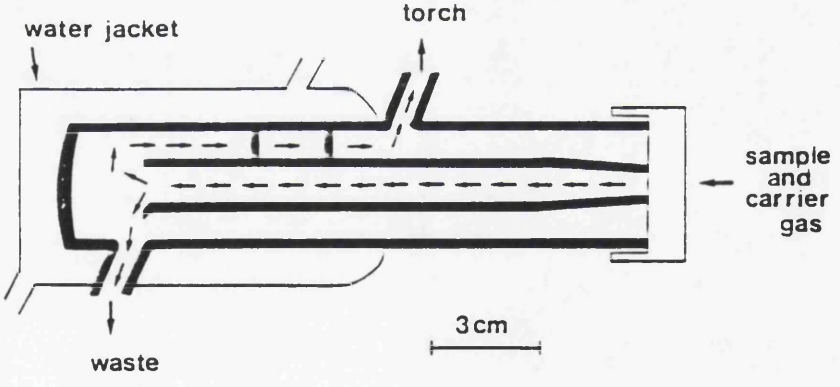

The electrothermal vaporisation unit is basically an electrically conductive vaporisation cell into which microlitre samples can be injected. Applying a current to the cell causes resistive heating. Changing the current using an electronic control system enables the cell to be heated in a sequence of temperature stages. Initially a low current is applied to the cell to dry the sample. In some cases an 'ash' stage is then used to remove some of the matrix from the sample. Finally a high current is applied to the cell for a short period (< 5 secs) to vaporise the sample. Argon is continuously passed through the cell and this sweeps the sample vapour into the plasma.

Electrothermal vaporisation can provide several advantages over pneumatic nebulisation. These include the analysis of small samples (5 - 100 μl), higher transport efficiency (20 - 80 %), the ability to analyse samples with higher solid and/or acid content, and possible separation of the analyte from the sample matrix [Shen *et al.*, 1990]. Potentially, this leads to reduced sample pretreatment, greater sample pre-concentration and higher sensitivity.

The electrothermal vaporisation unit used in the present study was a VG Microtherm Mark 1 manufactured by VG Elemental Ltd (Figure 2.3). It consisted of a pyrolytically coated graphite tube mounted in carbon bushes inside a quartz sleeve. 10-100 μl samples were injected into the graphite tube using a micropipette and the tube was then plugged with a graphite rod. A typical temperature profile is shown in Figure 2.4. During the vaporisation stage the sample is swept into the plasma by the carrier gas flow. This also contained approximately 1% freon (CHF_3) which is required to prevent the formation of carbides in the furnace and to increase the transport efficiency of refractory elements such as plutonium and neptunium.

2.1.4 The Inductively Coupled Plasma

The inductively coupled plasma (ICP) is required to volatilise, dissociate, and ionise the incoming sample and produce a source of representative ions which can then be mass analysed. It consists of a discharge in a gas at atmospheric pressure. The

Figure 2.3 The VG Microthem mark 1 ETV Unit used in this study showing (a) sample injection and (b) the gas flows during sample vaporisation [VG Isotopes, 1988]

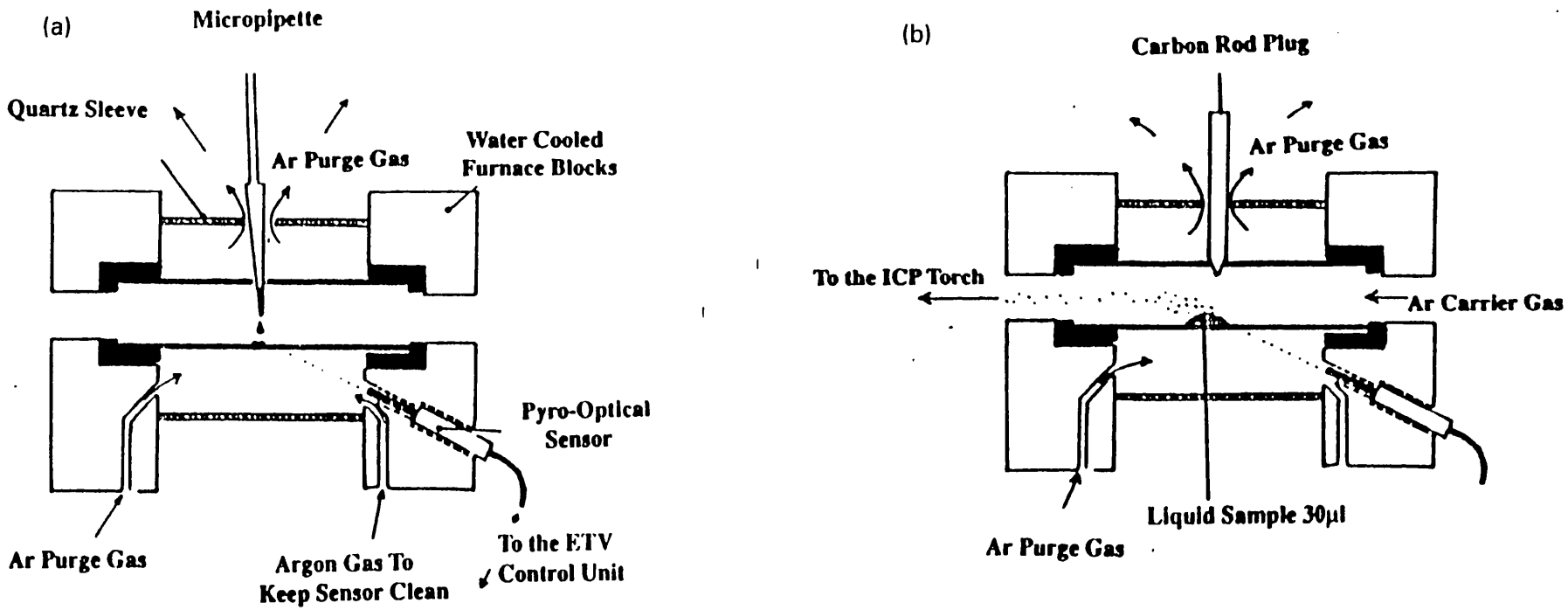

most commonly used gas is argon although other gases and gas combinations have been used [Williams, 1992]. Some of the fundamental properties and characteristics of the ICP are discussed below.

2.1.4.1 Plasma Generation

The production of an inductively coupled plasma has changed little since the pioneering work of Reed who established vorticular stabilisation of an argon plasma by introducing argon tangentially into a vertical plasma torch [Reed, 1961]. Modification of the plasma torch enabled samples to be efficiently introduced into the central channel of the plasma and led to its first application in an analytical technique [Greenfield *et al.*, 1964].

The main difference in the plasma system now used in ICP-MS is the horizontal configuration of the plasma torch. From the sample introduction system the samples are transported by the carrier or nebuliser gas to the plasma via the ICP torch. A typical torch including the gas flows and the induced magnetic field, is shown in Figure 2.5. It consists of three concentric quartz tubes through which are passed three separate gas flows. The coolant and the auxiliary flows enter the outer and inner annular spaces respectively at a tangent so as to create vorticular flow. The coolant gas flow (10-15 l min^{-1}) is the main support gas for the plasma, whilst the auxiliary flow (0 - 1.5 l min^{-1}) prevents the plasma from melting the tip of the central capillary tube. The carrier gas is passed through the central channel creating a cool jet of gas which punches a hole through the middle of the plasma. To initiate the plasma, the gas is seeded with free electrons produced from sparks from a tesla coil. The plasma is then maintained by coupling energy from a RF (radio-frequency) generator via 2 turns of a cooled copper coil which is placed around the torch a few millimetres from the end. An RF frequency of 27 MHz is used to create a field which lies along the axis of the torch. Free electrons in the plasma then precess around the magnetic field lines in circular orbits and the electrical energy supplied to the coil is converted into kinetic energy of the electrons. The mean free path of the electrons is approximately 10^{-3} mm, after which they collide and transfer their energy to the argon atoms. This heats the plasma and causes a bright discharge. At the frequencies used, the skin effect,

Figure 2.4 ETV temperature profile used in this study

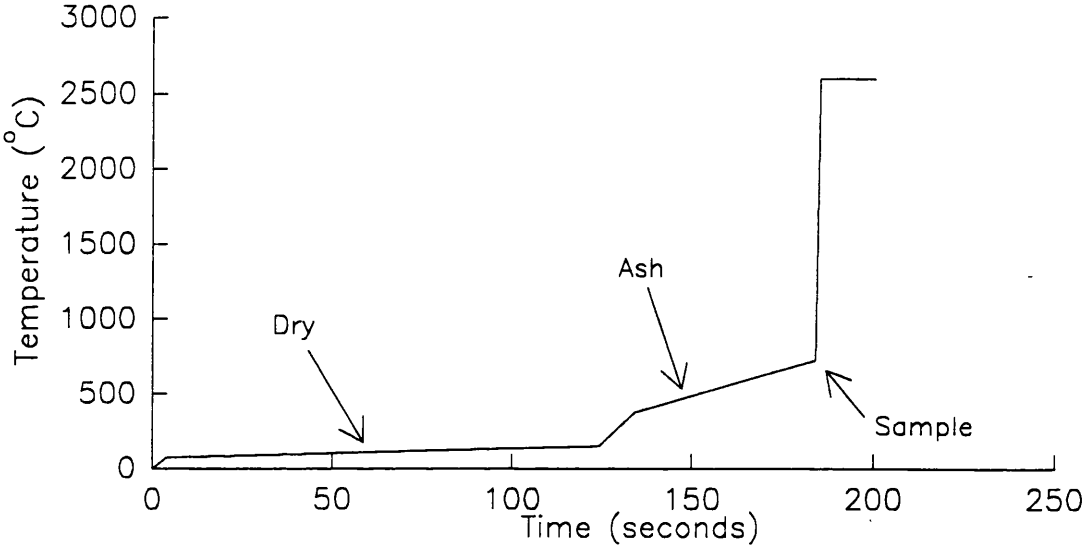

Figure 2.5 Schematic diagram of ICP torch, gas flows and the induced magnetic field. The shaded zones are observed when, a nebulised sample containing Y is introduced along the central Channel [Jarvis *et al*, 1992]

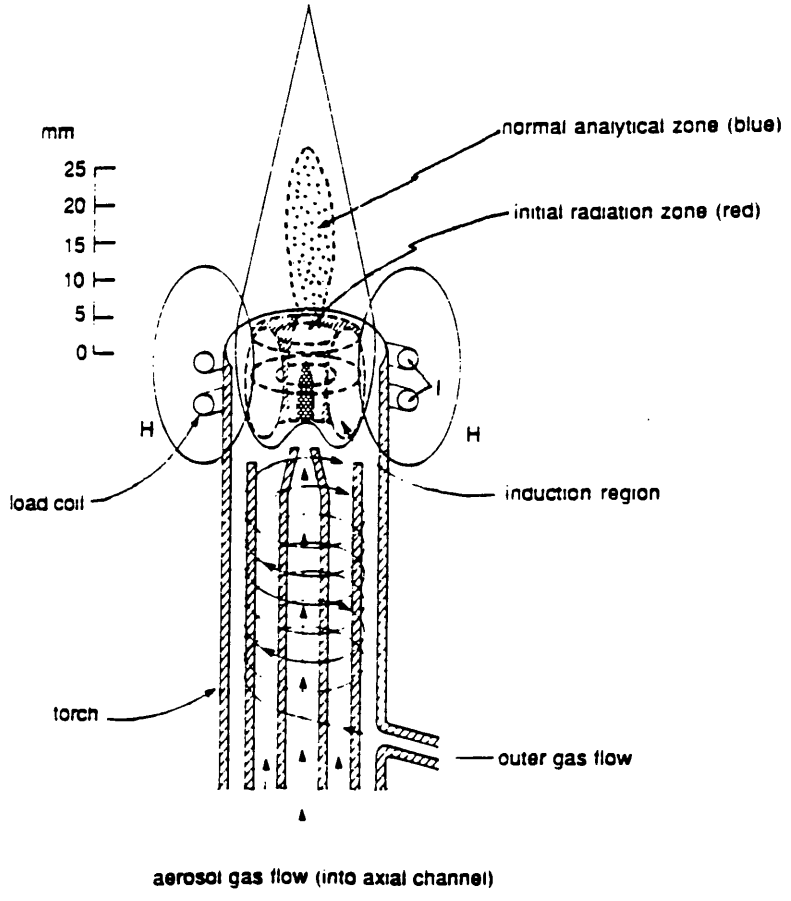

caused by RF induction heating, ensures that most of the energy is coupled to the outer or induction region of the plasma which attains a temperature of about 10,000 K [Scott *et al.*, 1974]. The gas in the centre is heated mainly by conduction and radiation from the induction region, the temperature ranging from 5,000 to 8,000 K. Samples entering the plasma from the central channel of the torch therefore have little effect on the electrical processes which maintain the plasma [Gray, 1989].

2.1.4.2 Fundamental Properties of the ICP

Much work has been done to determine the fundamental properties of the inductively coupled plasma, with the aim of improving its analytical capabilities and to elucidate the excitation mechanisms which take place within it [Hasegawa and Haraguchi, 1987]. Properties such as plasma temperature, electron number densities and number densities of analyte and argon species have been measured under different plasma conditions by a variety of techniques [Blades and Caughlin, 1985; Furuta *et al.*, 1985; Mao Huang *et al.*, 1992]. As a consequence of its inhomogeneous nature, the spatial distribution of these properties is required to characterise the plasma [Hasegawa and Haraguchi, 1987]. The plasma is said to be in local thermodynamic equilibrium (LTE) when the distribution functions (Boltzmann, Saha, Maxwell, etc) are characterised by unique temperature for all species. Empirical observations of the above parameters have led to the conclusion that the ionic and neutral species in the ICP are not in LTE [Boumans, 1987], although in the normal analytical region of the plasma 'close to LTE' conditions prevail [Furuta, 1986]. The reason for the departure from LTE is still under discussion, but a number of excitation mechanisms have been proposed [Hasegawa and Haraguchi, 1987].

2.1.4.3 Ionisation and distribution of ions in the Plasma

In the ICP, the analyte ions are not the dominant species present. Using the ideal gas laws the particle number densities can be calculated. With a pressure of 1 bar and a gas kinetic temperature of 5,000 K, the total particle density is 1.5×10^{18} cm^{-3}, the majority of which is argon [Jarvis *et al.*, 1992]. In a dry plasma the

number density of the argon ion (n_{Ar+}) and the electron number density (n_e) are calculated to be 1 x 10^{15} cm^{-3}. This compares favourably with measured values which range from 5 x 10^{14} to 5 x 10^{15} cm^{-3} [Hasegawa and Haraguchi, 1987]. Nebulising a solution of 1% nitric acid with an efficiency of 1% and at an uptake rate of 1 ml min^{-1} contributes electrons and ions from the ionisation of hydrogen (2 x 10^{14} cm^{-3}), oxygen (1 x 10^{14} cm^{-3}) and nitrogen (1 x 10^{12} cm^{-3}) [Jarvis *et al.*, 1992]. This increases the total electron number density of the plasma to 1.3 x 10^{15} cm^{-3}. The nebulisation of sample solution into the plasma therefore makes a significant contribution to the electron and ion population.

It is also worth considering the contribution made by trace elements in a sample solution. Elements that are present at a concentration of 1 μg ml^{-1} in solution contribute 1 x 10^{10} ions cm^{-3} to the plasma population, whereas a fully ionised matrix element at 5,000 μg ml^{-1} contributes 5 x 10^{13} ions cm^{-3}. Even at such a high concentration, a matrix element represents a barely significant contribution to the ion and electron population. Ionisation suppression in the plasma is therefore generally not a major cause of matrix interference [Olivares and Houk, 1986].

The degree of ionisation of analyte species can be predicted by the Saha equation:

$$\frac{n_i}{n_a} = \frac{1}{n_e}\left(\frac{2\pi m_e kT}{h^2}\right)^{3/2}\left(\frac{2Z_i}{Z_a}\right)\exp\left(\frac{-E_i}{kT}\right)$$

where n_i = conc. of ions; n_a = conc. of atoms; n_e = electron number density; m_e = mass of electron; T = ionisation temperature; z_i = partition function of ion i; z_a = partition function of atom a; and E_i = the ionisation potential.

With an ionisation temperature of 7,500 K and an electron number density of 1.3 x 10^{15} cm^{-3} this equation predicts that greater than 90% of most elements will be present as positively charged, singly ionised species [Houk, 1986]. Table 2.1 shows the distribution of ionisation energies among elements for singly and doubly charged species and Figure 2.6 shows how the degree of ionisation changes with

ionisation energy for singly charged ions in the ICP. The majority of the elements have first ionisation energies of less than 10 eV, an energy which corresponds to over 50% ionisation. In addition the second ionisation energies of most elements, with the exception of the alkaline and rare earth elements, uranium and thorium, are above 16 eV implying that elements introduced into the plasma will consist mainly of singly ionised species [Jarvis *et al.*, 1992].

Table 2.1: Distribution of ionisation energies among the elements for singly and doubly charged ions at 1eV intervals, from [Gray, 1989].

Ionisation energy (eV)	Elements	
< 7	Li, Na, Al, K, Ca, Sc, Y, Zr, Nb, Ti, V, Cr, Ga, Rb, Sr, La, Ce, Pr, In, Cs, Ba, Eu, Gd, Tb, Dy, Ho, Nd, Pm, Sm, Tm, Yb, Lu, Hf, Tl, Ra, Er, Ac, Th, U	
7 - 8	Mg, Mn, Fe, Co, Ni, Cu, Sn, Sb, Ge, Mo, Tc, Ru, Rh, Ag, Ta, W, Re, Pb, Bi	
8 - 9	B, Si, Pd, Cd, Os, Ir, Pt, Po	
9 - 10	Be, Zn, As, Se, Te, Au	2^+ ions
10 - 11	P, S, I, Hg, Rn	Ba, Ce, Pr, Nd, Ra
11 - 12	C, Br	Ca, Sr, La, Sm, Eu, Tb, Dy, Ho, Er
12 - 13	Xe	Sc, Y, Gd, Tm, Yb, Th, U, Ac
13 - 14	H, O, Cl, Kr	Ti, Zr, Lu
14 - 15	N	V, Nb, Hf
15 - 16	Ar	Mg, Mn, Ge, Pb
> 16	He, F, Ne	All other elements

To produce singly ionised species as efficiently as possible the incoming sample must first be desolvated, volatalised, dissociated and subsequently ionised. For these processes to occur the sample must remain in the hottest part of the plasma for several milliseconds [Houk, 1986], the exact time required depending on the size of the desolvated particles which in turn depends on the dissolved solids content of the sample. The time required to dissociate molecular species depends

Figure 2.6 Degree of ionisation vrs ionisation energy for singly charged ions in the ICP [Gray, 1989]

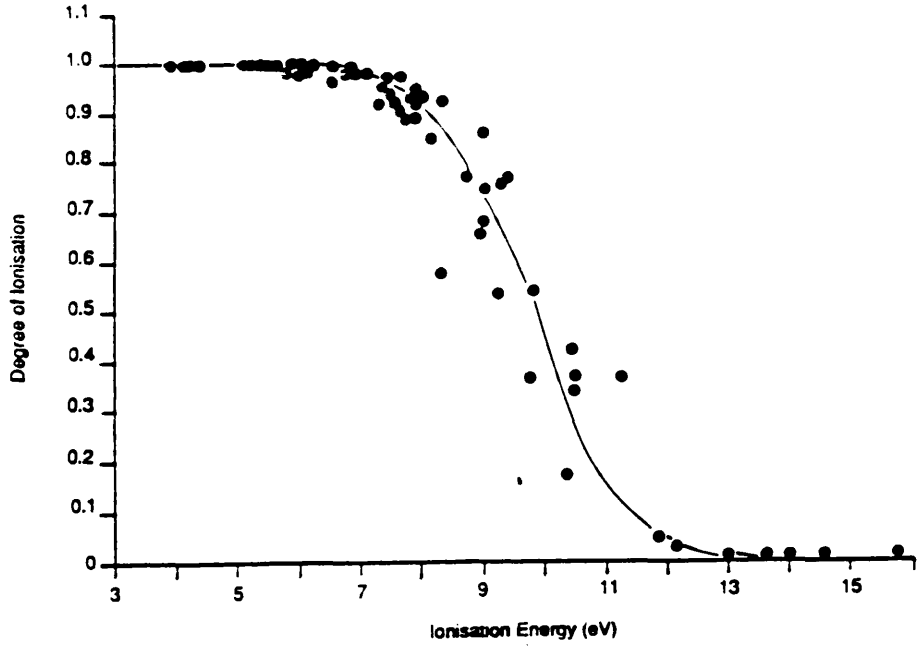

Figure 2.7 Transverse profile across the plasma flame at 5,10 and 15mm from the load coil in 1mm steps for a nebulised solution containing 100ng/ml Co [Jarvis *et al*, 1992]

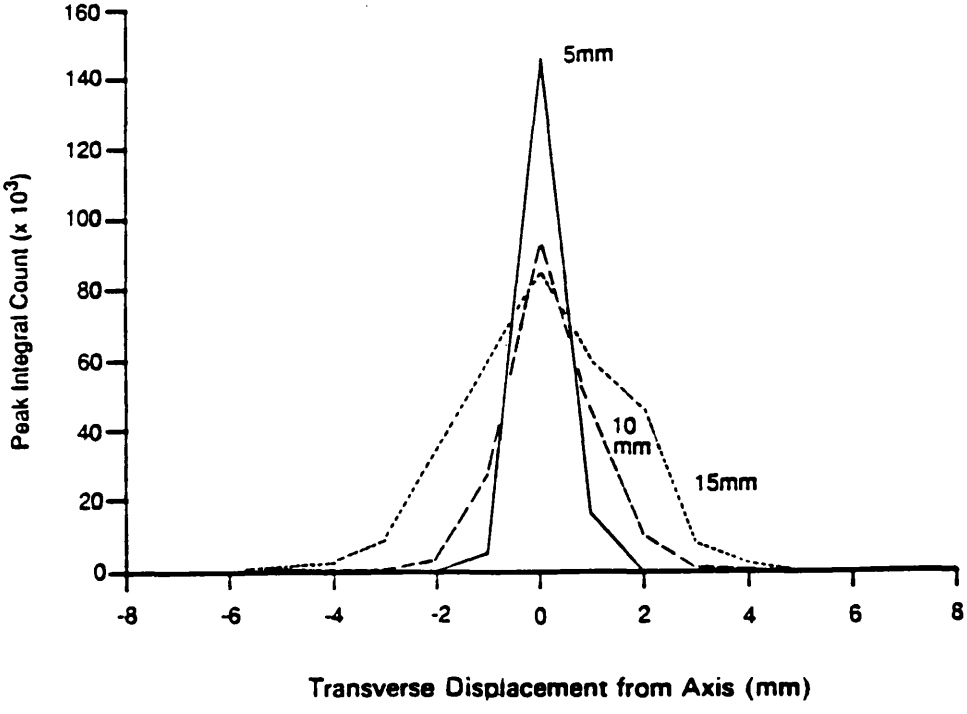

on their bond strengths, refractory species requiring longer residence times [Jarvis *et al.*, 1992]. The conditions in the plasma and the residence time of the sample, can to some extent, be optimised by changing the nebuliser flow rate and the RF power supplied to the plasma.

The processes occurring in the plasma can be rendered visible by introducing a concentrated (1,000 $\mu g\ g^{-1}$) solution of yttrium. This causes the initial radiation zone of the plasma to glow red, corresponding to emission from excited YO and neutral Y atoms. Further along the axial channel, singly charged Y ions are formed which emit blue light [Houk and Thompson, 1988]. The distribution of ions can also be observed by moving the sampling orifice and detection system across the plasma at various distances from the load coil. Figure 2.7 shows the transverse profile of an ICP at 5, 10 and 15 mm from the load coil, the signal being obtained from nebulising a solution of cobalt at 100 ng ml^{-1} [Jarvis *et al.*, 1992]. This profile shows that the central channel is about 3 mm wide with a sharp drop off at the sides. Further along the axis the central channel diffuses into the annulus. The optimum position for the sampling orifice is just after the initial radiation zone where interfering species still exist and before the ions diffuse out of the central channel.

In conclusion, the ICP is an excellent source of singly charged ions with few doubly charged species or polyatomic ions being formed. It enables easy sample introduction, with the sample composition having little effect on the processes which maintain the plasma. The main disadvantage is that representative ions have to be taken from the high temperature and pressure region of the ICP to the high vacuum region of the mass analyser.

2.1.5 The Sample Interface

2.1.5.1 Ion Extraction

The interface between the ICP and the mass spectrometer must be capable of extracting ions from the plasma at atmospheric pressure into the quadrupole mass spectrometer at a pressure of 10^{-5} torr. A schematic diagram of the interface used

Figure 2.8 The VG Plasma Quad interface [VG Isotopes, 1988]

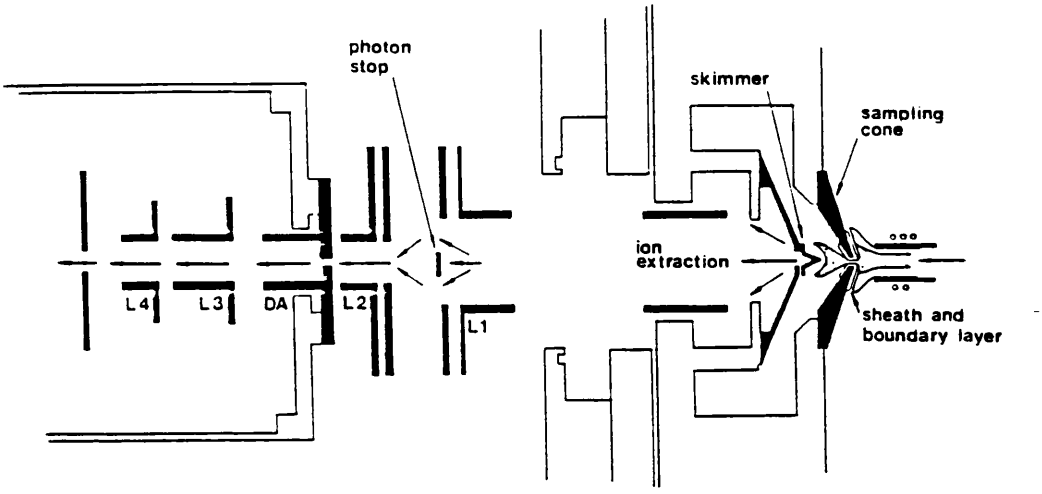

Figure 2.9 Interaction of the ICP with the sampling cone, showing boundary layer, sheath and flow of ions into the orifice [Jarvis *et al*, 1992]

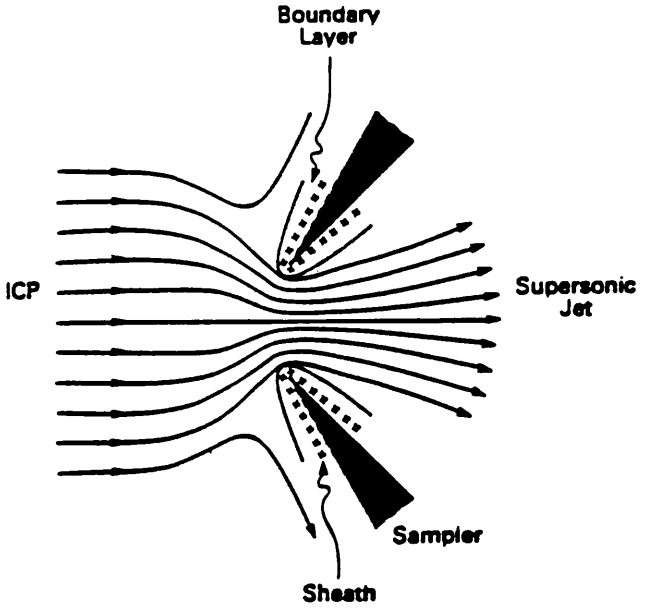

in the VG PlasmaQuad is shown in Figure 2.8.

As the plasma impinges on the water cooled nickel sampling cone, a boundary layer forms between the plasma and the cone surface (Figure 2.9). The gas flow through the sampling orifice (diameter 1mm) is sufficient to puncture this boundary layer and sampled ions flow directly from the plasma into the first vacuum stage [Gray, 1989]. Oxide formation and other chemical reactions resulting in the formation of polyatomic species readily take place in the cooler boundary layer. The extraction of these interfering species is kept to a minimum by keeping the skimmer cone orifice (0.75 mm diameter) smaller than the sampling cone [Vaughan and Horlick, 1990a; Gray, 1986]. In addition to the boundary layer, a sheath forms around the sampling cone (see Figure 2.9) as a consequence of electrical interaction of the plasma with the grounded sampling cone. As a result, the plasma assumes a net positive floating potential which affects the energy of the ions extracted which in turn affects the behaviour of the ions in the ion focusing region of the ICP-MS [Fulford and Douglas, 1986; Olivares and Houk, 1985a].

If the plasma potential is high enough it can cause a secondary discharge to occur between the plasma and the sampling orifice. This is detrimental as it erodes the sampling cone, generates multiple charged ions and induces high kinetic energies and a wide spread of kinetic energies in the extracted beam [Houk *et al.*, 1981; Douglas and French, 1986]. In Sciex Elan instruments the plasma potential is reduced significantly by grounding the load coil [Douglas and French, 1986]. The plasma potential can also be reduced by using a low aerosol flow rate (0.5 - 0.9 l min^{-1}), reducing the solvent load of the plasma and moving the sampling cone closer to the load coil [Jarvis *et al.*, 1992].

The pressure difference between the plasma and the first vacuum stage (1 bar to 1 mbar) is sufficient for the sampled gas to form a supersonic jet behind the sampling cone. Some collisions take place for the first few orifice diameters, after which expansion takes place freely [Douglas and French, 1988]. The supersonic jet is surrounded by a barrel shock and Mach disc, where collisions with the surrounding gas become significant. The small number of collisions within the jet and the short duration of expansion (approximately 3 μs) imply that the sampling

process is not complicated by extensive chemical reactions and that the ions extracted are more or less representative of those in the plasma [Douglas and French, 1988]. This is supported by ionisation temperature measurements [Crain *et al.*, 1990], and electron density measurements in the jet [Lim and Houk, 1990]. However, there is evidence that some charge separation takes place during the extraction process [Chambers *et al.*, 1991], although the extent of charge separation has not been determined [Tanner, 1992]. During the expansion stage the ions are entrained in the flow of the argon gas and attain a velocity equal to the terminal velocity of argon. The kinetic energy of the ions (the sum of $1/2\ mv^2$ and the plasma potential) is therefore dependent on the mass of the ions [Crain *et al.*, 1990].

The skimmer cone is placed within the supersonic jet, the optimum skimmer-sampler position found empirically to be approximately 2/3 of the distance from the onset of the Mach disc [Lam and Horlick, 1990; Douglas and French, 1988]. About 1% of the ions extracted from the plasma flow through the skimmer cone [Gillson *et al.*, 1988]. The condition of both the skimmer and sampling cone is significant to the instrument performance. During use, sample material builds up on the surfaces of the cones which also become pitted and corroded. To avoid memory effects, the cones should be cleaned daily and replaced if the instrument response has dropped significantly due to their deterioration.

2.1.5.2 Ion Focusing

To transmit the ions from the skimmer to the mass analyser, they are focused into a beam by an array of ion lenses, the principle operations of which are given by Jarvis *et al.* [1992]. For an ideal lens the trajectory of an ion, to the first approximation, is independent of m/z provided that the initial position and kinetic energy are the same. This implies that one set of lens voltages could transmit all ions with the same efficiency [Jarvis *et al.*, 1992]. However the ion's kinetic energy is mass dependent, the spread of kinetic energy across the mass range being a few eV [Crain *et al.*, 1990; Fulford and Douglas, 1986]. As a result, ions of different mass have different paths through the ion optics and a compromise set of lens voltages has to be found. This introduces mass discrimination into the

system, with some ions being transmitted more efficiently than others, and the extent of the mass discrimination depending on the plasma potential and on the ion lens settings. The trajectories of ions through the ion lens system have been modelled using a computer program, MacSimion, which illustrates the dependence of ion path on kinetic energy [Vaughan and Horlick, 1990b]. The program has been further adapted to account for space charge affects in the ion optics (see below) [Tanner, 1992].

The lens stack also contains a metal disc on the axis which acts as a photon stop, preventing photons emitted from the plasma from reaching the detector and contributing to the background count rate. Consequentially about 50-80% of the ions are also lost here [Jarvis *et al.*, 1992].

2.1.5.3 Space charge effects

The beam of ions passing through the skimmer cone can be considered to be quasi-neutral, the ion current being balanced by an equal electron current [Douglas and French, 1988]. However, as the beam leaves the skimmer, the electric field of the lens collects the ions and repels the electrons. Coulombic repulsion of ions of the same charge limits the number of ions that can be compressed into a beam of a given size. The ion current at the base of the skimmer has been calculated to be 1,500 μA [Gillson *et al.*, 1988] which well exceeds the maximum current of 1 μA where space charge effects are expected to be negligible [Olivares and Houk, 1985b]. As a result, ions are de-focused from the beam, the lighter, less energetic ions being affected more than the heavier, more energetic ions [Vickers *et al.*, 1989]. The mass bias effect is further enhanced within the ion optics where accelerating potentials induce a stronger mass-dependence to the ion's velocity, resulting in heavier ions moving more slowly than lighter ions [Tanner, 1992]. The heavier ions which were initially focused more tightly on the axis, now move more slowly and so make a greater contribution to the space charge. This is illustrated by Figure 2.10, which shows the suppression effect of matrix elements on the response for Li^+, Rb^+, and Th^+ as a function of the matrix element mass. Heavier matrix elements cause greater suppression than lighter matrix elements and, for a given matrix, light analytes are suppressed more than heavier analytes [Gillson *et*

Figure 2.10 Ratio of analyte signal in the presence of the matrix element to that in the absence of matrix element as a function of the matrix element for Li^+, Rb^+ and Th^+ analyte ions with matrix element concentration of 0.0042M [Gillson *et al*, 1988]

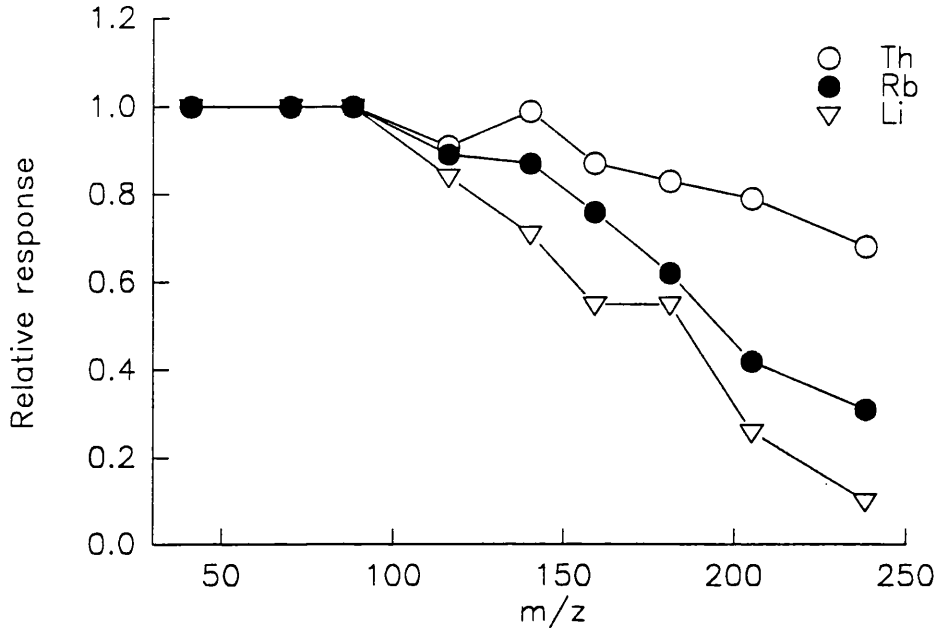

Figure 2.11 The Quadrupole mass filter, [Miller and Denton, 1986]

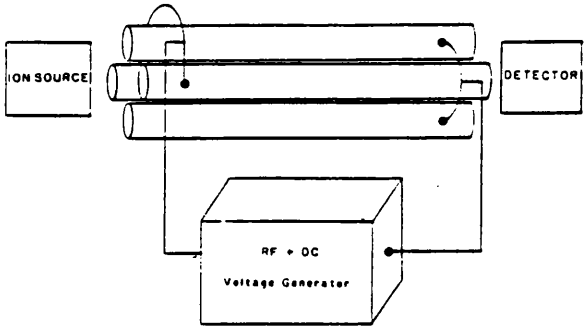

al., 1988]. Space charge effects in the interface are therefore the major cause of matrix interferences in ICP-MS.

2.1.6 Ion Selection and Detection

2.1.6.1 The quadrupole mass filter

Once the ions have passed through the ion optics they are focused into the quadrupole mass filter. This consists of four rods accurately machined to be parallel to and equidistant from the axis (Figure 2.11). Pairs of rods are connected together and a DC and RF voltage applied to each pair. To one pair the DC voltage is positive, to the other it is negative, the RF voltage being the same for each pair but 180° out of phase. Selecting RF and DC voltages appropriately allows only ions of a given m/z ratio to have stable paths through the rods, all other ions being deflected so that they hit the rods and become neutralised. The trajectory of the ions through the quadrupole can be calculated by considering the force acting on the ions by the electric field [Miller and Denton, 1986]. The solutions to the equations of motion require the definition of parameters a and q where:

$$a = \frac{4eU}{w^2 r_0^2 M} \qquad q = \frac{2eV}{w^2 r_0^2 M}$$

r_0 = radius between the rods; w = RF frequency; U = the magnitude of the DC voltage; V = the magnitude of the RF voltage.

The full mathematical calculation is given by Dawson [Dawson, 1976]. The stability of the appropriate solutions depends only on parameters a and q and a plot of a against q reveals regions where the solutions are stable or unstable (Figure 2.12). Keeping U/V constant restricts the operation of the mass filter to a set of operating points which lie on a straight line, known as the mass scan line (Figure 2.12). Only ions that fall on the scan line inside the sharply pointed tip of the

Figure 2.12 Stability diagram for ion transmission through quadrupole for fixed U and V, the (a, q) values for ions of different m/z = M, M-1 and M + 1 are indicated along the scan line [Miller and Denton, 1986]

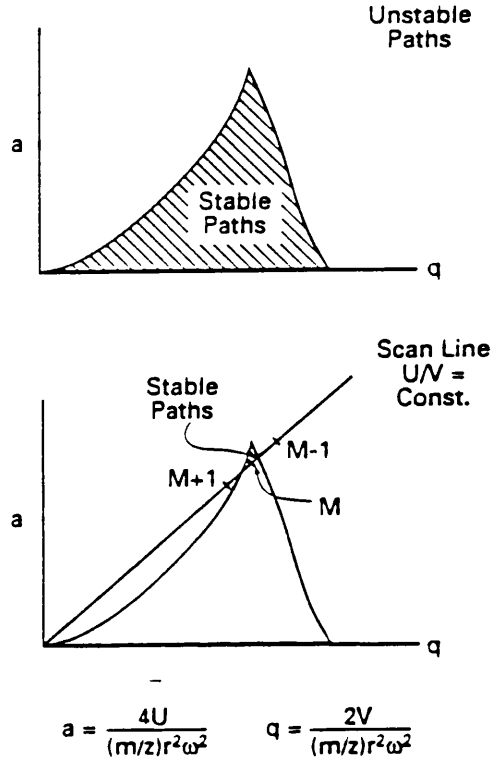

$$a = \frac{4U}{(m/z)r^2\omega^2} \qquad q = \frac{2V}{(m/z)r^2\omega^2}$$

stability region have stable paths through the rods. The quadrupole therefore acts as a narrow band-pass filter. Changing U and V alters a and q and this corresponds to moving from one m/z ratio to another along the scan line. Sweeping the voltages applied to the rods scans the band-pass region of the mass filter.

Adjusting the slope of the mass scan line by changing the U/V ratio alters the width of the m/z values transmitted. For example, increasing U/V narrows the mass-band of the filter and so in effect increases the resolution. However, the number of ions transmitted depends approximately on the area of the stability diagram that is enclosed, so increasing the resolution also decreases the fraction of the ions at the m/z ratio of interest getting through [Jarvis *et al.*, 1992]. Therefore, a compromise between resolution and ion transmission has to be made.

The quadrupole performs best with ions of low kinetic energy (< 20 eV). Ions with high kinetic energy pass too quickly through the quadrupole and do not experience enough RF cycles for proper resolution. The axial ion energy can be altered by applying a DC voltage uniformly to all rods, which would accelerate slow ions and retard fast ions.

To improve the performance of the quadrupole mass filter short, RF only quadrupoles are placed at the entrance and exit of the mass analyser. These act as high pass mass filters and collimate ions closer to the central axis and also reduce the effects of fringe fields at the exit and entrance of the analyser [Jarvis *et al.*, 1992].

The advantages of using a quadrupole mass filter are that it can tolerate high operating pressures (approximately 10^{-4} torr) and significant spreads in ion velocity. It also can be scanned rapidly and provide unit mass resolution [Houk and Thompson, 1988].

2.1.6.2 Ion detection

Mass resolved ions leaving the quadrupole mass filter are detected by a channeltron electron multiplier in pulse counting mode. This consists of an open glass tube

Figure 2.13 A Channeltron electron multiplier [Jarvis *et al*, 1922]

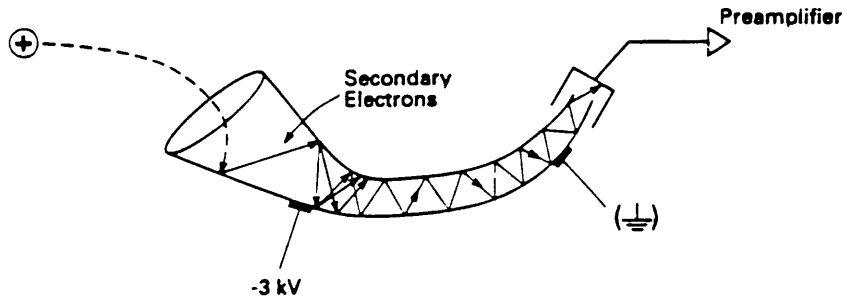

with a cone at one end (Figure 2.13). The interior surface of the tube and cone is coated with a lead oxide semiconducting material which enables a continuous potential gradient to be set up inside the tube by maintaining the cone at a high negative potential (approximately 3 keV) whilst keeping the other end of the tube at ground. A positive ion leaving the mass analyser is attracted to the negative potential. On collision with the interior surface of the cone it releases one or more electrons which are then accelerated by the potential gradient towards ground. If the electrons have acquired enough energy from the electric field, they will release secondary electrons on collision with the surface. This process repeats itself 10-20 times so that an incident ion results in a discrete pulse of typically 10^8 electrons at the collector. This pulse is then sensed and shaped by a fast pre-amplifier and the output passed to a digital discriminator and counting circuit. Only pulses above a set threshold amplitude will be counted, enabling discrimination against low amplitude pulses caused by spurious emission of electrons in the tube.

Channeltron electron multipliers have the advantage that they can be vented to the air without damage, as long as the high voltage is switched off. They are robust and can tolerate pressures up to 10^{-5} mbar. In addition the low instrumental

background (< 1cps) enables high sensitivity. In pulse counting mode a linear response is obtained over 5 - 6 decades of concentration, and this can be extended to 8 decades by using mean current detection. They have, however, a limited lifetime, dependent on the total accumulated charge and suffer from deadtime and counting fatigue at count rates greater than 10^6 s^{-1}.

2.1.6.3 Data collection

Pulses from the channel electron multiplier are counted into a multichannel scaler. This contains a 16 bit digital to analogue converter (DAC) which controls the quadrupole setting. The acquisition of data takes place for a defined dwell time at each DAC setting, after which the contents of the counter are passed into a latch so that the next acquisition can take place at the new DAC setting. The latch is subsequently read by a microprocessor which adds the contents to the appropriate location in the acquisition memory. This enables versatility in the acquisition of data which can be collected in two ways, peak jumping or scanning. In scanning mode the data are collected over a pre-defined mass range for a relatively large number of points per peak (15-20). With enough storage channels (4096), data can be collected for all isotopes of elements in the mass range 4-250 m/z, although more often a narrow region of interest is scanned. Skip scan regions can also be defined where data are not collected, although the quadrupole requires a settling time of a few milliseconds afterwards to equilibrate. Scanning has the advantage of collecting data over a wide mass range, making identification of interfering peaks easier, and also provides information on peaks which may not be of immediate interest.

In peak jumping mode data are collected at a number of fixed mass positions for selected isotopes. Usually the positions are taken as the central point of a peak, with two points either side. The dwell time on each isotope can be varied to improve the counting statistics. In this mode, time is not wasted collecting data on peaks which are not of interest, although this can make identification of interfering species more difficult. Peak jumping is advantageous if the isotopes of interest are spread over a wide mass range, or if only a small number of isotopes and isotope ratios are required.

2.2 ANALYTICAL PERFORMANCE

This section discusses the performance of the ICP-MS system used in this study. The system was bought in 1988, only four years after the first instruments were commercially available. The present study followed on from the work of Hursthouse [Hursthouse, 1990] at a time when ICP-MS was a relatively new technique and the system was still in a stage of development. With a growing community of ICP-MS users, the manufacturers were pressurised to make upgrades to the system, in order to improve its robustness and reliability. The extent and rapidity of the changes to the ICP-MS system mean that some of the development work present here, relating to the PlasmaQuad PQ1 and in particular to the Microtherm Mark 1 ETV, is now historical, although the underlying principles remain the same. As discussed earlier, there was little information in the literature relating to this particular application of the technique.

The initial section below, demonstrates the optimisation of the system for the analysis of actinides using standard solutions. The reliability and reproducibility of the system as a whole are discussed. Finally, the accuracy of the technique was tested by the analysis of a sediment sample which had been previously analysed by independent analytical techniques.

2.2.1 Optimisation

Theoretical studies of the fundamental properties of the ICP-MS system, such as the characteristics of the plasma and space charge effects, are important for understanding the behaviour of analyte species and for further development of the technique. However, the daily optimisation of the ICP-MS system is performed on a more empirical basis. A number of mutually interdependent parameters such as nebuliser flow rate, RF power, aperture-load coil separation and lens settings affect the performance of the ICP-MS system. In general, most of these parameters are kept at default values and optimisation consists of fine tuning the sampling position and the lens settings.

The analytical and developmental procedures were carried out periodically between

1989 and 1992, during which time the ICP-MS instrument was subjected to a wide variety of users and sample matrices. The results presented in this study were obtained during week long blocks of instrument time. At the start of each block the spray chamber and plasma torch were soaked overnight in 10% (1.6M) nitric acid, after which they were rinsed in doubly distilled, deionised water (DDI) and dried. The sampling and skimmer cones were cleaned daily with a proprietary stainless-steel cleaning preparation, Polaris, and rinsed with DDI water.

2.2.1.1 Lens settings and sampling position

Initially, the ion optics lens settings were optimised by maximising the $^{115}In^{+}$ signal obtained by aspirating a standard solution of 10 ng ml^{-1} ^{115}In in 2% (0.32M) nitric acid. Table 2.2 shows typical lens settings used during this study. The collector, extractor and L1 and L3 voltages were found to be critical. The ^{115}In tuning solution was later replaced by a 1 ng ml^{-1} ^{236}U solution to maximise the signal obtained for the mass region of interest (i.e. 235 - 242 a.m.u.). The optimum lens settings for the $^{115}In^{+}$ and the $^{236}U^{+}$ signals were found to vary slightly, but with no obvious trend. The sampling position was also optimised using the tuning solution. The distance between the load coil and the sampling aperture was fixed at approximately 10 mm so that dissociation and ionisation of the sample were as complete as possible. The positioning was checked occasionally by measuring the relative level of oxide to analyte species. Reduction of this distance may result in a higher ion response but carries an increased risk of incomplete dissociation of species [Gray and Williams, 1987]. The horizontal and vertical positioning of the torch were then adjusted to obtain the maximum ion signal. After any alteration of the sampling position the lens settings were re-optimised.

2.2.1.2 Nebuliser flow rate and RF power

The nebuliser flow rate and the RF power are important parameters for determining the distribution and relative abundance of species in the plasma at any given sampling position. Figure 2.14 shows the variation in signal response with nebuliser flow rate for uranium, neptunium and plutonium isotopes, at four different power settings (1250, 1300, 1350 and 1400 W). All other parameters were kept

constant. The results were obtained by aspirating a mixed standard solution and

Table 2.2 : Typical lens settings and supply voltages used during study

Lens	Average setting (PQ1 supply)	Average voltage	Recommended voltage
Extractor	1.14 ± 0.19	-200 ± 20	-190
Collector	4.84 ± 0.26	-5 ± 8	0
L1	5.01 ± 0.10	0 ± 3	0
L2	3.71 ± 0.68	-40 ± 20	-30
L3	4.75 ± 0.16	-13 ± 8	0
L4	3.24 ± 0.56	-90 ± 30	-50
Front Plate	5.07 ± 0.17	2 ± 5	4
Pole Bias	5.10 ± 0.36	0 ± 2	-3

recording the integral response over the mass range 235 - 246 using 512 MCA channels and a 1 minute integration time for each run. The optimum nebuliser flow rate increased with RF power, the maximum response being obtained at a power of 1400 W and a flow rate of 0.72 l min^{-1}. There was no significant variation in the optimum flow rate observed for Np, U, and Pu isotopes implying that the instrument parameters could be optimised using only one isotope. Subsequently, the RF power was fixed at 1350 W and the nebuliser flow rate optimised daily using a 1 ng ml^{-1} ^{236}U solution. Figure 2.15 shows the variation in nuclide ratios measured during this experiment. Excluding the initial ratio in each data set, the deviations of the nuclide ratios were all less than 2%. The probable cause of the deviation of the first result is initial instability in the plasma after the RF power was altered. The general stability of the nuclide ratios suggests that U, Np and Pu nuclides have similar behaviour in the ICP-MS system implying that ^{236}U can be used as an internal standard for ^{237}Np analysis.

2.2.1.3 Resolution

The resolution of the ICP-MS system can be adjusted by altering the ratio of the DC and RF voltages applied to the quadrupole mass filter (see section 2.1.6.1). However, an increase in resolution results in a decrease in sensitivity (Figure 2.16) and a compromise setting has to be reached. The most critical factor in this study

Figure 2.14 The variation in signal response with nebuliser flow rate at four different power settings for ^{236}U, ^{237}Np, ^{239}Pu and ^{242}Pu

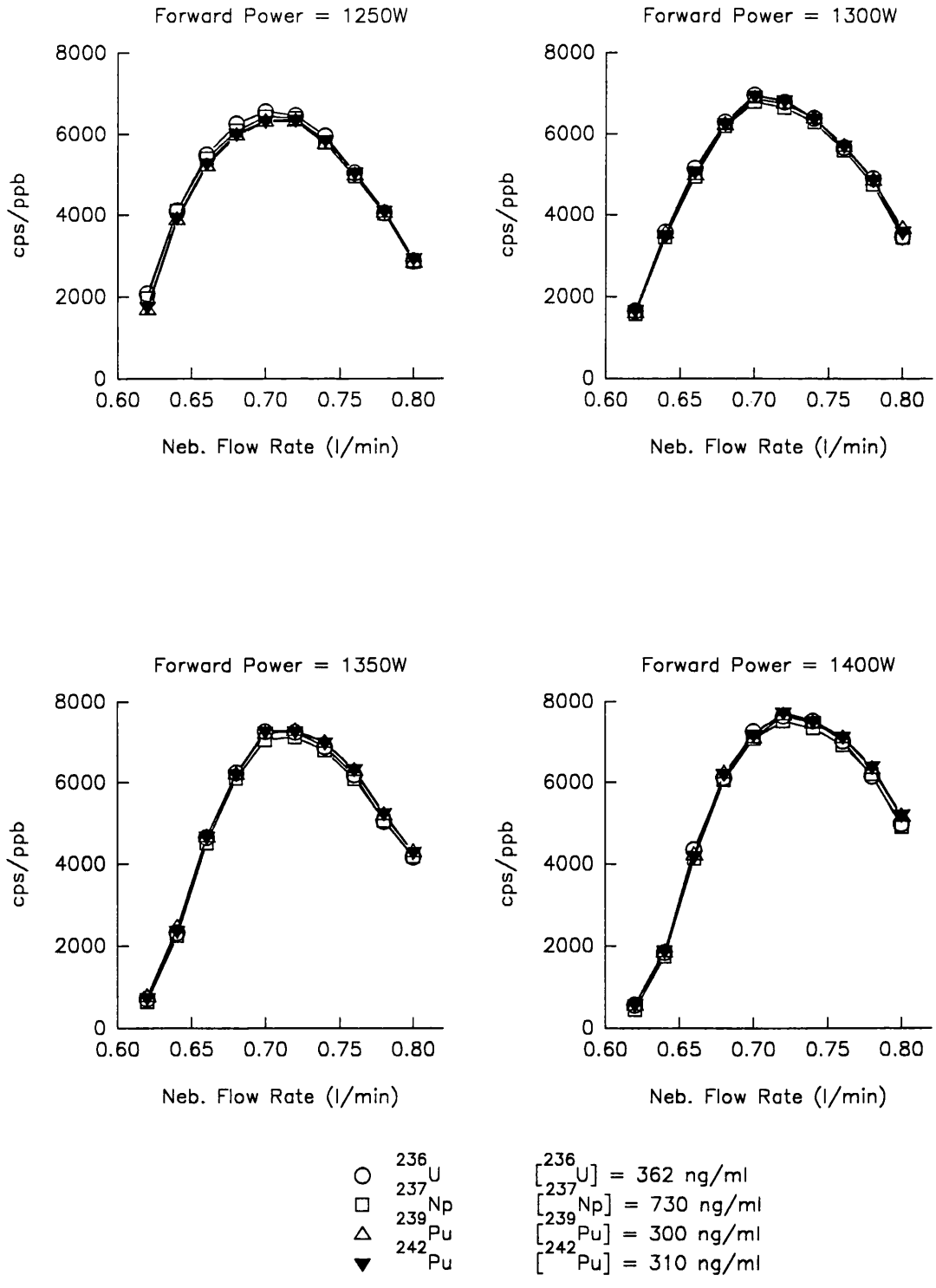

Figure 2.15 The variation in nuclide ratios with nebuliser flow rate at four different power settings

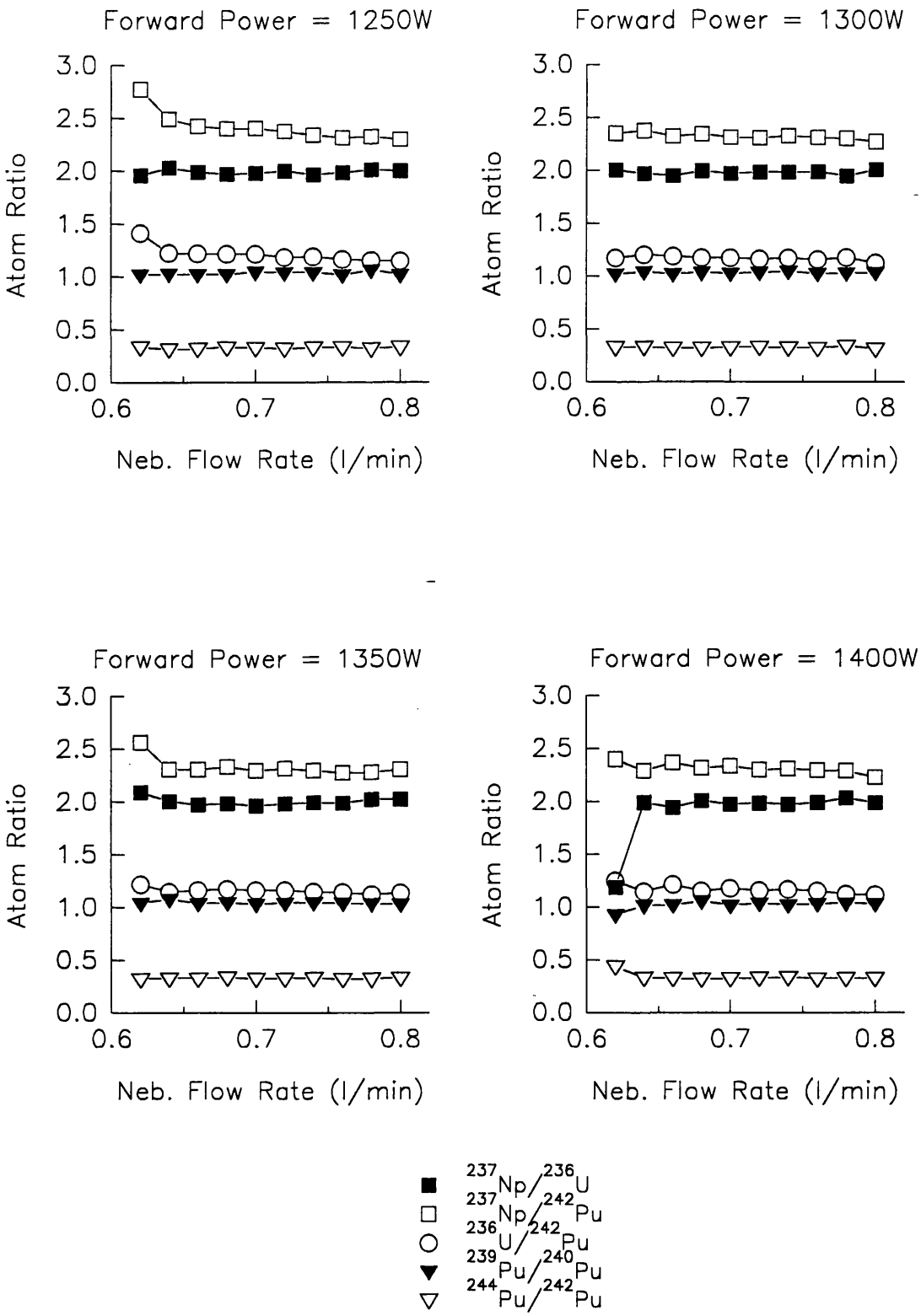

Figure 2.16 Variation in integrated counts with resolution for an aspirated solution of 100ng ml^{-1} ^{238}U in 2% HNO_3.

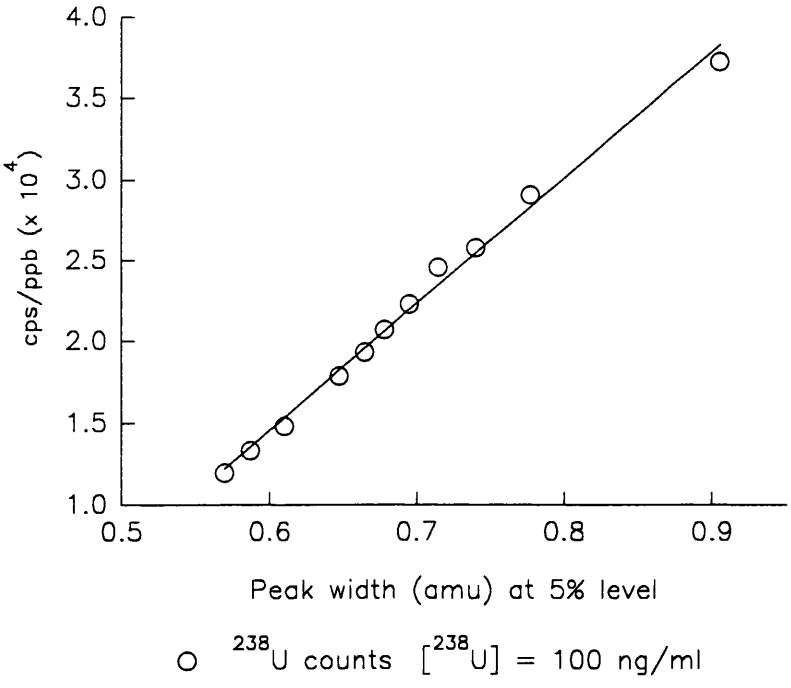

was the complete separation of adjacent peaks, as ^{237}Np and ^{239}Pu were measured on either side of ^{238}U, which was present at up to 10^5 times higher concentration. This required an abundance sensitivity of greater than 10^{-6}, which was readily achieved by setting the quadrupole to baseline resolution between adjacent peaks.

2.2.1.4 Data collection and sample throughput

In this study the nuclides of interest fell in a narrow mass range between 236 and 242 a.m.u. As all the peaks in this region were of interest both as analytes and potential interferents, data were collected by rapidly scanning across this mass range. The scanning parameters chosen are shown in Table 2.3. At a sample uptake rate of 1 ml min^{-1}, three consecutive one minute scans required a minimum volume of 5 ml of sample, taking into consideration a two minute sample uptake time. This allows time for the sample to reach the plasma and for the conditions in the plasma to reach equilibrium before data are collected. For each sample, a time of only 5 minutes was required to obtain data for three repeat runs. A three minute wash time between each sample was also applied, aspirating 2% HNO_3 to remove any sample memory from the system. Considering the time required for

optimisation, standards, checks and reference materials a typical throughput of samples was 20 a day.

Table 2.3: Typical scan parameters

a) Liquid nebulisation

Mass Range	235 - 246 a.m.u.
Number of channels	512
Number of scan sweeps	1600
Dwell Time (μs)	80
Approximate run time	66s
Number of runs per sample	3

b) ETV

Mass range	235 - 246 a.m.u
Number of channels	512
Number of scan sweeps	200
Dwell Time (μs)	80
Approximate run time	8s
Number of runs per sample	5

2.2.2 ETV Optimisation

The optimum settings for ETV-ICP-MS were not expected to be the same as those obtained for liquid nebulisation as the plasma is operated under 'dry' conditions with the ETV. However, the signal obtained during a normal analytical run by ETV-ICP-MS has a short duration (0.5 - 10 seconds), making optimisation of the instrument parameters exceedingly difficult. Several techniques were investigated during this study to produce a prolonged signal (Table 2.4). The results were variable, not only from day to day, but also from hour to hour. The most reliable technique was the bismuth optimisation. In many cases, the 'optimum' settings were inappropriate for a normal analytical run. In general, adequate signal response was obtained by optimising the instrument by liquid nebulisation, then converting directly to ETV without changing any parameters.

Table 2.4 : Techniques attempted to optimise the ETV-ICP-MS parameters

Isotope	Temperature profile	Injection	Comments
Bi	Dry, then vaporise from 125 to 1,825°C in 10s, holding for 60s	50 μl 100 ppb Bi solution in 2% HNO_3	High m/z, sharp peak observed, followed by a slow decrease in counts during which optimisation can take place
Xe	As above	100 μl H_2O	Generally, a small signal observed of short duration
Hg	Set furnace temperature to 50°C	Place a pipette tip filled with Hg in the furnace hole	Good steady signal observed, but optimum settings inappropriate for normal analysis
CHF_3 Impurity			None found at high enough concentration

2.2.2.1 Temperature profile

A typical temperature profile used to heat the graphite furnace is shown in Figure 2.4. The temperature profile consists of three stages namely; drying, ashing, and vaporisation. During the initial drying stage, the solvent is removed from the sample at a slow enough rate to produce a reproducible deposit, preventing spluttering or spreading of the sample over the surface of the furnace. From visual observation of the sample droplet, this required gradual ramping of the furnace temperature from 75 °C to 125 °C over a period of 100 seconds. The ashing stage removes residual organic matter and some matrix material from the sample. The maximum ashing temperature, which did not result in the loss of analyte material, was found to be 725 °C. This was not high enough to remove some of the major matrix components such as sodium.

Figure 2.17 shows the variation in signal response with vaporisation temperature for three different carrier gas flow rates. In each case the maximum signal was

Figure 2.17 The signal response for ^{236}U, ^{237}Np and ^{242}Pu as a function of vaporisation temperature, at carrier gas flow rates of 0.725, 0.750 and 0.800 ($lmin^{-1}$)

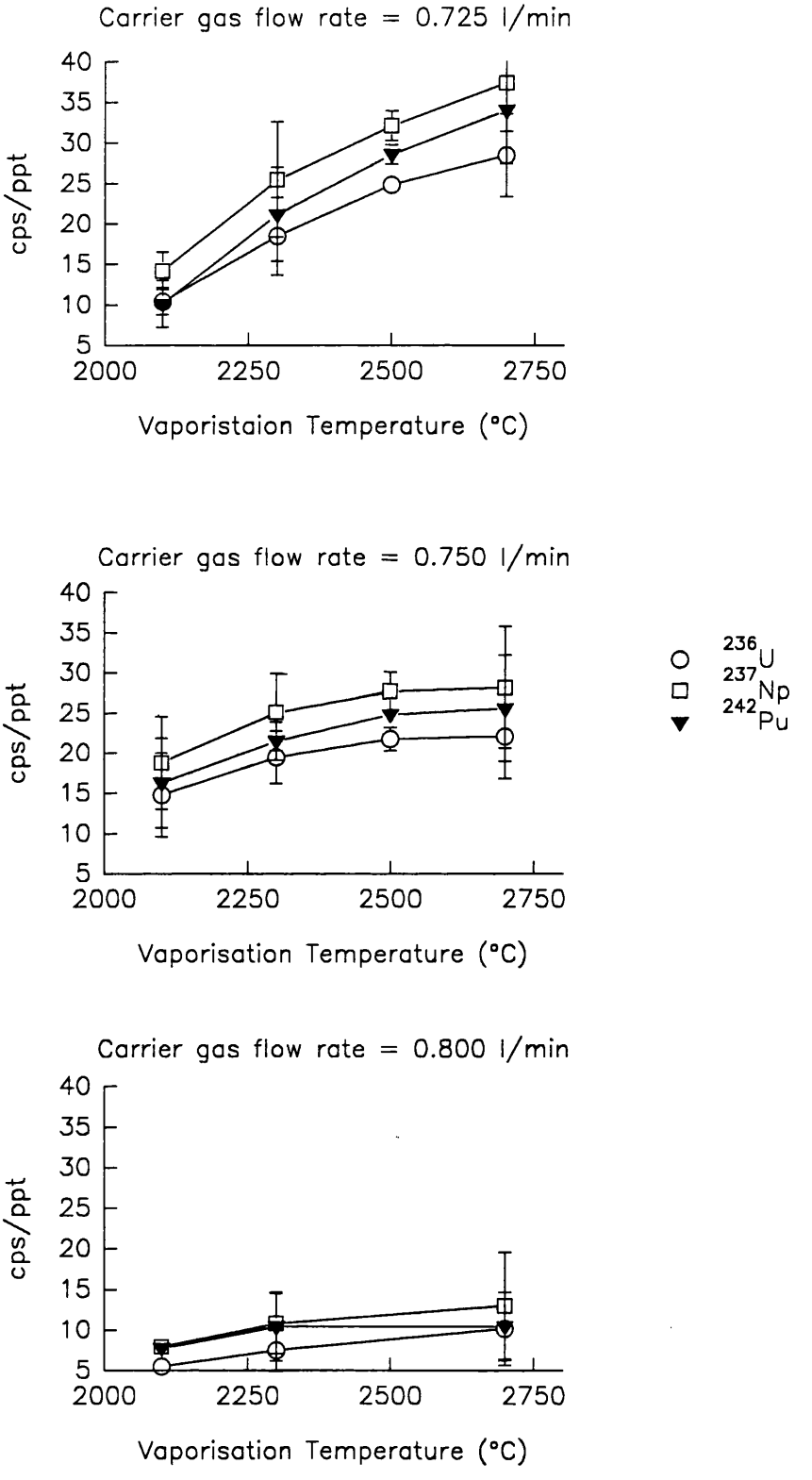

Figure 2.18 The variation in signal response for ^{236}U, ^{237}Np and ^{242}Pu with freon flow rate on three different days of ETV-ICP-MS analysis

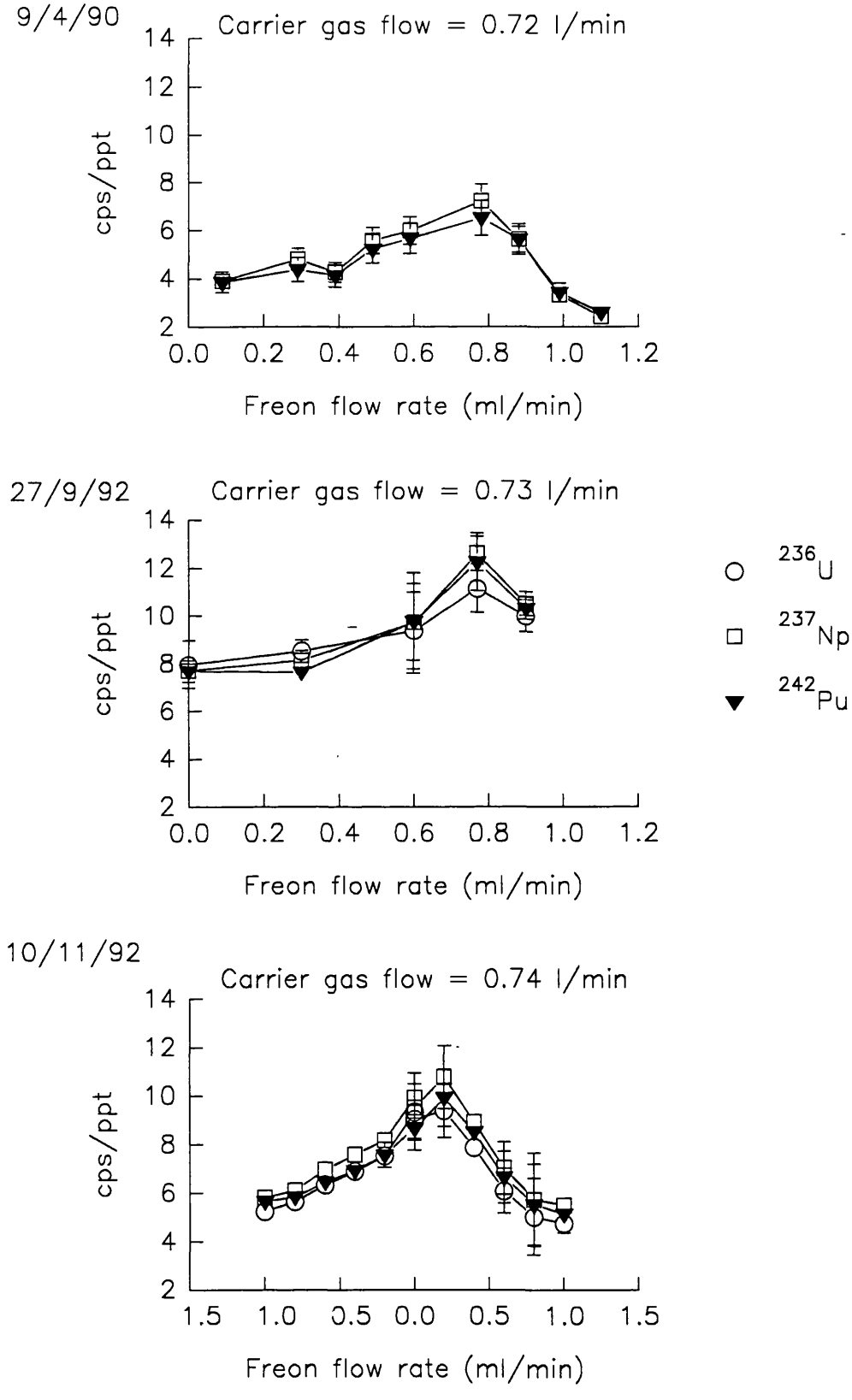

obtained at the maximum vaporisation temperature used, 2,750 °C. Temperatures above this tended to cause rapid ageing of the furnace, resulting in heavy carbon deposits on the cones and cracking of the furnace surface. Increasing the carrier gas flow rate decreased the signal response. The default temperature profile was set at a vaporisation temperature of 2,750 °C and at the optimum carrier gas flow rate determined by liquid nebulisation.

2.2.2.2. Freon flow rate

At the vaporisation temperatures used with ETV, refractory elements, such as the actinides, can form carbides which stick to the surface of the graphite tube. To overcome this, freon (CHF_3) was added to the carrier gas so that volatile fluorides formed preferentially, increasing the transport efficiency of the actinides from the furnace to the plasma [Hutton, 1990]. Figure 2.18 shows the results of three experiments investigating the effect of the freon flow rate on the signal response. The first two graphs display a similar trend, with the optimum freon flow rate occurring at 0.78 ml min^{-1}, approximately 0.11% of the carrier gas flow rate. The third graph displays a markedly different trend with the maximum signal response occurring at or close to zero freon flow. Although the results were reproducible on the day, this was a 'one off' set of results, thought to be caused by entrainment of air (instead of freon) in the furnace, resulting in the formation of oxides. In general the addition of freon increased the signal response. The default freon flow rate was set at 0.1% of the carrier gas flow rate.

2.2.2.3 Data Collection

ICP-MS data can be collected in two ways: single ion monitoring, where the quadrupole is left resting at the mass unit of interest, or multielement scanning where the quadrupole is scanned rapidly over a discrete number of mass units. Figure 2.19 shows the signals obtained from a 50 μl injection of a 100 pg ml^{-1} solution containing ^{236}U, ^{237}Np and ^{242}Pu by single ion monitoring and multielement scanning. In this case, 11,879 cps were measured by single ion monitoring at 236 m/z with a background count rate of 54 cps compared to 2,705 cps obtained by multielement scanning with a corresponding background of 34 cps. Although

Figure 2.19 Spectra obtained by (a) single ion monitoring at mass 236 and (b) multielement scanning, using a 50μl injection of a solution containing 100 pg ml^{-1} ^{236}U, ^{237}Np and ^{242}Pu

(a)

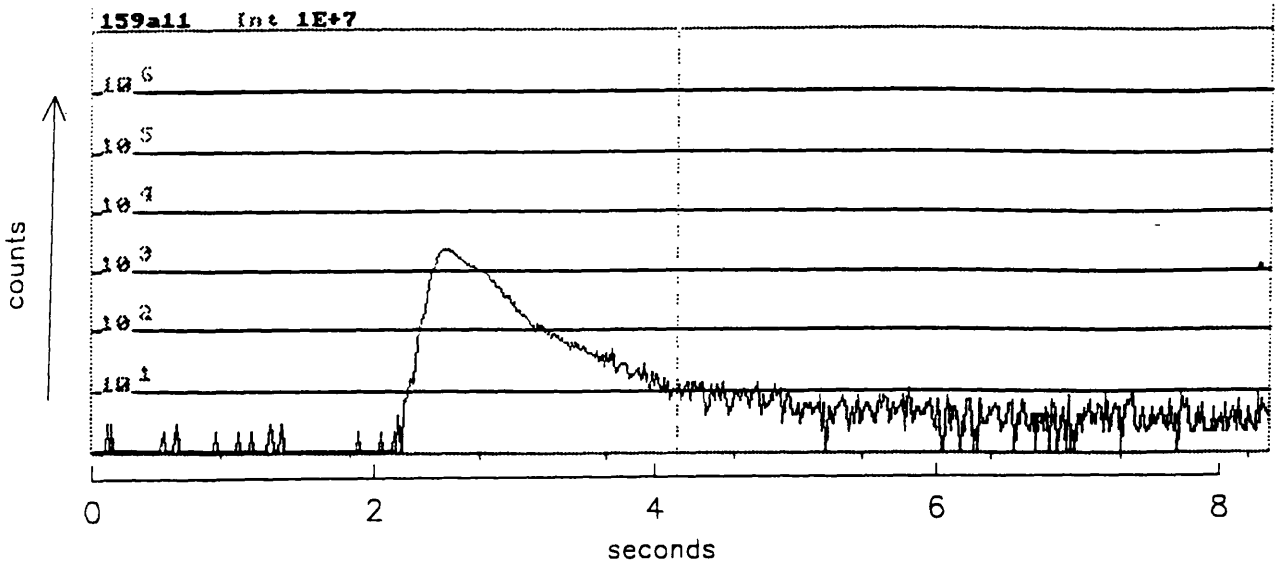

(b)

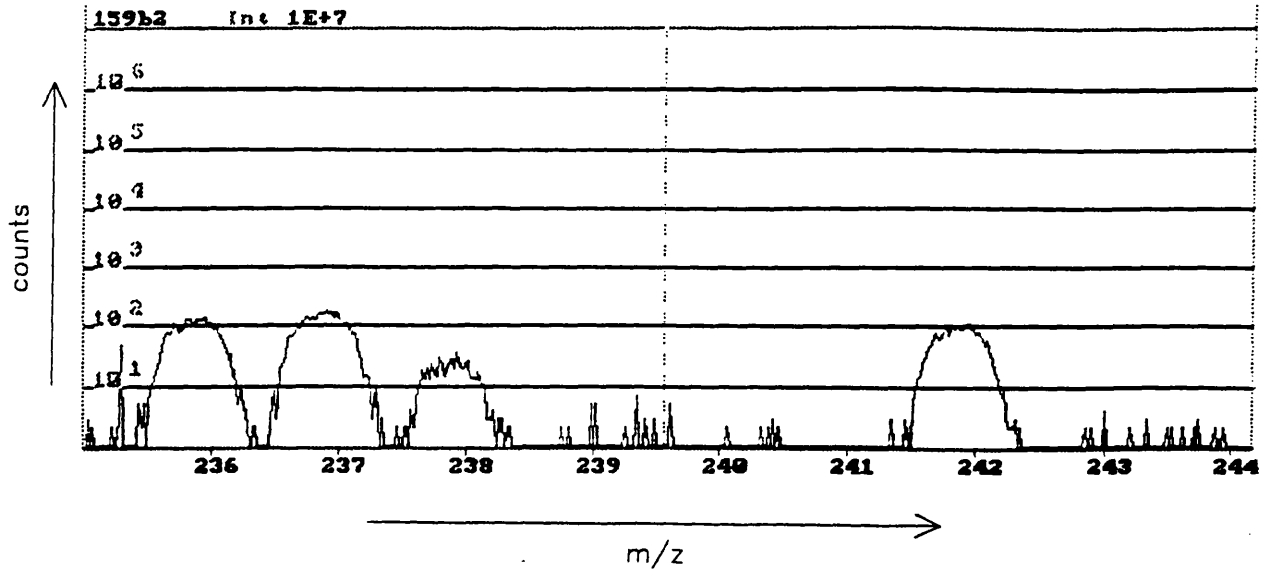

Figure 2.20 Signal response as a function of dwell time for a fixed integration time of 10 seconds

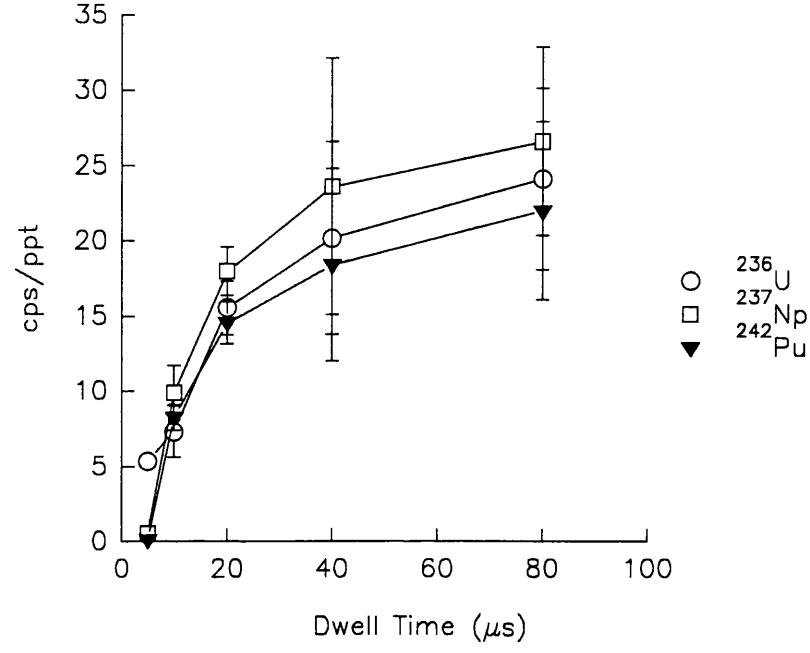

Figure 2.21 The relative signal response as a function of number of scan sweeps at a fixed dwell time of 80μs

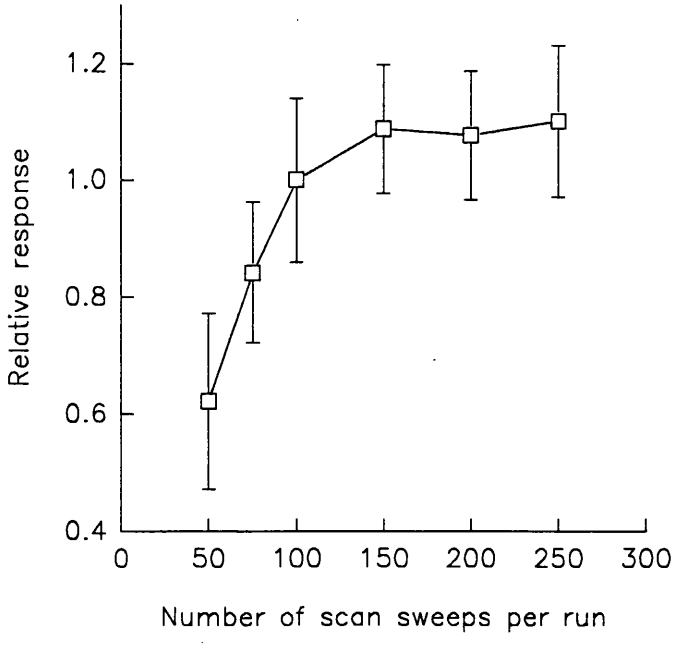

greater sensitivity is achieved by single ion monitoring as data are collected only at the mass of interest, multielement scanning can provide more information and enable internal standardisation of the technique. The total signal duration as shown in Figure 2.19a is only a few seconds. To obtain accurate nuclide information during a multielement scan, short dwell times are required. Figure 2.20 shows the effect of increasing the dwell time, whilst keeping the total integration time constant. For small dwell times ($< 40\ \mu s$) the finite time required for the quadrupole to change mass and the resting time required between scans (~ 10ms), as well as the time for the ions to be transmitted through the quadrupole ($\sim 20\mu s$) become significant. The minimum dwell time for maximum integrated counts was found to be 80 μs with an optimum number of scan sweeps of 200 (see Figure 2.21).

2.2.3 Signal response, stability and reliability

Figure 2.22 Signal response curve across the mass range

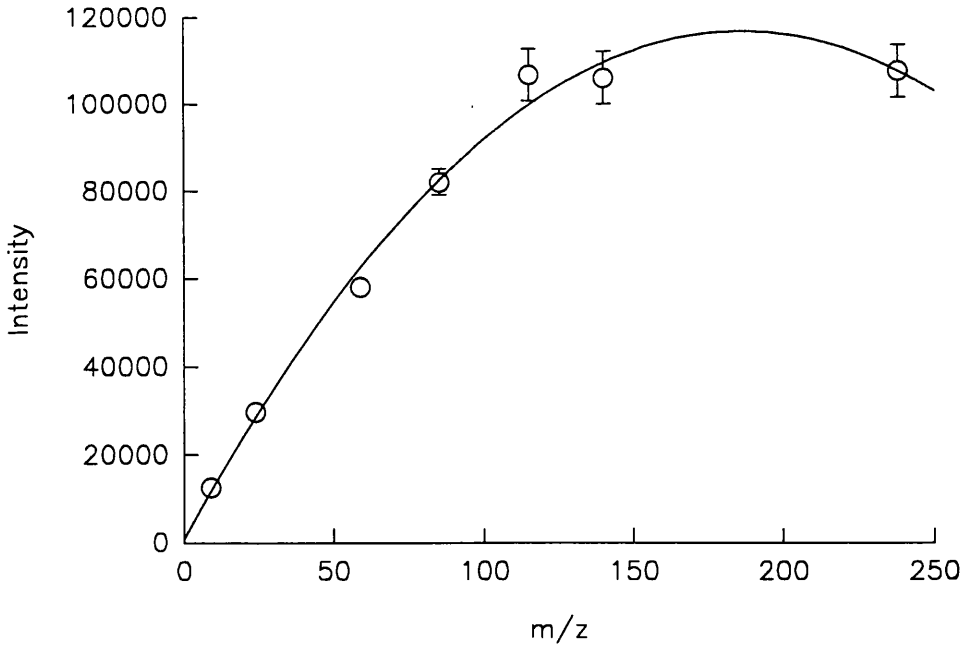

Figure 2.23 Long term signal response observed for (a) ^{115}In and (b) ^{237}Np by liquid nebulisation, and (c) ^{237}Np by ETV

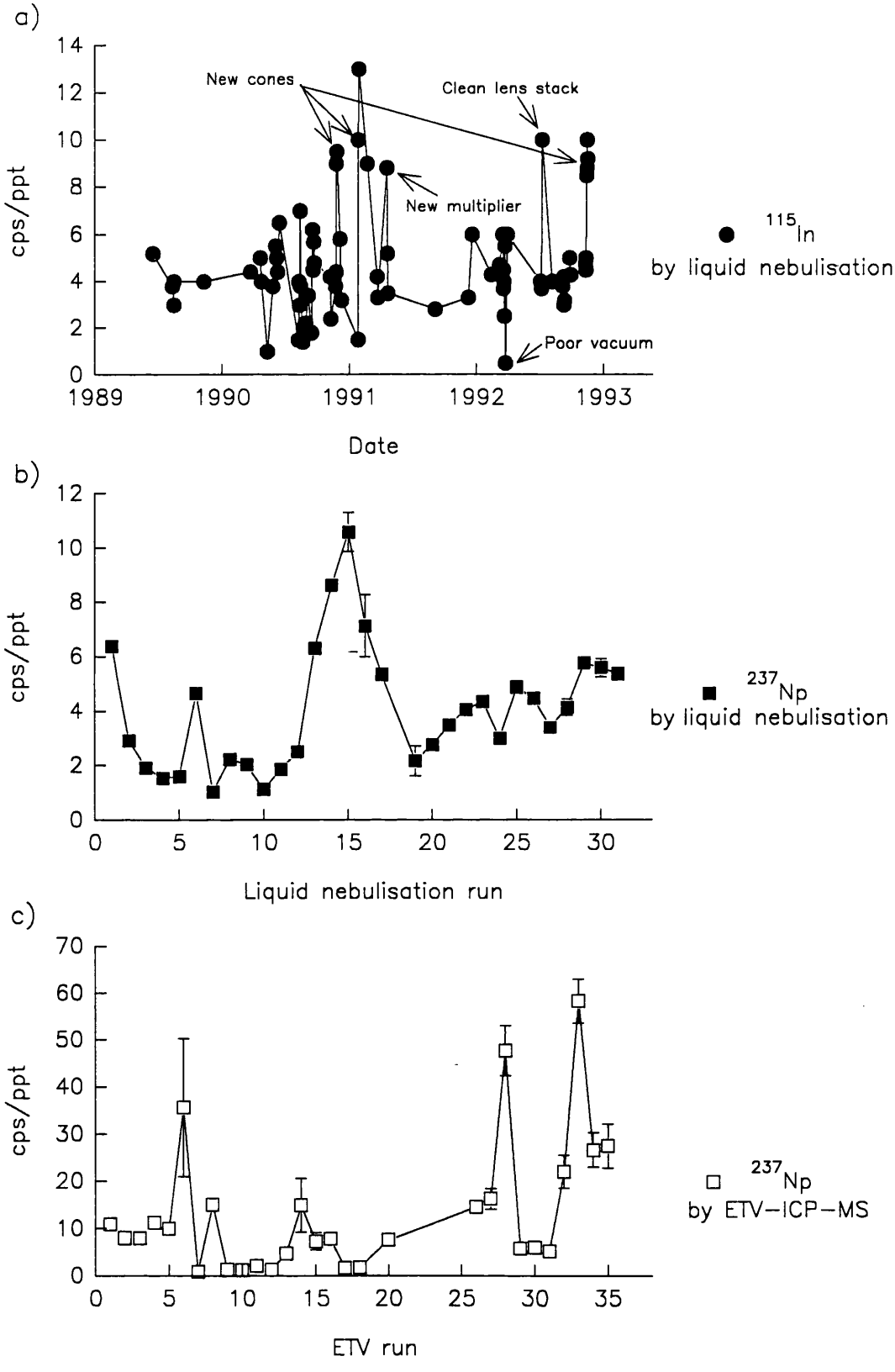

2.2.3.1 Response across the mass range

Figure 2.22, showing the signal response of the ICP-MS system across the mass range, indicates that the sensitivity is greater for the heavier elements, with the response curve flattening out in the mass range of interest in this study. The shape of the curve is dependent on the parameters of the system and on space charge effects in the interface.

2.2.3.2 Long term signal response

On any one day, the signal response is dependent on all the parameters of the ICP-MS system as well as factors such as the condition of the skimmer and sampling cones, the lens system and the age of the detector. Figure 2.23 shows how the initial signal response varied during the study for the indium tuning solution, and for neptunium, both by liquid nebulisation and ETV. For liquid nebulisation, a threshold response of 2 cps/ppt was set, below which steps were taken to improve it. In general, a low response was caused by the condition of the cones or lens system. With new cones and a clean lens stack a response as high as 8-10 cps/ppt was obtained although the average response was 4 cps/ppt.

The signal response measured for ETV-ICP-MS showed much more variability, with a maximum response of 50-60 cps/ppt for ^{237}Np, but with a minimum well below the 2 cps/ppt threshold. This is due to additional factors which affect the signal, such as the condition of the graphite furnace, and the difficulty of optimising the instrument parameters.

In general, the signal responses for uranium, neptunium and plutonium isotopes were not significantly different in either liquid nebulisation or ETV-ICP-MS.

2.2.3.3 Short term signal response and signal stability

The change in signal response over one day of analysis is shown in Figure 2.24. In general, the signal response deteriorates during the day as sample material deposits on the surface of the cones. For liquid nebulisation the signal reduced to

a minimum of 64% of the maximum level. The drop in the signal response for the ETV is more marked, with the signal dropping to a minimum of 42% of the initial signal. One cause is the deterioration of the graphite furnace, resulting in deposition of carbon onto the cone surfaces and less efficient transfer of the sample into the plasma as a result of leakage of sample from the tube and bushes. Evidence of this is shown in Figure 2.24b where the replacement of the furnace resulted in an immediate improvement of the signal response. It was observed that the addition of freon into the carrier gas, accelerated the rate of decay of the furnace.

The variation in the signal over ten consecutive runs of a 1 ppb solution for both liquid nebulisation and ETV is shown in Figure 2.25. Once again the signal for ETV is more variable than liquid nebulisation, with typical standard deviations of 12%, and 4% respectively. Another factor causing signal variation for ETV is the manual injection of each sample. Reproducibility can be improved by the use of an automatic sampler.

2.2.3.4 Reliability

During the study the instrument had a high percentage of "down time". Apart from the regular replacement of skimmer and sampling cones and plasma torches, the quadrupole, detector(x3), generator, torch box, expansion chamber front plate, rotary pump, RF quadrupole valves (x4), and quadrupole control electronics were replaced or upgraded.

2.2.4 Validation

2.2.4.1 Calibration and sampling protocol

As shown by the above discussion, the signal response of the ICP-MS system changes from day to day and from hour to hour. Several techniques can be employed to correct for instrument drift; internal standardisation, external calibration, isotope dilution and standard addition [Jarvis *et al.*, 1992]. The most powerful of these techniques for mass spectrometry is isotope dilution, where the

Figure 2.24 ^{237}Np **signal variation during 4 days of analysis by (a) liquid nebulisation and (b) ETV**

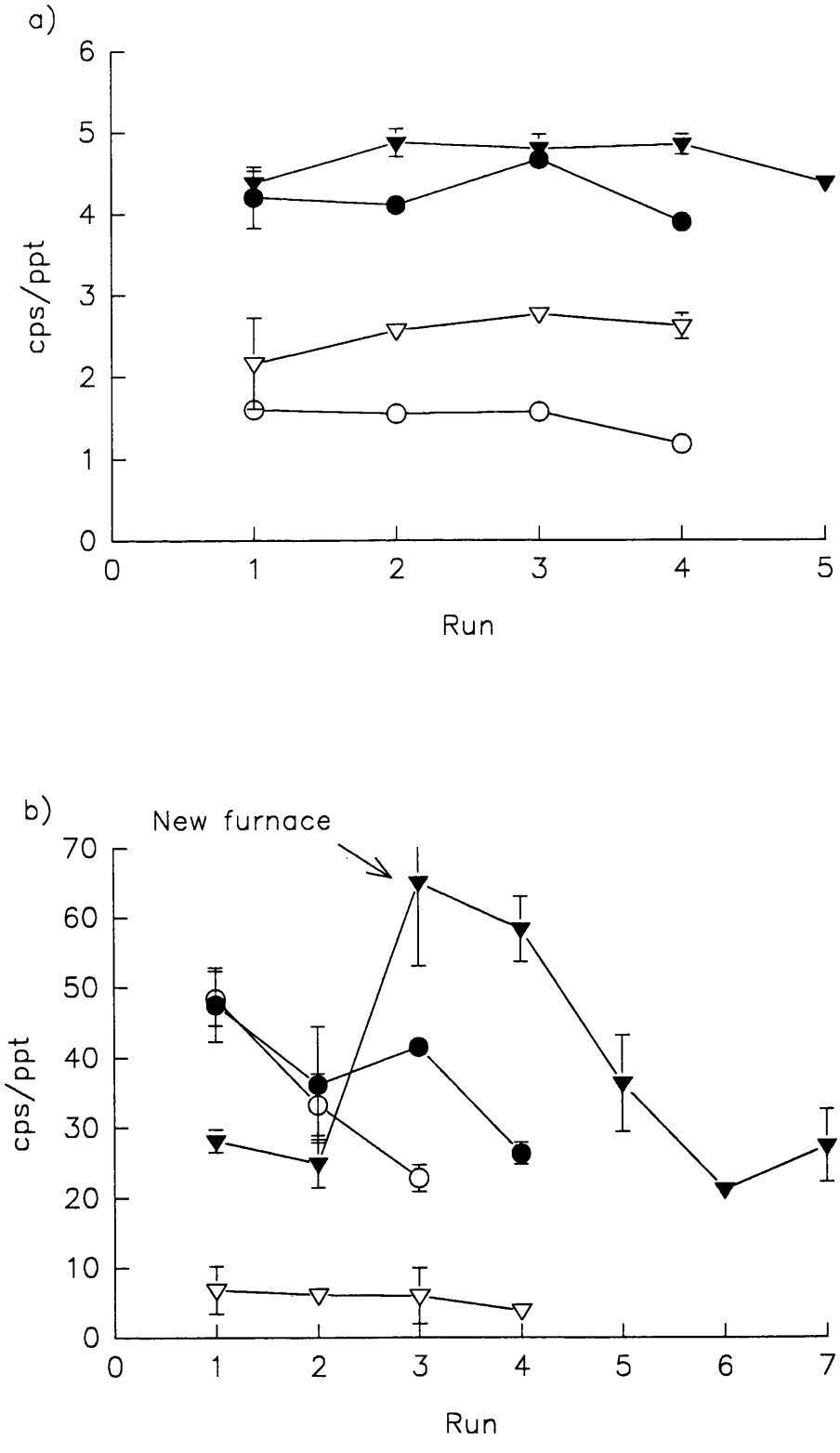

Figure 2.25 Short term variation in signal response over 10 consecutive runs for (a) liquid nebulisation and (b) ETV

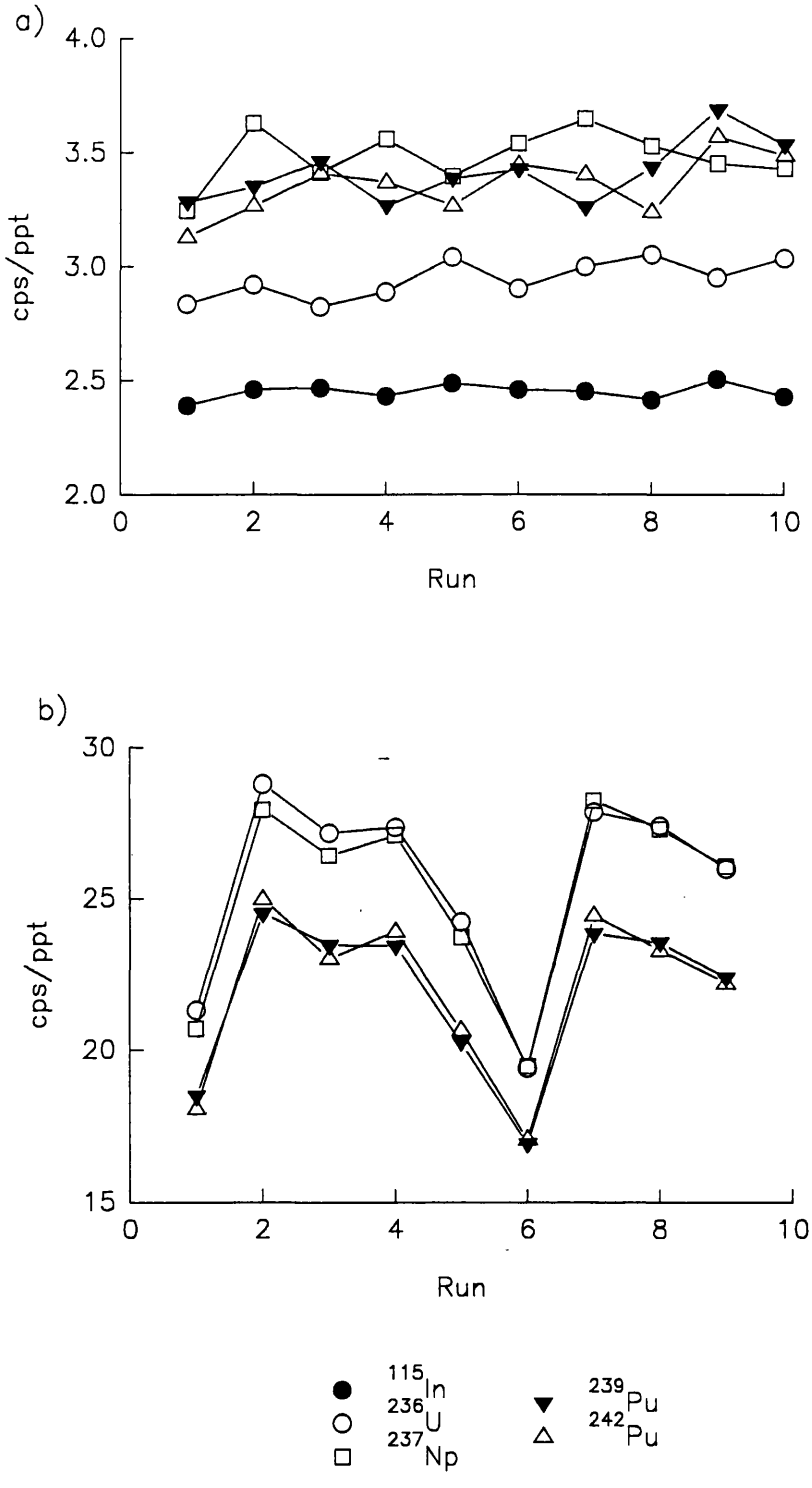

elemental concentration of a sample can be calculated by measuring the change in intensity of two selected isotopes after the addition of a known quantity of spike enriched in one isotope. In the case of plutonium analysis, this is possible by the addition of the long-lived ^{242}Pu isotope. The advantage of this technique is that the plutonium isotopes have very similar behaviour in the ICP-MS system and ^{242}Pu can be used simultaneously as an internal standard and a chemical yield tracer. Unfortunately no long-lived isotope is available for the analysis of ^{237}Np by isotope dilution. Instead a system of internal standardisation and external calibration was used. A known quantity of a high purity ^{236}U standard in 2% HNO_3 (Harwell, UK) was added to each sample as an internal standard. ^{236}U was chosen as an internal standard as it is free from interference and close in mass to ^{237}Np. Although they have differing first ionisation energies, ^{236}U and ^{237}Np display similar behaviour in the ICP-MS system as discussed above. Each run was started by a three point calibration curve with standard calibration checks after every five samples. A standard sediment sample (section 2.2.4.2) and a certified isotope ratio standard were also analysed randomly throughout each procedure to check the accuracy of the technique. ^{237}Np standards were prepared by dilution of a high purity stock solution in 2% HNO_3 (CIS, UK). A typical calibration curve is shown in Figure 2.26 with linearity over 3 orders of magnitude and a correlation coefficient of 0.99999.

2.2.4.2 Accuracy and precision

A review of the standard reference materials which had certified values for the elements of interest and were available at the time of this study revealed that none had values for the ^{237}Np content of the sample, or the individual ^{239}Pu and ^{240}Pu concentrations. However a bulk homogenised sample of Ravenglass silt which had been analysed by a previous study for ^{237}Np and plutonium isotopes both by ICP-MS and by independent techniques [Hursthouse, 1990] was available for analysis, and this was used to validate the technique. A comparison of results is shown in Table 2.5.

Figure 2.26 Typical ETV-ICP-MS calibration curves for ^{237}Np

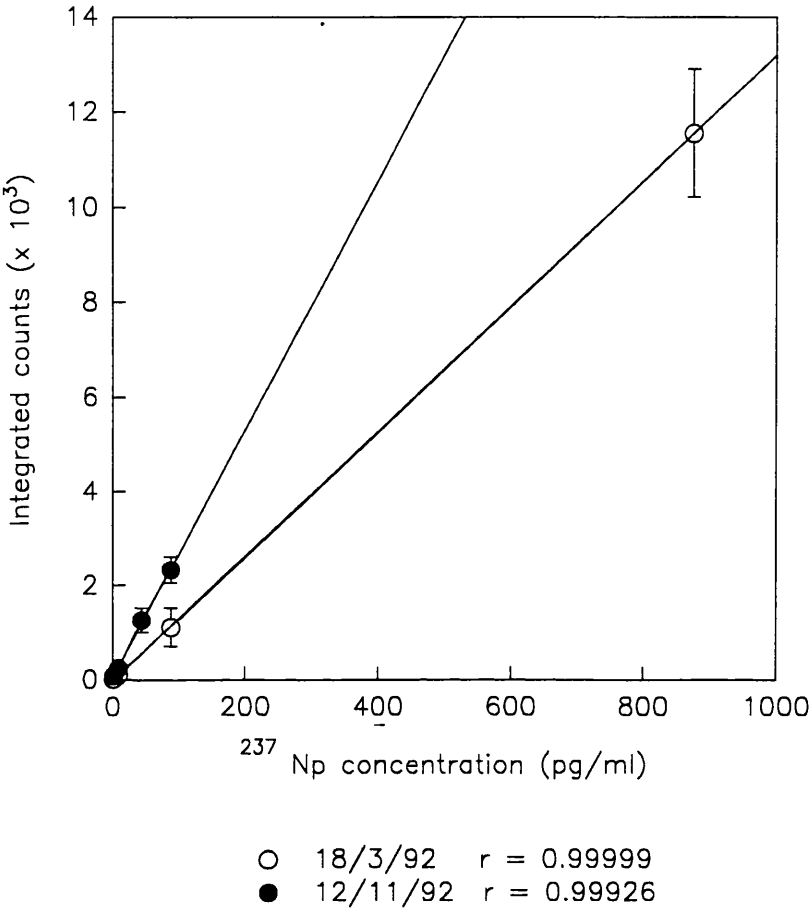

Table 2.5: Summary of results for Ravenglass sediment sample (errors are ± 1σ)

a) Neptunium concentrations (pg g^{-1})

Technique	This Study	*Previous Study
Liquid Nebulisation	101 ± 24	139 ± 21
ETV-ICP-MS	103 ± 25	-
Alpha Spectrometry	-	116 ± 7
Neutron Activation	-	81 ± 36

b) $^{239+240}Pu$ (Bq kg^{-1})

Technique	This study	*Previous Study	*Institute of Terrestrial Ecology
Liquid Nebulisation	1,020 ± 120	1,038 ± 36	-
ETV-ICP-MS	1,110 ± 180	-	-
α-spectrometry	-	870 ± 220	1,060 ± 80

* from Hursthouse, 1990.

The results of the plutonium analysis show close agreement, within ± 1σ. The difference in the standard deviations in the results obtained by ICP-MS for this study and the previous study reflect the different methods used. In this study, chemical processing was performed on separate aliquots of the sediment material whereas, for the previous study, data were obtained from a single processed bulk sample [Hursthouse, 1990]. Table 2.6 includes the results of replicate analyses of a bulk sample which display comparable deviation to those obtained by Hursthouse. The disparity of the deviations by the two methods indicates possible inhomogeneity in the bulk Ravenglass sample.

The neptunium results acquired by liquid nebulisation and ETV-ICP-MS show close agreement, and agree to within ± 2σ with those obtained by different techniques. The precision of the ICP-MS results reflects both the chemical recovery and the

performance of the instrument on the day of analysis and is therefore subject to large variation. From Table 2.6 it can be seen that the deviation in the liquid nebulisation results is comparable to those obtained by ETV. Once again, repeat analysis of a single sample on different days showed a smaller deviation than analyses of a series of discrete subsamples indicating inhomogeneity of the bulk sample.

A certified isotopic standard containing ^{239}Pu, ^{240}Pu, ^{242}Pu and ^{244}Pu (Harwell, UK) was also analysed as part of the analytical scheme to assess the accuracy of the isotope ratio data, and the results are presented in Figure 2.27. In general, the expected isotope ratio value was within the precision of each individual result. Where the measured isotope ratio was greater than one standard deviation from the expected value, the results were treated with caution and, where possible, the analyses were repeated. The variation in the precision of each measurement and the overall deviation of the results was much greater for the ETV results than for those acquired by liquid nebulisation, the standard deviations being 8% and 2.3% respectively. The poorer reproducibility of the ETV results (Figure 2.27b) is again a factor of manual injection and the condition of the graphite furnace as discussed above.

Table 2.6: ICP-MS results for bulk Ravenglass sediment sample

a) $^{239+240}$Pu activity (Bq g^{-1}) ± 1σ

Analysis of individual sub-sample		Repeat analysis of single sample	
Liquid Neb.	ETV	Liquid Neb.	ETV
1.041 ± 0.216	0.848 ± 0.017	1.010 ± 0.060	1.107 ± 0.095
1.162 ± 0.200	0.908 ± 0.020	1.041 ± 0.075	1.104 ± 0.085
1.022 ± 0.079	1.089 ± 0.017	0.931 ± 0.114	1.136 ± 0.046
0.929 ± 0.187	1.110 ± 0.056	1.013 ± 0.057	1.113 ± 0.042
0.890 ± 0.200	1.065 ± 0.068	1.008 ± 0.022	1.120 ± 0.059
0.768 ± 0.129	1.342 ± 0.348	1.026 ± 0.038	1.060 ± 0.123
0.870 ± 0.134	1.259 ± 0.083	1.059 ± 0.072	1.106 ± 0.039
0.848 ± 0.071	1.293 ± 0.174	1.013 ± 0.060	
1.072 ± 0.142	1.160 ± 0.202	1.001 ± 0.031	
0.938 ± 0.192	1.417 ± 0.250	0.999 ± 0.065	
1.094 ± 0.180	1.273 ± 0.139		
1.067 ± 0.176	1.278 ± 0.102		
1.092 ± 0.202	1.129 ± 0.037		
1.133 ± 0.083	1.195 ± 0.087		
1.140 ± 0.084	0.689 ± 0.132		
1.181 ± 0.104	0.847 ± 0.151		
1.149 ± 0.065	0.871 ± 0.246		
1.009 ± 0.034	1.331 ± 0.292		
	1.158 ± 0.083		
	1.118 ± 0.187		
	0.940 ± 0.519		
	1.168 ± 0.115		
	1.107 ± 0.086		
	1.126 ± 0.037		
	1.100 ± 0.027		
	1.107 ± 0.023		
Mean = 1.023	Mean = 1.113	Mean = 1.010	Mean = 1.107
σ = 0.122	σ = 0.175	σ = 0.033	σ = 0.023

b) ^{237}Np concentration (pg g^{-1}) ± 1σ

Analysis of individual sub-samples		Repeat analysis of single sample	
Liquid neb.	ETV	Liquid neb.	ETV
91.0 ± 6.1	91.8 ± 9.8	-	137 ± 31
78 ± 16	111 ± 12		133.2 ± 6.5
76.2 ± 4.2	113 ± 38		105.8 ± 6.3
137.8 ± 6.8	76.9 ± 15.6		127.9 ± 9.5
113 ± 11	169 ± 23		119.0 ± 8.0
109.6 ± 4.0	65.3 ± 3.5		108.2 ± 10.9
	81.0 ± 1.9		107.8 ± 8.0
	113 ± 38		
	100.4 ± 5.6		
	86.4 ± 6.9		
	120 ± 13		
	100.8 ± 6.8		
	99.6 ± 1.9		
	111 ± 14		
Mean = 101	Mean = 103	-	Mean = 120
σ = 24	σ = 25	-	σ = 13

2.2.5 Detection limits

Table 2.7 shows the detection limits (based on 3σ background count rate) obtained for liquid nebulisation and ETV, both by multielement scanning and single ion monitoring. The typical range and the average value of the detection limits have been quoted as these are dependent on the performance of the instrument on any particular day. The observed range of the background count rate for both liquid nebulisation and multielement scanning ETV were similar (3-40 cps), and in both cases the average background count rate was 13 cps. However, in general, the signal response for ETV-ICP-MS was greater than that for liquid nebulisation

Figure 2.27 Plutonium standard isotope ratio variations observed during this study for (a) liquid nebulisation and (b) ETV

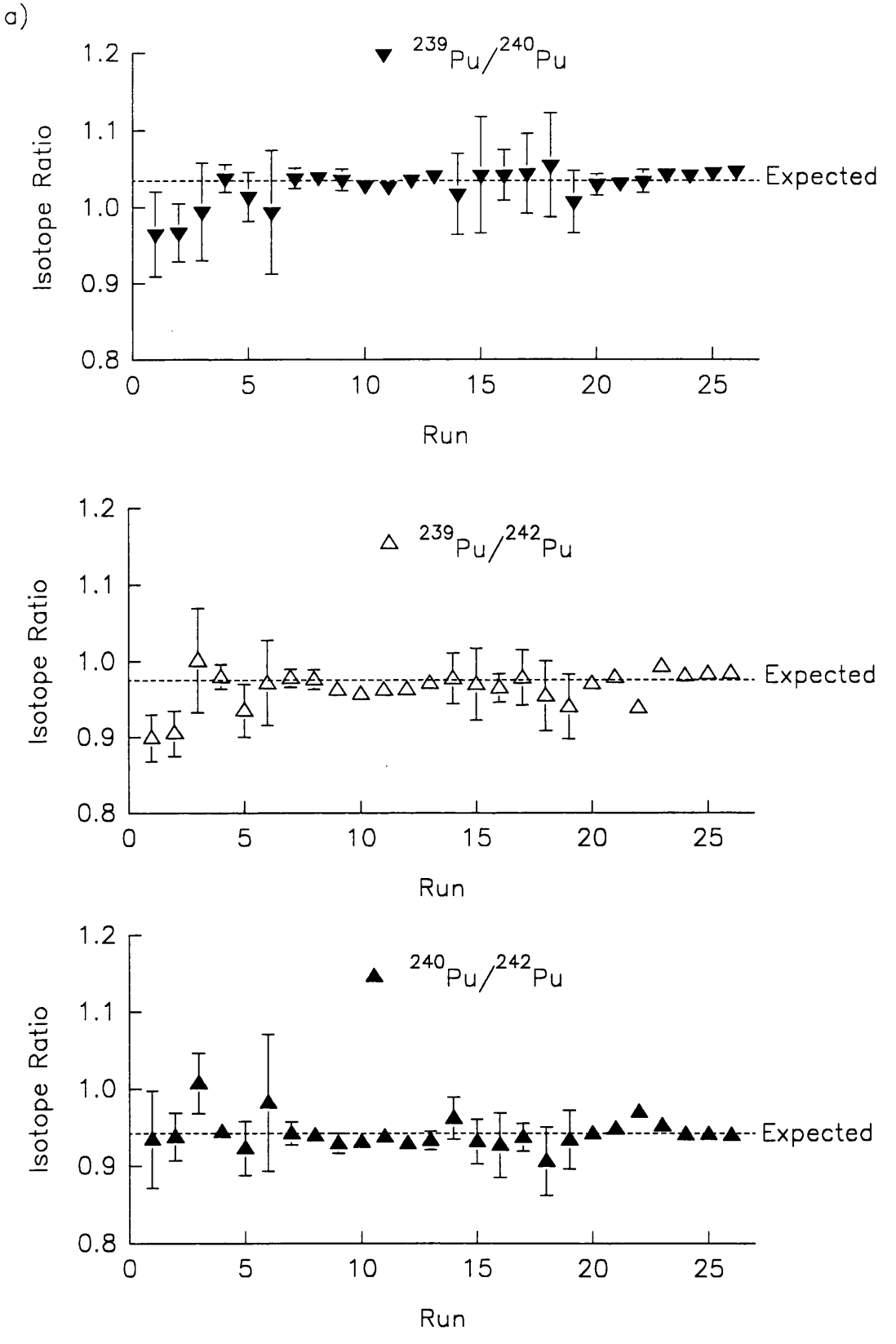

Figure 2.27 (continued)

b)

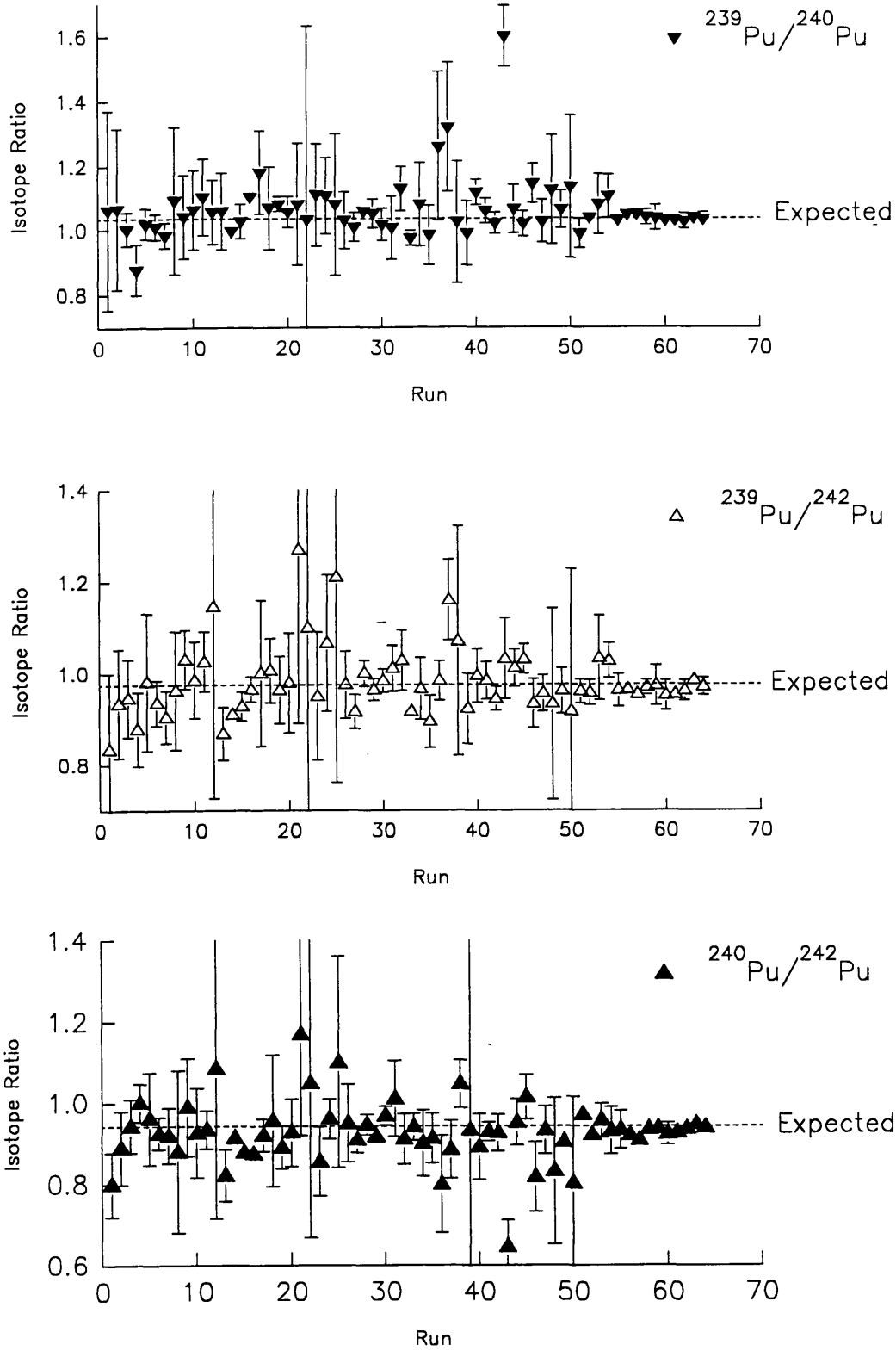

resulting in a reduction in the average detection limit by a factor of 5, with a value of 1 pg ml^{-1}. This corresponds to an absolute detection limit of 50 fg. To substantiate these detection limits, Figure 2.28 shows a spectrum obtained by injection of 50 μl of a standard solution containing 1.1 pg ml^{-1} ^{236}U, 1.9 pg ml^{-1} ^{237}Np, 1.2 pg ml^{-1} ^{239}Pu, ^{240}Pu and ^{242}Pu and 0.4 pg ml^{-1} ^{244}Pu, along with a spectrum obtained by injection of 50 μl of 2% HNO_3 blank solution. All the peaks are clearly distinguishable above the background count rate. In the case of single ion monitoring, both the background count rate and the signal response are increased but with a resultant detection limit lower than that for multielement scanning, the average absolute value being 20 fg. During this study the best absolute detection limit obtained was 0.7 fg, obtained by single ion monitoring.

Table 2.7: ICP-MS detection limits observed during this study

	Liquid nebulisation	ETV Multielement scanning	ETV Single ion monitoring
Range (pg ml^{-1})	1 - 16	0.3 - 3.0	0.014 - 1.8
Typical value	5 pg ml^{-1}	1 pg ml^{-1}	0.4 pg ml^{-1}
Background counts	3 - 30 cps	4 - 39 cps	2 - 340 cps

2.2.6 Summary

ICP-MS is a rapid and sensitive technique which can provide information on both isotopic and elemental composition within one sample in a matter of minutes. Once the instrument parameters have been optimised, the operation of an ICP-MS is relatively simple enabling a high sample throughput. Using liquid nebulisation the performance of the ICP-MS used in this study was in general reliable with a sensitivity between 2 and 10 cps/ppt. The performance of the mark 1 ETV unit was more erratic, with the sensitivity of the system varying considerably from day to day and even within days. However, on average, the response of the instrument using ETV was 5 times that of liquid nebulisation giving average detection limits for isotopes of the actinide elements of 1 ng ml^{-1}. One of the main advantages of

Figure 2.28 ETV-ICP-MS spectra of a 50μl injection of (a) a standard solution containing 1.08 pg ml^{-1} ^{236}U, 1.93 pg ml^{-1} ^{237}Np, 1.16 pg ml^{-1} ^{239}Pu, 1.20 pg ml^{-1} ^{240}Pu, 1.24 pg ml^{-1} ^{242}Pu and 0.40 pg ml^{-1} ^{244}Pu, and (b) a 2% HNO_3 solution

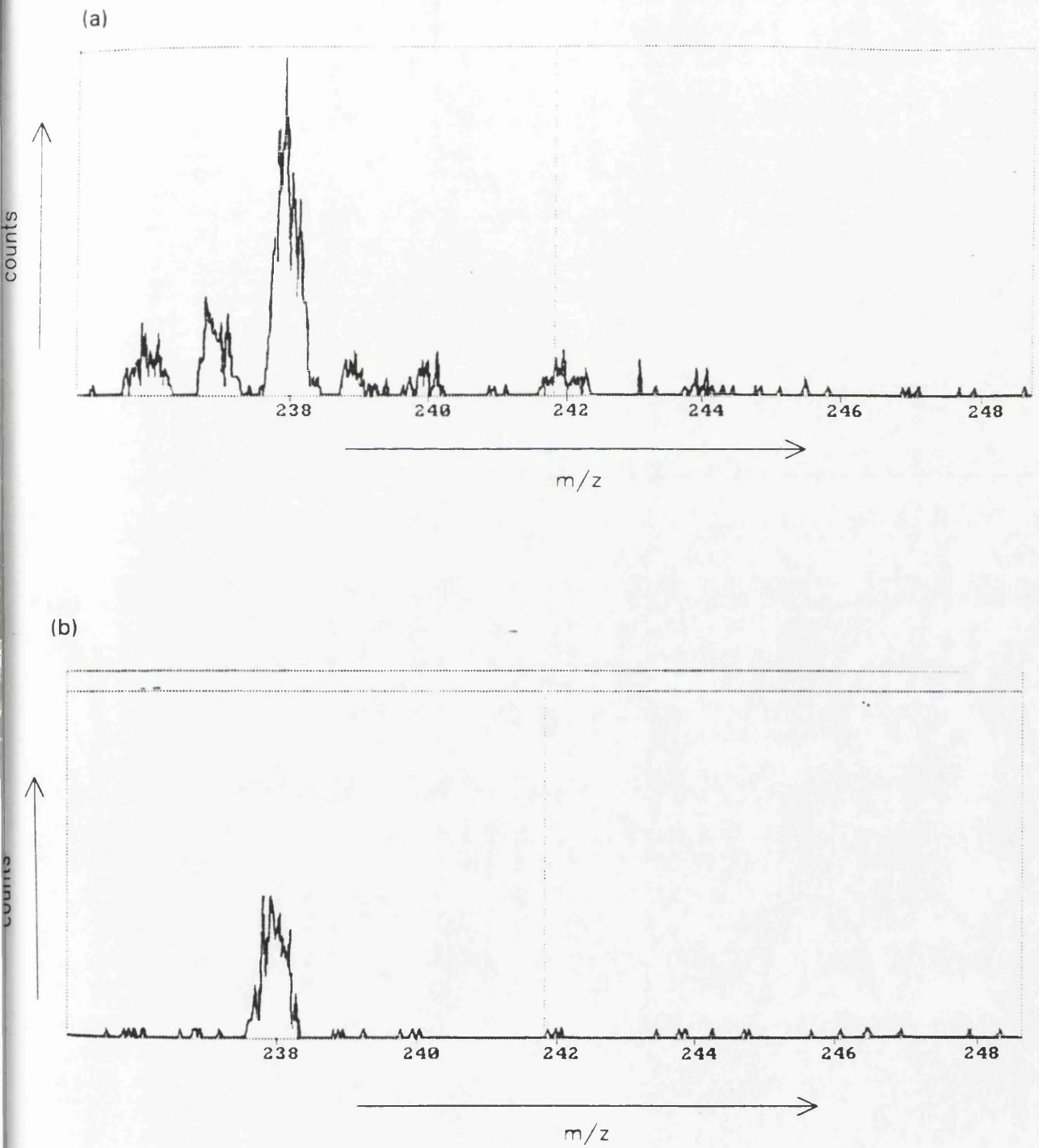

using ETV as opposed to liquid nebulisation, is the small sample volumes required for analysis.

2.3 LIMITATIONS FOR THE ANALYSIS OF 'REAL' SAMPLES

Section 2.2 discussed the performance of the ICP-MS system when analysing standard solutions. However, in the analysis of 'real' samples the effect of the physical form and content of the sample must also be taken into consideration as these may cause interference with the analyte species and disrupt the performance of the ICP-MS system.

2.3.1 Spectroscopic Interferences

The interferences observed in ICP-MS fall into two main categories; spectroscopic interference from isobaric, polyatomic and oxide ions, and non-spectroscopic interference including matrix effects and physical effects from high dissolved solid concentrations. These are discussed below.

2.3.1.1 Polyatomic and Oxide Interferences

Background spectral interferences can be formed from the plasma gas, gases entrained into the plasma or from the sample solvent. The main interfering species are those formed from the dominant species in the plasma, ie Ar, H and O which can combine together and with elements from the sample matrix to form polyatomic ions. The severity of background interferences depends strongly on the choice of solvent used, with water and nitric acid producing similar background spectra, while hydrochloric and sulphuric acids result in much more complex spectra [Jarvis *et al.*, 1992]. Most of the interfering species are well characterised and occur below mass 80. Tables have been produced which list all the possible combinations of background ions and the major and minor isotopes of elements with which they might interfere [Tan and Horlick, 1986]. Less detail is given on the magnitude of the species as this is dependent on the instrument design and the operating conditions [Gray and Williams, 1987].

In this study 2% nitric acid was chosen as the solvent to maintain the background species to as low a level as possible while maintaining the analytes in solution. A background spectrum produced by aspiration of 2% HNO_3 (Figure 2.29) indicates that the background in the mass region of interest is very low. Figure 2.28b also shows a background spectrum obtained by ETV-ICP-MS. This shows a small peak at ^{238}U which is present at a low concentration (< 5 pg ml^{-1}) in Aristar HNO_3.

Another source of spectroscopic interference is from refractory oxides which occur either as a result of incomplete dissociation of the sample or from recombination in the plasma tail. The level of oxides in general does not exceed 1.5 % although this is again dependent on the conditions in the plasma, particularly on the nebuliser flow rate [Horlick *et al.*, 1985]. Doubly charged ions also occur, especially for those elements which have low second ionisation energies. In this case reducing the nebuliser flow rate increases the level of doubly charged ions as a result of the increased plasma temperature, although under normal operating conditions the levels remain less than 1 % [Jarvis *et al.*, 1992].

In the m/z region from 236 to 242, the only polyatomic species to cause interference is that from MH^+, and in most cases the magnitude of this species is insignificant compared to the background count rate. However, ^{238}U concentrations in environmental samples are 3-4 orders of magnitude or more higher than the concentrations of plutonium and neptunium. In this case the $^{238}UH^+$ species can be a significant contribution to the ^{239}Pu peak. This is illustrated in Figure 2.30 which shows a spectrum obtained from the aspiration of a 1 μg ml^{-1} uranium solution. This spectrum was obtained in the early stages of this study and shows a spurious precursor signal at approximately m/Z = 237.4. This was an artifact of the early system and was removed by changing the wiring of the quadrupole. The $^{238}UH^+$ species was observed using both liquid nebulisation and ETV. The $^{238}UH^+/^{238}U^+$ ratio was found to vary from $(2.7 \pm 0.2) \times 10^{-5}$ to $(3.2 \pm 0.3) \times 10^{-5}$ during this study. To maintain the UH^+ interference to below background levels, it is necessary to reduce the uranium concentration in the final solution to below 100 ppb.

Figure 2.29 Liquid nebulisation, ICP-MS spectrum of a 2% HNO_3 solution over the mass range of interest

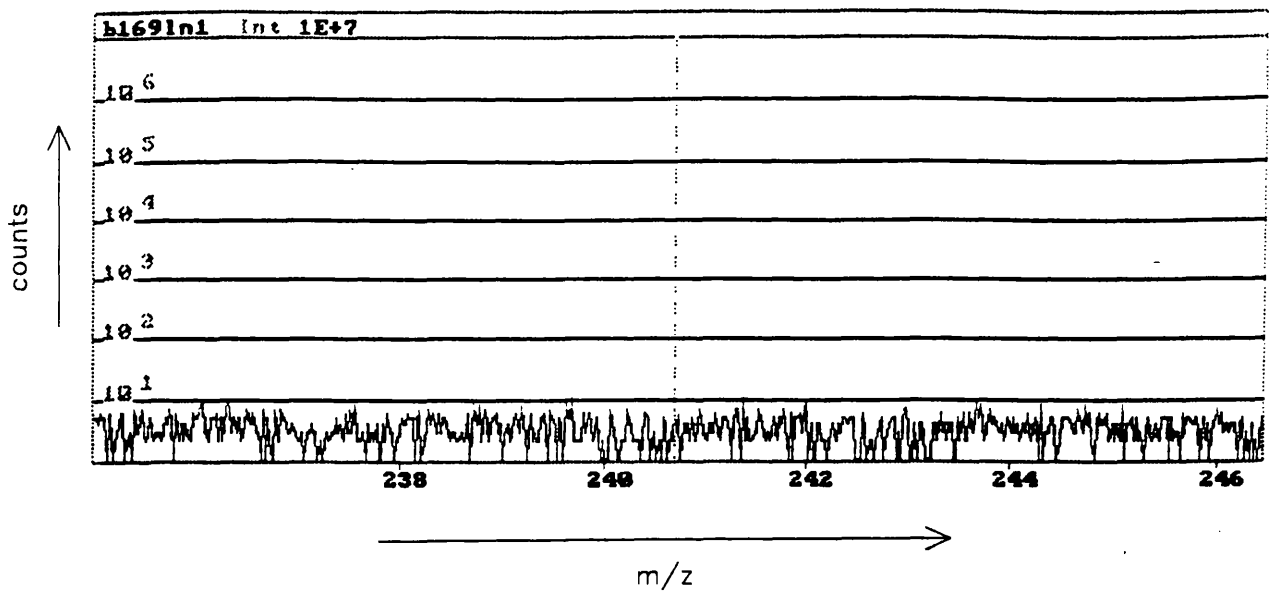

Figure 2.30 Liquid nebulisation, ICP-MS spectrum of a solution containing 1μg ml^{-1} ^{238}U, showing the $^{238}UH^+$ interference at mass 239

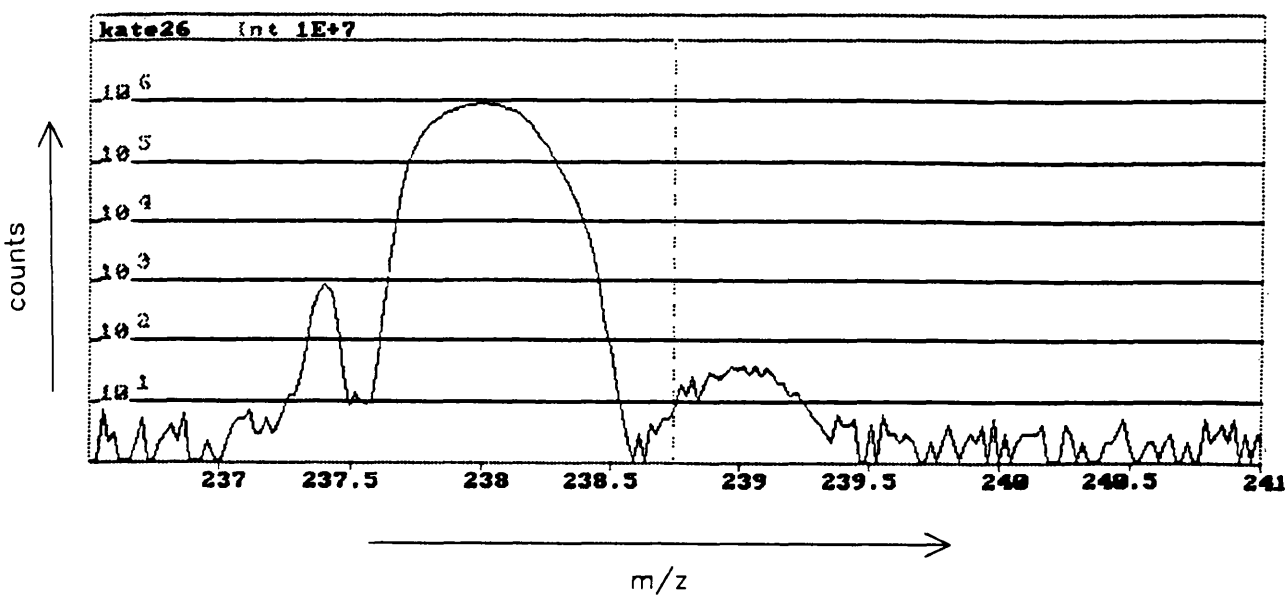

2.3.1.2 Isobaric Interferences

Isobaric interferences can occur anywhere in the mass spectrum where two elements have isotopes of similar mass (to approximately within 0.7 a.m.u.) which are unresolved by the ICP-MS system. The severity of the interference depends on the composition of the sample and in some cases can be reduced or removed by chemical separation. Usually, isotopes which are free from isobaric interference can be found and used for determination of the elemental concentrations.

In the mass region of interest there are two isobaric interferences, ^{238}U with ^{238}Pu, and ^{241}Am with ^{241}Pu. The first of these is insignificant as the concentrations of the short-lived ^{238}Pu are undetectable by ICP-MS, especially when considering the decontamination factors which would be required to remove ^{238}U from any sample (even the concentration of uranium in *Aristar nitric acid at 2% v/v would mask the ^{238}Pu signal). The ^{241}Am interference on ^{241}Pu is more significant. However americium can be removed easily from the sample without loss of plutonium and the decontamination factors checked by γ-spectrometry.

2.3.2 Non-spectroscopic interferences

Non-spectroscopic interferences include the physical effects caused by the dissolved solid content of the sample and suppression or enhancement effects which occur in the presence of high concentrations of matrix or concomitant elements.

The continuous aspiration of a high dissolved solid content sample results in deterioration of the analytical precision and a rapid decrease in the signal during the first 20 min, after which the response stabilises. These effects are caused by the deposition of sample material on the sampling orifice, resulting in fewer ions entering the system and reducing the efficiency of the extraction system [Jarvis *et al.*, 1992]. To avoid this affect, the total dissolved solids content of samples were maintained at less than 0.2% w/v throughout the study.

A review of the effects on analyte signals in the presence of concomitant elements

presents a confusing picture. In general, suppression of the analyte signal is observed [Thompson and Houk, 1987], but some studies have reported both signal enhancement and no effect [Beauchemin *et al.*, 1987]. For example, Olivares and Houk [1986] investigated the effect of increasing salt concentrations on the signal obtained from a 1.2 mg l^{-1} solution of Co. Suppression of the Co ion signal was observed for salt concentrations above 0.01 M, the degree of suppression increasing with decreasing ionisation energy (Na > Mg > I > Br > Cl). This suggests a shift in ionisation equilibrium as a possible mechanism. These findings were contrary to those of Beauchemin *et al.* [1987] who found that 0.01M solutions of Na, K, Cs, Mg, and Ca induced enhancement of the signals obtained from 100 μg l^{-1} solutions of Cr, Mn, Ni, Co, Cu, Zn, Cd and Pb. Of the matrix elements investigated, B, Al and U were found to cause signal suppression, while Li had no effect. It was concluded that because the easily ionised elements caused signal enhancement, a shift in the ion-atom equilibrium in the plasma was not the only mechanism to cause these effects as, in such a case, signal suppression would be expected. The deposition of refractory oxides on the interface was suggested as the cause for the signal suppression observed with U, Al and B. The matrix effect was found to be strongly dependent on the nebuliser flow rate [Tan and Horlick, 1987] although plasma power and sampling depth appeared to have little significance. A strong mass dependence of the matrix effect has been observed by several authors, with heavier matrix elements causing more severe suppression and being affected less that lighter elements [Gregoire, 1987; Gillson *et al.*, 1988; Tan and Horlick, 1987; Beauchemin, 1987]. An explanation of this could be space charge effects (see section 2.1.5.3).

In this study, the effect of sample matrix on the signal response for actinide nuclides was investigated by increasing the dissolved NaCl content of a standard solution from 0 to 1% w/v. The results, shown in Figure 2.31, reveal that for both liquid nebulisation and ETV, increasing the NaCl content of the sample resulted in a suppression of the analyte signal. This was more marked in the case of ETV, with the signal dropping to 18% of the original value when the NaCl content was increased to 1.0% w/v. In all cases, the results were corrected for drift in the original signal response throughout the experiment.

Figure 2.31 Suppression of analyte signal by NaCl for (a) liquid nebulisation and (b) ETV

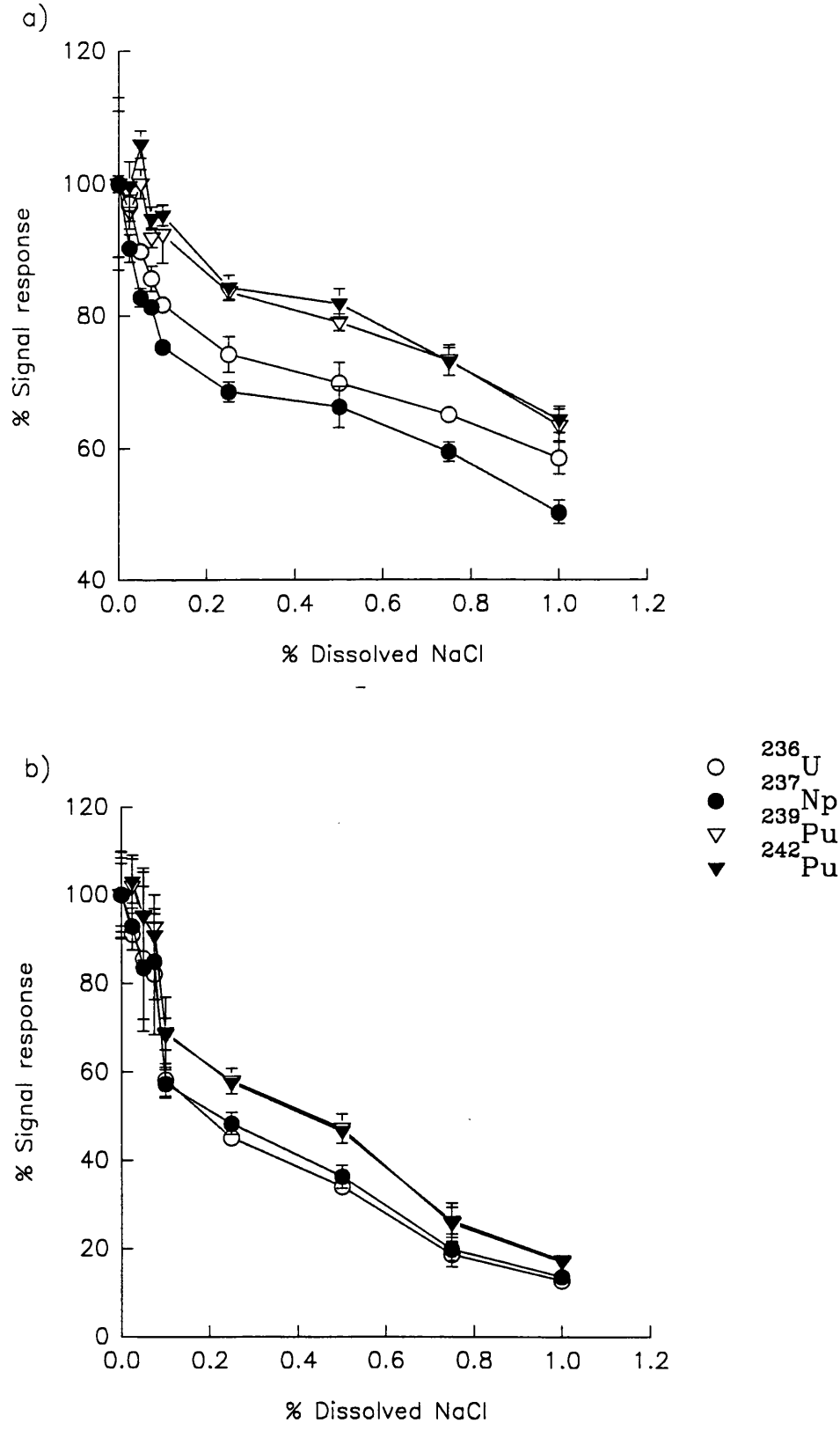

Although in the above experiment NaCl was used to simulate the effect of sample matrix on the analyte signal, for environmental samples the sample matrix is complex and not easily reproduced using laboratory solutions. To further investigate the effect of sample matrix on the analyte signal a sediment sample taken from Loch Long in the Clyde Sea Area was prepared in the same manner as the samples (see section 3.3) along with a reagent blank. The final solutions were split into three and spiked with ^{237}Np to concentrations of 10, 50 and 100 ng ml^{-1} respectively. In addition 10, 50 and 100 ng ml^{-1} solutions of ^{237}Np were made up in 2% HNO_3. All the samples were spiked to 100 ng ml^{-1} of ^{236}U which was used as an internal standard. The uncorrected signal responses obtained for each matrix are shown in Figure 2.32a which reveals that signal suppression was in the order: sediment matrix > reagent blank > 2% HNO_3 blank. Interestingly the suppression observed for the reagent blank and the sediment matrix solutions were of a similar magnitude, indicating that the 'purity' of the samples is restricted not by the original matrix of the samples but by the solutions used during sample preparation. It is also interesting to note that the sediment sample contained a small concentration of ^{237}Np as indicated by the intercept of the y-axis. This was not observed with the reagent blank and can therefore be attributed to a ^{237}Np contribution from the sediment sample.

Several methods have been proposed to compensate for non-spectroscopic interferences, including using an internal standard [Thompson and Houk, 1987], isotope dilution [McLaren *et al.*, 1987], standard addition [Beauchemin *et al.*, 1987] and flow injection [Vickers *et al.*, 1989]. In this study a system of internal standardisation was used for ^{237}Np analysis and isotope dilution for plutonium analysis. Figure 2.32b shows the results of the above experiment normalised to the ^{236}U counts. This supports the evidence that ^{236}U is a suitable internal standard for ^{237}Np analysis, capable of correcting for both instrument drift and for matrix suppression within each individual sample.

2.4 SAMPLE REQUISITES SUMMARY

As discussed above, the analysis of real samples by ICP-MS presents some restrictions on the final sample solution to be aspirated into the plasma. The

Figure 2.32 Effect of matrix on ^{237}Np calibration curves with (a) no internal standard and (b) ^{236}U used as an internal standard, by ETV-ICP-MS

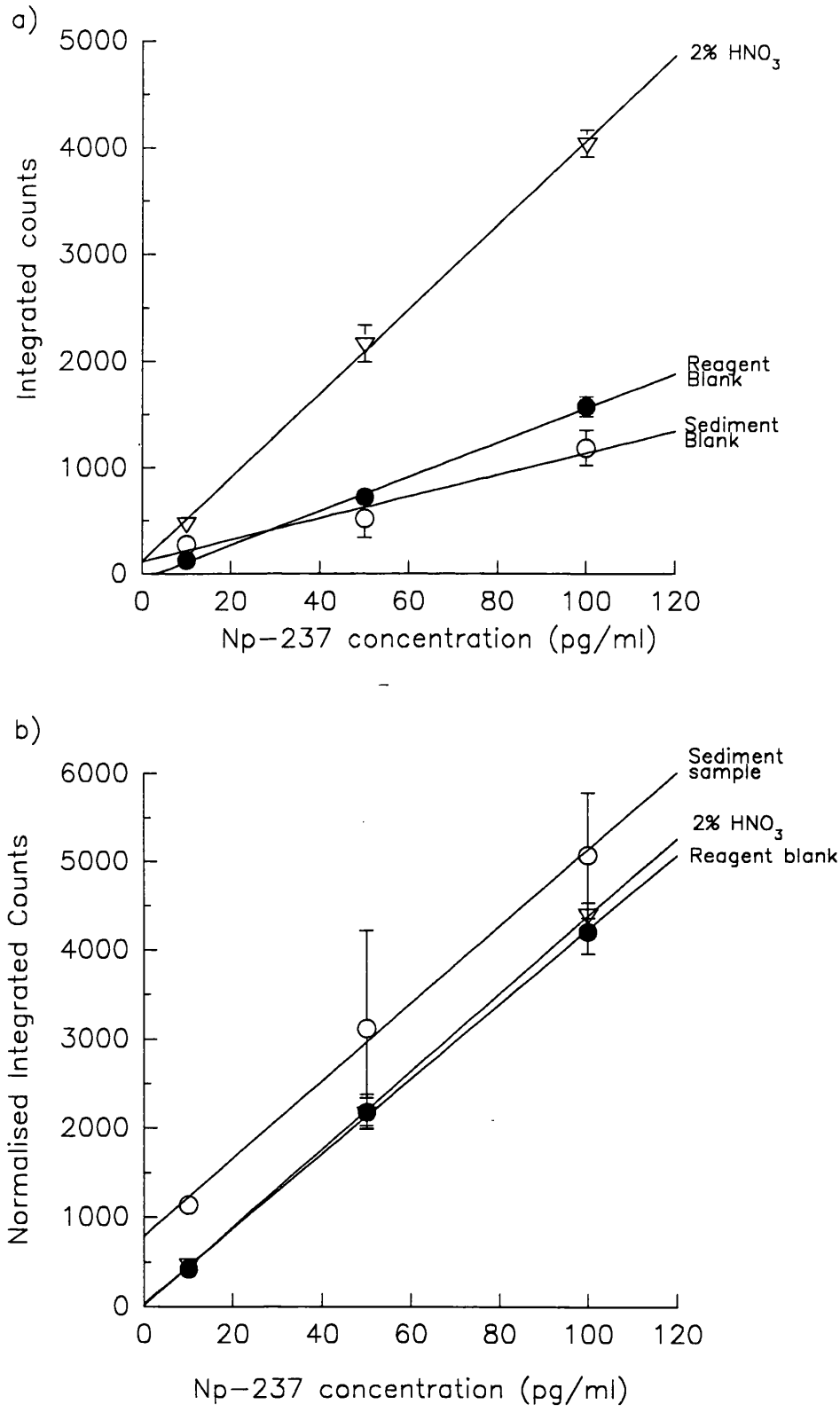

dissolved solids content limitation of 0.2% w/v coupled with the detection limits of the system, the matrix suppression effects, and the ultra-trace levels of neptunium and plutonium in environmental samples implies that some sample preconcentration is required. In addition to this, the $^{238}UH^{+}$ interference with ^{239}Pu limits uranium concentrations to below 100 $\mu g\ ml^{-1}$ in the final solution. Another consideration is the isobaric interference of ^{241}Am with ^{241}Pu. In conclusion, for the analysis of environmental levels of plutonium and neptunium, ICP-MS is not a panacea for an environmental chemist tired of lengthy laboratory procedures, as some chemical pretreatment is required.

CHAPTER 3 : DEVELOPMENT AND VALIDATION OF A METHOD FOR ANALYSIS OF SEDIMENT SAMPLES

3.1 INTRODUCTION

In Chapter 2 it was shown that ICP-MS is a sensitive and rapid technique capable of the determination of ^{237}Np concentrations and $^{240}Pu/^{239}Pu$ atom ratios in environmental samples. Originally, it was envisaged that ICP-MS could be applied to the analysis of environmental samples without the laborious and lengthy sample preparation procedures which are required for α-spectrometry. However, as discussed in section 2.3.2, samples presented to the ICP-MS are restricted to a solids content of less than 0.2% (w/v), introducing a dilution factor of over 500 for solid samples. If environmental samples were analysed directly in this way, the actinide concentrations would be well below the detection limits of the system. This can be overcome by preconcentrating the analytes of interest after separating them from the bulk matrix. In addition, it was shown that the high natural abundance of ^{238}U, led to a $^{238}UH^+$ interference with ^{239}Pu, and increased the risk of the ^{238}U peak tailing into the ^{237}Np and ^{239}Pu peaks (see section 2.3.1.1). Application of ICP-MS to the determination of ^{237}Np concentrations and $^{240}Pu/^{239}Pu$ atom ratios in environmental samples therefore requires sample preparation procedures which are capable of separating Np and Pu from the bulk matrix and uranium.

In this chapter, chemical separation techniques for the actinides are discussed generally, followed by details of a method adapted in the present study for analysis of sediment samples by ICP-MS. The technique has been validated by the analysis of intercomparison samples which were analysed independently, using different chemical separation and analysis techniques.

3.2 CHEMICAL SEPARATION TECHNIQUES FOR THE ACTINIDES

One of the key aspects of the solution chemistry of the actinides which is important for their analytical separation is their ability to form multiple oxidation states (see section 1.2.1). Other important properties include covalent bonding

with oxygen and halogens, with the stability of the bonds decreasing in the order $M^{4+} > MO_2^{2+} \approx M^{3+} > MO_2^{+}$, and the formation of anionic complexes between M^{4+} and fluoride, chloride or nitrate (see section 1.2.2 and 1.2.3). Both solvent extraction and anion exchange, the main separation techniques used in actinide chemistry, rely on the manipulation of the oxidation states of the actinides to create or destroy these complexes in order to obtain the desired separation of the elements [Harvey and Thurston, 1988].

The industrial reprocessing of irradiated nuclear fuels and the extraction of uranium from ores have resulted in wide scale research into the separation chemistry of the actinides. Some of the basic techniques are outlined below, with particular reference to methods which have been used in this study. Recent developments in the extraction chemistry of the actinides are described by Ahrland [1986]; Musikas, [1987]; and Myasoedov [1987]. In addition, Hursthouse [1990] has reviewed the techniques available for the separation of ^{237}Np from solution, with reference to Pu and U.

3.2.1 Co-precipitation

Co-precipitation is a technique widely used to isolate trace elements from large volume solutions and provides an effective method for pre-concentrating and separating the actinides from environmental matrices. The extent of co-precipitation of the actinides is dependent on their oxidation states, which can be manipulated to provide effective separation from solution. For example, iron hydroxide co-precipitation schemes are used from slightly alkaline solution as actinides in their lower oxidation states (M^{3+} and M^{4+}) readily co-precipitate with small quantities of iron hydroxide, whereas actinides in their higher oxidation states (MO_2^{+} and MO_2^{2+}) remain in solution [Lovett et al., 1990]. Other commonly used methods include co-precipitation of actinides with rare-earth fluorides or calcium oxalate from acid solutions [Lovett et al., 1990; Harvey and Thurston, 1988]. These techniques provide a good preliminary step for separating the actinides from many elements and anions, but are not selective enough to provide the pre-concentration and isolation factors required for the final solution for ICP-MS analysis.

3.2.2 Liquid-liquid extraction

Liquid-liquid extraction (or solvent extraction) is based on the differential distribution of actinide complexes between two immiscible liquid phases, normally an aqueous and an organic phase [De et al., 1970]. The vast range of organic reagents which is used to extract actinides from various aqueous phases can be split into three main groups; anionic extractants, where the chelating agents are coordinated to the metal ions as anions (e.g. β-diketones); neutral extractants, where extractable compounds are formed by electrostatic attraction (e.g. organophosphates and amines); and mixtures of extractants which have a synergistic effect, resulting in a higher extraction ability than when each extractant is used separately [Ahrland, 1986; Hursthouse, 1990].

3.2.2.1 Anionic extractants

Strong complexes of actinide ions are formed with the β-diketones, the tropolones, the 8-hydroxyquinolines (oxines), ethylenediaminetetraacetic acid (EDTA), and other complexones [Ahrland, 1986]. Of these, the most widely used chelating agent is the β-diketone: thenoyltrifluoroacetone (TTA).

TTA is slightly soluble in water and highly soluble in organic solvents. In benzene, it exists in two forms, 11% as the keto form and the rest as the enol form, which forms complexes through dissociation of the OH group [Poskanser and Forman, 1961]. The extraction mechanism can be described as:

$$M^{z+}(aq) + zHTTA(org) \rightleftharpoons M(TTA)_z(org) + zH^+$$

The extraction of different metal ions by TTA is highly dependent on pH (see Figure 3.1), enabling the separation of one metal ion from another [Poskanser and Forman, 1961]. For the actinides, M^{4+} ions are more strongly complexed and extracted than other oxidation states, with Pu^{4+} forming a stronger complex than Np^{4+} [Ramanujan et al., 1978].

Quantitative extraction of Pu^{4+} and Np^{4+} from 0.5M HCl can be achieved using

Figure 3.1 Effect of pH on the extraction of actinides by HTTA (benzene) [Hursthouse, 1990; Stary, 1964]

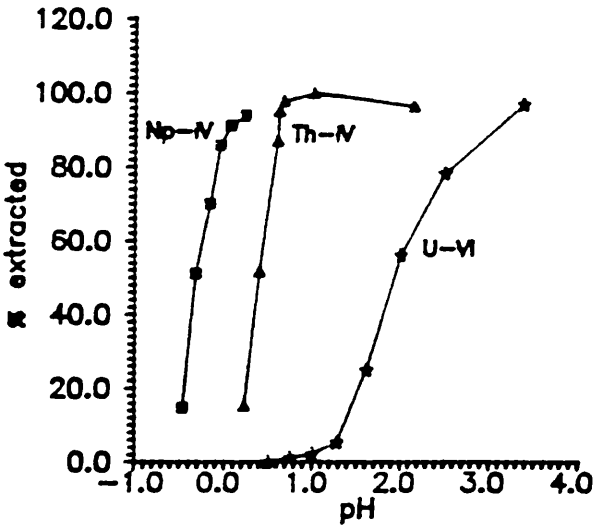

0.5M TTA(xylene), with 99% extraction occurring after an optimal equilibration time of 10 - 15 mins [Moore, 1957]. However, for environmental samples, separation from the bulk matrix is required prior to TTA extraction as the salt content of the samples increases the solubility of TTA in the aqueous phase and formation of ferric iron causes interference by simultaneous extraction [Hursthouse, 1990].

3.2.2.2 Neutral extractants

For extraction with neutral or cationic extractants, the properties and concentration of the anions present in the aqueous phase are very important. Efficient extraction is only possible if the anion can participate in the formation of mixed complexes which can be accepted into the organic phase. An example of this is the Purex process where tetra- and hexavelant actinides are extracted by tributly phosphate (TBP). The reactions taking place from nitric acid solutions are:

$$M^{4+}(aq) + 4NO_3^-(aq) + 2TBP(org) \rightleftharpoons M(NO_3)_4(TBP)_2(org)$$

and

$$MO_2^{2+}(aq) + 2NO_3^-(aq) + 2TBP(org) \rightleftharpoons MO_2(NO_3)_2(TBP)_2(org)$$

respectively [Ahrland, 1986]. The extraction efficiency of TBP for the actinides is highly dependent on the concentration of nitric acid in the aqueous phase. Initially extraction increases with acid concentration, but reaches a maximum at approximately 5 M, after which competing reactions, such as the formation of HNO_3.TBP in the organic phase and anionic nitrate complexes in the aqueous phase, reduce the efficiency of the extraction [Ahrland, 1986]. The Purex process using TBP is one of a wide range of processes involving neutral extractants which have been utilised by the nuclear industry. A summary of these is shown in Table 3.1.

The ketones and ethers are also effective extractants for the actinides. For example, di-isopropyl ether can be used to quantitatively extract Np, Pu and Am from nitric acid solutions. Extraction decreases in the order $Pu^{4+} > NpO_2^{2+} > PuO_2^{2+} > Np^{4+}$ (see Figure 3.2)[Grindler, 1962]. However, the extraction of the actinides with di-isopropyl ether is poor compared to other extractants and no extraction takes place from hydrochloric acid solutions.

3.2.3 Ion exchange

Ion exchange is a commonly used analytical technique which involves the exchange between free species in solution with species immobilised or sorbed onto an inert solid phase, as described by:

$$A_{resin} + B_{soln} \rightleftharpoons B_{resin} + A_{soln}$$

Both anionic and cationic resins are available, usually with copolymers of styrene and divinylbenzene to provide a framework for the active ion exchange groups. The functional groups present determine the exchange characteristics of the resins. For example, strong cation exchangers possess $-SO_2OH$ groups and strong anion exchange resin contains $-NR_3OH$. Anionic exchange is most commonly used for actinide separation [e.g. Burney and Harbour, 1974; Lally and Eakins, 1978; Harvey

Table 3.1: Extraction processes used in the nuclear industry

Process	Extractant	Comments	Reference
BUTEX	bis(2-butoxyethyl) ether (butex)	initial waste reprocessing technique	Howells et al., 1958
REDOX	methyl isobutyl ketone (MIBK)	early technique used for large scale irradiated fuel processing	Burney and Harbour, 1974
PUREX	tributly phosphate (TBP)	technique now used in spent fuel reprocessing, selective for U and Pu, good chemical and radiation stability	De et al., 1970
TUREX	octylphenyl-N,N-diisobutlycarbomoyl-methylene phosphine oxide (CMPO)	isolates actinides in III, IV and VI oxidation states, from high-level radioactive wastes	Schultz and Howitz, 1987; Musikas, 1987
DAPEX	diethylhexylphosphoric acid (HDEHP)	used to recover uranium from ores	Mannone et al., 1984; Musikas, 1987

Figure 3.2 Extraction of actinides by diisopropylether from HNO_3 [Hursthouse, 1990; Grindler, 1962]

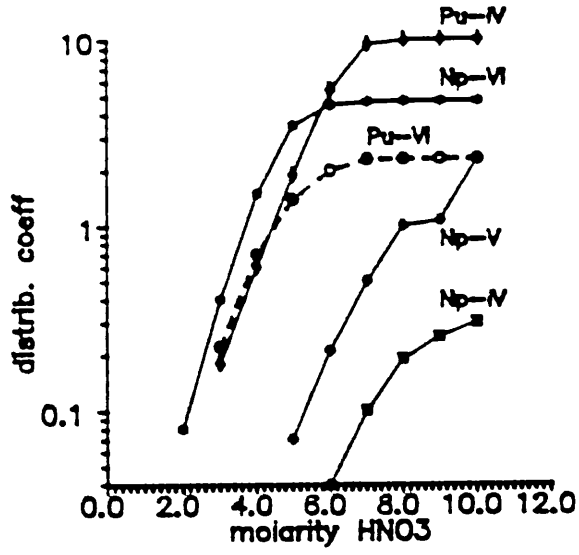

and Thurston, 1988; Lovett et al., 1990].

The adsorption behaviour of a given solute on ion exchange resins is represented by the equilibrium distribution coefficient. This can be defined either as a volume distribution coefficient, D_v (amount of solute adsorbed per millilitre resin bed/amount of a solute per millilitre of solution), or as a weight distribution coefficient, D_g (amount of solute adsorbed per gram dry resin/amount of a solute per ml of solution) [Saito, 1984].

The distribution coefficients for the adsorption of the actinides by Dowex 1X8, an anion exchange resin used in this study, from both nitric acid and hydrochloric acid are shown in Figure 3.3. Although the separation characteristics are better from nitric acid than hydrochloric acid, the oxidising nature of nitric acid can lead to disruption of the organic resin bed, making its application impractical [Hursthouse, 1990].

Figure 3.3 Anion exchange distribution coefficients for aqueous actinide ions on Dowex 1X8 [Coleman, 1965; Burney and Harbour, 1974; Satio, 1978; Harvey and Thurston, 1988]

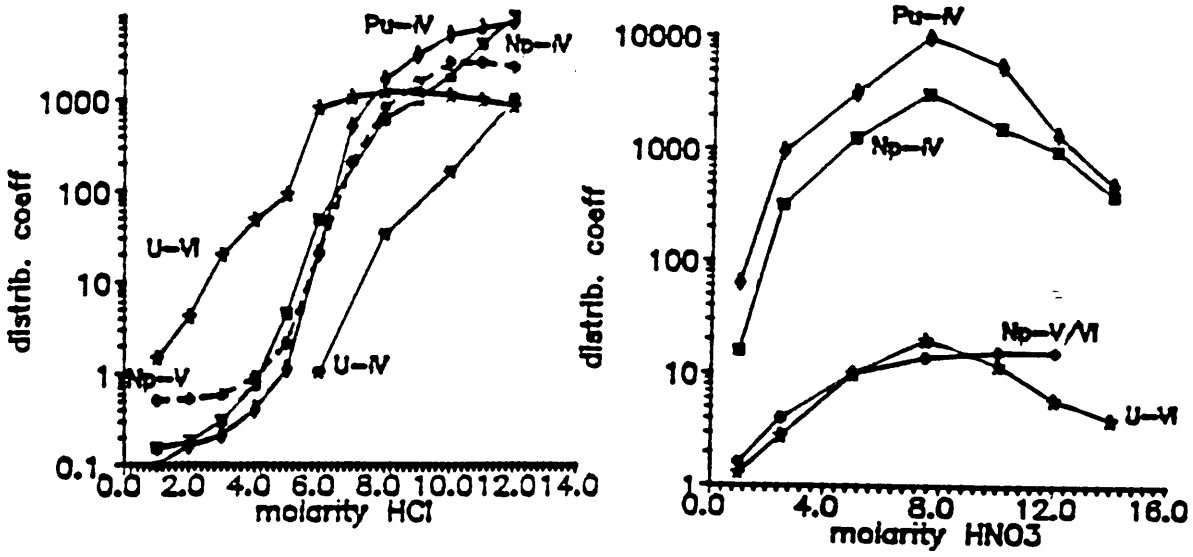

3.3 METHOD DEVELOPMENT

For the determination of plutonium and neptunium from marine sediments by ICP-MS, an analytical procedure was required which would:

i) separate the actinides from the bulk matrix to enable some preconcentration of the analytes prior to analysis, whilst restricting the dissolved solid content of the final sample to less than 0.2% (w/v)

ii) eliminate uranium from the sample to the extent where the UH^+ interference in the ^{239}Pu peak was below detectable limits and to reduce the risk of tailing of the ^{238}U peak in to the ^{237}Np and ^{239}Pu peaks

iii) involve simple chemical separation techniques to take full advantage of the less stringent sample requirements of ICP-MS compared to α-spectrometry.

This study followed on from the work of Hursthouse [1990], who developed a

Figure 3.4 A schematic summary of the analytical procedure used to determine ^{237}Np concentrations and $^{240}Pu/^{239}Pu$ atom ratios in marine sediments by ICP-MS, adapted from Hursthouse [1990] and Byrne [1986]

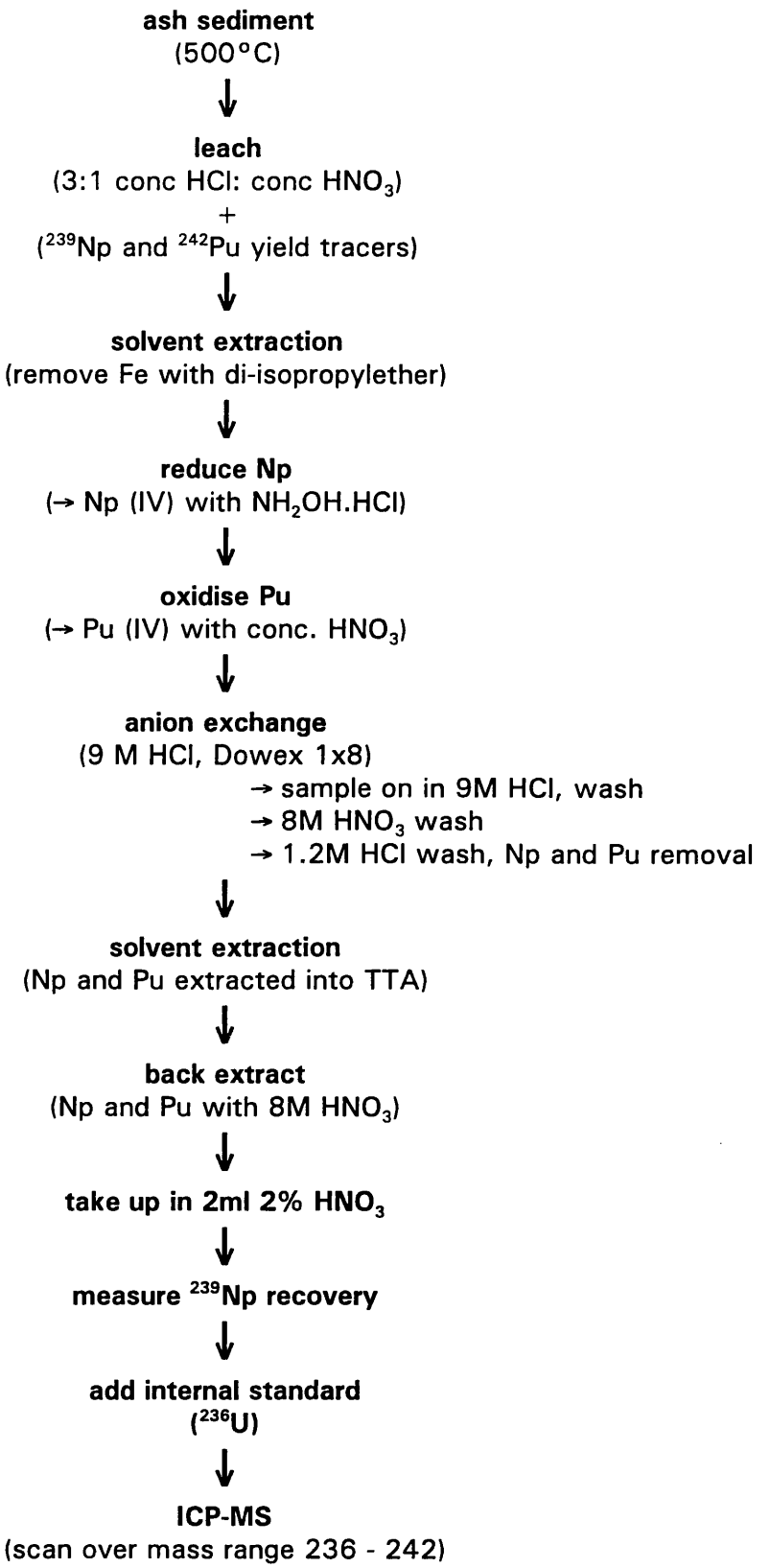

method for the analysis of ^{237}Np by ICP-MS based on an analytical procedure used by Byrne [1986] to determine ^{237}Np by neutron activation. This method was investigated and developed for the analysis of ^{237}Np and plutonium isotopes from the same sample by ICP-MS. A summary of the resulting procedure is shown in Figure 3.4.

3.3.1 Radiochemical yield tracers

For accurate determination of radionuclide concentrations it is essential to account for any losses which may occur during the chemical procedures. As discussed in section 2.2.4.1, the ideal technique is isotope dilution where an isotope with similar characteristics as the determinand is added to the sample, enabling simultaneous determination of both the determinand and yield tracer from the final solution, thus reducing errors associated with matrix effects and systematic errors which may occur from the use of more than one detection system. This is possible for the determination of ^{239}Pu and ^{240}Pu by ICP-MS by the addition of ^{242}Pu which has a half-life of 3.76×10^5 years. For ^{237}Np analysis, a potential candidate for a yield tracer is ^{236m}Np with a half-life of 10^7 years [Landrum et al., 1969], but isotopically pure standards are difficult to produce due to ^{237}Np contamination [Hursthouse, 1990]. There are also no strong α-emitting isotopes of Np which can be used as a tracer for α-spectrometry. As a result, the most commonly used chemical yield tracer for ^{237}Np analysis is the short-lived isotope ^{239}Np which can be determined by γ or β-spectrometry [Holm and Nilsson, 1980; Holm, 1984; Harvey and Lovett, 1984; Hursthouse, 1990].

In this study, 1 - 2 ml aliquots of ^{242}Pu (0.1445 Bq ml^{-1}) in 8 M HNO_3, were weighed into each sample during the preliminary leaching stage along with aliquots of ^{239}Np. ^{239}Np is the short-lived (2.35 day half-life) daughter of ^{243}Am. Separation of the daughter from the parent can be achieved by a single cycle TTA solvent extraction [Byrne, 1986; Hursthouse, 1990; and section 3.2.2.1]. A solution of ^{243}Am (obtained by A. Hursthouse from E. Hamilton and R.Clifton of I.M.E.R.) with an activity of approximately 4 kBq was separated into (nominally) 800 Bq aliquots which were placed into 10 ml solutions of 0.5 M HCl, containing 0.5 g of hydroxylamine hydrochloride ($NH_2OH.HCl$, BDH AnalaR) [Hursthouse, 1990]. An

equal volume of 0.2 M TTA (toluene) was added to this solution and ^{239}Np extracted into the organic layer by mixing thoroughly for 10 - 15 minutes. The solutions were then centrifuged to separate the layers, and the upper, organic layer removed and retained. ^{239}Np was back-extracted from this solution with 5 ml of 8 M HNO_3. Again, the layers were separated by centrifugation, the 8M HNO_3 pipetted off into a 20 ml polythene pot and counted (see section 3.3.6). Weighed aliquots of the spike were then added to each sample. The ^{243}Am solution was left for at least 2 weeks to allow time for the solution to reach secular equilibrium, after which ^{239}Np could once again be milked from its parent.

3.3.2 Spiked sediment sample

To investigate the application of some of the techniques outlined in section 3.2, and the procedure shown in Figure 3.4, a sediment sample was required with enhanced and known concentrations of neptunium and plutonium. This was produced by spiking a 'background' sediment sample (obtained from Crombie point, Rosyth (Grid reference 3035 6844) on 8th August, 1988) with ^{237}Np and ^{242}Pu. This sample was dried for 24 hours at 30°C, sieved using a 2 mm mesh, and ground. 76% of the sediment sample was in the less than 2 mm fraction, which consisted of fine to coarse sand and shell fragments. The sediment contained 0.08 ± 0.02 Bq kg^{-1} $^{239+240}Pu$ and 0.4 μg g^{-1} ^{238}U [Bradley, 1989]. A 20 gram aliquot was taken and ashed in a muffle furnace at 500°C for 12 hours after which the sample was heated gently for a further 12 hours in 500 ml of aqua regia (3:1, 11.4 M HCl and 15.6 M HNO_3 respectively). After cooling, the sample was filtered, the aqueous phase taken to near dryness and the volume made up to 100 ml with 8 M HCl. This solution was spiked with ^{237}Np and ^{242}Pu to a concentration of 4.8 and 8.2 ng ml^{-1} respectively. Aliquots of this solution were then used to investigate the performance of analytical procedures as described below. In addition, the 'in-house' standard reference sample of Ravenglass silt, (see section 2.2.4.2) was used to assess the analytical procedures.

3.3.3 Initial sample preparation and dissolution

Aliqouts of the sediment samples which had been previously dried, sieved using a

2 mm mesh, and ground, were dried overnight at a temperature of 110°C. This process was checked by comparing the weight loss per gram of sediment with freeze drying and no significant difference was found between the two techniques.

The dried samples were then ashed overnight in a muffle furnace at 500°C to combust any organic material. After cooling, the samples were heated gently with aqua regia in the presence of the chemical yield tracers. For sediment samples, Pu and Np originating from Sellafield discharges are unlikely to be present in primary mineral phases, so a simple acid leach is sufficient to release the analytes into solution [Popplewell and Ham, 1987]. This is advantageous for analysis by ICP-MS as only 30 - 50% of the total weight of the sample is released into solution [Krey and Bogen, 1987], reducing the need for sample clean up procedures.

Table 3.2 Effect of initial sample weight on final $^{239+240}$Pu sediment concentrations for Ravenglass silt

Sample weight (g)	Final sample volume (ml)	No. of samples	$^{239+240}$Pu specific activity (Bq kg^{-1})
30	5	5	861 ± 60
20	5	3	926 ± 89
10	5	5	1,065 ± 75
2	1	3	1,102 ± 36
1	1	3	1,104 ± 48

Table 3.2 shows the effect of the initial sample weight on the final $^{239+240}$Pu specific activity of the Ravenglass silt sample. For sample weights of greater than 10 g the sample leaching processes used here were less efficient at releasing the plutonium from the sample, most probably due to insufficient volume of aqua regia compared to the weight of sample. The relative proportion of leaching solution for the larger sediment samples was increased to a minimum of 10:1 with satisfactory results as a subsequent bulk sample with an initial sample weight of 100 g was found to have a $^{239+240}$Pu specific activity of 1,020 ± 14 Bq kg^{-1}. The reagent volumes used in the following procedure applies to sediment samples with an initial sample weight of 2 - 10 g.

3.3.4 Anionic exchange

After leaching, the samples were cooled and the solid phase removed by filtration. The aqueous sample was then taken to low volume and made up to 20 ml using 8 M HCl. Iron was removed by extraction with equal volumes of di-isopropyl ether [Nachtrieb and Conway, 1948a,b]. This was repeated until the aqueous phase was clear or pale yellow, in general requiring a single cycle extraction for samples of 5 g or less. The samples were then heated gently to remove any residual ether, cooled and the volume and acidity of the solution altered to produce a 20 ml solution of 9 M HCl. At this stage approximately 1 g of $NH_2OH.HCl$ was added to the solution to reduce Np to the IV state. Meanwhile a 1 x 10 cm column of Dowex 1X8 (100-200 mesh) anionic exchange resin was prepared and pre-conditioned with 9 M HCl. Just before addition of the sample solution to the exchange column, 10 drops of 15.6 M HNO_3 were added to the solution to ensure that Pu was in the IV state. After addition of the sample, the column was washed with an equal volume of 9 M HCl, followed by 4 x 50 ml washes of 8 M HNO_3, to remove a proportion of uranium from the sample (see below). Finally both Pu and Np were eluted from the column using 150 ml 1.2 M HCl. Elution curves for the removal of uranium and the final elution of Pu and Np are shown in Figure 3.5. These were obtained by using the spiked sediment sample which had a ^{238}U concentration of 28.3 $\pm$ 0.5 ng ml^{-1}. In this case 60% of ^{238}U was removed from the sample, and 87 and 73% of ^{237}Np and ^{242}Pu respectively were in the final elution solution. Repetition of this experiment produced variable results (see Table 3.3), however in general the anionic exchange column was effective in removing over 50% of ^{238}U with over 70% recovery for both Pu and Np. Semiquantitative analysis of the wash solutions, by ICP-MS, revealed that the main components of the sediment sample solution (Ca, Mg, Na, Al and Mn) were not adsorbed by the anionic exchange resin and remained in the 9 M HCl solution.

The distribution coefficients for Np, Pu and U in the IV oxidation state (see Figure 3.3) indicate that they are strongly sorbed onto the anionic exchange column in HCl, the adsorption increasing with HCl molarity. However, if U is first oxidised to U(VI) then it can be removed, to a certain extent, by 8 M HNO_3 (the distribution coefficient in 8 M HNO_3 for U(VI) is < 10, compared with $> 10^3$ for Np(IV) and

Figure 3.5 Elution curves for DOWEX 1X8 anion exchange resin showing % recoveries for (a) ^{238}U in 8M HNO_3 wash, (b) ^{237}Np and (c) ^{242}Pu in 1.2M HCl wash

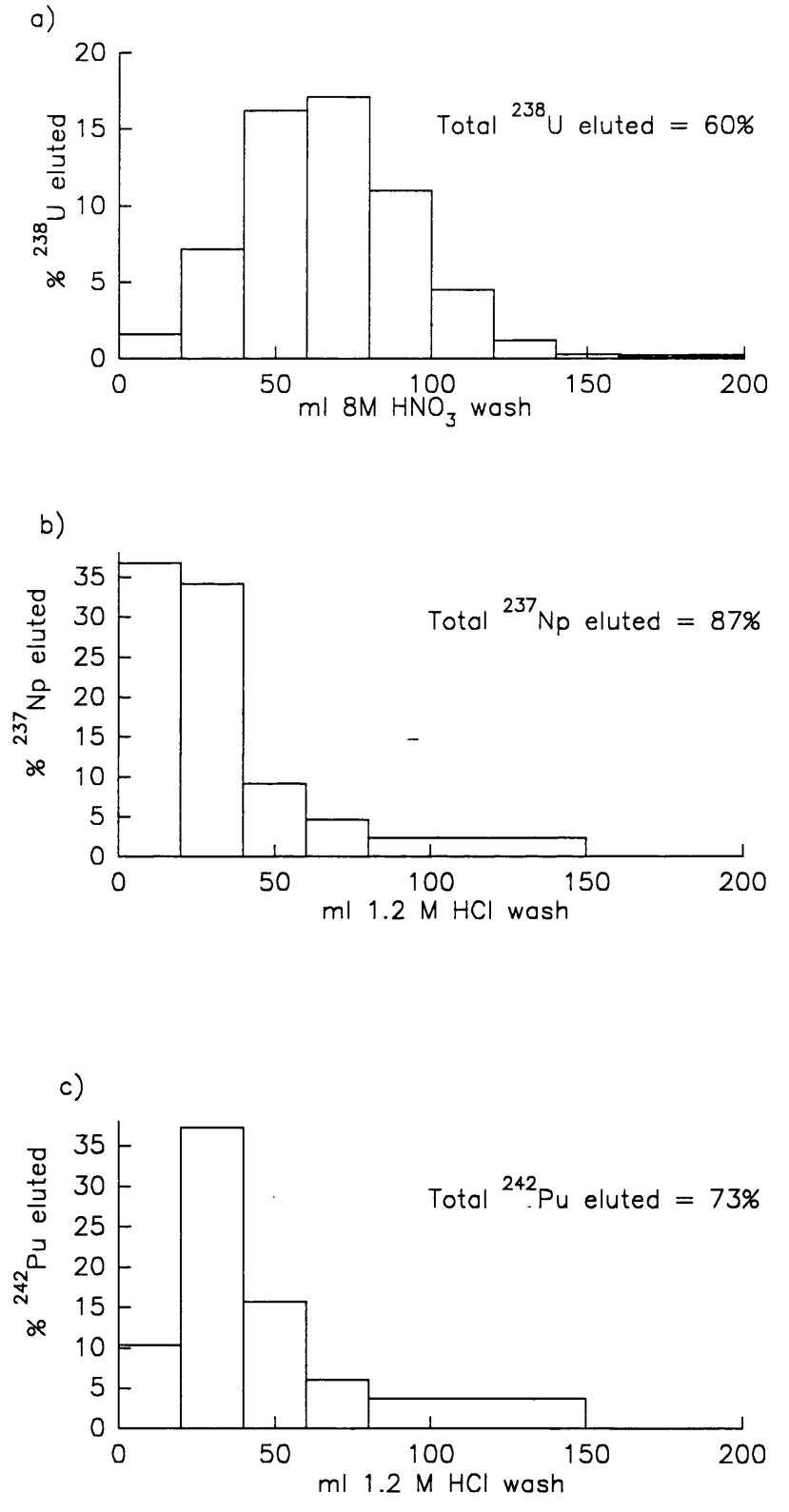

Table 3.3 Results of experiments to adjust the oxidation state of Pu and Np before addition of sample solution onto anionic exchange column in terms of % recovery in each solution

Experiment	Wash	^{238}U	^{237}Np	^{242}Pu
No reducing agents	9M HCl	-	-	-
	8M HNO_3	0.4 - 3	1 - 4	6 - 14
	1.2M HCl	69 - 86	55 - 77	26 - 55
Addition of $NH_2OH.HCl$	9M HCl	< 1	< 1	8 - 15
	8M HNO_3	< 1	< 1 - 2	3 - 14
	1.2M HCl	66 - 76	75 - 84	8 - 62
Addition of $NH_2OH.HCl$ and HNO_3	9M HCl	< 1 - 23	< DL	< DL - 7
	8M HNO_3	104 - 140	< DL	< DL
	1.2M HCl	5 - 41	88 - 108	89 - 101

Pu(IV)). By comparison, all actinides in the VI and IV oxidation states have low distribution coefficients at low acidity, and should be eluted from the anionic exchange column by 1.2 M HCl. The effect of the addition of oxidising\reducing agents to the sample prior to anionic exchange can be seen in Table 3.3. Best recoveries of both Np and Pu were obtained by the addition of HNO_3 and $NH_2OH.HCl$. The results for ^{238}U were variable and in some cases unexpected, with 8M HNO_3 failing to remove the uranium and with > 100% recoveries observed. This suggested that the anion exchange resin contained significant quantities of uranium in the 4+ oxidation state. A similar conclusion was reached by Hursthouse [1990], and a fresh batch of resin was acquired which was relatively free of uranium.

The ^{238}U concentration of 20 g aliquots of the Ravenglass silt sample after anionic exchange was found to be 400 - 500 ng ml^{-1}. An ETV-ICP-MS spectrum obtained for one of these samples is shown in Figure 3.6. In this case the ^{238}U peak tails into ^{237}Np, although the peaks could have been separated by increasing the resolution at the expense of the signal response (see section 2.2.1.3). However, the ^{238}U concentration was high enough for $^{238}UH^+$ to interfere with ^{239}Pu, as confirmed by the average $^{240}Pu/^{239}Pu$ atom ratio which was found to be 0.214 ± 0.006 compared to an average value of 0.250 ± 0.020 found for samples which had lower ^{238}U concentrations. As a result, further removal of uranium was required.

Figure 3.6 ETV-ICP-MS spectrum obtained from analysis of a 20g Ravenglass sediment sample after anionic exchange.

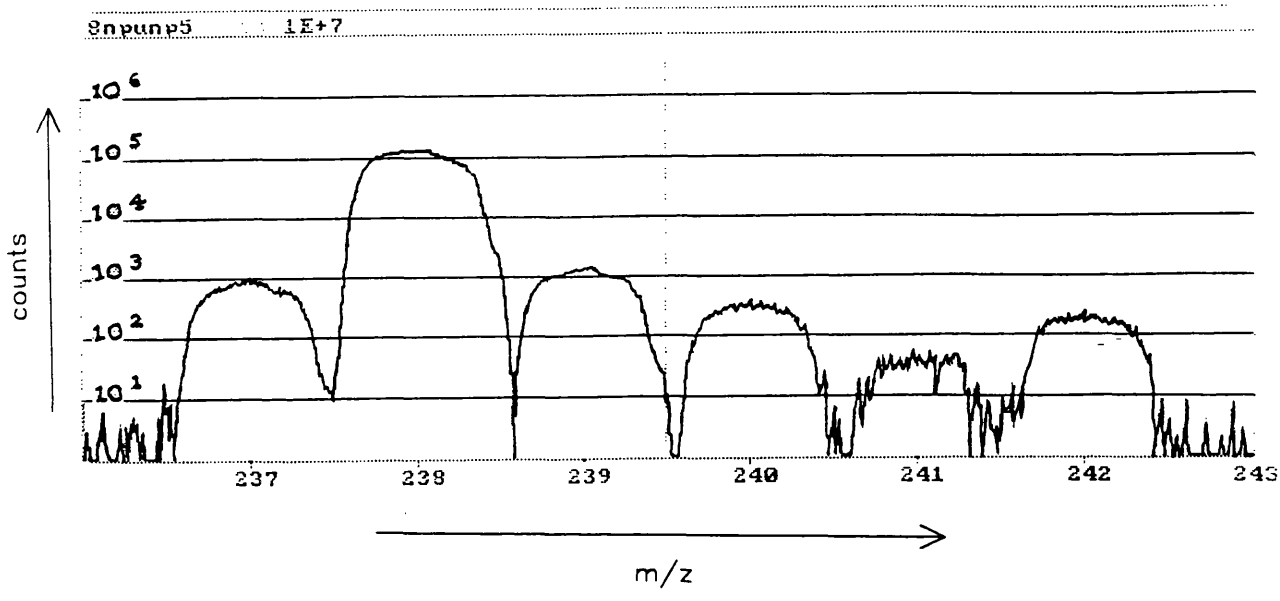

3.3.5 TTA solvent extraction

Separation of Np and Pu from uranium was achieved by a single cycle TTA extraction from 0.5 M HCl. Firstly, the 1.2 M HCl wash solution was taken to near dryness and the remaining solution was taken up in 25 ml of 0.5 M HCl. Extraction was performed with an equal volume of pre-conditioned TTA with thorough mixing of the solvent and aqueous phase for 15 minutes. The aqueous layer was removed and Np and Pu were back extracted with 25 ml of 8 M HNO_3. This was then taken to near dryness and made up to 2 - 5 ml using 2% HNO_3. The sample was placed in a polythene pot and the gamma spectrum recorded to obtain the Np recovery (see section 3.3.6).

Several experiments were performed to investigate the effect of adding reducing and oxidising agents to the 0.5 M HCl solution, prior to TTA extraction, using 10 g aliquots of the Ravenglass silt sample which had previously undergone anion exchange separation. The results of these experiments are summarised in Table 3.4. All the experiments resulted in the effective removal of uranium to a final

Table 3.4 Results of experiments investigating the effect of reducing\oxidising agents on the extraction of Pu and Np by TTA, showing % final recovery for Np and Pu, and final ^{238}U concentration for an initial sample weight of 10 g.

Oxidation/reducing agents added to 0.5 M HCl solution prior to TTA extraction	% Np recovery	% Pu recovery	^{238}U concentration in final solution (ng ml^{-1})
None	53 - 107	50 - 104	0.4 - 1.1
1 g $NH_3OH.HCl$	67 - 96	3 - 6	1.6 - 6.1
10 drops 15.6M HNO_3	26 - 66	96 - 101	0.6 - 4.7
$NH_2OH.HCl$ and HNO_3	41 - 101	6 - 83	6.3 - 9.5
None, 2 x TTA extraction	33 - 89	29 - 60	0.04 - 0.07

Figure 3.7 ETV-ICP-MS spectrum obtained from analysis of a 10 g Ravenglass sediment sample after anionic exchange and a single cycle TTA extraction

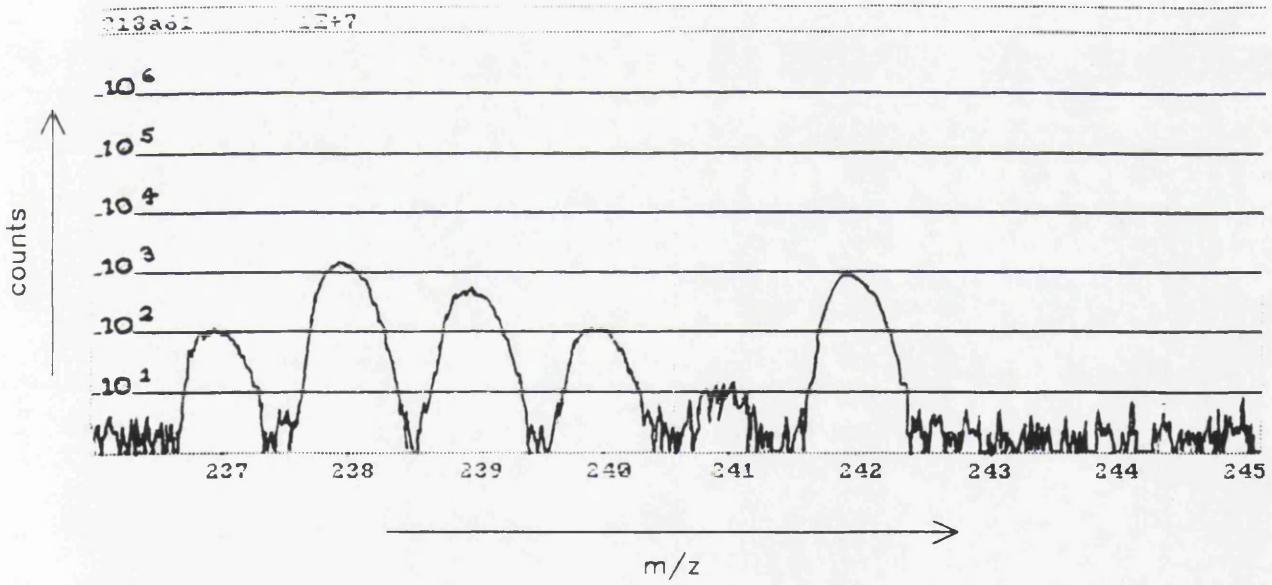

concentration of less than 10 ng ml^{-1}, which caused no interference with analysis of ^{237}Np and ^{239}Pu (see Figure 3.7). The recoveries for both Pu and Np were variable, the best results obtained by adding no oxidising or reducing agent between anion exchange and solvent extraction steps. Table 3.4 also shows the results obtained after performing two TTA extraction steps. As expected, the final ^{238}U recovery was lower, as were the recoveries for both Np and Pu. Considering the requirement for minimum chemistry, the second TTA extraction step was redundant.

The replacement of anion exchange with TTA extraction was also investigated, but the results were unreliable, probably due to the levels of salt in the samples effecting the solubility of TTA in the aqueous phase (see section 3.2.2.1).

3.3.6 Determination of ^{237}Np recoveries

^{239}Np was used as a yield tracer for Np analysis as described in section 3.3.1. Np recoveries were calculated by comparing the counts obtained for the 228 keV (11.8%) and 277 keV (14.1%) emissions (using high resolution γ-spectrometry) for the initial ^{239}Np spike with the counts obtained for the final solution. The more abundant 106 keV (22.8%) emission was not used due to interferences from Pu K_α and K_β lines. Corrections were made to account for decay during counting using an equation derived by Hoffman and Van Camerik [1967] such that:

$$\Delta t = \frac{t_{1/2}\ln((1-e^{-R\ln 2})/R\ln 2)}{\ln 2}$$

where Δt is the time correction, determining the time from the start of counting for which the observed activity is the true activity of the sample, and R is the number of half-lives counted ((counting time, T)/$t_{1/2}$). Addition of Δt to the time taken for processing the samples enabled calculation of the complete decay corrections. Since only the relative ^{239}Np activity of the final sample was required, the absolute efficiency of the γ-detector was not needed as both the spike and the sample were

measured in a fixed geometry. However, the sample volumes were variable within the 1 - 2 ml range. To check that changes in sample volume did not affect the measured activity, the absolute efficiency of the detector was measured for this volume range using a standard γ-source, and the variation in efficiency was found to be insignificant.

γ-counting the samples prior to analysis also confirmed that the peaks observed at 241 m/z in the ICP-MS spectra were due only to ^{241}Pu in the samples as the high intensity 60 keV ^{241}Am γ-ray was not observed. ^{241}Am was not expected to be present in the final solution as the dominant oxidation state of Am is the III state which does not form stable, negatively charged chloro complexes implying that it would pass straight through the anionic exchange column [Cleveland, 1970].

3.4 APPLICATION TO IRISH SEA SEDIMENT SAMPLES

To establish the ^{240}Pu/^{239}Pu atom ratios and obtain data on the ^{237}Np distribution within the sediments of the Irish Sea, intertidal sediment samples from the coast of West Cumbria and sediment core samples taken from Maryport and the Solway Firth were obtained.

The analysis of these samples by ICP-MS provided the opportunity to study the environmental record of Sellafield discharges. In Chapter 4, the results are discussed in terms of the current understanding of the dynamics of the Irish Sea and the environmental behaviour of these radionuclides, and conclusions are drawn on the interpretations that such data can provide on unpublished releases from Sellafield.

3.4.1 Sample site locations

3.4.1.1 Intertidal surface sediments

Intertidal sediment samples were collected from the coastline of West Cumbria, between the 10 and 12th November, 1988 (Figure 3.8). Bulk sediment samples were taken from 1 m squares, up to 50 m below the high tide mark, to a depth of

Figure 3.8 Intertidal sediment sample collection sites

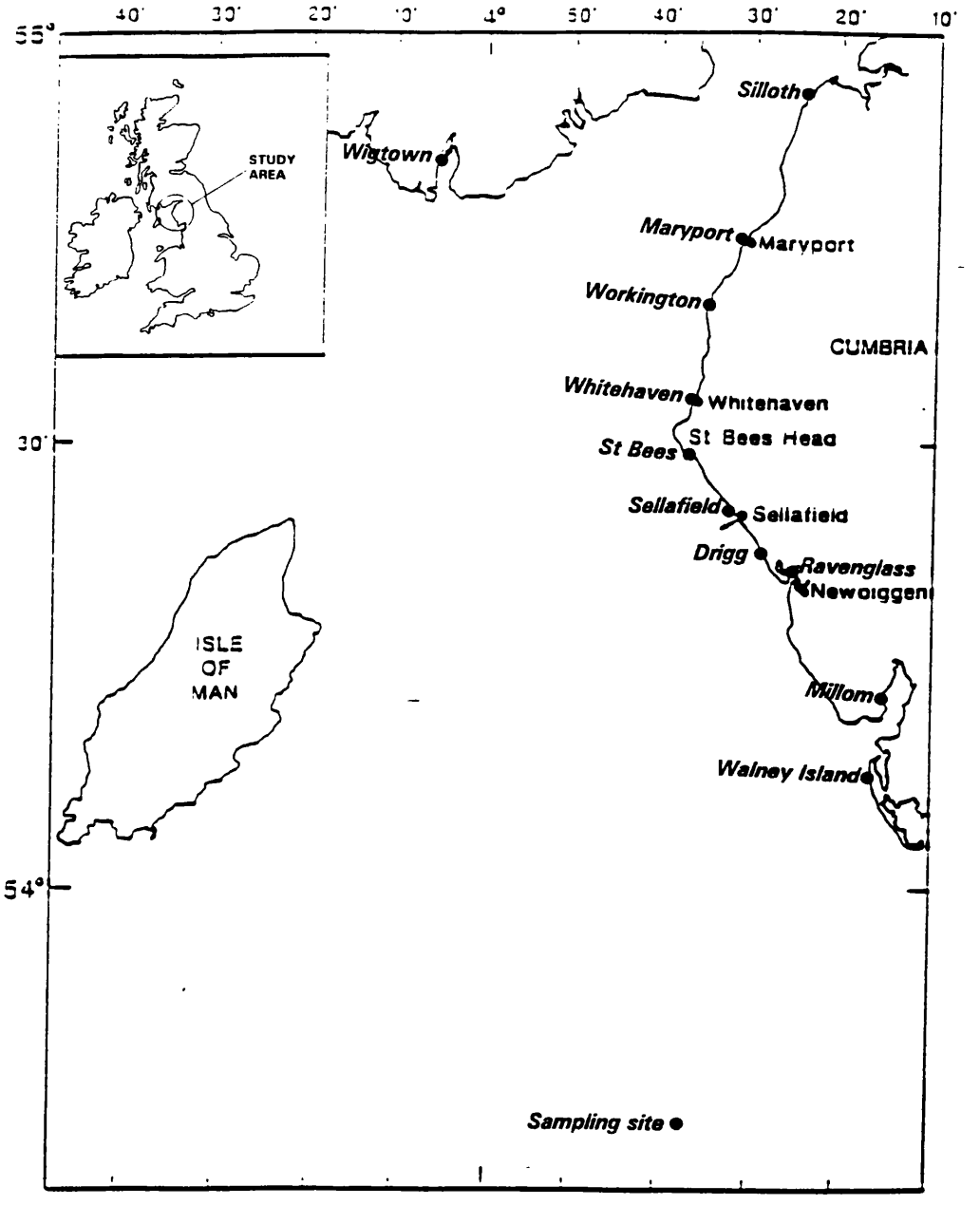

Figure 3.9 Schematic diagram showing the collection site of cores taken from Maryport Harbour, Cumbria [Kershaw *et al.*, 1990]

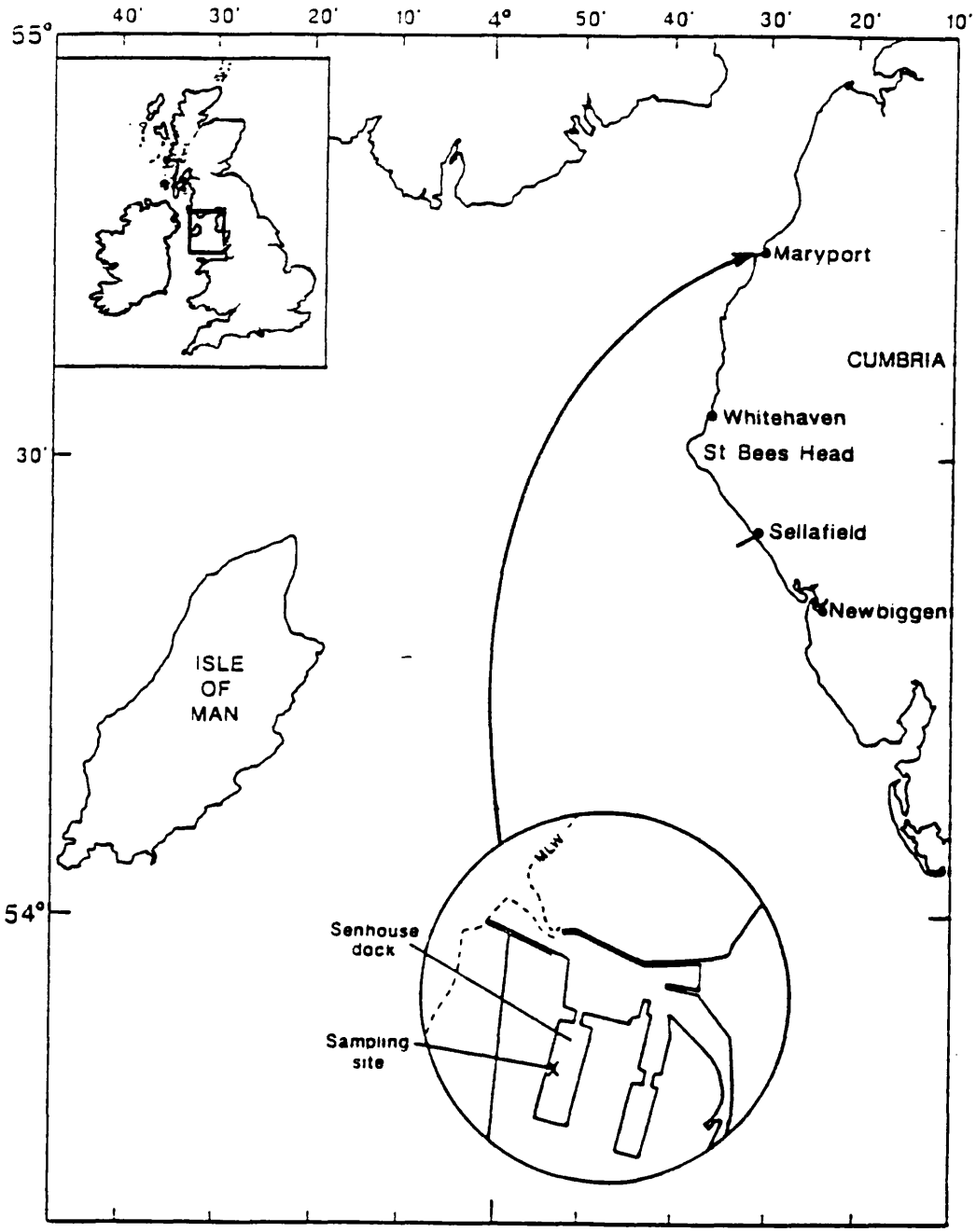

Figure 3.10 Sampling site of Southwick Core (SC1) [Allan, 1993]

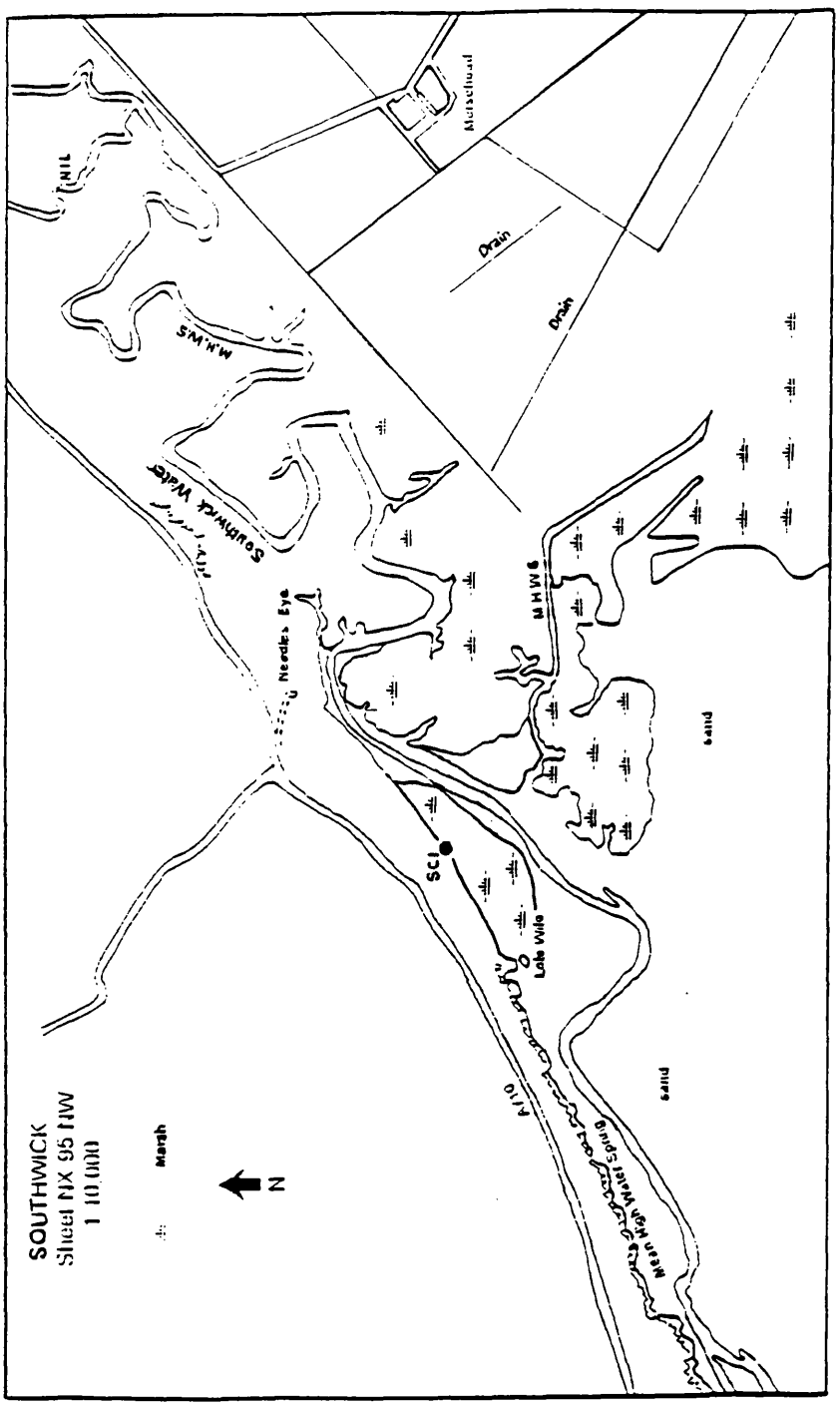

1 cm. The sediment types ranged from coarse sands to fine silt (based only on visual characterisation). At each sampling site, the samples were placed in polythene pots, which were then sealed in bags to prevent cross contamination. Each sample was dried, sieved using a 2 mm mesh and ground using a TEMA disc mill. The homogenised samples were then sub-sampled prior to analysis. The analysis procedure has been detailed in section 3.3.

3.4.1.2 Sediment core samples

Sections of sediment cores collected from Maryport and the Solway Firth were kindly donated by Dr. P.J. Kershaw and Dr. R.L. Allan respectively. The sampling techniques employed to extract and sub-section these cores, detailed by Kershaw et al. [1990] and Allan [1993], are summarised below.

Several sediment cores were taken from Senhouse Dock in Maryport harbour. This was dredged in the early 1950s, at about the time of the first discharges from Sellafield (then Windscale). The dock rapidly silted up and was left undisturbed until 1988, when it was redredged as part of a harbour redevelopment project. Core samples were collected at low water on 17th February, 1988 (Figure 3.9). Square section (15 x 15 cm), steel 'Kasten' barrels were lowered onto the exposed sediment surface using a 12 ton crane. The core sections analysed in the present study originated from two cores, M1 and M2, which were 210 and 108 cm in length respectively. These cores were sectioned into 1, 2, or 5 cm intervals, and each section homogenised and sub-sampled. 2 - 5 grams of core sub-sections, spanning the whole length of the cores, were made available for ICP-MS analysis.

The Solway core was extracted from a vertical river bank of Southwick Water. This sample location is subject to an oscillatory pattern of erosion caused by the slumping of the banks, followed by periods of rapid sediment accumulation [MacKenzie et al., 1994]. The sediment core was collected as part of a project to assess the transfer of Sellafield discharges to the Solway coast. Figure 3.10 shows the sample collection site of the Solway core (SC1), located 200 m downstream from the intersection of the path from the entrance to the Scottish

Wildlife Trust's Southwick Coast nature reserve at Netherclifton [Allan, 1993]. A 70 cm core was extracted by preparing a clean vertical face at the stepped edges of the merse and extracting the sediment samples in 5 cm depth intervals, the surface area of each section being approximately 10 x 15 cm. Each sub-sampled section was placed in polythene bags, dried overnight at 60°C then sieved through a 2 mm mesh prior to analysis.

3.5 VALIDATION OF RESULTS

The results obtained by ETV-ICP-MS for the Maryport core and Solway core (SC1) samples are shown in Table 4.4 and 4.5 respectively. Validation of the plutonium results was possible by comparison of the $^{239+240}$Pu specific activities (derived from the ^{239}Pu/^{242}Pu and ^{240}Pu/^{242}Pu atom ratios obtained by ICP-MS), with the results obtained by Kershaw et al. [1990] and Allan [1993] by α-spectrometry. In addition, some of the electrodeposited sources used for α-spectrometry by Kershaw et al. [1990] were sent to W. McCarthy (AWE, Harwell) for analysis by TIMS. This enabled direct comparison of the ^{240}Pu/^{239}Pu atom ratios obtained by ICP-MS with those obtained by TIMS. The differences between ICP-MS, α-spectrometry and TIMS techniques were outlined in section 1.7. Unfortunately, no data were available for comparison with ^{237}Np specific activities obtained by ICP-MS for Maryport core samples. Instead the 'in-house' Ravenglass silt reference standard was analysed as part of each analytical procedure and the ^{237}Np results checked with the expected ^{237}Np specific activity (see section 2.2.4.2).

3.5.1 $^{239+240}$Pu results

Figure 3.11 shows a plot of the $^{239+240}$Pu specific activity obtained by ICP-MS compared to α-spectrometry [Kershaw et al., 1990], for the Maryport core samples. The agreement between the results is good, with a correlation coefficient of 0.955. Figure 3.12 shows a plot of the difference between the individual results obtained by each technique against their mean value. This reveals two types of variation between the two data sets: a systematic difference in which the mean ICP-MS value is 142 Bq kg^{-1} higher than the equivalent α-spectrometry result, suggesting a difference between the two yield tracer spikes; and a random difference where,

Figure 3.11 Comparison of $^{239+240}$Pu specific activities obtained by ICP-MS and α-spectrometry [Kershaw *et al.*, 1990] for Maryport core samples

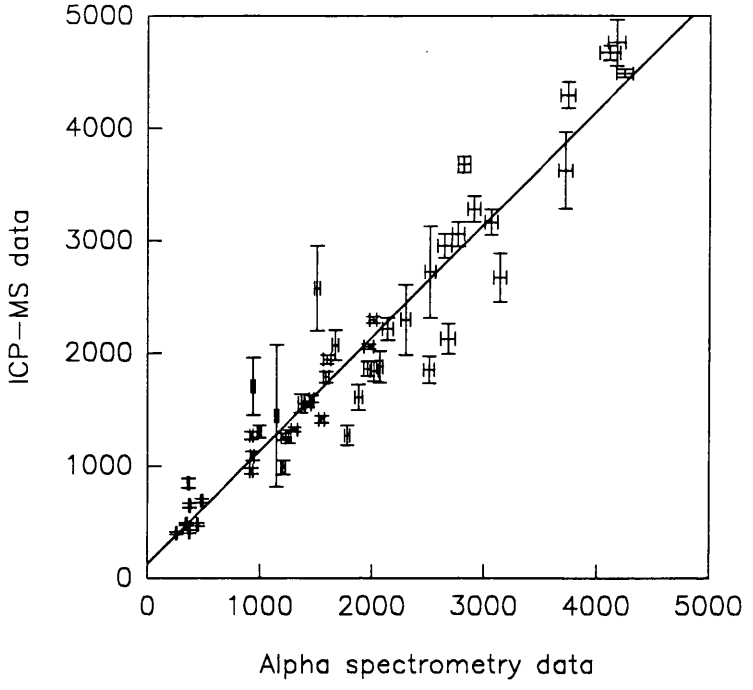

Figure 3.12 Plot of the difference between individual results obtained by ICP-MS and α-spectrometry [Kershaw *et al.*, 1990] against their mean value

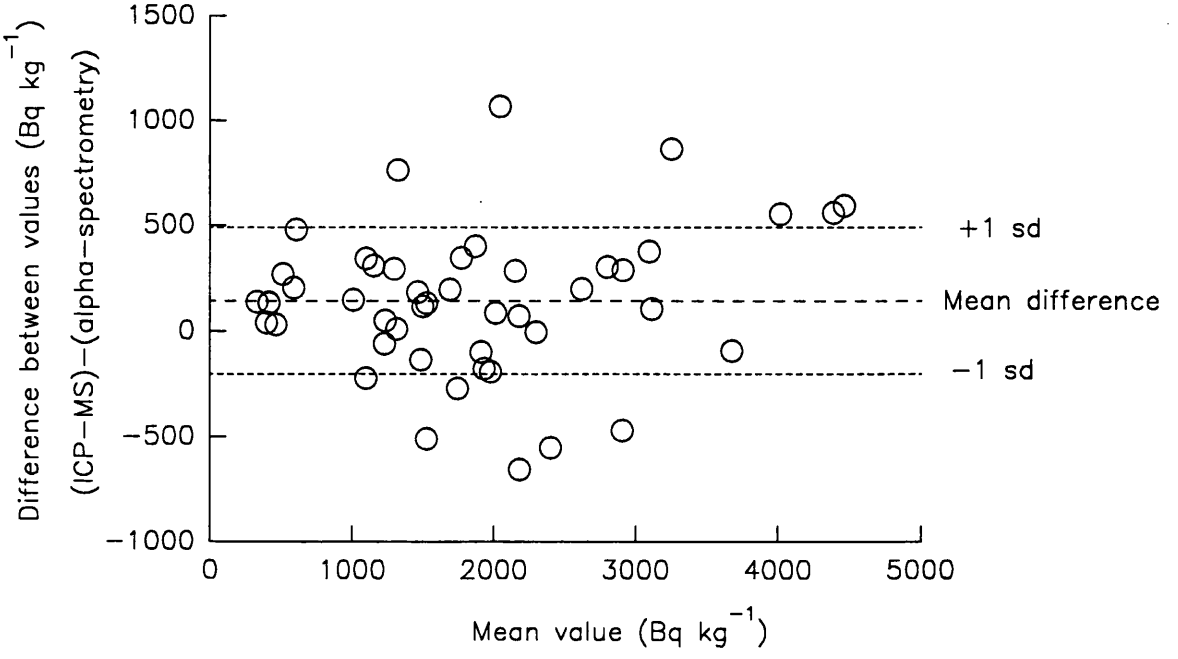

in a few cases, there are large disparities between the data sets, possibly the result of sub sampling or an artifact of the different analytical procedures. Absolute validation of the concentration of the ^{242}Pu spike used in this study was not possible, but each dilution of the original certified material was checked.

The $^{239+240}Pu$ specific activities for samples from the Solway core obtained by ICP-MS and α-spectrometry [Allan, 1993] are compared in Figure 3.13. Once again, the agreement between the two data sets is good with a linear correlation coefficient of 0.951. Interestingly, a plot of the difference between the results against their mean value (Figure 3.14) reveals a greater correspondence between the two data sets than was observed for the Maryport core data, with a mean ICP-MS value only 15 Bq kg^{-1} lower than the mean α-spectrometry value. In this case, the systematic error due to the yield tracer is removed as the same spike solution was used for both techniques.

3.5.2 $^{240}Pu/^{239}Pu$ results

The $^{240}Pu/^{239}Pu$ atom ratio profiles for the Maryport core obtained by ETV-ICP-MS and by TIMS [McCarthy, 1994] are shown in Figure 3.15. The agreement between the two data sets is excellent, with a correlation coefficient of 0.980 (Figure 3.16). In this case, the average difference between the results was 0.0039 (Figure 3.17). The main difference between the two data sets was the precision, typically 4.4% for ICP-MS compared to 0.35% for TIMS. Direct comparison of the precision for specific samples is not possible as different sample preparation procedures were used, and only 1 - 2 grams of material were available for ICP-MS analysis. For ICP-MS, the precision was dependent on the sensitivity of the instrument and on the concentration of plutonium in the final solution. The precision could therefore be improved by increasing the initial sample size and by the use of the latest generation ICP-MS instruments (PQ2 series) which have improved sensitivity of typically an order of magnitude.

Figure 3.13 Comparison of $^{239+240}$Pu activities obtained by ICP-MS and α-spectrometry [Allan, 1993] for Solway core (SC1) samples

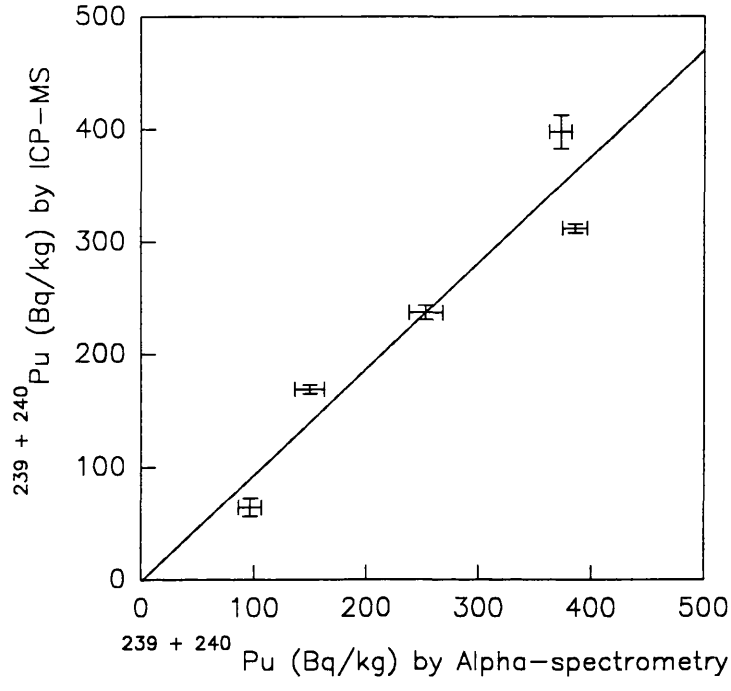

Figure 3.14 Plot of the difference between individual results obtained by ICP-MS and α-spectrometry [Allan, 1993] against their mean value

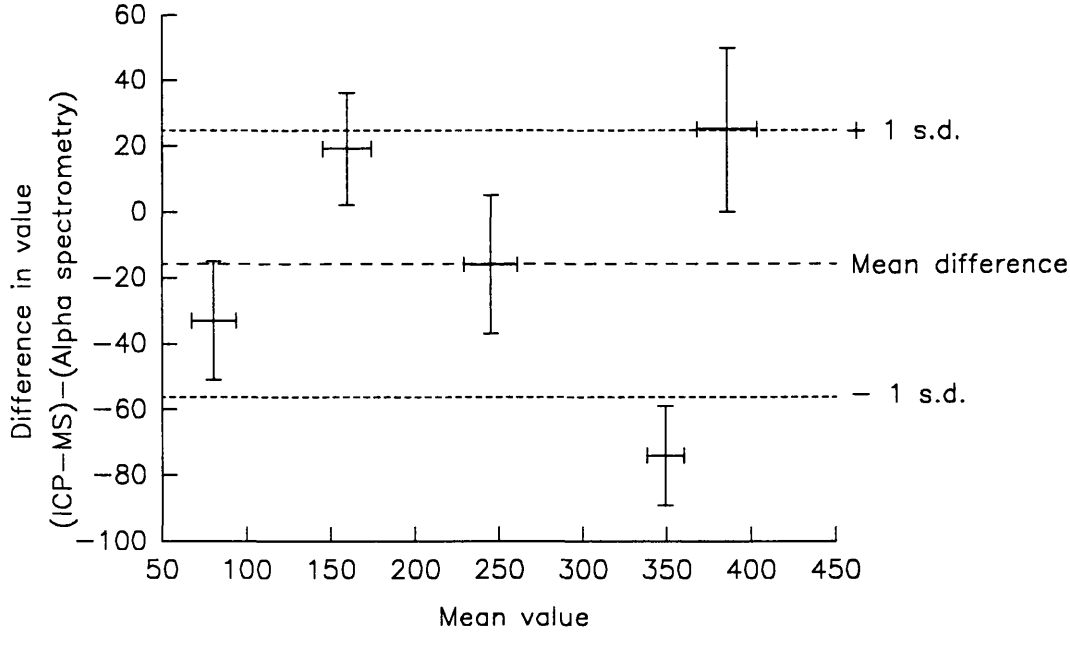

Figure 3.15 $^{240}Pu/^{239}Pu$ atom ratio profile for Maryport core samples obtained by ICP-MS and TIMS [McCarthy, 1994]

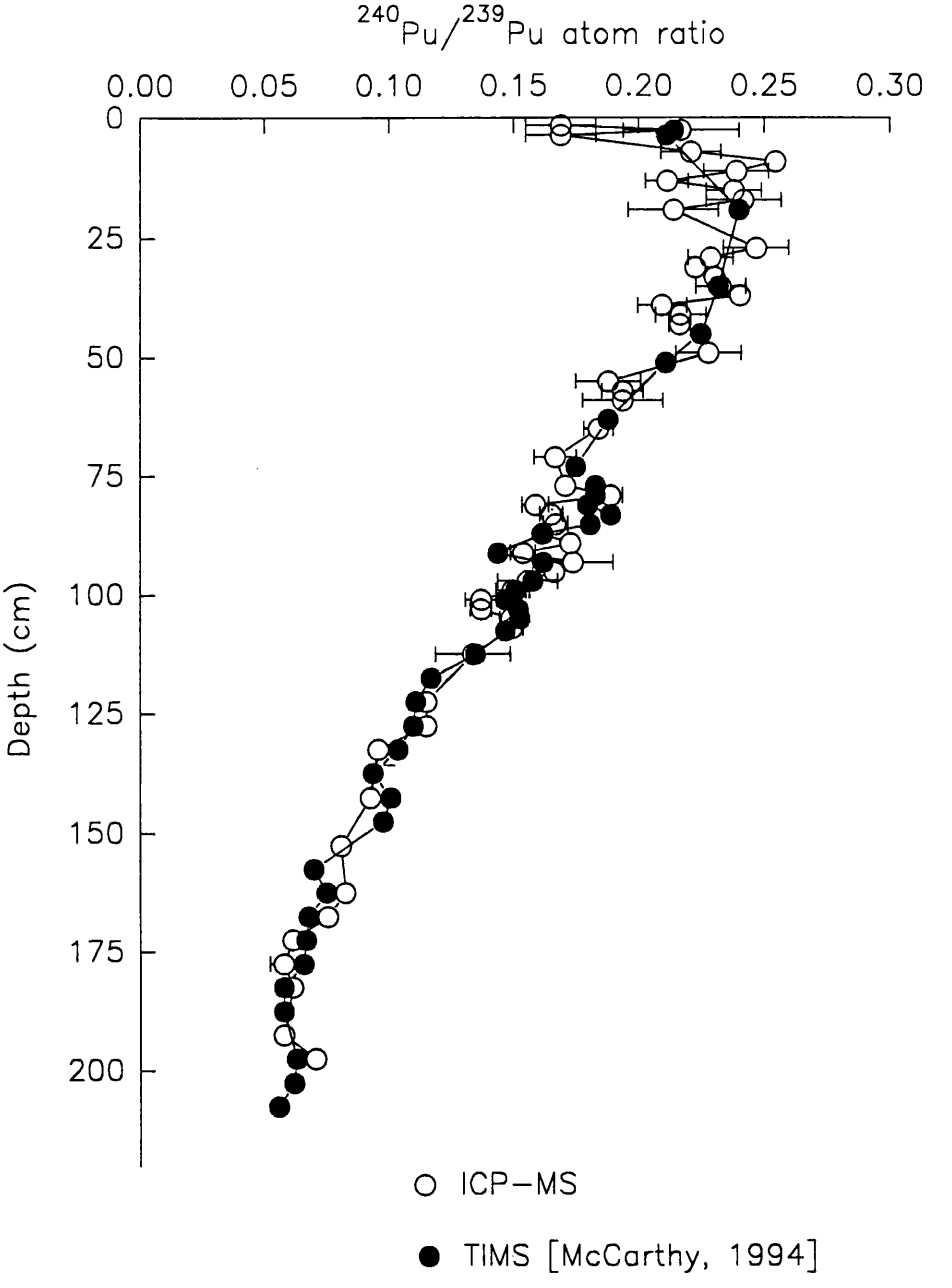

Figure 3.16 Comparison of $^{240}Pu/^{239}Pu$ atom ratios obtained by ICP-MS and TIMS [McCarthy, 1994] for Maryport core samples.

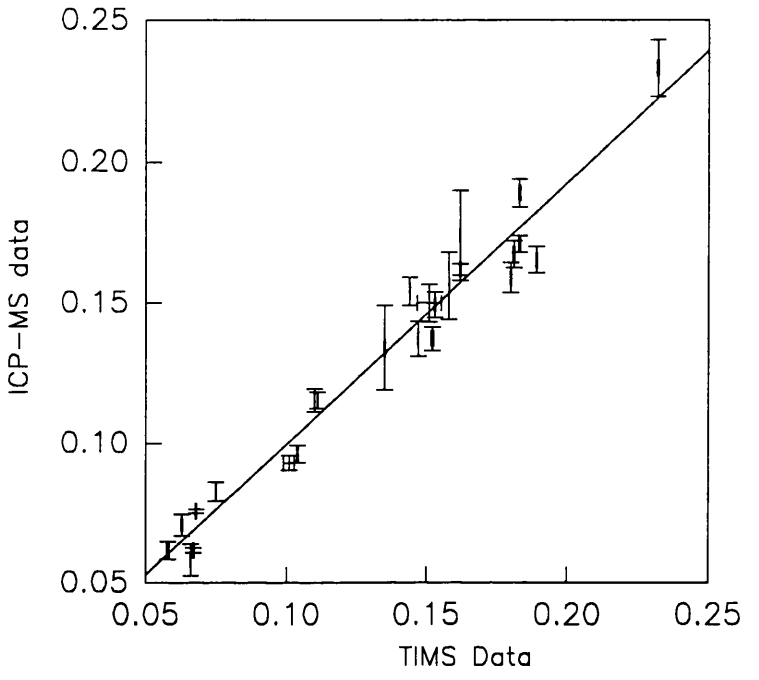

Figure 3.17 Plot of the difference between individual results obtained by ICP-MS and TIMS [McCarthy, 1994] against their mean value

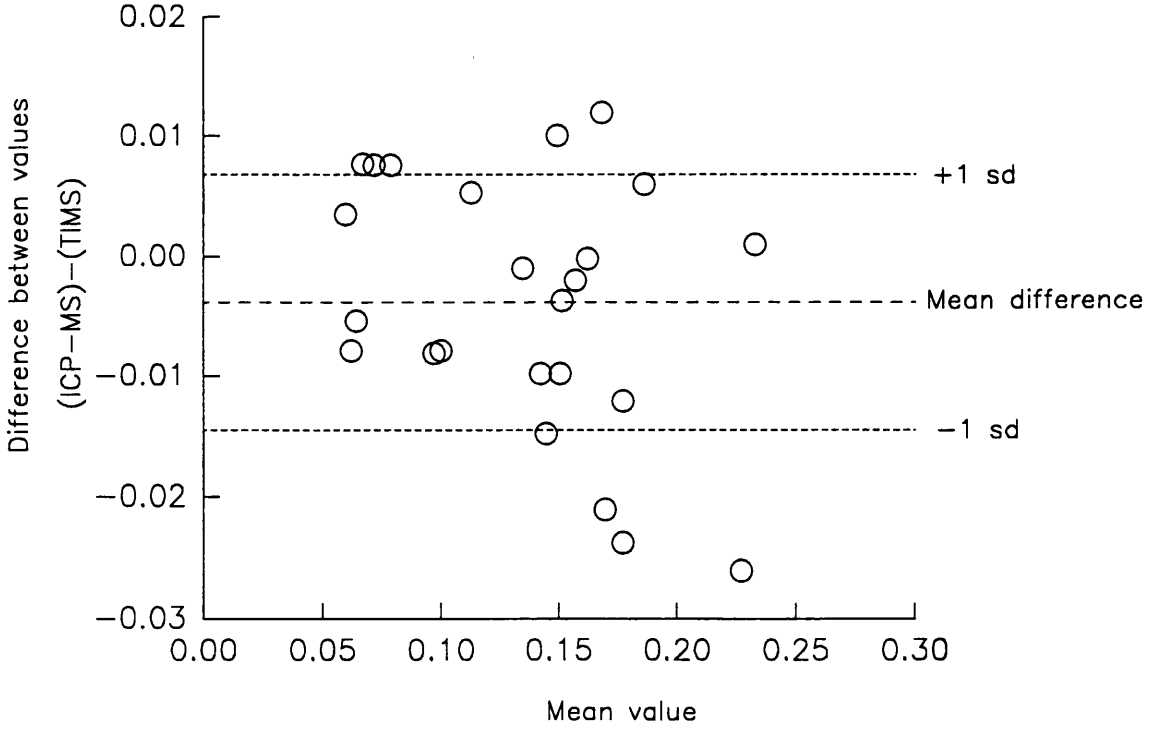

CHAPTER 4
AN ENVIRONMENTAL APPLICATION

4.1 INTRODUCTION

The Sellafield discharges offer an opportunity to study the environmental behaviour of radionuclides, such as plutonium and neptunium, which were not present in the marine system before the discharges started, or were at a relatively low concentration compared to the present levels. As the isotopes of plutonium and neptunium are of long-term significance in terms of nuclear waste disposal (see section 1.6.3), it is important to assess the environmental behaviour of these radionuclides in order to address the omissions in the Sellafield discharge record and to predict the potential sources and sinks of the actinides in the future.

The isotopic signature of the Sellafield discharges has changed with time, and this can potentially help to untangle the environmental record of the discharges. For the heavy elements, such as Np and Pu, it can be assumed that no isotopic fractionation occurs during biological or chemical reactions in the environment, so that the isotope ratios observed in environmental media are related to those observed in the discharges, although the individual contributions from each year's discharge may vary from sample to sample. Some separation of different elements does occur during environmental processes as a result of each element's individual biogeochemical behaviour, although elements from the same group, for example the actinides, tend to have similar behaviour. This can be highlighted by observing nuclide ratios in different environmental media.

One limitation in interpreting the environmental signature of radionuclides discharged from Sellafield is the incomplete record of the releases. For example, ^{237}Np and ^{238}Pu discharge data only exist since 1978, after the peak discharges of the early to mid 1970s. In addition, some isotope ratios in the discharges, such as $^{240}Pu/^{239}Pu$, have never been recorded. In the case of plutonium, a nearly complete record of the Sellafield releases exists for $^{239+240}Pu$, and this can be used to interpret the observed $^{239+240}Pu$ concentrations in environmental media. If a model is then established which relates the discharges to the environmental signature, it

can be applied to other isotopes of plutonium, such as ^{238}Pu, for which limited discharge data exist. Once a model predicts and agrees with the available Sellafield discharge data, it can be used to predict the level of releases for which no data exists. Likewise, a model which predicts the recorded $^{238}Pu/^{239+240}Pu$ ratios in the discharge from the sediment record, could be applied to the $^{240}Pu/^{239}Pu$ ratios. For some radionuclides, such as ^{237}Np, the discharge data are limited and the environmental behaviour is not well characterised. In such a case nuclide ratios, for example the $^{237}Np/^{239+240}Pu$ activity ratio, can be used to provide a comparison with radionuclides for which the behaviour is well known.

In this study, $^{240}Pu/^{239}Pu$ atom ratio data and ^{237}Np specific activity data were obtained by ICP-MS for intertidal surface sediment and core samples. The interpretation of these data is discussed below, as well as the potential for deconvolution of the environmental signature to provide information on the source term.

4.2 RESULTS FOR INTERTIDAL SURFACE SEDIMENTS FROM THE IRISH SEA

Table 4.1 $^{240}Pu/^{239}Pu$ atom ratios and $^{239+240}Pu$ specific activities found in intertidal sediments by ICP-MS

Sample Site	Type	$^{240}Pu/^{239}Pu$ atom ratio	$^{239+240}Pu$ (Bq kg^{-1})
Wigtown	Sand	0.2083 ± 0.021	26 ± 5
Silloth	Sand	0.1799 ± 0.0068	33 ± 7
Maryport	Silt	0.2043 ± 0.029	931 ± 108
Workington	Sand	0.1832 ± 0.0047	110 ± 8
Whitehaven	Sand	0.2326 ± 0.027	57 ± 7
St Bees	Sand	0.1429 ± 0.0082	35 ± 2
Sellafield	Sand	0.1852 ± 0.0062	170 ± 11
Drigg	Sand	0.1908 ± 0.0025	201 ± 4
Ravenglass	Silt	0.2188 ± 0.0072	1117 ± 36
Millom	Sand	0.2132 ± 0.0050	281 ± 13
Walney Island	Sand	0.250 ± 0.013	42 ± 2

4.2.1 $^{239+240}$Pu specific activity

$^{239+240}$Pu specific activities measured in intertidal sediments collected from the coastline of West Cumbria are shown in Table 4.1. As expected, the data show a relationship between the $^{239+240}$Pu concentrations and sediment type, the sand samples having lower concentrations than the silt samples. The variation in the $^{239+240}$Pu concentrations within the broad 'sand' classification used here, based only on visual characterisation, is likely to be a function of both the particle size distribution within the sediments and the distance of the sampling point from the Sellafield pipeline. Table 4.2 lists published $^{239+240}$Pu concentration data, obtained by α-spectrometry, for intertidal sediments collected from similar locations during the 1980s. In general, the results obtained by ICP-MS show good agreement with those obtained by α-spectrometry, although there are some striking differences. For example, the sediment sample collected at Workington by MAFF contained 970 Bq kg^{-1} $^{239+240}$Pu, whereas the sample analysed in this study contained only 110 Bq kg^{-1}. In this case, the difference can be attributed to sample types. Studies have shown that even within a small area with similar sediment types, the concentrations of radionuclides can vary considerably [Aston and Stanners, 1982a]. This highlights the limitations of environmental data in that they can only provide a snapshot of what is happening at one moment in time and at one specific location. This can be overcome by collecting a number of samples from any one site and obtaining an average to ascertain the general trend.

4.2.2 ^{240}Pu/^{239}Pu atom ratios

Interpretation of ^{240}Pu/^{239}Pu atom ratios observed in environmental materials from the Irish Sea is difficult as there are few data available in the literature for comparison (Table 4.3) and no information is published on ^{240}Pu/^{239}Pu ratios in the Sellafield discharge or the average burn-up of nuclear waste reprocessed at any given time. However, it is known that the initial reprocessing program was developed to produce nuclear weapons, so it would be expected that early discharges from Sellafield would have characteristically low ^{240}Pu content (see section 1.3.1) and that the ^{240}Pu/^{239}Pu ratio in the discharges would increase as higher burn-up material from nuclear power stations was subsequently reprocessed.

Table 4.2 Comparison of $^{239+240}Pu$ specific activities in intertidal sediments from the Cumbrian and Solway coast

Reference	This study	Aston *et al.*, 1985	Eakins *et al.*, 1988	Others
Sampling date	1988	1978-80	1982-84	1985-88
Wigtown	26 ± 5	120 ± 3		[a] 132 ± 9
Silloth	33 ± 7	242 ± 5	10 ± 1	
Maryport	931 ± 108	1818 ± 33	94 ± 6	[b] 970
Workington	110 ± 8	37 ± 1		
Whitehaven	57 ± 7		33 ± 4	[b] 810
St Bees	35 ± 2		110 ± 8	[c] 103 ± 25
Sellafield	170 ± 11		142 ± 9	
Drigg	201 ± 4	116 ± 3	113 ± 7	
Ravenglass	1117 ± 36	1297 ± 33		
Millom	281 ± 13	2921 ± 38		
Walney Island	42 ± 2	964 ± 29	72 ± 4	

[a] Sample collected during 1985 [MacKenzie *et al.*, 1987]
[b] Samples collected during 1988 [MAFF, 1989]
[c] Sample collected 1986-87 [McKay and Walker, 1990].

The $^{240}Pu/^{239}Pu$ atom ratios obtained for the intertidal sediments collected from West Cumbria are listed in Table 4.1. Figure 4.1 shows the variation in $^{240}Pu/^{239}Pu$ atom ratios with distance from the Sellafield pipeline, for the results obtained in the present study and those obtained by McCarthy and Nicholls [1990] by TIMS. The results from each study show a close correspondence, despite the three year gap between sample collection, indicating that the $^{240}Pu/^{239}Pu$ atom ratio in the intertidal sediments did not significantly change during this time. In general, the $^{240}Pu/^{239}Pu$ atom ratios are indicative of high burn-up material, showing little variation with distance from Sellafield. Interestingly, most of the values to the north of Sellafield are within error of the average fallout value, implying that the $^{240}Pu/^{239}Pu$ atom ratio alone cannot be used to determine the source of the plutonium. However, the concentrations of plutonium in the samples indicate that the dominant source is

Table 4.3 Published $^{240}Pu/^{239}Pu$ atom ratios for marine samples

Irish Sea intertidal sediment samples

Place	Date	$^{240}Pu/^{239}Pu$	Reference
Ravenglass	1989	0.197 ± 0.003	Kim *et al.*, 1989
Ravenglass	1986	0.217 ± 0.089	Hursthouse, 1990
Ravenglass	1985	0.194 ± < 1%	McCarthy and Nicholls,
Seascale	1985	0.180 "	1990
Braystones	1985	0.182 "	"
Nethertown	1985	0.187 "	"
Nethertown	1983	0.188 "	"
Newbiggin	1985	0.198 "	"
Saltcoats	1977	0.158 "	"
Whitehaven	1985	0.1943 - 0.200	Koide *et al.*, 1985

Samples contaminated with fallout

Sample	$^{240}Pu/^{239}Pu$	Reference
Average fallout, soils	0.179 ± 0.014	Perkins and Thomas, 1980
Atlantic sediment cores	0.105 - 0.193	Buesseler and Sholkovitz, 1987
Atlantic pore waters	0.052 - 0.163	
Atlantic sediments	0.142 - 0.179	Buesseler and Halverson, 1987
" pore waters	0.179 - 0.188	
" seawater	0.180 - 0.211	"
" sediment trap material	0.179 - 0.180	"
Coral	0.194 - 0.239	"
Gulf of Mexico		
Sediment cores	0.069 - 0.185	Scott *et al.*, 1983
Antarctic and Artic ice		
Post-moratorium	0.09 - 0.22	Koide *et al.*, 1985
Pre-moratorium	0.21 - 0.34	"
Enewetak		
Lagoon water, 1972	0.092 - 0.116	Noshkin, 1980
Fish bone	0.309 ± 0.067	"
Bikini coral, 1976	0.207 ± 0.017	"

Sellafield. In both studies, there is one data point that is much lower than the others and lower than the average fallout value (see Figure 4.1). Both of the samples which exhibit low $^{240}Pu/^{239}Pu$ atom ratios occurred in sediments close to Sellafield, the probable source of low burn-up material. The low $^{240}Pu/^{239}Pu$ atom ratios in these sediments indicate that either earlier discharge material forms a significant proportion of the surface sediment, or Sellafield has recently been releasing plutonium with a low $^{240}Pu/^{239}Pu$ atom ratio.

For comparison, the $^{238}Pu/^{239+240}Pu$ activity ratios found in intertidal sediments are shown in Figure 4.2. These show a similar general trend to the $^{240}Pu/^{239}Pu$ atom ratios, with the $^{238}Pu/^{239+240}Pu$ activity ratios remaining fairly constant in the sediments over distances up to 100 km from Sellafield, the average values being 0.208 ± 0.009 for samples collected between 1978 and 1980, and 0.233 ± 0.019 for samples collected from 1982-1984. The ratios recorded for the Sellafield discharges at these times were 0.31 and 0.32 respectively. The lower values found in the sediments and the increase in the ratio observed with time, indicate that the $^{238}Pu/^{239+240}Pu$ activity ratios in the intertidal sediments are influenced by earlier discharges from Sellafield which had a higher proportion of $^{239,240}Pu$. This is supported by the evidence of Eakins *et al.* [1988] who found that Pu concentrations within intertidal sand cores were fairly constant to a depth of 50 cm, suggesting that the sediments were well mixed and that the $^{238}Pu/^{239+240}Pu$ activity ratios are indicative of cumulative discharges. Likewise, it is expected that the $^{240}Pu/^{239}Pu$ ratios found in intertidal areas are also representative of the cumulative Sellafield discharges.

At large distances (> 100 km) from Sellafield the $^{238}Pu/^{239+240}Pu$ activity ratios decreased. No discharge data exist for ^{238}Pu before 1978 and the best available estimates of the early $^{238}Pu/^{239+240}Pu$ activity ratios are provided by Hetherington [1975] who measured the annual $^{238}Pu/^{239+240}Pu$ activity ratio in surface sediments from Newbiggin between 1966 and 1974. The data show an increase in the $^{238}Pu/^{239+240}Pu$ ratio from 0.053 in 1966 to 0.200 in 1973 (see Figure 4.3). Comparison of the results obtained by Hetherington [1975] with those found above (Figure 4.2), suggests that the samples at large distances from Sellafield are more influenced by 'older' discharges, resulting in lower $^{238}Pu/^{239+240}Pu$ activity ratios.

Figure 4.1 Variation in $^{240}Pu/^{239}Pu$ atom ratios in intertidal surface sediments with distance from Sellafield

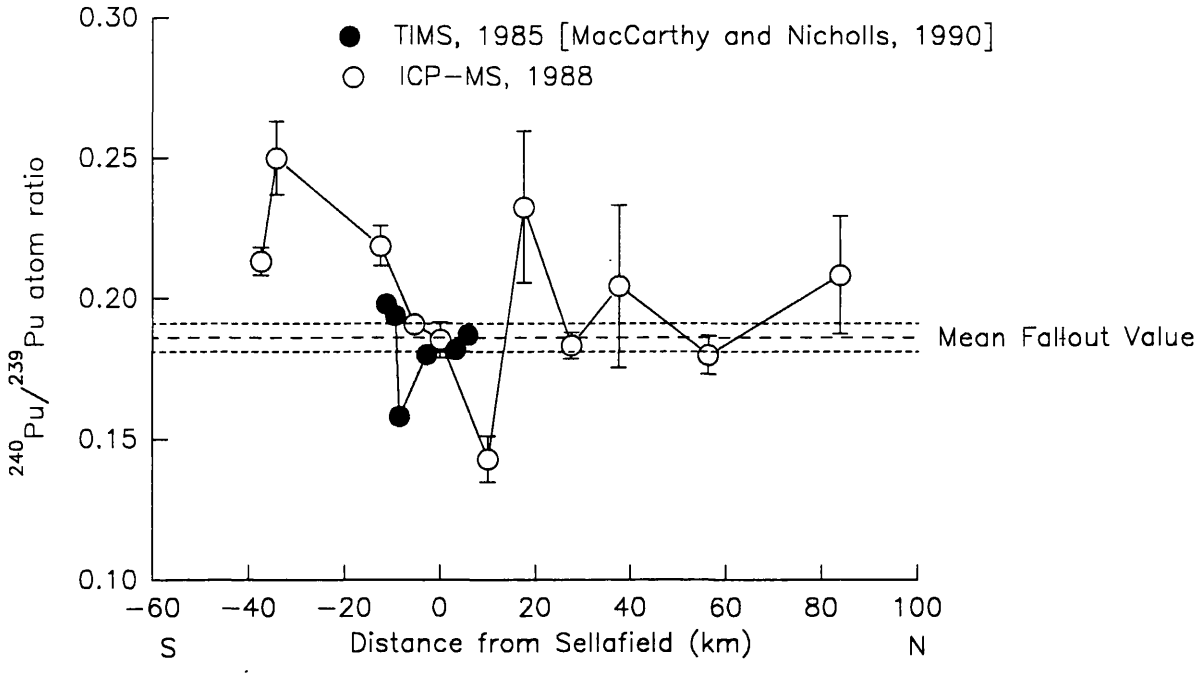

Figure 4.2 Variation in $^{238}Pu/^{239+240}Pu$ activity ratios in intertidal surface sediments with distance from Sellafield

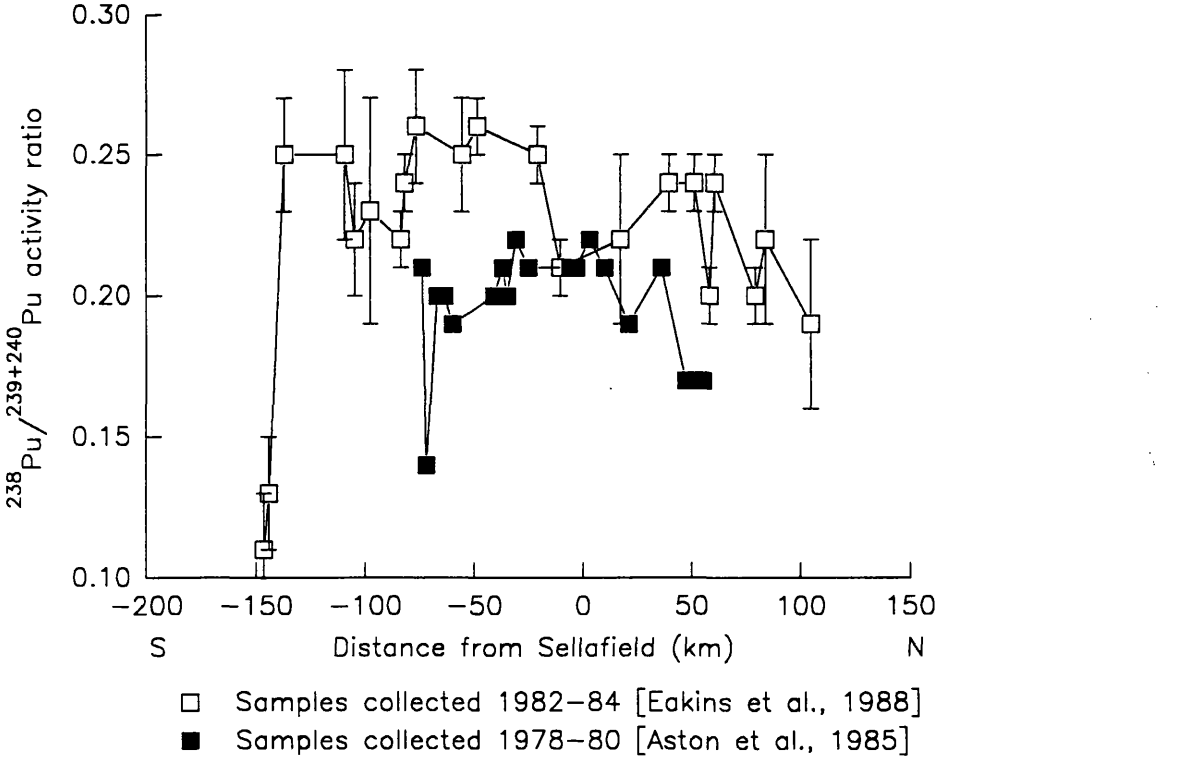

Figure 4.3 Annual $^{238}Pu/^{239+240}Pu$ activity ratios found in intertidal surface sediments from Newbiggin from 1966 to 1974 [Hetherington, 1975]

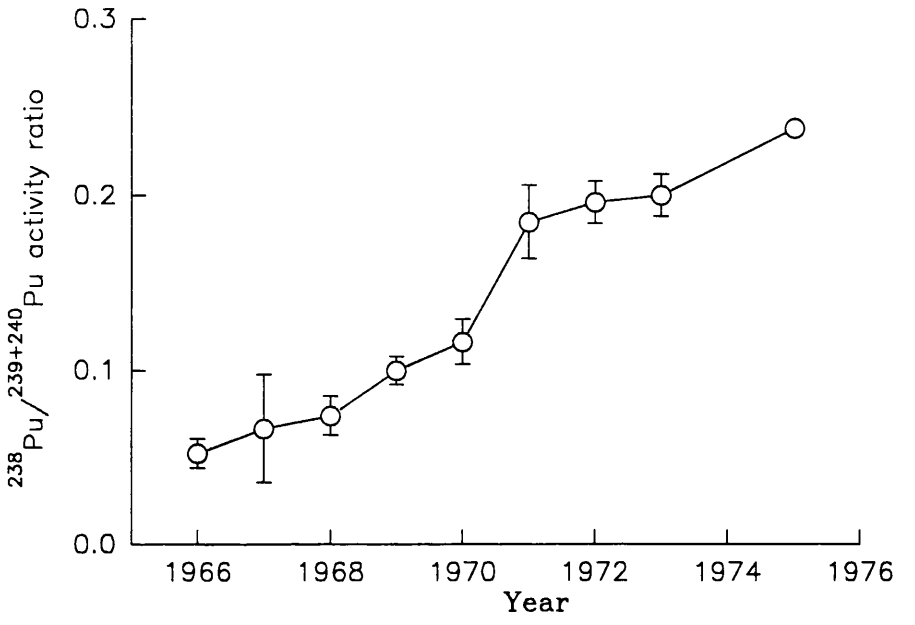

An alternative explanation could be that fallout $^{238}Pu/^{239+240}Pu$ ratios become more significant as the dominance of the Sellafield discharges decreases with distance. The $^{238}Pu/^{239+240}Pu$ fallout activity ratio is characteristically low (0.031 in 1982, from Pentreath [1988]) so the mixing of sediments contaminated with fallout with those contaminated with diluted Sellafield discharges, would result in the observation of lower $^{238}Pu/^{239+240}Pu$ activity ratios. However, the plutonium inventory for all the samples collected by Eakins *et al.* [1988] was significantly higher than the expected fallout inventory, with even the southern most sampling site having a $^{239+240}Pu$ content of 5 kBq m^{-2}, compared to 48 Bq m^{-2} expected from fallout. Unfortunately, in the present study, samples were not collected at such distances from Sellafield as it would have been interesting to observe $^{240}Pu/^{239}Pu$ atom ratios in sediments which had low $^{238}Pu/^{239+240}Pu$ activity ratios.

4.3 SEDIMENT CORE DATA

The analysis of two cores taken from Maryport and the Solway Firth (SC1) has been described in Section 3.3. Several publications also relate to these specific

Table 4.4 ETV-ICP-MS results showing ^{237}Np and $^{239+240}Pu$ concentrations, and $^{240}Pu/^{239}Pu$ atom ratios for Maryport core samples.

Sample	^{237}Np concentration (pg g^{-1})	$^{239+240}Pu$ concentration (Bq kg^{-1})	$^{240}Pu/^{239}Pu$ atom ratios
M1 0 - 1	54 ± 2	-	-
M1 1 - 2	50 ± 1	631 ± 14	0.169 ± 0.014
M1 2 - 3	38 ± 2	758 ± 50	0.217 ± 0.023
M1 3 - 4	-	1113 ± 94	0.169 ± 0.014
M1 4 - 5	32 ± 5	-	-
M1 5 - 6	45 ± 7	-	-
M2 6 - 8	28 ± 5	956 ± 26	0.221 ± 0.012
M2 8 - 10	-	912 ± 12	0.2546 ± 0.0030
M2 10 - 12	-	1087 ± 40	0.239 ± 0.013
M2 12 - 14	-	1700 ± 250	0.2114 ± 0.0085
M2 14 - 16	34 ± 2	1261 ± 30	0.238 ± 0.011
M2 16 - 18	-	1549 ± 29	0.242 ± 0.015
M2 18 - 20	71 ± 4	987 ± 61	0.214 ± 0.018
M2 26 -28	-	1594 ± 31	0.247 ± 0.013
M2 28 - 30	76 ± 3	1843 ± 90	0.2288 ± 0.0089
M2 30 - 32	32 ± 1	1322 ± 19	0.2228 ± 0.0031
M2 32 - 34	-	1789 ± 49	0.2304 ± 0.0026
M2 34 - 36	101 ± 6	1271 ± 89	0.233 ± 0.010
M2 36 - 38	-	1862 ± 67	0.2405 ± 0.0035
M2 38 - 40	-	2580 ± 380	0.2096 ± 0.0098
M2 40 - 42	-	1556 ± 80	0.217 ± 0.010
M2 42 - 44	40 ± 5	1416 ± 31	0.2166 ± 0.0043
M2 44 - 46	67 ± 9	-	-
M2 46 - 48	119 ± 12	-	-
M2 48 - 50	70 ± 10	3630 ± 340	0.228 ± 0.013

Sample	^{237}Np concentration (pg g^{-1})	$^{239+240}Pu$ concentration (Bq kg^{-1})	$^{240}Pu/^{239}Pu$ atom ratios
M2 50 - 52	178 ± 17	-	-
M2 54 - 56	-	1945 ± 40	0.188 ± 0.013
M2 56 - 58	57 ± 8	2058 ± 24	0.1938 ± 0.0083
M2 58 - 60	23 ± 3	2720 ± 410	0.194 ± 0.016
M2 60 - 62	113 ± 8	-	-
M2 64 - 66	-	3060 ± 110	0.1842 ± 0.0058
M2 70 - 72	32 ± 2	2130 ± 130	0.1669 ± 0.0084
M2 74 - 76	29.6 ± 0.7	-	-
M2 76 - 78	16.9 ± 0.8	2296 ± 27	0.1709 ± 0.0029
M2 78 - 80	32 ± 1	2210 ± 100	0.1890 ± 0.0050
M2 80 - 82	-	2960 ± 110	0.1590 ± 0.0053
M2 82 - 84	-	4669 ± 64	0.1653 ± 0.0046
M2 84 - 86	64 ± 2	3350 ± 77	0.1672 ± 0.0048
M2 86 - 88	-	3290 ± 120	0.1618 ± 0.0020
M2 88 - 90	75 ± 27	3170 ± 110	0.1730 ± 0.0015
M2 90 - 92	99 ± 7	4290 ± 120	0.1541 ± 0.0050
M2 92 - 94	-	4760 ± 210	0.174 ± 0.016
M2 94 - 96	-	4490 ± 37	0.1667 ± 0.0033
M2 96 - 98	-	2300 ± 310	0.156 ± 0.012
M2 98 - 100	-	1850 ± 120	0.1499 ± 0.0067
M2 100 - 102	-	2070 ± 140	0.1372 ± 0.0062
M2 102 - 104	100 ± 3	2670 ± 220	0.1372 ± 0.0043
M2 104 - 106	130 ± 5	3680 ± 71	0.1493 ± 0.0045
M2 106 - 108	-	1880 ± 140	0.1499 ± 0.0043
M1 110 - 115	-	1610 ± 120	0.134 ± 0.015
M1 120 - 125	-	1390 ± 25	0.1153 ± 0.0029
M1 125 - 130	-	1202 ± 60	0.1153 ± 0.0041
M1 130 - 135	9.1 ± 0.6	1306 ± 53	0.0961 ± 0.0031
M1 140 - 145	-	1271 ± 33	0.0929 ± 0.0026
M1 150 - 155	6.3 ± 2.5	485 ± 15	0.0809 ± 0.0029

Sample	^{237}Np concentration (pg g^{-1})	$^{239+240}Pu$ concentration (Bq kg^{-1})	$^{240}Pu/^{239}Pu$ atom ratios
M1 160 - 165	-	691 ± 15	0.0826 ± 0.0034
M1 165 - 170	-	649 ± 19	0.07559 ± 0.00063
M1 170 - 175	-	482 ± 5	0.06165 ± 0.00091
M1 175 - 180	-	848 ± 41	0.0581 ± 0.0057
M1 180 - 185	-	418 ± 13	0.0615 ± 0.0032
M1 190 - 195	-	480 ± 13	0.0579 ± 0.0028
M1 195 - 200	6.0 ± 2.5	402 ± 10	0.0707 ± 0.0039

cores. In particular, the Maryport core is referred to by Kershaw *et al.* [1990] and MacKenzie *et al.* [1994], and the Solway core (named here SC1) is referred to by MacKenzie *et al.* [1994] as S2 and Allan [1994] as SC1. The $^{240}Pu/^{239}Pu$ atom ratio, $^{239+240}Pu$ activity concentrations and ^{237}Np concentrations of samples taken from the Maryport core, determined by ETV-ICP-MS, are listed in Table 4.4., and the $^{240}Pu/^{239}Pu$ atom ratios in samples from SC1 are shown in Table 4.5. The $^{240}Pu/^{239}Pu$ atom ratios and the $^{239+240}Pu$ specific activities have been validated by comparison with the results obtained by independent techniques as discussed in section 3.5. The relationship between the sediment core profiles and the Sellafield discharges is discussed in detail in section 4.3.3.

Table 4.5 $^{240}Pu/^{239}Pu$ atom ratios for Solway core, SC1 obtained by ETV-ICP-MS

Sample depth (cm)	$^{240}Pu/^{239}Pu$ atom ratio
5 - 10	0.1988 ± 0.0059
20 - 25	0.2070 ± 0.0021
30 - 35	0.1957 ± 0.0027
45 - 50	0.1543 ± 0.0033
60 - 65	0.090 ± 0.014

Figure 4.4 $^{240}Pu/^{239}Pu$ atom ratio profile for Maryport core obtained by ETV-ICP-MS

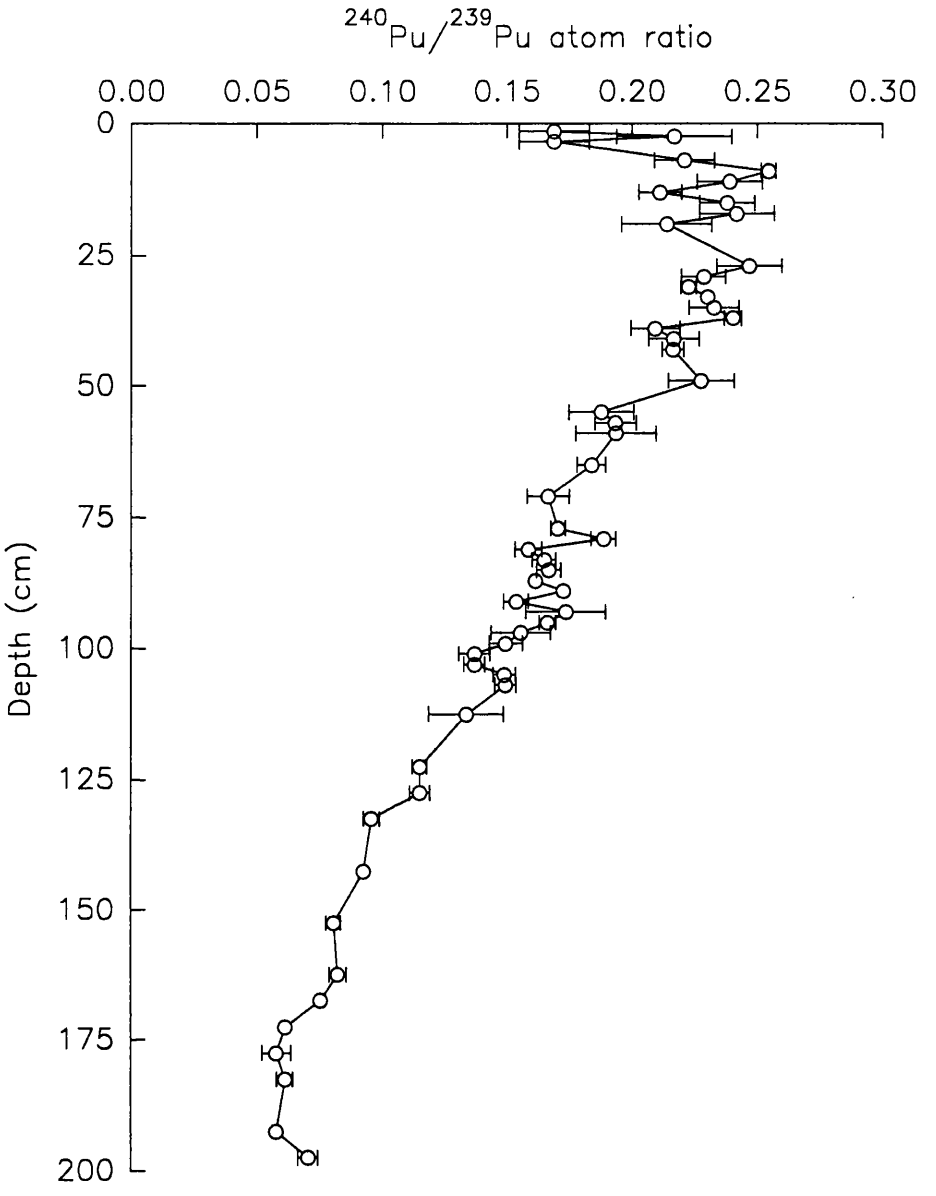

4.3.1 $^{240}Pu/^{239}Pu$ atom ratios

4.3.1.1 The Maryport core

Figure 4.4 shows the $^{240}Pu/^{239}Pu$ atom ratio profile down the Maryport core. The ratio changes significantly with depth, varying from 0.058 ± 0.006 at depths of 175-180 cm to a maximum value of 0.255 ± 0.003 at 8-10 cm, but with the values levelling off between 6 and 50 cm to an average of 0.229. The $^{239+240}Pu$ specific activities and $^{238}Pu/^{239+240}Pu$ activity ratios [Kershaw *et al.*, 1990] in the sediment indicate that the source of the plutonium is dominantly Sellafield. Using the relationship between the degree of burn-up and the $^{240}Pu/^{239}Pu$ atom ratios in nuclear fuel (as shown by Figure 1.2), the maximum and minimum ratios found in the core correlate to a burn-up in Magnox fuel of 4 and 0.65 GWD/Te respectively. It is worth considering that the expected $^{240}Pu/^{239}Pu$ atom ratios for low-burn up material, characteristic of weapons grade plutonium, is less than 0.14, whereas the ratio found in Magnox fuel after an average burn-up in a nuclear power station is greater than 0.2 (see section 1.3.1). The $^{240}Pu/^{239}Pu$ atom ratios observed at depth in the Maryport core are therefore representative of low burn-up weapons grade plutonium, whereas those nearer the surface are characteristic of high burn-up material. In simple terms, if the $^{240}Pu/^{239}Pu$ atom ratios at depth are representative of early discharges from Sellafield, and those near the surface are representative of more recent discharges, then it can be concluded that the bulk of the material initially reprocessed was low burn-up, but with time, inclusion of higher burn-up material resulted in an increase in the average $^{240}Pu/^{239}Pu$ ratios.

One interesting trend observed both by ICP-MS and by TIMS (see Figure 3.15) is the drop in the $^{240}Pu/^{239}Pu$ atom ratio in the top 5 cm of the sediment core. This could be caused by several mechanisms: bioturbation might have brought 'older' material from the depths of the core to the surface after or while the sediments were deposited, or the discharges from Sellafield in the late 1980s had lower $^{240}Pu/^{239}Pu$ atom ratios and this material formed a significant fraction of the plutonium in the surface sediments, or the sediment being deposited at Maryport was well mixed with low burn-up material before deposition. Evidence against bioturbation causing the lower $^{240}Pu/^{239}Pu$ surface ratios is provided by the

observation that only a few worm burrows were present in the core, and these were restricted to a depth of 1 m [Kershaw *et al.*, 1990]. The $^{240}Pu/^{239}Pu$ ratios at 1 m are of the order of 0.15, with a $^{239+240}Pu$ concentration of approximately 2000 Bq kg^{-1}, significantly higher than the 550 Bq kg^{-1} observed at the surface. Consider a theoretical situation where the sediment deposited on the surface at Maryport was well mixed with a $^{240}Pu/^{239}Pu$ ratio of 0.222 (the average value obtained for the top 50 cm), and a $^{239+240}Pu$ concentration of 550 Bq kg^{-1}. Under these conditions a worm depositing material from a depth of 1 m would have to deposit approximately 10% of the surface material for the final ratio to be 0.169 with a $^{239+240}Pu$ concentration of 700 Bq kg^{-1} (as observed in the 1-2 cm sample). Incursion of sediment from closer to the surface would require even more material to be deposited to significantly reduce the ratio, but this would also result in an increase in the activity of the sample. Considering the density of worm burrows found in the core and the average apparent accumulation rate of 6.4 cm y^{-1} [Kershaw *et al.*, 1990], this process would appear unlikely. In addition, X-ray radiographs taken by Kershaw *et al.* [1990] suggested that there was little post-depositional mixing in the sediments. Similarly, if pre-depositional mixing of the sediments were to result in the reduction of the $^{240}Pu/^{239}Pu$ atom ratio at the surface of the core, then this would require an incursion of significant quantities of low burn-up material, which either did not occur previously or was insignificant compared to the quantities of high burn-up material deposited at lower depths. From the surface data of the Maryport core and the data presented in section 4.2.2., which also showed spuriously low $^{240}Pu/^{239}Pu$ atom ratios in surface sediments near to Sellafield in 1985 and 1988, it is difficult to ascertain if the low ratios were caused by mixing with sediments contaminated with much 'older' discharges or if the ratios were characteristic of the discharge values in the late 1980s.

For comparison, the $^{238}Pu/^{239+240}Pu$ activity ratios in samples from the Maryport core, obtained by Kershaw *et al.* [1990], are shown in Figure 4.5. The shape of the $^{238}Pu/^{239+240}Pu$ activity profile is similar to that of the $^{240}Pu/^{239}Pu$ atom ratio profile, but with a larger variation, changing from 0.0208 ± 0.0005 at depths of 180-185 cm to 0.256 ± 0.006 at depths of 46-48 cm. However, it should be noted that the shape of the profile is complicated by the radioactive decay of ^{238}Pu,

Figure 4.5 $^{238}Pu/^{239+240}Pu$ activity ratio profile for Maryport core using (a) measured ratios and (b) decay-corrected ratios [Kershaw *et al.*, 1990]

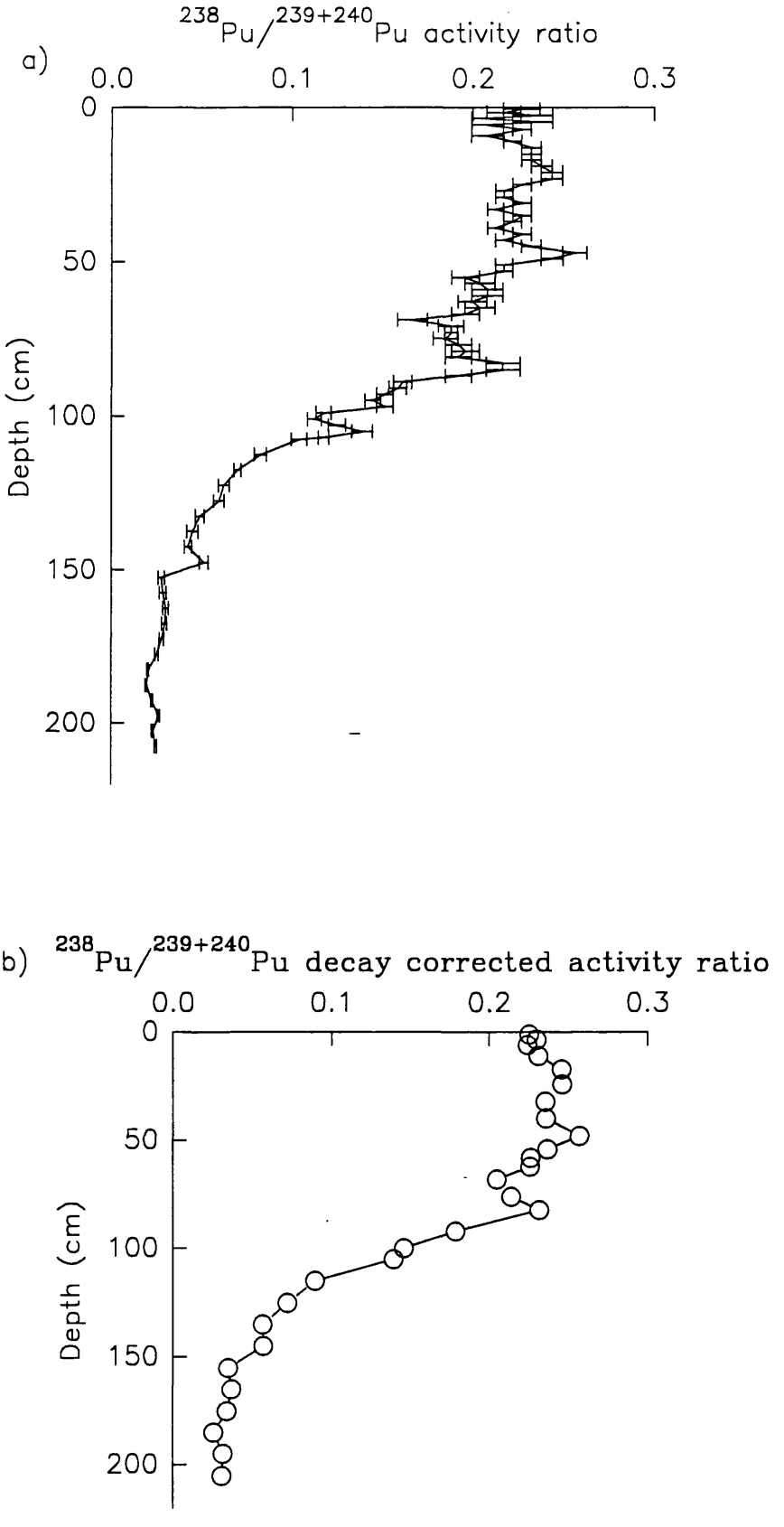

whose 87.8 year half-life is significant in terms of the 40 years of Sellafield discharges. Decay correcting the $^{238}Pu/^{239+240}Pu$ ratios requires some assumptions on the 'age' of the material deposited. Figure 4.5b shows the decay corrected profile, based on the chronology established by Kershaw *et al* [1990]. Like the $^{240}Pu/^{239}Pu$ atom ratio profile, the $^{238}Pu/^{239+240}Pu$ activity ratios level off in the top 6 to 50 cm and show a decrease, but to a lesser extent, near the surface of the core. This would be expected as the $^{238}Pu/^{239+240}Pu$ activity ratios are also indicative of the degree of burn-up, but in a more indirect way than the $^{240}Pu/^{239}Pu$ atom ratio (see section 1.3.1).

4.3.1.2 The Solway core (SC1)

The $^{240}Pu/^{239}Pu$ atom ratio profile for the Solway core (SC1) is shown in Figure 4.6. The general shape of the profile is similar to that observed at Maryport. The $^{240}Pu/^{239}Pu$ atom ratios in SC1 change from 0.090 ± 0.014 at a depth of 60-65 cm, to 0.2069 ± 0.0023 at a depth of 20-25 cm, with the values levelling off in the top 35 cm to an average of 0.201. The rate of change of the $^{240}Pu/^{239}Pu$ ratio with depth is much greater for SC1 than for the Maryport core, as the average sedimentation rate for the Solway core was 2.4 cm y^{-1} [Allan, 1992], compared to 6.4 cm y^{-1} observed at Maryport [Kershaw *et al.*, 1990]. Allan [1992] obtained an average sedimentation rate for SC1 by matching the depth of the maximum of the nuclide profiles with the year of the maximum Sellafield discharges for $^{239+240}Pu$, ^{241}Am and ^{137}Cs. The average sedimentation rate was then used to establish a chronology for the core. Using this, and the chronology obtained by Kershaw *et al.* [1990] for the Maryport core, direct comparison of the $^{240}Pu/^{239}Pu$ atom ratio data from each site can be made (Table 4.6). The data show remarkable correspondence considering possible discrepancies in the individual chronologies, and factors such as the location and topography of each site, and the dynamic nature of the Irish Sea. One difference is the higher $^{240}Pu/^{239}Pu$ atom ratios observed near the surface of the Maryport core, which has an average $^{240}Pu/^{239}Pu$ plateau value of 0.229 ± 0.013, compared to the equivalent value of 0.201 ± 0.006 observed for SC1. Since there was little evidence of post-depositional mixing within SC1 [Allan, 1993], the lower $^{240}Pu/^{239}Pu$ atom ratios in the near surface samples from the core are likely to be the result of greater mixing with

Figure 4.6 $^{240}Pu/^{239}Pu$ **atom ratio profile for Solway core, SC1**

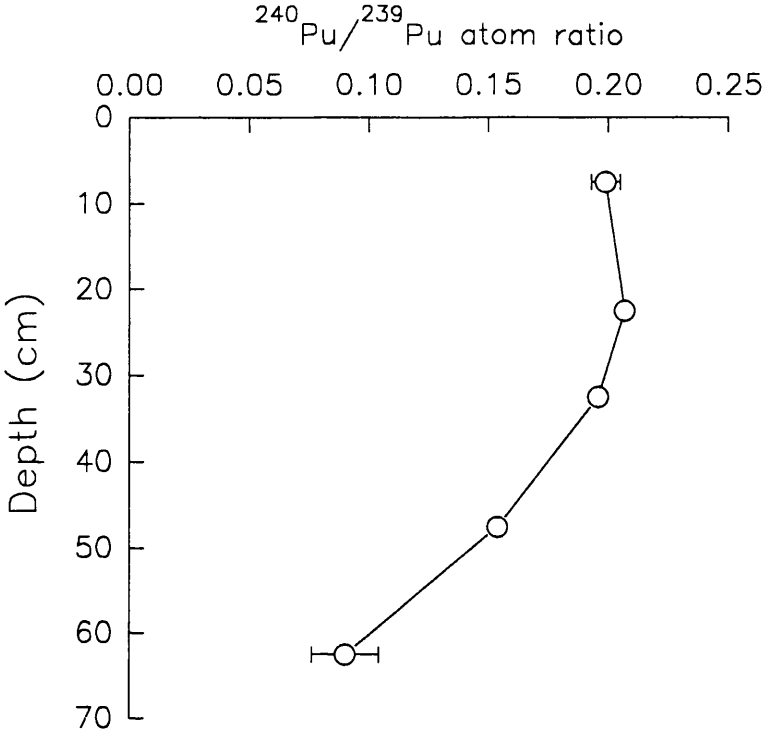

Figure 4.7 $^{238}Pu/^{239+240}Pu$ **activity ratio profile for SC1 [Allan, 1993]**

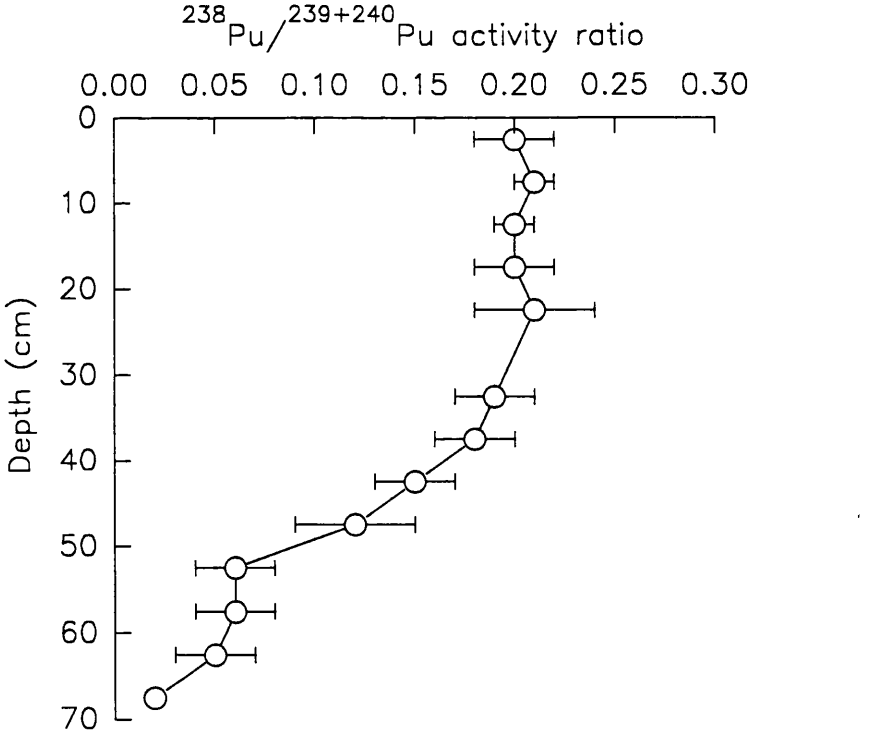

'older' material before deposition, compared to the sediments deposited at Maryport. This is not unexpected considering that sediment transport has been shown to be the dominant mechanism for the transfer of plutonium in the Sellafield discharges to the Solway [MacKenzie *et al.*, 1987], and considering the difference in the distance between the Sellafield pipeline, Maryport and the Solway, with the chance for the sediments to mix before deposition increasing with distance from Sellafield.

Table 4.6 : Comparison of $^{240}Pu/^{239}Pu$ atom ratios obtained for the Solway core with the average ratios for the Maryport core at the equivalent depths, based on the chronologies established by Allan [1994] and Kershaw *et al.* [1990] for the Solway and Maryport core respectively.

	Solway core		Maryport core	
'Date'	Depth (cm)	$^{240}Pu/^{239}Pu$	Depth (cm)	Average $^{240}Pu/^{239}Pu$
1988-1986	5-10	0.1988 ± 0.0059	-	-
1982-1980	20-25	0.2069 ± 0.0023	14-36	0.232 ± 0.011
1977-1975	30-35	0.1958 ± 0.0027	52-66	0.1896 ± 0.0042
1971-1969	45-50	0.1543 ± 0.0033	88-110	0.155 ± 0.013
1963-1965	60-65	0.090 ± 0.014	140-170	0.0830 ± 0.0073

Figure 4.7 shows the $^{238}Pu/^{239+240}Pu$ activity ratios obtained by Allan [1993] for SC1. As was observed for the Maryport core, the $^{238}Pu/^{239+240}Pu$ activity and $^{240}Pu/^{239}Pu$ atom ratio profiles down SC1 are similar, but with the $^{238}Pu/^{239+240}Pu$ activity ratios showing a larger range of values. The $^{238}Pu/^{239+240}Pu$ activity profiles for the Maryport and Solway cores are similar after consideration of the different sedimentation rates at each site. Again, the plateau ratios for the Solway show a lower average value of 0.204 ± 0.005 in the top 25 cm compared to 0.224 ± 0.013 in the equivalent top 65 cm of the Maryport core. This supports the evidence that the sediments recently deposited at the Solway have been better mixed with material contaminated with 'older' discharges than the sediments deposited at Maryport.

Figure 4.8 (a) ^{237}Np specific activity, (b) $^{239+240}Pu$ specific activity and (c) $^{237}Np/^{239+240}Pu$ activity ratio profiles for Maryport core

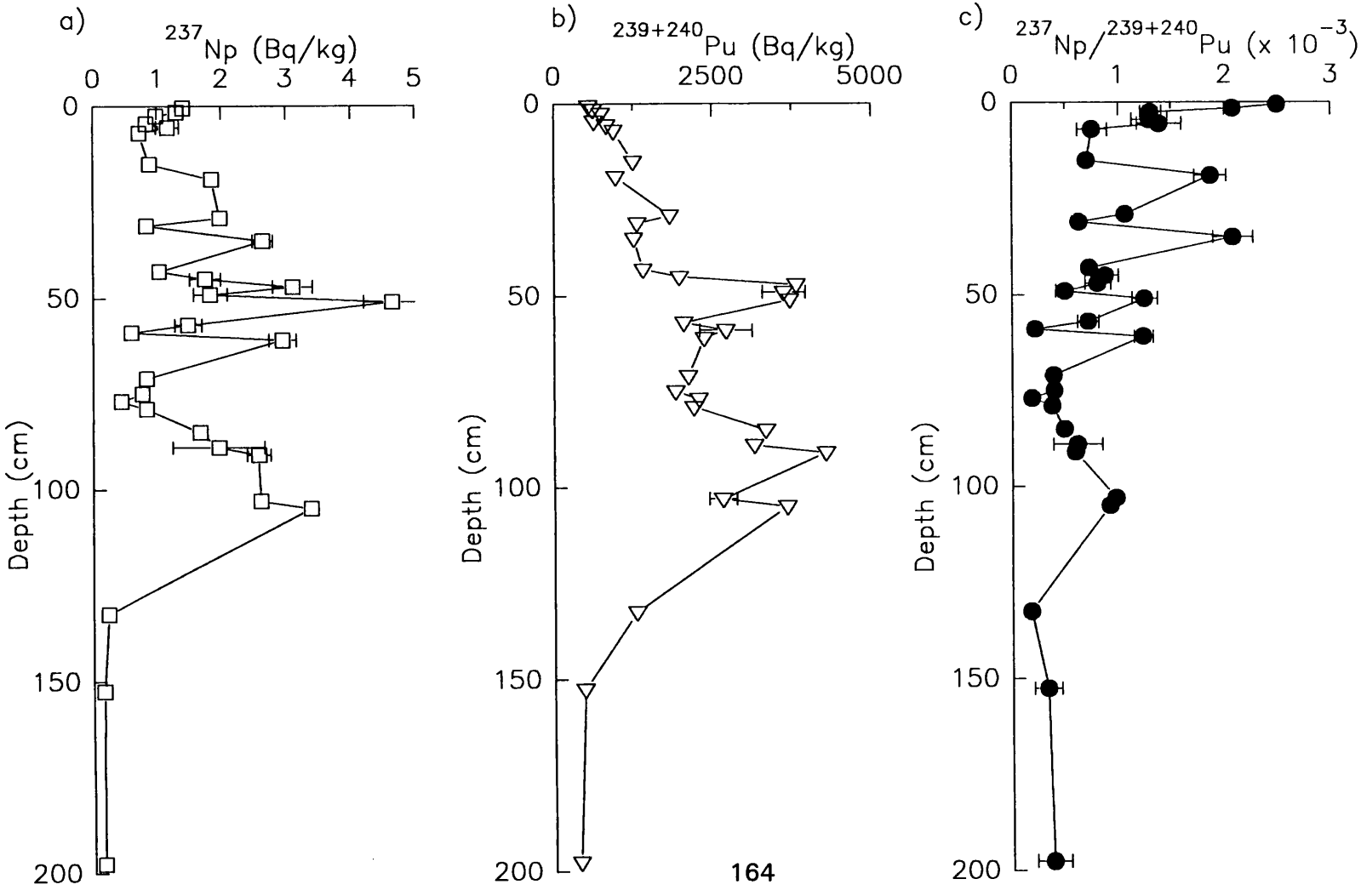

4.3.2 ^{237}Np specific activity in the Maryport core

The ^{237}Np specific activities of samples from the Maryport core are shown in Figure 4.8, along with the corresponding $^{239+240}Pu$ specific activity and $^{237}Np/^{239+240}Pu$ activity ratio profiles. The ^{237}Np profile has more structure than the $^{239+240}Pu$ profile, but both profiles display two sub-surface maxima at depths of approximately 50 and 105 cm. A notable difference between the two profiles is the increase in ^{237}Np specific activities from a depth of 8 cm to the surface. In general, there is a relatively constant relationship between ^{237}Np and $^{239+240}Pu$ in the samples, but with a gradual increase in the relative proportion of ^{237}Np towards the surface. This reflects the trend observed in the Sellafield discharges, which have shown an increase in $^{237}Np/^{239+240}Pu$ activity ratios since 1982 (see Table 4.7). The correlation between the ^{237}Np specific activities and $^{237}Np/^{239+240}Pu$ activity ratios for the core samples, averaged in yearly increments using the chronology established by Kershaw *et al.* [1990], and the corresponding Sellafield discharge data (see Figure 4.9) is fairly good, with linear correlation coefficients of 0.81 and 0.93 respectively.

Table 4.7 ^{237}Np and $^{239+240}Pu$ activities and the $^{237}Np/^{239+240}Pu$ activity ratios for discharge from Sellafield, 1978-1988 [BNFL, 1979-1990].

Year	^{237}Np discharge (TBq)	$^{239+240}Pu$ discharge (TBq)	$^{237}Np/^{239+240}Pu$ ratio
1978	0.592	45.62	0.0130
1979	0.333	37.44	0.0089
1980	0.666	20.35	0.0327
1981	0.407	15.32	0.0266
1982	0.307	16.06	0.0191
1983	0.324	8.73	0.0371
1984	0.3	8.3	0.0361
1985	0.2	2.6	0.077
		Total Pu(α) discharge (TBq)	^{237}Np/Pu(α) ratio
1986	0.4	2.7	0.148
1987	0.23	1.3	0.177
1988	0.28	1.4	0.200

Figure 4.9 Comparison of Maryport core and Sellafield discharge data for (a) ^{237}Np (b) ^{237}Np with the available discharge data normalised to 1984 core data and (c) $^{237}Np/^{239+240}Pu$ activity ratios using the chronology established by Kershaw *et al.*, [1990]

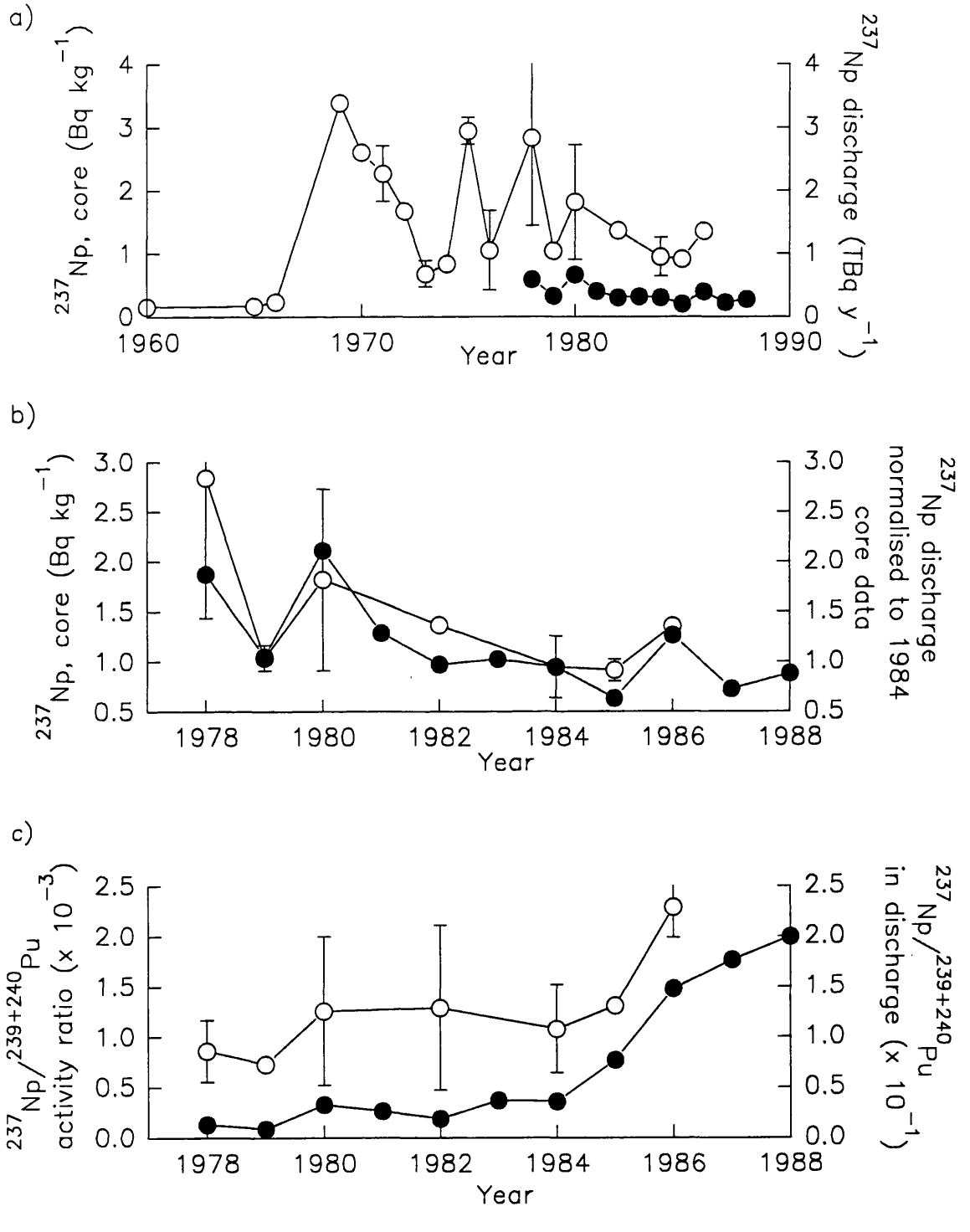

Table 4.8 ^{237}Np activities and $^{237}Np/^{239+240}Pu$ activity ratios observed in sediments from the Irish Sea.

Reference	Sediment sample	^{237}Np specific activity (Bq kg^{-1})	$^{237}Np/^{239+240}Pu$ activity ratio
Assinder *et al.*, 1991	Intertidal, from Solway to N. Welsh coast, 1988	0.012 - 4.5	0.0017 - 0.0052
Hursthouse, 1990	Ravenglass silt, 1987	3.26 ± 0.05	0.0038
	Offshore cores, 1987	0.25 - 0.56	0.0007 - 0.0023
Byrne, 1986	Newbiggin	4.35	-
	Grange-over-sands	0.55	-
	Ravenglass	5.9	-
Harvey and Kershaw, 1984	Offshore core, 1982	0.8 - 14.4	0.0037 - 0.012
Pentreath and Harvey, 1981	Suspended particulates	0.19 - 38.9	-
Holm, 1981	Sediment, 1977	1.4	3.44×10^{-4}

Figure 4.10 Ratio of $^{237}Np/^{239+240}Pu$ activity ratios in the Sellafield discharges to averaged Maryport core data for the equivalent 'year', with depth

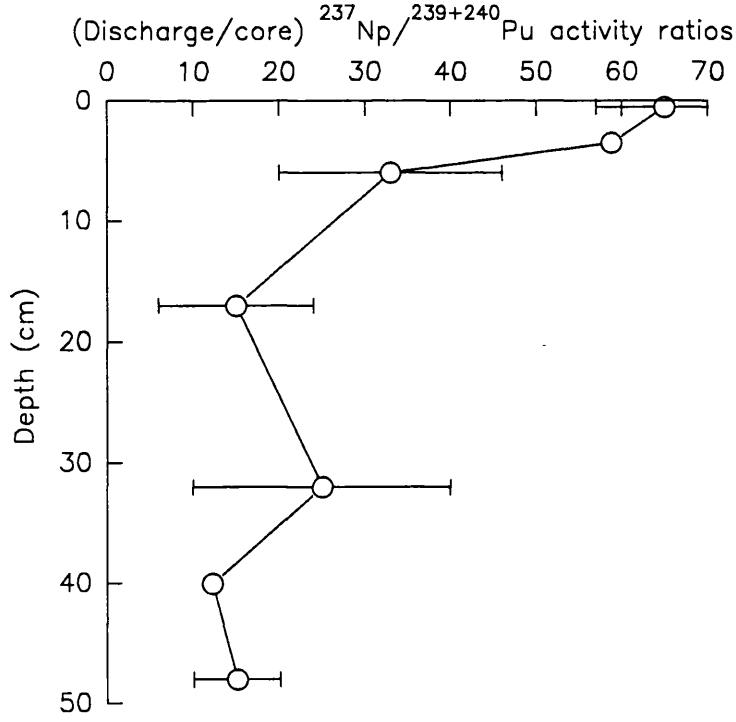

Interestingly, the $^{237}Np/^{239+240}Pu$ activity ratios throughout the Maryport core agree well with published $^{237}Np/^{239+240}Pu$ activity ratios observed in Irish Sea sediments (Table 4.8), but are an order of magnitude, or more, lower than the ratios in the discharges. This reflects the relative bulk K_d values for Pu and Np in the Irish Sea which are of the order 10^5 and 10^4 respectively, suggesting that Pu should be relatively enhanced in the sediments by a factor of approximately 10 compared to Np (see section 1.5.2). Figure 4.10 shows the ratio of the $^{237}Np/^{239+240}Pu$ activity ratios in the discharge to the equivalent ratio in the averaged core segments against the depth down the core, corresponding to each 'year'. At depths of greater than 10 cm, the factors between the discharge and core ratios are fairly constant at approximately 15, as expected. However, towards the surface of the core, the factor increases, up to a value of 70. This suggests that in the top 10 cm of the core there is a relative lack of Np in the solid phase compared to Pu. Interpretation of this requires an understanding of the chemical processes occurring in the sediments which could effect the relative proportions of the oxidation states of Np between the more particle reactive Np(IV) and Np(V).

Interstitial water profiles obtained from nearby cores collected at the same time, indicated that SO_4^{2-} reduction was taking place in the Maryport sediments [Kershaw *et al.*, 1990]. The absence of NO_3^- below 0-1 cm suggested that anoxic conditions occurred below the sediment surface and the enhanced titration alkalinity concentration measured in the top 0-1 cm segment suggested that sulphate reduction began immediately below the sediment surface [Kershaw *et al.*, 1990; Elderfield *et al.*, 1981]. However, the rate of sulphate reduction appeared to be lower in the top 10 cm compared to the sediments at greater depths, despite the greater availability of metabolisable organic matter near the sediment surface. To account for this discrepancy, it was concluded that irrigation of the sediments was occurring in the top 10 cm [Kershaw *et al.*, 1990].

The chemistry of the transitional zone between the oxidising seawater and the relatively reducing sediment is complex, and is further complicated by the irrigation of the surface sediments. From considerations of porewater chemistry and Eh/pH conditions, it is expected that reduction of Np(V) to Np(IV) should occur in the sediments below the top 10-20 cm [Harvey, 1981]. Predictions of the behaviour

of Np in the transitional zone, however, is difficult and experiments observing the reduction of Np(V) in the upper layers of disturbed sediments were inconclusive [Harvey, 1981]. Harvey and Kershaw [1984] observed that the percentage of reduced Np in the interstitial waters of an Irish Sea core, increased from the surface to a depth of approximately 8 cm, suggesting reduction of Np to Np(IV), which may have then formed soluble complex species with organic ligands. Similar behaviour would be expected for Pu. For example, Malcolm *et al.* [1990] found that > 96% of Pu was in the reduced form at all depths of several sediment cores, except for the top 2 cm where 27 - 67% was found in the oxidised form due to the irrigation of the sediment with oxidising seawater.

The evidence above suggests that in the top 10 cm of the Maryport core both Np and Pu may be present in more mobile oxidised forms due to the irrigation of the sediments. In addition, discrepancies in the relative proportions of Np and Pu in the solid phase compared to that expected from the relative K_ds of each element, indicate that this effect is more significant for Np than Pu, suggesting that Np is more likely to be remobilised from the surface sediment than Pu. Confirmation of this requires the measurement of the oxidation states of Np and Pu both in the solid phase and the interstitial water.

4.3.3 Matching core profiles with Sellafield discharge data

The relationship between the Sellafield discharges and their distribution within the sediments of the Irish Sea is complex, depending on factors such as: fluctuations of the discharges between years and within individual years; changes in the chemical associations in the effluent as a result of changes in the reprocessing procedures; mixing of recently contaminated sediments with 'older' material, corresponding to earlier discharges; redistribution of the radionuclides within the sediments by bioturbation, diffusion or diagenesis; and changes in the dynamics of the Irish Sea [Kershaw *et al.*, 1990; and section 1.5.4]. Despite the complexity of the environmental system, there have been numerous attempts to match temporal variations in the Sellafield discharges with sediment core profiles (see section 1.5.5), including the use of techniques such as simple visual matching of core profile shapes with the discharge record and $^{210}Pb_{ex}$ dating techniques to determine

Figure 4.11 Vertical profiles of Sellafield-derived artificial radionuclides for Maryport cores together with with decay-corrected discharges [Kershaw *et al.*, 1990]

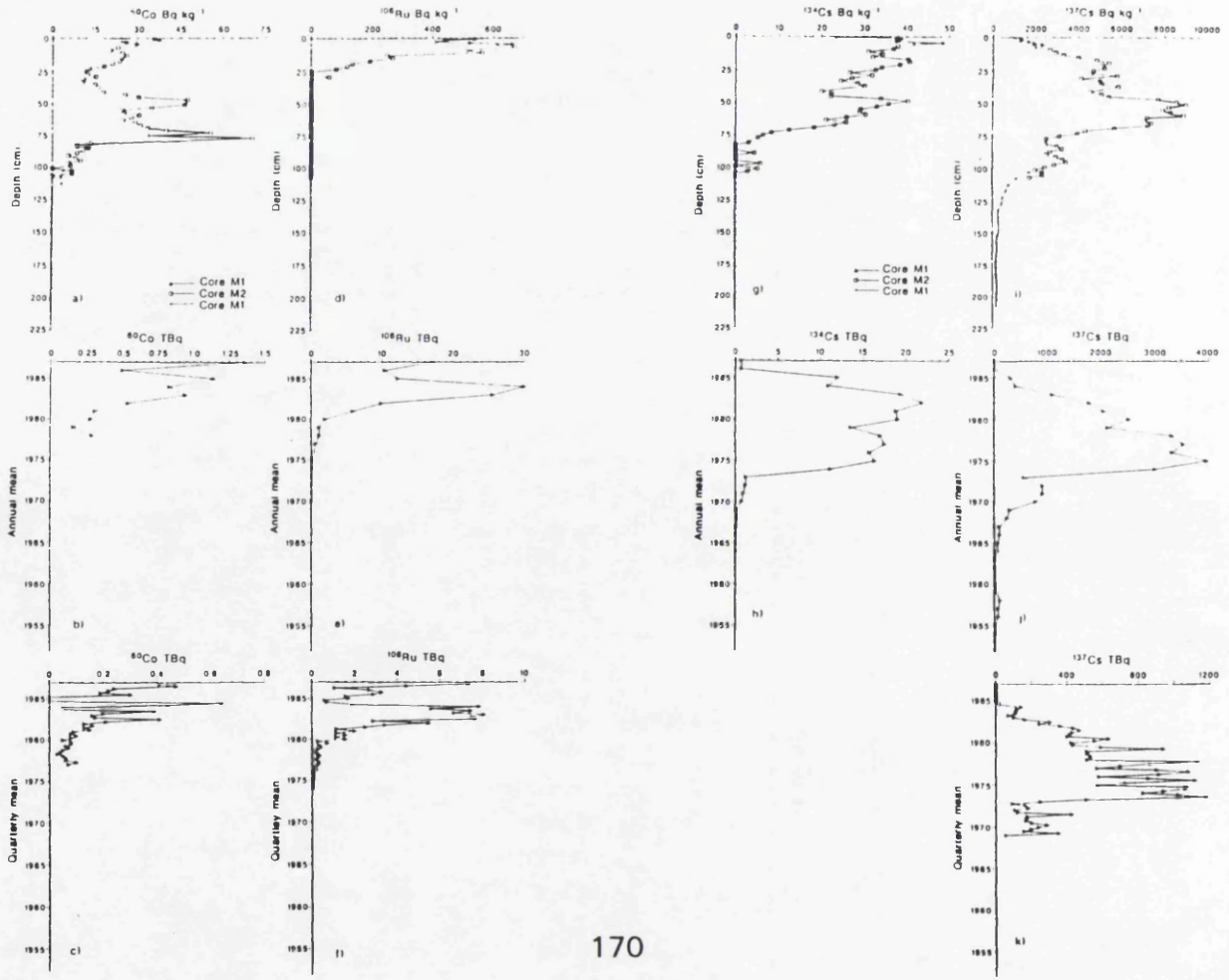

Figure 4.11 continued

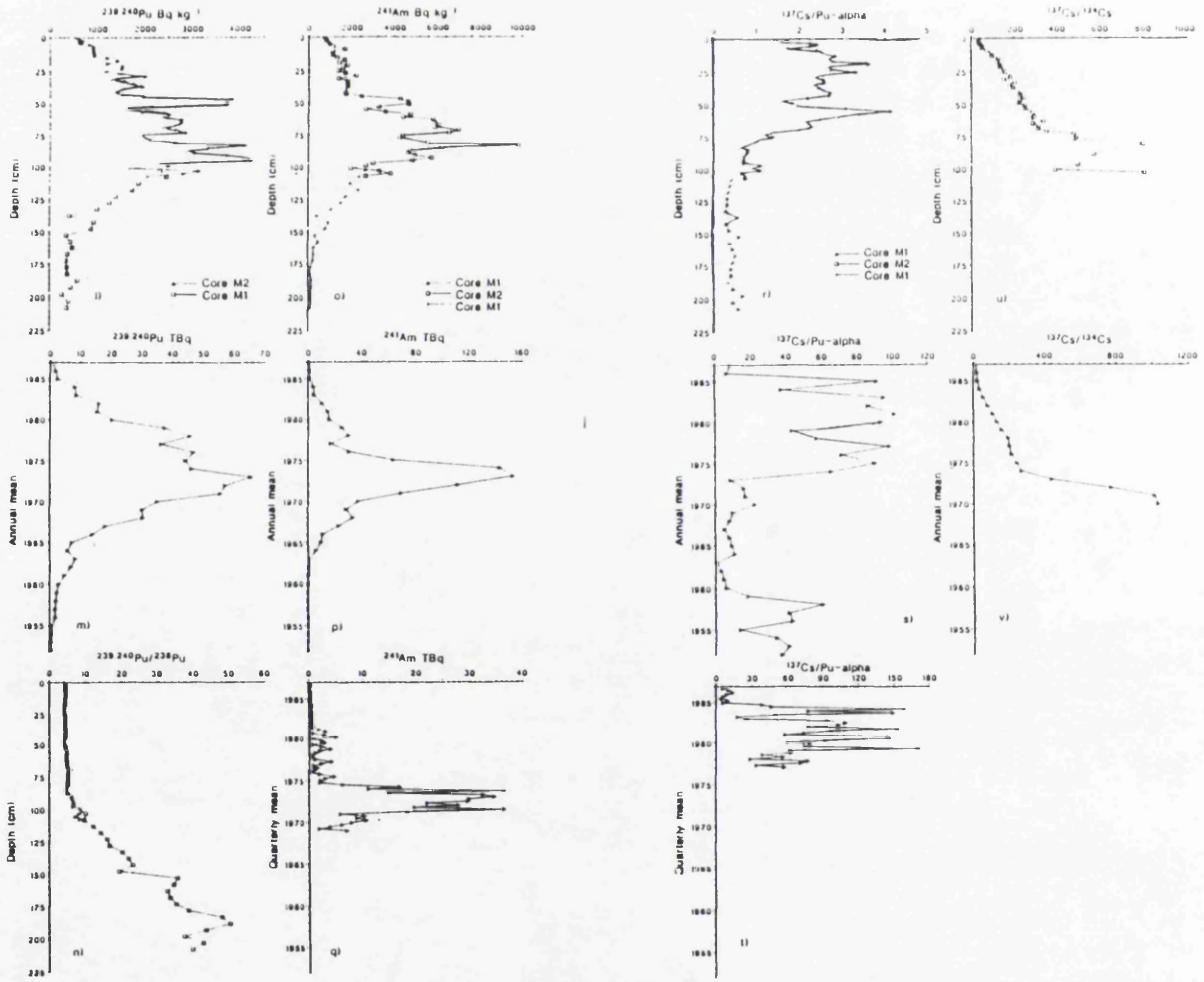

independent sedimentation rates.

4.3.3.1 The Maryport core

Kershaw *et al.* [1990] obtained data from the Maryport core samples for a wide range of radionuclides. Some of these profiles and the corresponding Sellafield discharge data are shown in Figure 4.11. On first glance, the shapes of the radionuclide profiles in the sediment appear to match the shapes of the annual Sellafield discharge data closely, particularly for $^{239+240}Pu$, ^{241}Am and ^{137}Cs. However, there are some exceptions. For example the ^{60}Co profile shows no obvious relationship with the discharge data. Kershaw *et al.* [1990] established a chronology for the Maryport core by visually matching the core profile shapes, for both radionuclides and nuclide activity ratios, with the discharge data, combining the individual radionuclide chronologies to obtain an overall 'best-fit' chronology. This required the assumption of a 'lag' time of approximately 1 - 2 years for discharged radionuclides to become incorporated into the sediments at Maryport, some 40 km north of the discharge point. The resulting 'date' of the top of the sediment core (which was collected in 1988) was 1986. Attempts to use the $^{210}Pb_{ex}$ concentrations in the core samples, to provide an independent estimate of the sedimentation rate, were limited due to an additional and variable source of ^{210}Pb from a phosphate factory at Whitehaven [Kershaw *et al.*, 1990; McCartney *et al.*, 1990]. The implications of the chronology derived by Kershaw *et al.* [1990] were that the concentrations of radionuclides in the sediment core at specific depths were directly proportional to the Sellafield discharges in the equivalent 'year'. However, from the differences observed between the $^{154}Eu/^{155}Eu$ and $^{239+240}Pu/^{238}Pu$ activity ratios in the core, with the equivalent decay-corrected activity ratios in the discharges, it was noted that some mixing of the sediments deposited at Maryport with 'older' material must have occurred [Kershaw *et al.*, 1990]. In particular, it was found that the decay-corrected $^{239+240}Pu/^{238}Pu$ activity ratios in the core were consistently higher by a factor of 1.31 $\pm$ 0.13, than those of the discharge between 1978 and 1986. This factor was used to modify the $^{239+240}Pu/^{238}Pu$ activity ratios throughout the core, to obtain an approximate value for the discharges of each year, which was then applied to the total Pu(α) discharge data, giving an estimate for the ^{238}Pu discharge from 1959 to 1986 (see Figure

4.12) [Kershaw *et al.*, 1990]. Although the results of the predicted ^{238}Pu discharge agree well with the recorded Sellafield discharge data, where such data are available (1978-1986), the use of a constant mixing factor in this way for the whole of the core is questionable. It might be expected that for some time after the mid 1970s, the sediment concentrations and nuclide ratios would be dominated by the peak discharges which occurred in the early to mid 1970s. Between 1978 and 1986 the $^{239+240}Pu/^{238}Pu$ activity ratios in the discharges did not vary significantly. As a result, mixing of sediments contaminated by these discharges with a sediment pool dominated by the peak discharges would result in the observed consistent relationship between the average activity ratios in the deposited sediments and the discharge data. However, the situation was very different before the peak discharges, when plutonium was released into a relatively uncontaminated environment. In this case, the significance of the previous discharges would be expected to have a lesser and variable influence on the deposited sediment activity ratios, depending on the degree of contamination of the sediment pool. The relationship between the sediment core profiles and Sellafield discharge data is discussed further below.

Figure 4.12 Actual and predicted discharges of ^{238}Pu (TBq y^{-1}) [Kershaw *et al.*, 1990]

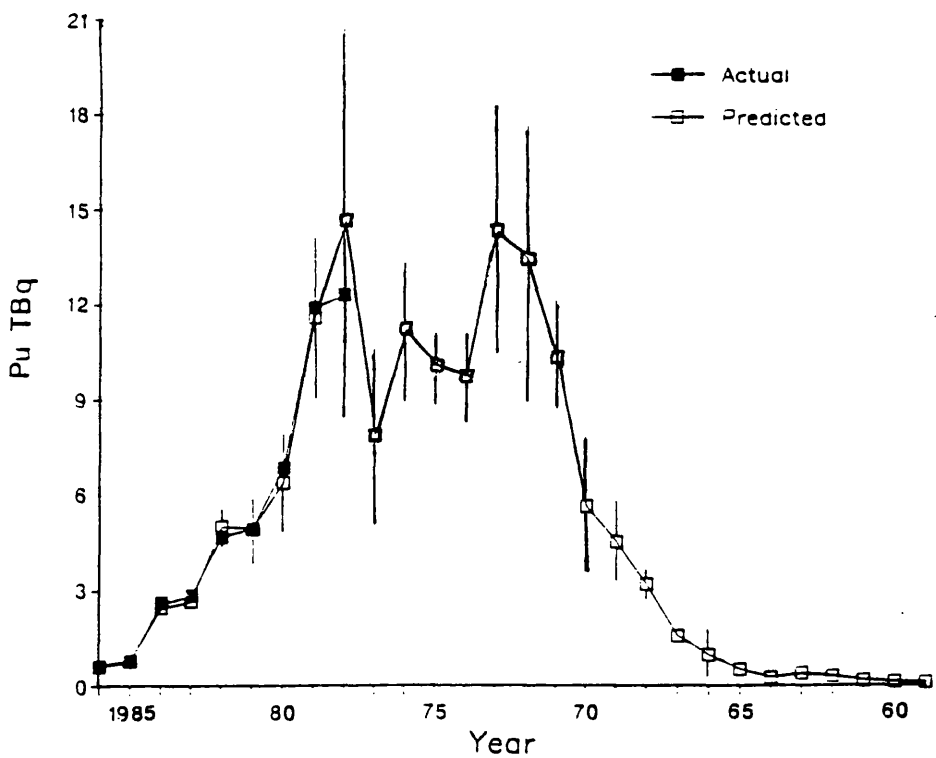

On closer inspection, there are several inconsistencies between the sediment core profiles and the Sellafield discharge data.

For example, for ^{137}Cs, $^{239+240}Pu$ and ^{241}Am, the ratios between the maximum and surface nuclide concentrations of the core samples were one to two orders of magnitude lower than the equivalent ratios in the Sellafield discharges, suggesting a non-linear relationship between the sediment concentrations and the quantities of radionuclides discharged [MacKenzie *et al.*, 1994]. In addition, the surface concentrations of these radionuclides are much higher than would be expected, considering the recent levels of the Sellafield discharges. The similarities and differences between the $^{239+240}Pu$ specific activity profile in the Maryport core and the Sellafield discharge data can be seen from Figure 4.13 which compares the core data, averaged over yearly increments, with the discharge data. Much of the fine structure of the Sellafield discharges is mimicked in the core profile. However, the maximum to surface ratio for the $^{239+240}Pu$ concentrations is 7.5, compared to 30.6 observed in the equivalent Sellafield discharge data, with the surface $^{239+240}Pu$ concentrations being higher than expected from the recent discharge data.

MacKenzie *et al.* [1994] hypothesised that if particle transport was the dominant mechanism of transfer of Sellafield waste to the intertidal sediments of the Irish Sea, and assuming that the contaminated offshore sediments are completely vertically mixed (with respect to radionuclide activity ratios) before redistribution, then the radionuclide concentrations and activity ratios in accumulating intertidal sediments would be related to the time-integrated discharges. Further, in an accumulating sediment environment, such as the sample sites of Maryport and the Solway, then deposits to the surface of the sediment from the mixed sediment pool, and subsequent radionuclide activity ratios at any given depth, should be directly related to the discharge integrated up to the time of deposition, after taking into account radioactive decay and ingrowth. The authors contended that the empirical data supported this hypothesis by comparing $^{241}Am/^{239+240}Pu$ and $^{137}Cs/^{241}Am$ activity ratios normalised to the annual discharges with those normalised to the time-integrated discharges, accounting for the ingrowth of ^{241}Am from ^{241}Pu (Figure 4.14). The $^{241}Am/^{239+240}Pu$ ratios for the Maryport core, normalised to the time-integrated discharges, showed little variation, with a mean

Figure 4.13 $^{239+240}$Pu core profile for (a) all samples, (b) averaged data in yearly increments, and (c) $^{239+240}$Pu Sellafield discharge data [Kershaw *et al.*, 1990; BNFL, 1971-1986; Cambray, 1982]

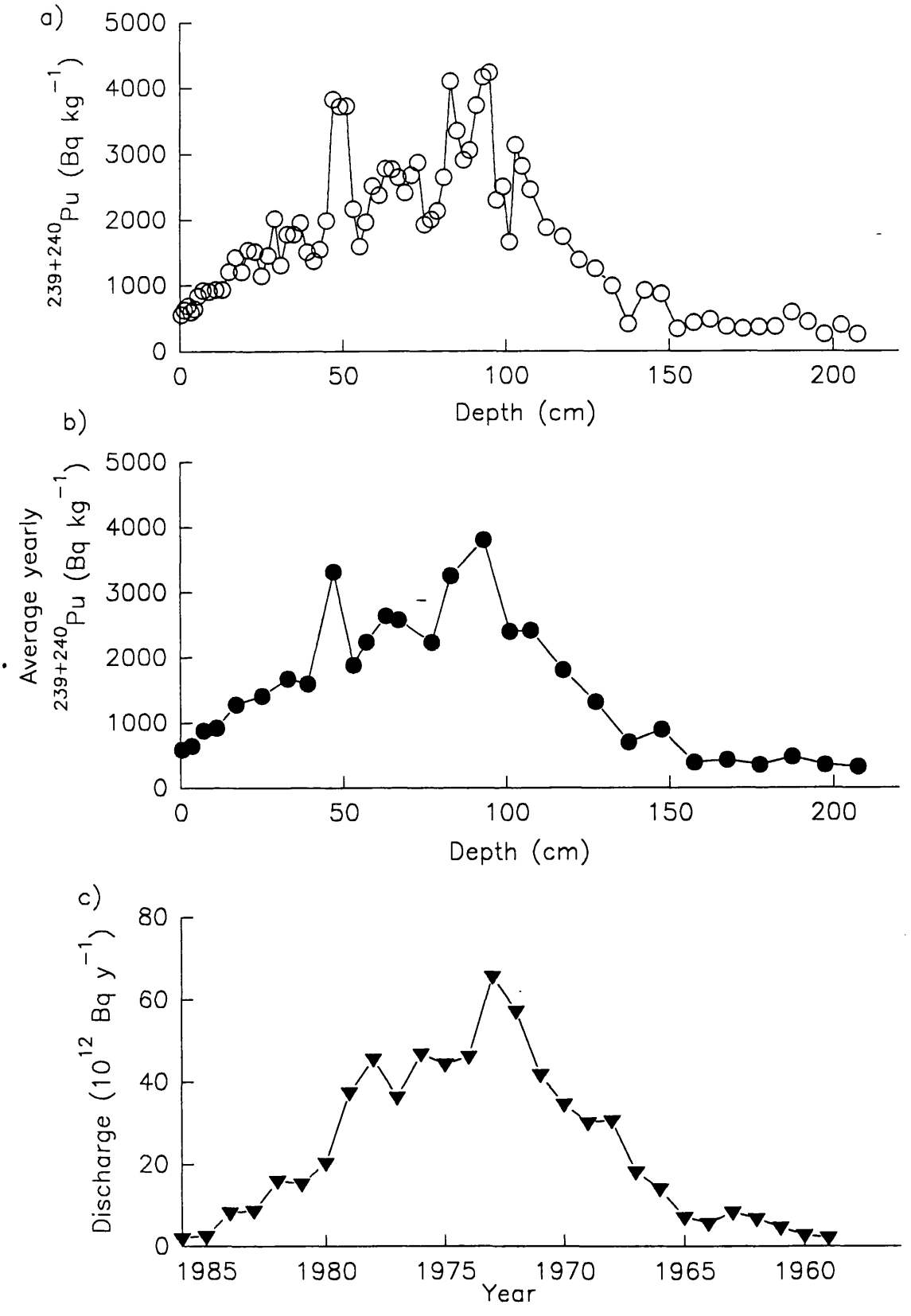

Figure 4.14 (a) $^{241}Am/^{239,240}Pu$ activity ratios and (b) decay corrected $^{137}Cs/^{241}Am$ activity ratios for Maryport cores [Kershaw *et al.*, 1990], normalised to the corresponding ratio in: Sellafield annual discharges; Sellafield annual discharges plus ingrowth of ^{241}Am from decay of corresponding ^{241}Pu discharges; and the time-integrated Sellafield discharge [MacKenzie *et al.*, 1994]

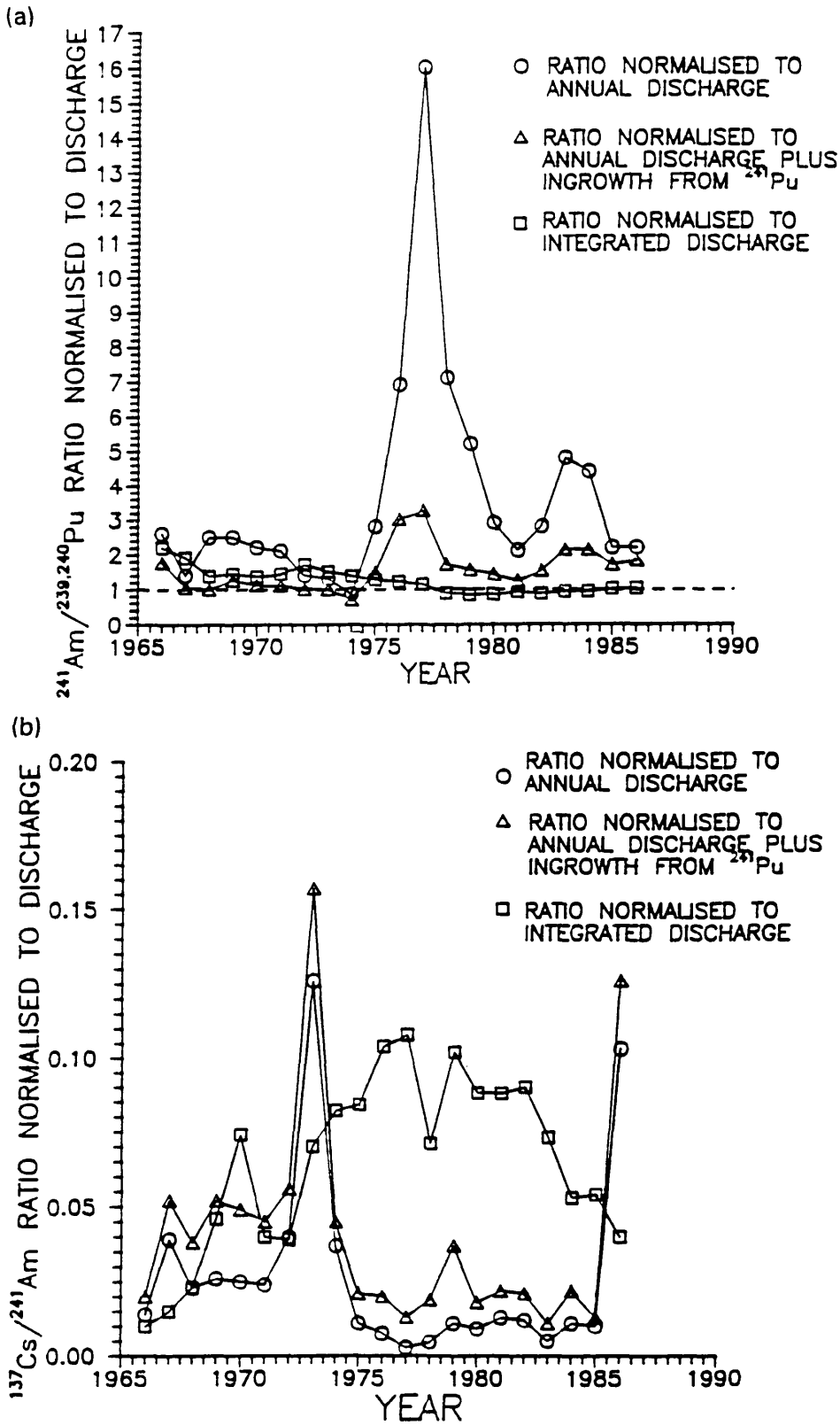

value of 1.3 ± 0.3. Ratios obtained after the peak Sellafield discharges, in the mid 1970s, were even more consistent, with a mean value of 0.99 ± 0.14. In contrast, the ratios normalised to the annual discharges showed large and inconsistent variations, changing from 2 to 16, and from 1.1 to 3.8 when taking into account ingrowth from ^{241}Pu. This was supported by $^{241}Am/^{239+240}Pu$ ratios for Solway cores which displayed similar consistencies when normalised to the time-integrated discharges, and variations when normalised to the annual discharges.

The $^{137}Cs/^{241}Am$ activity ratios normalised to the time-integrated discharges showed more variation, and for both the Maryport and Solway cores, displayed a systematic decrease after the peak discharges. This was interpreted as the result of re-dissolution of ^{137}Cs from the sediment [MacKenzie *et al.*, 1994]. Unfortunately, such comparisons cannot be made for $^{237}Np/^{239+240}Pu$ activity ratios as the time integrated discharges for ^{237}Np cannot be calculated from the available discharge data.

The time-integrated environmental inventories for Sellafield waste ^{241}Am and $^{239+240}Pu$ have been increasing continuously. The corresponding ^{137}Cs inventory has shown only a small decrease since 1983 when radioactive decay has exceeded fresh Sellafield inputs. However, the sediment profiles show distinct sub-surface maxima corresponding approximately to the sediments deposited in the mid-1970s. To account for this, MacKenzie *et al.* [1994] contended that physical dispersion and dilution of the contaminated sediments have caused a decrease in the sediment concentrations deposited since the 1970s. This is supported by observation of the temporal change in radionuclide concentrations in Irish Sea surface sediments. For example, Pentreath *et al.* [1984] observed in 1977/78, that radionuclide concentrations decreased in surface sediments by two orders of magnitude between the discharge point and the coast of south-west Scotland, whereas by 1987, McDonald *et al.* [1990] found that radionuclide concentrations were a function of the sediment composition and that for silts the concentrations were effectively constant over a distance of 60 km. Vertical mixing of sediment has been shown to reduce the radionuclide concentrations by mixing the surface contaminated material with deeper uncontaminated sediments [Kershaw *et al.*, 1983; 1984].

MacKenzie *et al.* [1994] described these processes in terms of a simple model in which discrete volumes of sediment from a well mixed sediment pool are transferred to an accumulating intertidal deposit, providing a record of the changes in the sediment radionuclide concentrations, as described by:

$$\frac{dC_t}{dt} = I_t - \Lambda C_t$$

where C_t is the radionuclide concentration in the sediment pool at time t, I_t is the annual input from the Sellafield discharge and Λ is a removal probability per unit time which represents a sum of contributions from radioactive decay, dispersion/dilution and redissolution. An outcome of this model is that if the value of I_t tends towards zero, as observed in recent years, then C_t should show an exponential decrease with time. This is supported by plots of the natural logarithm of the sediment $^{239+240}$Pu concentration, normalised to the time-integrated discharge (shown in Figure 4.15 for Maryport and Solway cores), which reveal a highly linear decrease as a function of time, particularly for the sections of the plot relating to post 1975 [MacKenzie *et al.*, 1994]. From the linear portions of these plots, half-value periods for the reduction of radionuclide concentrations ($\ln 2/\Lambda$) can be derived. For $^{239+240}$Pu, these are calculated to be approximately 5.6 and 3.7 years for SC1 and the Maryport core respectively, implying that a more rapid reduction of the $^{239+240}$Pu concentrations by dilution/dispersion is observed at Maryport than in the Solway. MacKenzie *et al.* [1994], suggested that this could be the result of non-uniform distribution of radionuclides in offshore sediments resulting in redistribution of material from areas of relatively high concentration to areas of lower concentration, but leading to an increase of the radionuclide inventory in accumulating sediments such as those sampled in the Solway.

Figure 4.16 shows the year by year relative values of C_t, as derived from the integrated $^{239+240}$Pu discharge data, with no dilution/dispersion, and with half-time values of 5.6 and 3.7 years, as calculated for the Maryport and Solway (SC1) cores. One of the interesting aspects of this model is that the maximum

Figure 4.15 Plot of the natural logarithm of the ratio of the sediment $^{239+240}Pu$ concentration to the corresponding integrated Sellafield discharge for (a) Maryport cores [Kershaw *et al.*, 1990] and (b) Solway core SC1 [MacKenzie *et al.*, 1994]

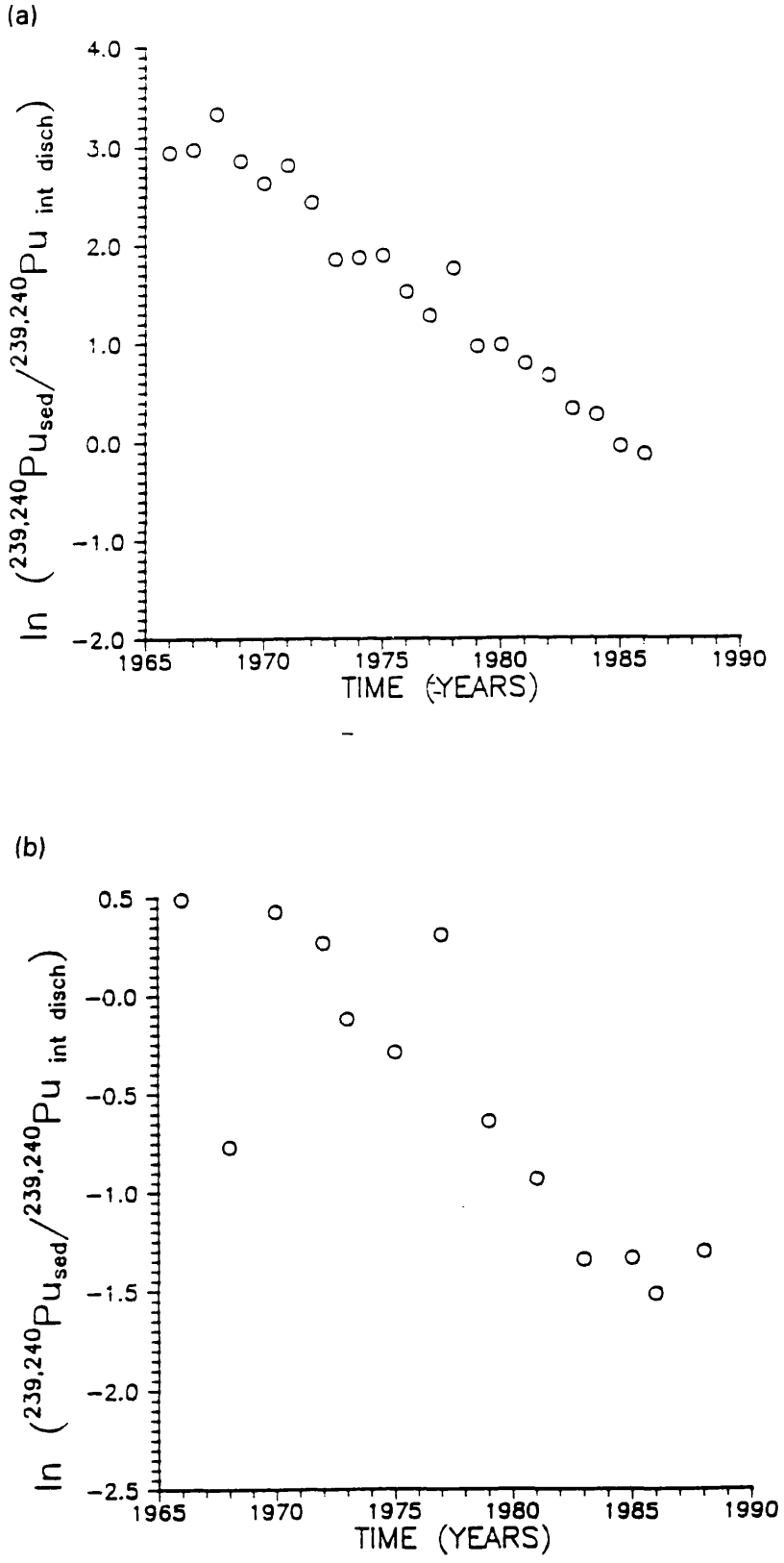

Figure 4.16 Model curves for temporal variations in relative concentrations of $^{239+240}Pu$

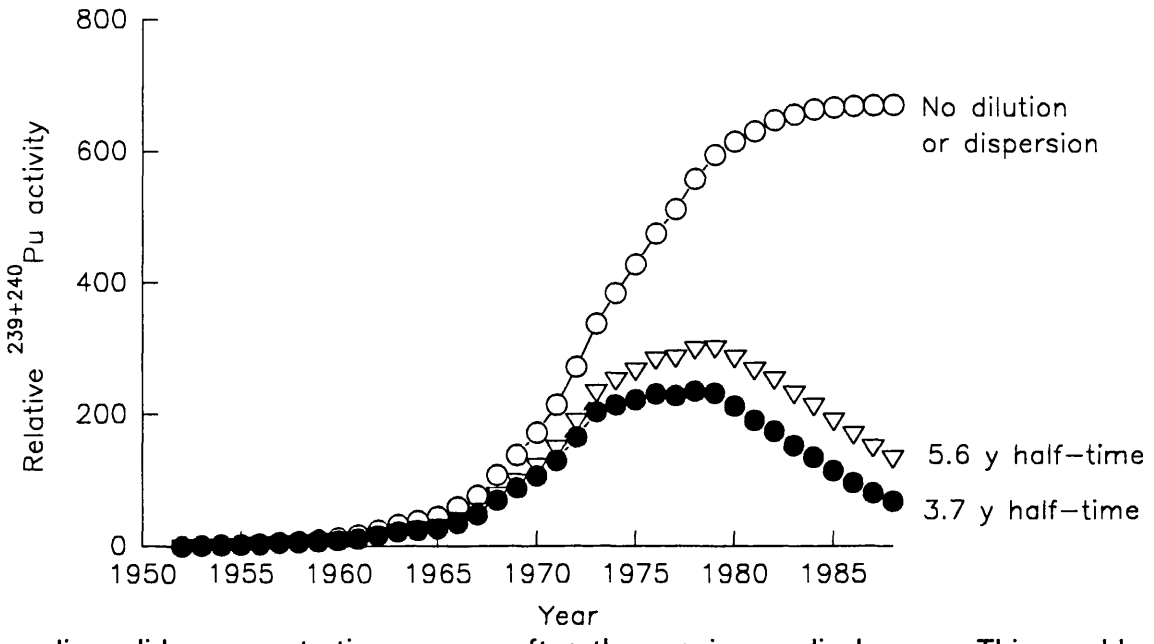

radionuclide concentrations occur after the maximum discharge. This could account for the lag-times required in previous studies [Stanners and Aston, 1981 a,b; Aston and Stanners, 1982] to match the sub-surface maxima with the peak Sellafield discharges. Kershaw *et al.* [1990], also required a lag-time of approximately 1 to 2 years to match the observed radionuclide profiles in the Maryport core with the annual Sellafield discharge data. Figure 4.17a shows the model predictions (normalised to the 1975 core data) with the observed $^{239+240}Pu$ concentration profile (averaged for yearly increments) for the Maryport core, based on the chronology established by Kershaw *et al.* [1990]. Although the general shape of the model curve is similar to the observed sediment profile, it appears translocated to the right of the core profile. Shifting the chronology by a few years would bring the core profile in line with the model predictions. This is justifiable as the model is based on the sediment concentrations reflecting the integrated discharges up to the time of deposition, suggesting that 2 years should be added to each year of the original chronology so that the surface 'age' corresponds to the date of collection. Comparisons of the model predictions with a shifted chronology are shown in Figure 4.17b and 4.17c. The model predictions match remarkably well (linear correlation coefficient of 0.91) with the underlying sediment profile after a three year shift in the chronology. This would, however, bring the date of

Figure 4.17 Model predictions for $^{239+240}Pu$ with observed concentrations in Maryport core averaged in yearly increments using (a) original chronology [Kershaw *et al.*, 1990], (b) a two year shifted chronology, and (c) a three year shifted chronology

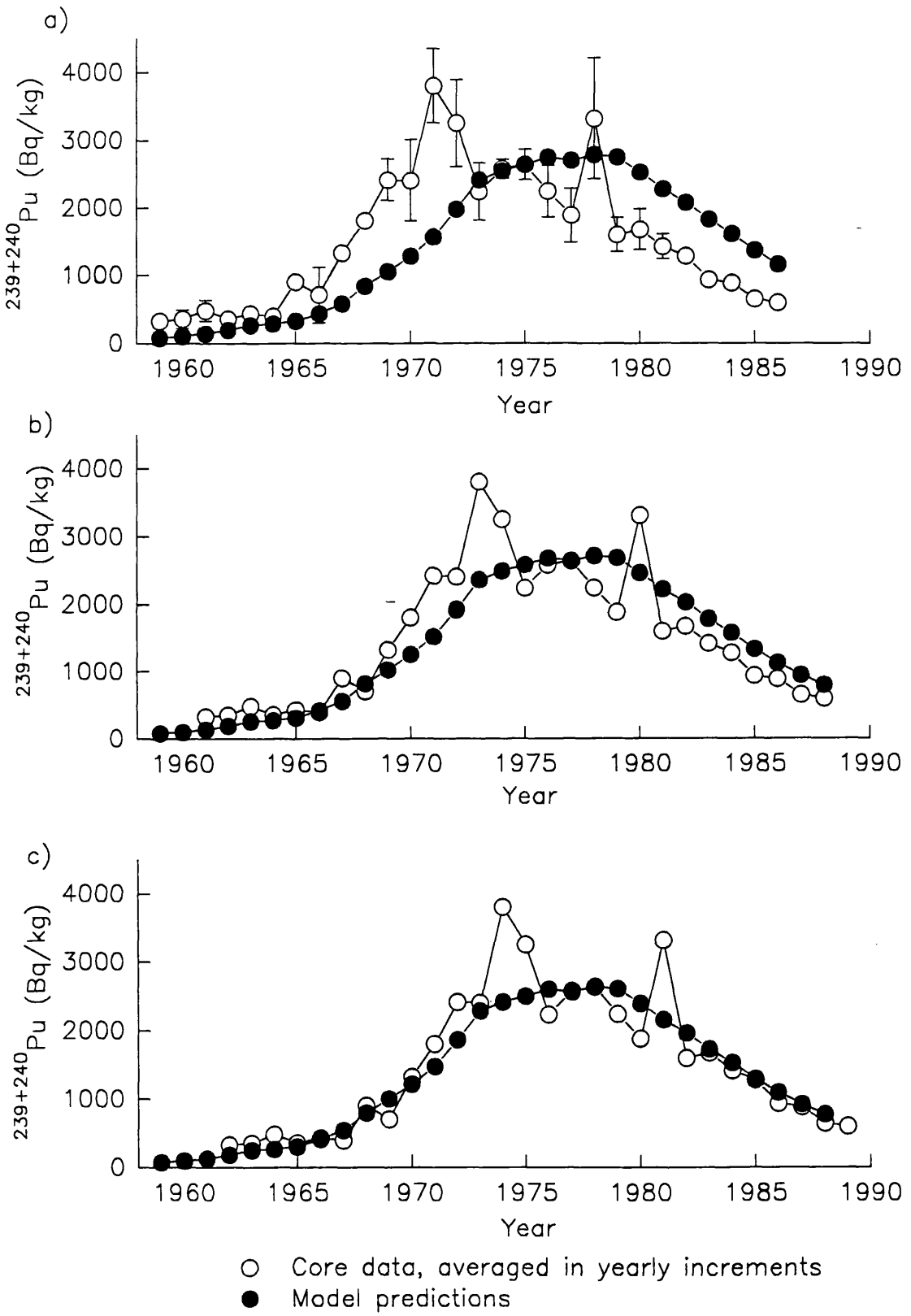

the surface of the core to after the time of collection, and the sharp peaks, relating to the 1973 and 1978 discharges (see below), to 1974 and 1981 respectively. However, the errors associated with the chronology may well be of the order of years. In particular it was noted that the sharp peak in the $^{239+240}$Pu core profile relating to the 1973 discharge was given an 'age' of 1971 in the original chronology. A two year shifted chronology has a linear correlation coefficient with the integrated discharge model of 0.865. For convenience, the terminology 'two year shifted chronology' will refer to a chronology based on the original version obtained by Kershaw *et al.* [1990], but with 2 years added to each 'date' to correct for the lag-time, so that the date of the core surface corresponds with the sample collection date.

Although the model discussed above matches well with the underlying sediment profile of the Maryport core, there are still significant deviations between the sediment profile and the model curve. Figure 4.18a shows the $^{239+240}$Pu annual discharge profile normalised to the Maryport core samples, with the core data, using a two year shifted chronology. This clearly demonstrates that the fine structure of the Maryport core corresponds well with variations in the annual discharge data, with two sharp peaks relating to the 1973 and 1978 Sellafield releases. However, the underlying core profile deviates from the annual discharge profile as discussed above. If a fraction of the relative $^{239+240}$Pu concentrations obtained from the integrated discharge data, with a dilution half-time of 3.7 years, is added to the annual discharge data, the resulting profile becomes a mixture of both the annual and integrated discharge model profiles (Figure 4.18b,c,d). From Figure 4.18c, it can be seen that the addition of 30% of the yearly integrated discharge data (correcting for dilution) to the annual releases produces a profile very similar in shape to the Maryport core profile, with a linear correlation coefficient of 0.92. Altering the chronology to fix the sharp peaks at 1973 and 1978 would result in an even closer match. This suggests that the Maryport $^{239+240}$Pu profile does not reflect only the annual discharge data, as suggested by Kershaw *et al.* [1990], or the integrated discharge data, as suggested by MacKenzie *et al.* [1994], but reflects a combination of both. An implication of this model is that the relative significance of the annual discharges to the sediment

Figure 4.18 Model predictions for $^{239+240}Pu$ with observed Maryport core data averaged in yearly increments using a two year shifted chronology and model curves based on the annual Sellafield discharge plus (a) 0%, (b) 10% (c) 30% and (d) 50% of the integrated discharge profile with a 3.7 yr half-time for dilution and dispersion, normalised to 1977 data

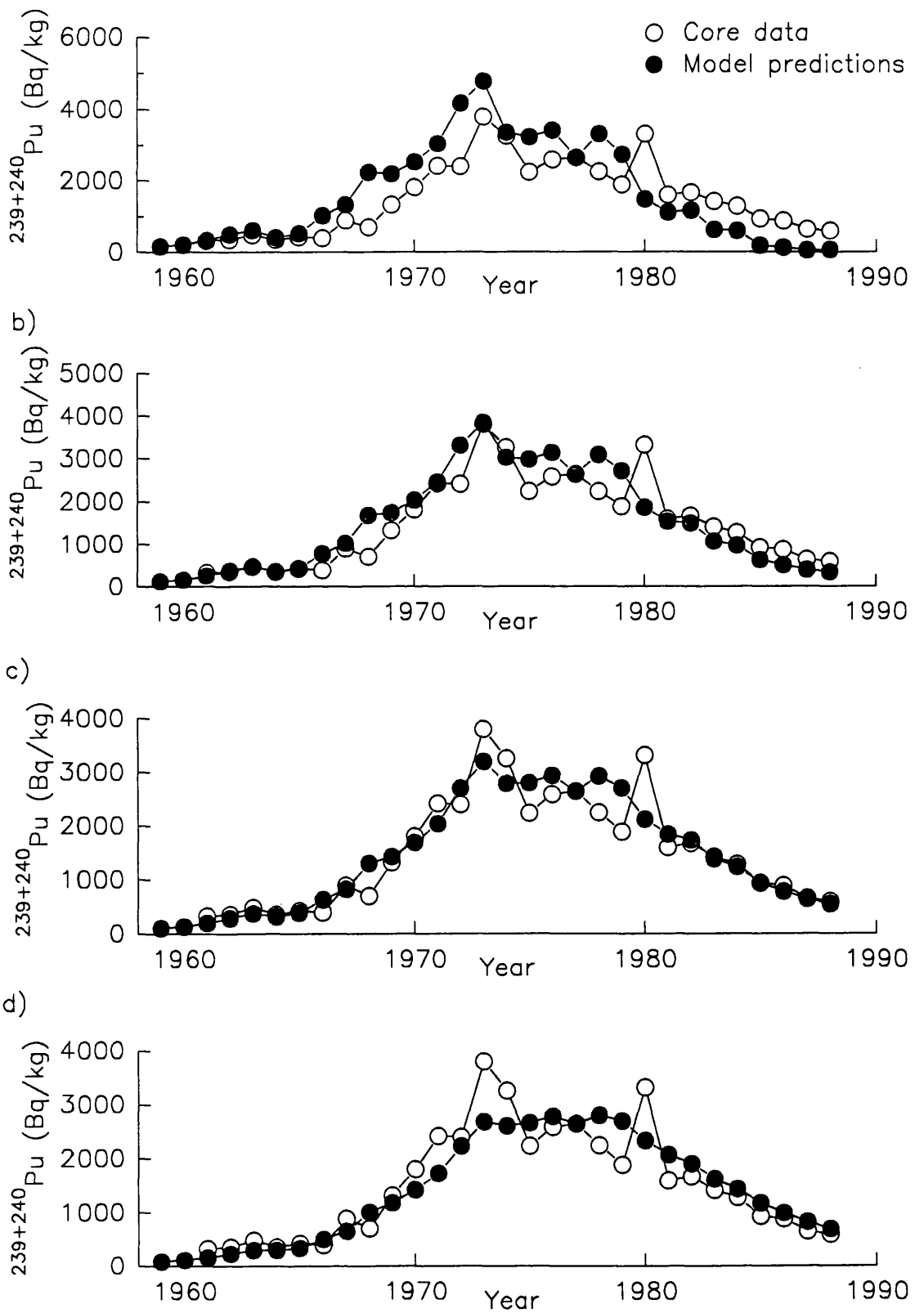

Figure 4.19 Comparison of factors obtained to calculate the ^{238}Pu annual discharges with published Sellafield discharge data

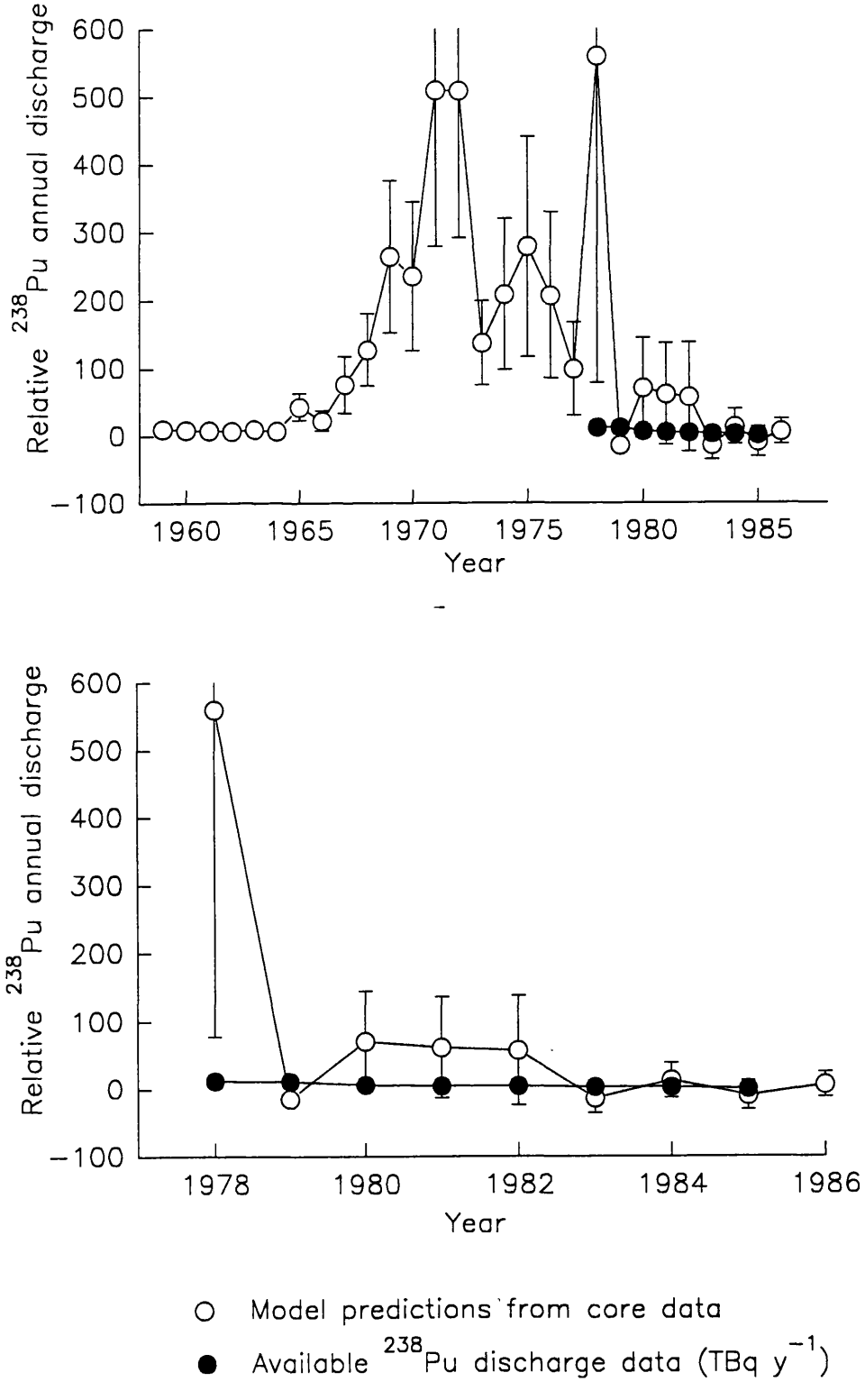

profiles would alter with time as the relative contribution from the integrated discharge values increases. Attempts to deconvolute the ^{238}Pu core profile in order to obtain the ^{238}Pu annual discharge data met with difficulties (see Figure 4.19). Unfortunately, the complex fine structure of the ^{238}Pu profile led to large errors in the estimated integrated discharge data, which also led to significant errors in the factors which were to be used to calculate the annual discharge data. Comparison of these factors with the published Sellafield discharge data provides no useful information.

A sediment profile influenced by both the annual and integrated Sellafield releases could be produced by two mechanisms; namely 1) the contaminated sediments do not totally mix with 'older' sediments before deposition in areas of accumulation close to Sellafield, or 2) a combination of both contaminated sediment transport, representing the integrated Sellafield discharge data, and solution transport, contaminating the surface sediment material with radionuclide concentrations representative of the annual discharge data. If the timescales for solution and sediment transport were significantly different then these mechanisms could be differentiated. However, soluble species are rapidly removed from the Irish Sea in a time of less than one year [Jefferies *et al.*, 1973], and sediment transport also occurs in a similar timescale [Hunt, 1985].

4.3.3.2 The Solway Core

The $^{239+240}Pu$ sediment profile for the Solway core SC1 is compared to the annual Sellafield discharge data in Figure 4.20. The general shape of the core profile is similar to the discharge data, except for the top portion of the core which has enhanced levels of $^{239+240}Pu$ indicating that the sediment profile does not merely reflected the annual discharges. The maximum to surface $^{239+240}Pu$ concentration for this core is 2.1, compared with a ratio of 89.8 observed in the discharges for the equivalent years. The sediment profile does not display the fine structure observed in the Maryport core, in part due to the 5 cm depth sampling increments which span nearly 2 years due to the low sedimentation rate (on average 2.4 cm y^{-1}).

Figure 4.20 Showing (a) $^{239+240}$Pu concentration profile for SC1 [Allan, 1993] compared with (b) $^{239+240}$Pu annual Sellafield discharges

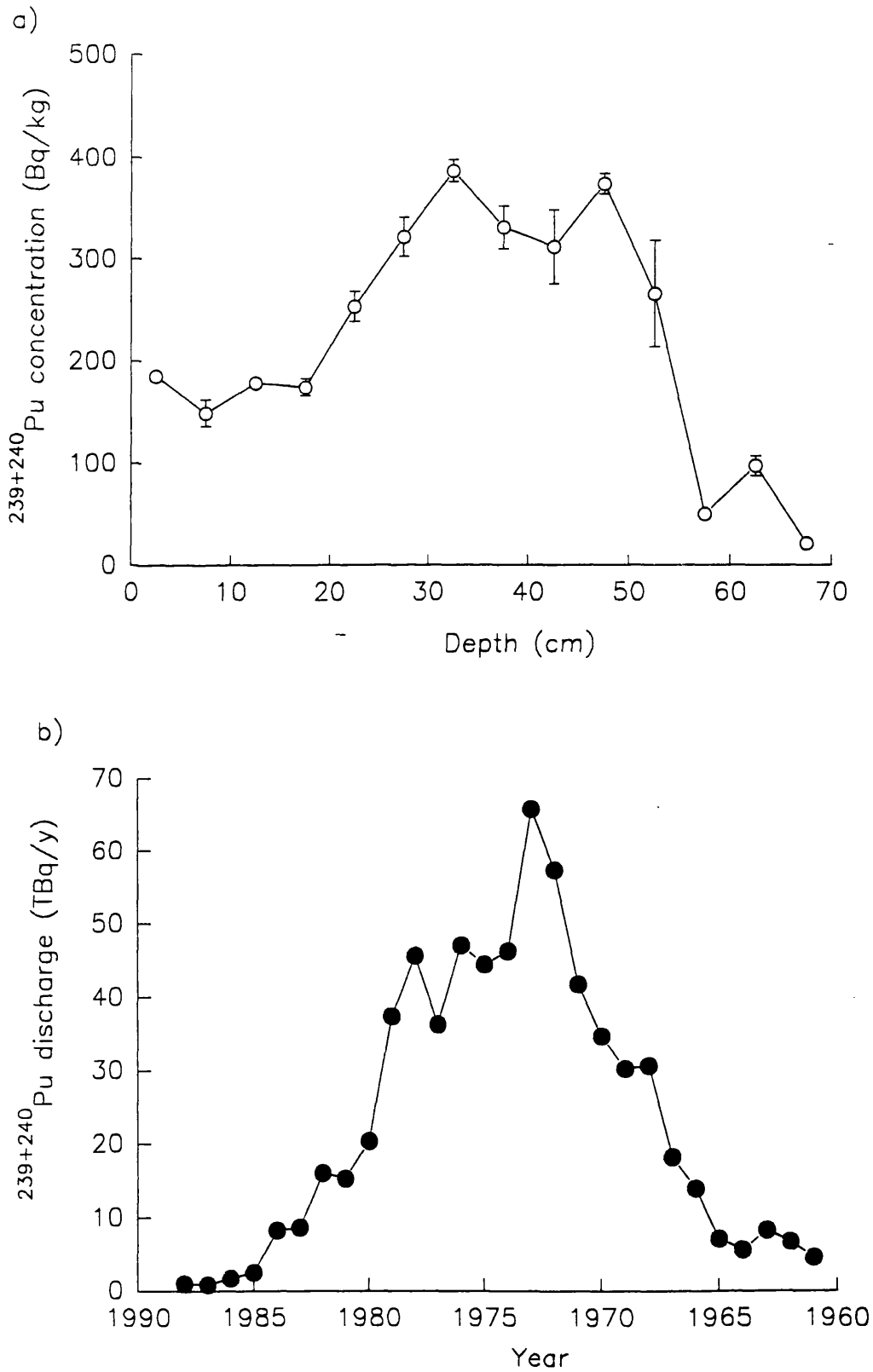

Figure 4.21 (a) $^{241}Am/^{239+240}Pu$ activity ratios and (b) decay corrected $^{137}Cs/^{241}Am$ activity ratios for SC1, normalised to the corresponding ratio in: Sellafield annual discharges; Sellafield annual discharges plus ingrowth of ^{241}Am from decay of corresponding ^{241}Pu discharges; and the time integrated Sellafield discharge [MacKenzie *et al.*, 1994]

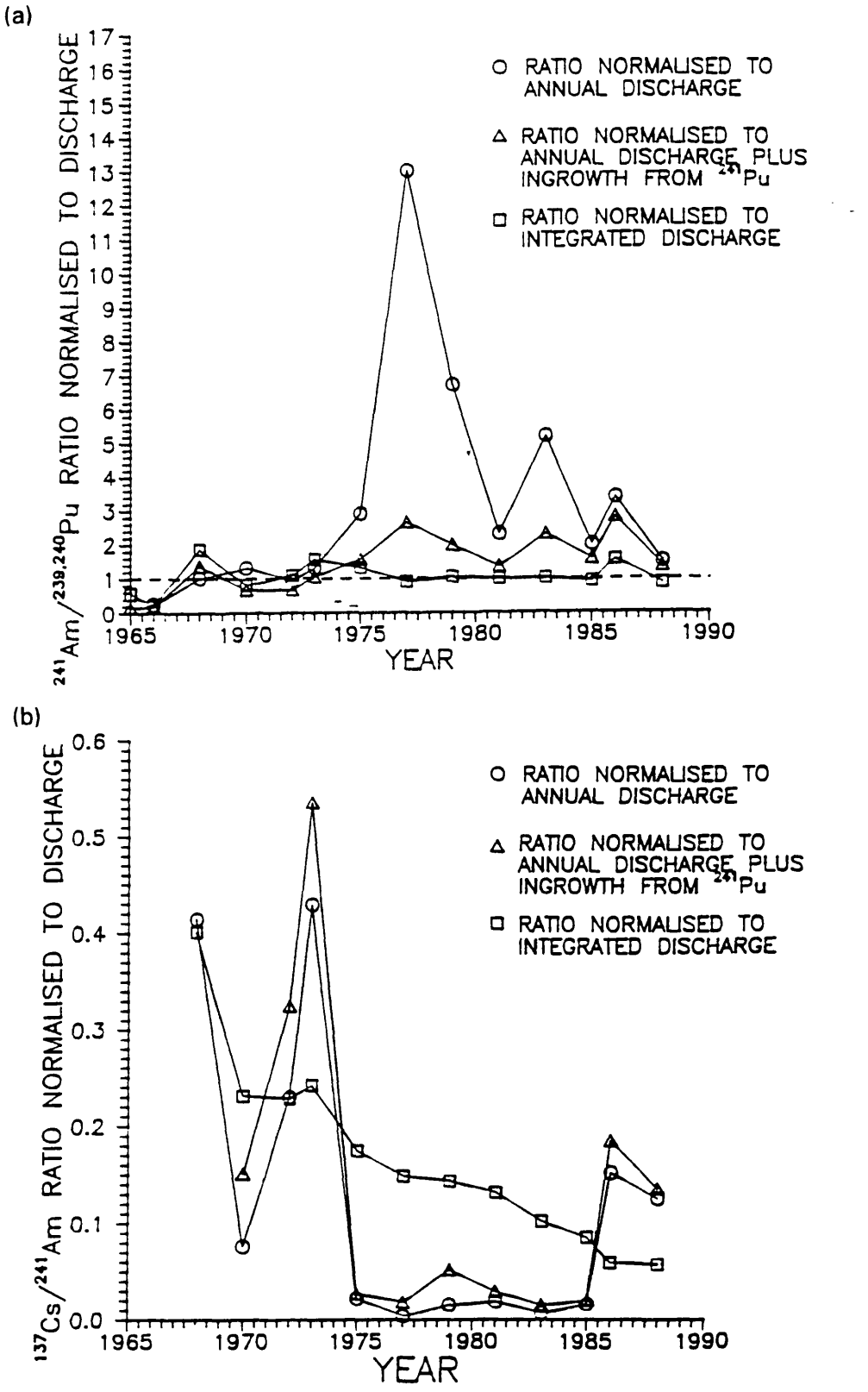

Plots of the $^{241}Am/^{239+240}Pu$ activity ratio and $^{137}Cs/^{241}Am$ activity ratio normalised to the annual and integrated discharges, accounting for the ingrowth of ^{241}Pu, are shown in Figure 4.21 [MacKenzie *et al.*, 1994]. As with the Maryport core, the radionuclide data for SC1 have a more consistent relationship with the integrated Sellafield discharge data than with the annual discharges. For example, the $^{241}Am/^{239+240}Pu$ activity ratios normalised to the integrated discharges have an average value of 0.99 ± 0.14, since 1975. Plots of the natural logarithm of the ratio of $^{239+240}Pu$ concentrations to the integrated $^{239+240}Pu$ discharge (see Figure 4.15) show a high degree of linearity, particularly after 1979, consistent with the mixed sediment pool model discussed above. From the linear portions of this plot the half-value period for reduction of $^{239+240}Pu$ concentrations by dispersion/dilution of the contaminated sediments is 5.6 years.

Figure 4.22 Model predictions for $^{239+240}Pu$ with observed concentration in SC1 using a sedimentation rate of 2.95 cm y^{-1} [Allan, 1993]

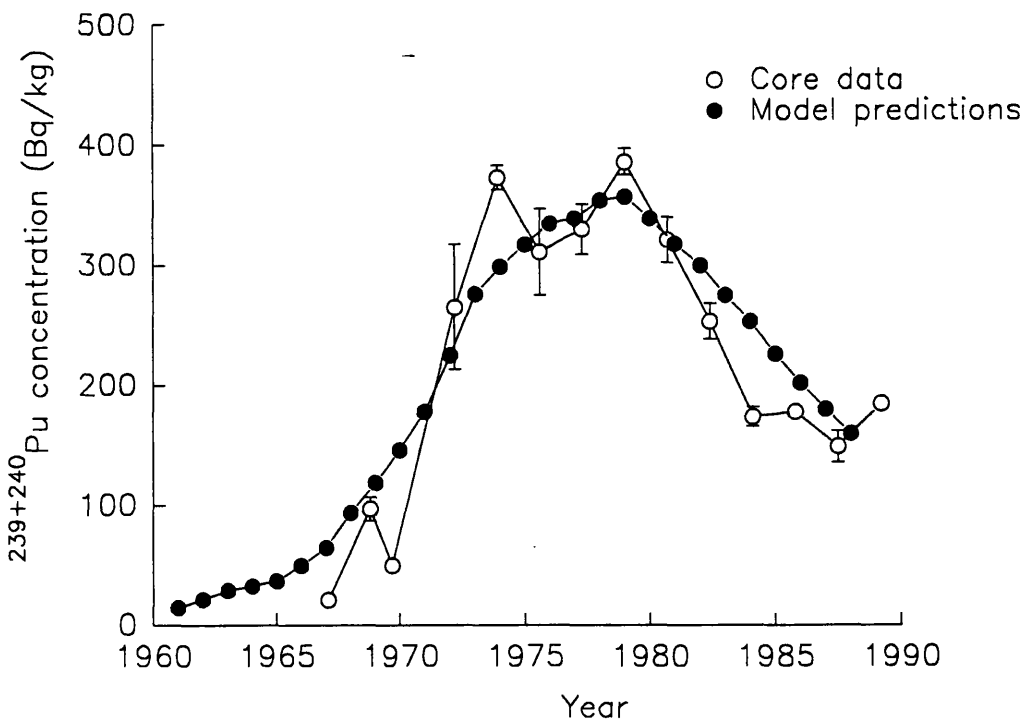

In the case of the Solway core, if the maxima of the core radionuclide profiles are matched to the integrated discharge profile, with the predicted half-value period, then the average sedimentation rate is increased to 2.95 cm y^{-1} [Allan, 1994]. Figure 4.22 shows the observed sediment profile for $^{239+240}Pu$ in SC1 (using a chronology based on a sedimentation rate of 2.95 cm y^{-1}), with the model predictions, normalised to the 1978 values. The model profile shows close agreement with the observed $^{239+240}Pu$ profile, but, as was observed for the Maryport core, fails to predict the two peaks which correspond to the maximum discharges in 1973 and 1978. Figure 4.23 shows the correspondence of the observed $^{239+240}Pu$ data with profiles produced by different combinations of the integrated and annual discharge data. Neither the integrated nor annual discharge profiles could account for the rapid decrease in the $^{239+240}Pu$ concentrations near the bottom of the core, or the slight increase in activity near the surface of the core, both of which may be caused by a change in the sediment composition. Interestingly, unlike the Maryport core profile, the SC1 data correspond closer to the integrated discharge profile than the annual profile. This suggests that although both particulate and solution transport contribute to the transfer of Sellafield waste to the Solway, the relative contribution from solution transport is lower than for areas close to Sellafield.

One weakness of the Solway data is that the sediment core was sub-sampled in incremental depths of 5 cm, and as a consequence each data point represents an average of several years of accumulated sediment. The resulting profiles show little of the fine structure observed at Maryport and it is difficult to tell if this is because the annual discharges have little influence on the sediment profiles or if their influence has been averaged out. This is unfortunate as the fine structure of core profiles can be used to establish a more precise chronology. Sub-sampling cores in increments representative of less than a year, however, can also lead to problems due to seasonal variations in the sediment composition [Graham, 1994]. The SC1 data show that the sediment concentrations in the Solway are dominated by the integrated discharges, suggesting that further sediment cores collected from this area may well provide data which could be used to produce a history of the Sellafield discharges.

Figure 4.23 Model predictions for $^{239+240}$Pu with observed concentrations in SC1 with model curves based on; the integrated discharge data with a 5.6 year half-time and (a) 0% and (b) 50% of annual discharge data; and the annual discharge profile with (c) 0% and (d) 50% of integrated discharge data with 5.6 yr half-time all normalised to 1973 data.

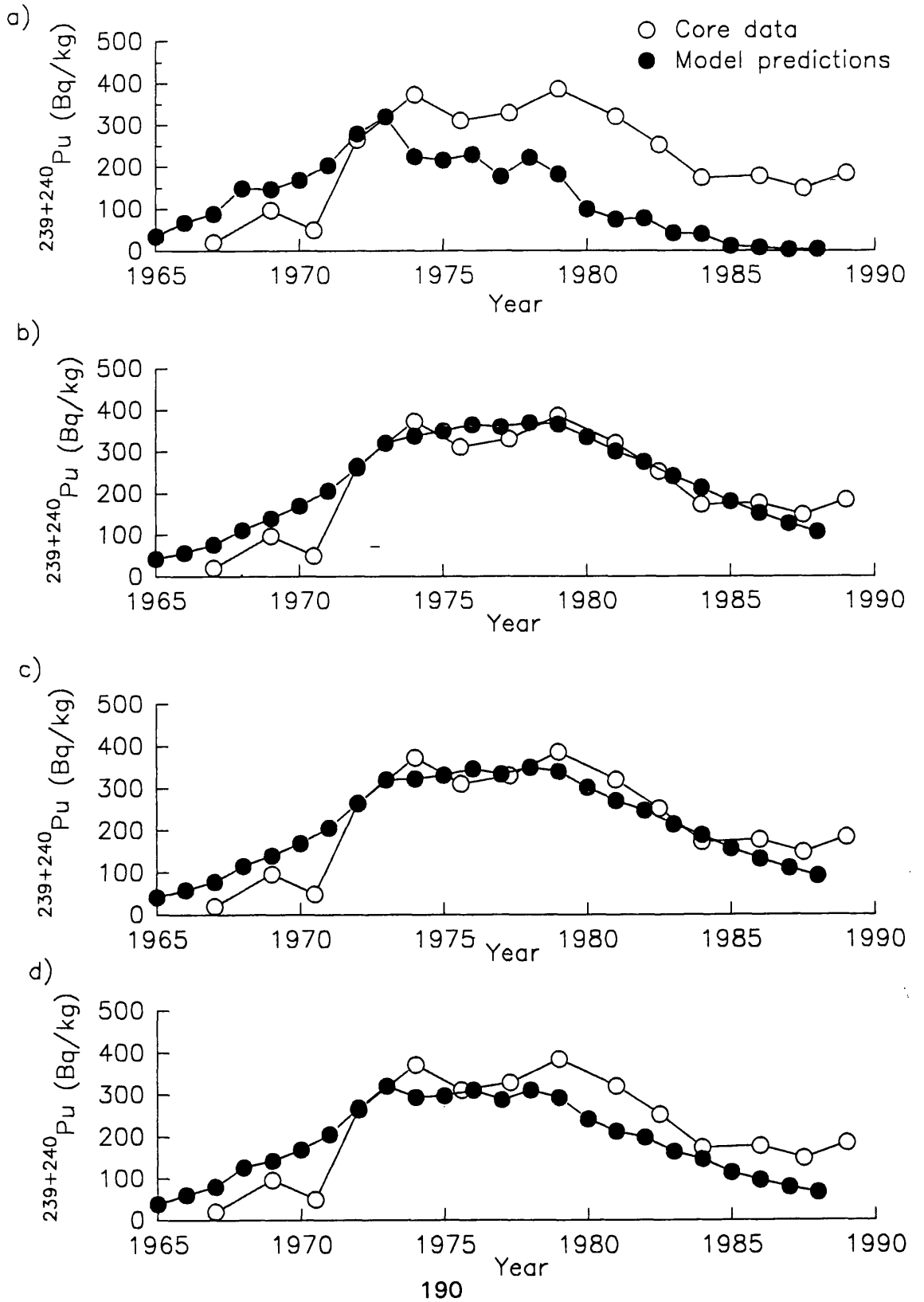

4.3.3.3 Establishing core chronologies

One of the key factors in interpreting the sediment core profiles in terms of the Sellafield discharge data, is the sediment chronology. In the Maryport core, the original chronology [Kershaw *et al.*, 1990] was established by visually matching the core profiles with the annual discharge data. Although this technique has worked well in the case of Maryport, it gives no indication of how well the chronology fits the data.

As an illustration of an independent technique to match discharge data with core profiles, and to provide a measure of how well the data sets correspond, a statistical program, 'SLOTSEQ', (developed to compare and correlate two sets of physical log data from boreholes [Gordon, 1980; Gordon and Reyment, 1979]), was used to match the decay corrected discharge data with the radionuclide data obtained by Kershaw *et al.* [1990]. In order that direct comparisons can be made between the two dissimilar data sets, they were first standardised in terms of the number of standard deviations from the mean value for each individual sequence. The program then slots one sequence into the other, whilst maintaining the order of original sequences [Gordon, 1980]. Consider two sequences A and B, with individual objects A_0, A_1 A_2, A_3, etc, and B_0, B_1, B_2, etc, respectively, the program will slot A and B together to produce a single sequence (see Figure 4.24). For each object in each sequence, the local discordance of the object in the slotting can be defined [Gordon, 1988]. In this case, the local discordance of an object C was defined as the smallest dissimilarity between C and the pair of objects from the other sequence between which C is located, e.g., the local discordance of A_2 is the minimum value of the difference between A_2 and B_1, and A_2 and B_2. The global discordance of two sequences is then defined as the sum, over each object in each sequence, of the local discordances (ie the sum of the dashed lines in Figure 4.24)[Gordon, 1988]. The program obtains the optimum slotting of one sequence into the other by finding the minimum value of the global discordance. The program also defines a statistic κ, which is related to the global discordance [Gordon, 1988]. Although the characteristics of this statistic have not been fully assessed, it can be predicted that large values of κ brings into question any agreement between the two sequences, but values close to 1 indicate a good

correspondence [Gordon, 1988; Gordon, 1980].

Figure 4.24 The slotting of sequences A and B [Gordon, 1988]

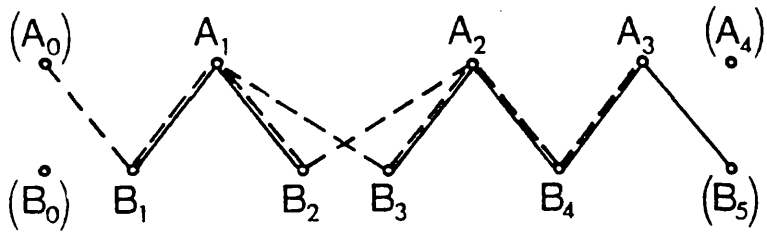

SLOTSEQ was applied to the Sellafield decay corrected annual discharge data and Maryport core data for $^{239+240}$Pu, ^{238}Pu, ^{241}Am and ^{137}Cs. The resulting single sequences are shown in Table 4.9. From the values of κ obtained for the data sets, $^{239+240}$Pu and ^{137}Cs showed the best matching of core profiles with discharge data. Interestingly, the chronologies obtained in this way closely matched the chronology obtained by Kershaw *et al.* [1990], but with the maximum annual $^{239+240}$Pu discharge of 1973 corresponding to the distinct $^{239+240}$Pu concentration peak observed at depths of 90 to 94 cm. This gives further evidence of inconsistencies in the original Maryport core chronology and suggests that the fine structure of the core profile matches with the annual discharges.

One of the short fallings of this technique is that the initial standardisation of the data tends to smooth out any major differences between the two data sets such as those highlighted by MacKenzie *et al.* [1994].

Table 4.9 Comparison of the Kershaw et al. [1990] chronology with the SLOTSEQ results

Depth (cm)	Date	$^{239+240}$Pu	^{238}Pu	^{241}Am	^{137}Cs
0-1	86	84	85	81	85
1-2		-	84	-	84
2-3	85	-	-	-	-
3-4		-	-	-	-
4-5		83	-	80/77	-
5-6	84	-	-	76	83
6-8		82	-	-	-
8-10	83	-	83	-	-
10-12		-	-	-	-
12-14		81	-	-	82
14-16	82	-	82	-	81
16-18		-	-	-	80
18-20		-	-	-	-
20-22	81	-	-	-	-
22-24		-	-	-	-
24-26		-	-	-	-
26-28		-	-	-	-
28-30	80	-	-	-	-
30-32		-	-	-	-
32-34		80	-	-	-
34-36		-	-	-	-
	79	-	-	-	-

Depth	Date	$^{239+240}$Pu	^{238}Pu	^{241}Am	^{137}Cs
36-38		-	-	-	-
38-40		-	-	-	-
40-42		-	-	-	79
42-44	78	79	-	-	78
44-46		-	-	75	77/76
46-48			81	74/73	-
48-50		-	-	-	-
50-52	77	-	-	-	-
52-54		-	-	-	-
54-56	76	-	-	-	75
56-58		-	-	-	-
58-60	75	-	-	-	-
60-62		-	-	-	-
62-64		78/75	-	-	-
64-66	74	-	-	-	74
66-68		-	-	-	-
68-70		-	-	-	-
70-72	73	-	-	-	73
72-74		-	-	-	72
74-76		-	-	-	-
76-78		-	-	-	-
78-80	72	-	-	-	-
80-82		-	-	-	-

Depth	Date	$^{239+240}$Pu	^{238}Pu	^{241}Am	^{137}Cs
82-84		-	-	-	-
84-86		74	-	-	-
86-88	71	-	-	-	-
88-90		-	-	-	-
90-92		73	-	-	-
92-94		-	-	-	-
94-96	70	72	-	72	-
96-98		71	-	-	-
98-100		-	-	-	71
100-102		-	-	-	-
102-104	69	-	-	-	70
104-106		-	-	-	-
106-108		-	-	-	69
100-105		-	-	-	-
105-110	68	70	-	71	68
110-115		69	-	-	-
115-120	67	68	-	-	67
120-125		67	-	-	-
125-130		-	-	70	-
130-135		-	-	-	66
135-140		-	-	-	-
140-145		-	-	-	65
145-150					
		κ = 1.2	κ = 4.2	κ = 2.2	κ = 1.3

4.4 CONCLUSIONS

ICP-MS is a quick and sensitive technique capable of the determination of ^{237}Np concentrations and $^{240}Pu/^{239}Pu$ atom ratios in sediment samples contaminated by Sellafield discharges. Chemical separation of Np and Pu from the bulk matrix and ^{238}U (to comply with the sample restrictions of < 0.2 % dissolved solids content and < 100 ng ml^{-1} ^{238}U, while maintaining the levels of Pu and Np above the detection limits of the system) was achieved by a combination of solvent extraction and anion exchange. Radionuclide profiles in sediment cores from areas of accumulating sediment were found to provide a temporal record of the Sellafield releases, related to both the annual and time-integrated discharge data. However, full deconvolution of the radionuclide profiles was not possible.

REFERENCES

Aarkrog, A. (1986) Long-lived radionuclides important in marine disposal. In: The behaviour of long-lived radionuclides associated with the deep-sea disposal of radioactive wastes, IAEA-TECDOC-368, IAEA, Vienna, 149-154.

Aarkrog, A. (1988) Worldwide data on fluxes of $^{239,240}Pu$ and ^{238}Pu to the oceans. In: Inventories of selected radionuclides in the oceans, IAEA-TECDOC-481, IAEA, Vienna, 103-138.

Ahrland, S. (1986) Solution chemistry and kinetics of ionic reaction. In: The Chemistry of the Actinide Elements, Katz, J.J., Seaborg, G.T. and Morss, L.R. (eds.), Chapman and Hall Ltd., London, 1480-1546.

Allan, R.L. (1993) Distribution, geochemistry and geochronology of Sellafield waste in contaminated Solway Firth floodplain deposits. Ph.D. Thesis, Glasgow University.

Allard, B., Olofsson, V. and Torstenfelt, B. (1984) Environmental actinide chemistry. Inorg. Chim. Acta, **94**, 205-221.

Allardice, R.H., Harris, D.W. and Mills, A.L. (1983) Nuclear fuel processing in the UK. In: Nuclear Power and Technology, Volume 2, Marshall, W. (ed.), Clarendon, Oxford, 209-281.

Askew, J.R., Campbell, C.G. and Tyror, J.G. (1983) Reactor Physics. In: Nuclear power and technology, Volume 1 Reactor technology, Marshall, W. (ed.), Clarendon, Oxford, 50-137.

Assinder, D.J., Yamamoto, M., Kim, C.K., Seki, R., Takaku, Y., Yamauchi, Y., Komura, K., Ueno, K. and Bourne, G.S. (1991) Neptunium in intertidal coastal and estuarine sediments in the Irish Sea. J. Environ. Radioactivity, **14**, 135-145.

Aston, S.R., Assinder, D.J. and Kelly, M. (1985) Plutonium in intertidal coastal and estuarine sediments in the northern Irish Sea. Estuarine, Coastal and Shelf Sci., **20**, 761-771.

Aston, S.R., Gastaud, P., Oregioni, B. and Parsi, P. (1983) Observations on the adsorption and geochemical associations of Tc, Np, Pu, Am and Cf with a deepsea sediment. In: Int. Symp. on the behaviour of the long-lived radionuclides in the marine environment, Cigna, A. and Myttenaere, C. (eds.), EUR 9214 EN, CEC, Brussels, 179-188.

Aston, S.R. and Stanners, D.A. (1982a) The transport to and deposition of americium in intertidal sediments of the Ravenglass estuary and its relationship to plutonium. Environ. Pollut., **3B**, 1-19.

Aston, S.R. and Stanners, D.A. (1982b) Local variability in the distribution of Windscale fission products in estuarine sediments. Estuarine Coastal Shelf Sci., **14**, 167-174.

Baxter, M.S., Scott, R.D. and Ledingham, K.W.D. (1987) Resonance ionisation mass-spectrometry: a review of its status and potential as a radioanalytical technique. DOE Rep. Contract PECD 7/9/341.

Beauchemin, D., McLaren, J.W. and Berman, S.S. (1987a) Study of the effects of concomitant elements in inductively coupled plasma mass spectrometry. Spectrochim. Acta, **42B**, 467-490.

Beauchemin, D., McLaren, J.W., Mykytiuk, A.P. and Berman, S.S. (1987b) Determination of trace metals in a river water reference material by inductively coupled plasma mass spectrometry. Anal. Chem., **59**, 778-783.

Begg, F.H. (1992) Anthropogenic ^{14}C in the natural (aquatic) environment. Ph.D. Thesis, Glasgow University.

Belderson, R.H. and Stride, A.H. (1969) Tidal currents and sand wave profiles in the north-eastern Irish Sea. Nature, Lond., **222**, 74-75.

Bertell, R. (1985) The problem: nuclear radiation and its biological effects. In: No immediate danger, The Woman's Press, Lond., 15-65.

Blades, M.W. and Caughlin, B.L. (1985) Excitation temperature and electron density in the Inductively Coupled Plasma - aqueous vrs organic introduction. Spectrochim. Acta, **40B**, 579-591.

BNFL (1986b) Fuel reprocessing services. BNFL plc, Risley.

BNFL (1992b) Nuclear fuel reprocessing technology. BNFL plc, Risley.

BNFL (1977-1993) Annual report on radioactive discharges and monitoring of the environment. BNFL plc, Risley.

Bondietti, E.A. and Trabalka, J.K. (1980) Evidence for plutonium (V) in an alkaline freshwater pond. Radiochem. Radioanal. Chem. Lett., **42**, 169.

Boumans, P.W.J.M. (1987) Inductively coupled plasma emission spectrometry Part 1: Methodology, instrumentation, and performance. In: Chemical Analysis vol 90, John Wiley and Sons, New York.

Bowen, V.T., Noshkin, V.E., Livingston, H.D. and Volchok, H.L. (1980) Fallout radionuclides in the Pacific Ocean: vertical and horizontal distributions, largely from Geosecs stations. Earth Planet. Sci. Lett., **49**, 411-434.

Bradley, P.E. (1989) pers. comm.

Brown, R.M., Long, S.E. and Pickford, C.J. (1987) Measurement of long-lived radionuclides by non-radiometric methods. Sci. Total Environ., **70**, 265-274.

Buesseler, K.O. and Halverson, J.E. (1987) The mass-spectrometric determination of fallout ^{239}Pu and ^{240}Pu in marine samples. J. Environ. Radioact., **5**, 425-444.

Buesseler, K.O. and Sholkovitz, E.R. (1987a) The geochemistry of fallout plutonium in the North Atlantic. I: A pore water study in shelf, slope, and deep-sea sediments. Geochim. Cosmochim. Acta, **51**, 2605-2622.

Buesseler, K.O. and Sholkovitz, E.R. (1987b) The geochemistry of fallout plutonium in the North Atlantic. II: $^{240}Pu/^{239}Pu$ ratios and their significance. Geochim. Cosmochim. Acta, **51**, 2623-2637.

Burney, G.A. and Harbour, R.M. (1974) Radiochemistry of neptunium. NAS-NS-3060.

Burton, L.L. and Blades, M.W. (1990) A simple method for calculating deviations from local thermodynamic equilibrium in the inductively coupled plasma. Spectrochim. Acta, **45B**, 139-144.

Byrne, A.R. (1986) The determination of ^{237}Np in Cumbrian (UK) sediments by neutron activation analysis: preliminary results. J. Environ. Radioact., **4**, 133-144.

Calmet, D. and Guegueniat, P.M. (1985) Les rejects d'effluents liquides radioactifs du centre de traitement des combustibles irradie de la Hague (France) et l'evolution radiologique du domaine marine. In: Behaviour of radionuclides released into coastal waters, IAEA-TECDOC-329, IAEA, Vienna, 111-144.

Cambray, R.S. (1982) Annual discharge of certain long-lived radionuclides to the sea and to the atmosphere from the Sellafield works, Cumbria, 1957-1981. UKAEA Harwell, AERE-M-3269, HMSO.

Cambray, R.S. and Eakins, J.D. (1980) Studies of environmental radioactivity in Cumbria Part 1: Concentrations of plutonium and caesium-137 in environmental samples from West Cumbria and a possible maritime effect. AERE-R9807, HMSO.

Cambray, R.S. and Eakins, J.D. (1982) Pu, 241-Am and 137-Cs in soil in West Cumbria and a maritime effect. Nature, **300**, 46-48.

Camplin, W.C. and Aarkrog, A. (1989) Radioactivity in North European waters: report of working group II of CEC project MARINA. Fisheries Research Data Rep., **No. 20**, MAFF, Lowestoft.

Carter, M.W. (1979) Nuclear Testing 1975-1978. Health Phys., **36**, 432-437.

Carter, M.W. and Moghissi, A.A. (1977) Three decades of nuclear testing. Health Phys., **33**, 55-71.

Cawse, P.A. and Beedham, M.A. (1979) Survey of radionuclides in UK soil. In: Environmental and Medical Sciences Division Progress Report 1978, Hainge, M. (ed.), AERE-PR-EM5/6, HMSO, Lond.

Chambers, D.M., Poehlman, J., Yang, P. and Hieftje, G.M. (1991) Fundamental studies of the sampling process in an inductively coupled plasma mass spectrometer. 1: Langmuir probe measurements. Spectrochim. Acta, **46B**, 741-760.

Choppin, G.R. (1983) Aspects of Pu solution chemistry. In: Plutonium Chemistry, Carnal, W.T. and Choppin, G.R. (eds.), ASC Symp. Ser., **216**, 213-230.

Choppin, G.R. and Morse, J.W. (1987) Laboratory studies of actinides in marine systems. In: Environmental research on actinide elements, Pinder III, J.E., Alberts, J.J., McLeod, K.W. and Schreckhise, R.G. (eds.), USDoE, Conf-841142.

Choppin, G.R. and Rydberg, J. (eds.) (1980) Nuclear chemistry: theory and applications. Pergammon, Oxford.

Cleveland, J.M. (1970) Aqueous coordination complexes of plutonium. Coordin. Chem. Rev., **5**, 101-137.

Clifton, R.J. and Hamilton, E.I. (1982) The application of radioisotopes in the study of estuarine sedimentary processes. Estuar. Coastl. Mar. Sci., **14**, 438-446.

Clifton, R.J., Stevens, H.E. and Hamilton, E.I. (1983) Concentration and depuration of some radionuclides present in a chronically exposed population of mussels (Mytilus edulis). Mar. Ecol., Prog. Ser., **11**, 245-256.

Cohen, B.L. (1982) Effect of the ICRP Publication 30 and the 1980 Bier Report on hazard assessments of high-level wastes. Health Phys., **42**, 133-143.

Cohen, B.L. (1983) Effects of recent neptunium studies on high-level waste hazard assessment. Health Phys., **44**, 567-569.

Coleman, G.H. (1965) Radiochemistry of plutonium. NAS-NS-3058.

Coughtrey, P.J., Jackson, D., Jones, C.H., Kane, P. and Thorne, M.C. (eds.) (1984) Radionuclide distribution and transport in terrestrial and aquatic ecosystems. A.A. Balkema, Rotterdam.

Crain, J.S., Smith, F.G. and Houk, R.S. (1990a) Mass spectrometric measurement of ionisation temperature in an ICP. Spectrochim. Acta, **45B**, 249-259.

Cross, J.E. and Hooper, E.W. (1987) Review of radioanalytical methods for low-levels of α-emitting transuranic elements, AERE-R12559.

Curtis, E.J.C., Popplewell, D.S. and Ham, G.J. (1991) Radioactivity in environmental samples taken in the Sellafield, Ravenglass and Morecambe Bay areas of west Cumbria. Sci. Total Environ., **105**, 211-231.

Davies, A.M. and Jones, J.E. (1992) A three dimensional wind driven circulation model of the Celtic and Irish Seas. Contin. Shelf Res., **12**, 159-188.

Date, A.R. and Gray, A.L. (1981) Plasma source mass spectrometry using an inductively coupled plasma and a high resolution quadrupole mass filter. Analyst, **106**, 1255-1267.

Date, A.R. and Gray, A.L. (1989) Applications of inductively coupled plasma mass spectrometry. Blackie, Glasgow.

Dawson, P.H. ed. (1976) Quadrupole mass spectrometry and its applications. Elsevier, Amsterdam.

Day, J.P. and Cross, J.E. (1981) ^{241}Am from the decay of ^{241}Pu in the Irish Sea. Nature, **292**, 43-45.

De, A.K., Khopkar, S.M. and Chalmers, R.A. (1970) Solvent extraction of metals. Van Nostrand Reinhold Co., London.

Dickson, R.R. and Boelens, R.G.V. (1988) The status of current knowledge on anthropogenic influences in the Irish Sea. Coop. Res. Rep., Int. Coun. Explor. Sea, **Vol 55**, 1-88.

Dickson, R.R. (1987) Irish Sea status report of the marine pollution monitoring group. Aquatic Environment Monitoring Report No. 17, MAFF, Lowestoft.

Dobson, M.R. (1977a) The geological structure of the Irish Sea. In: Quaternary History of the Irish Sea, Kidson, C. and Tooley, M.J. (eds.), Seel House Press, Liverpool, 13-26.

Dobson, M.R. (1977b) The history of the Irish Sea basins. In: Quaternary History of the Irish Sea, Kidson, C. and tooley, M.J. (eds.), Seel House Press, Liverpool, 93-98.

Douglas, D.J. and French, J.B. (1986) An improved interface for inductively coupled plasma-mass spectrometry (ICP-MS). Spectrochim. Acta, **41B**, 197-204.

Douglas, D.J. and French, J.B. (1988) Gas dynamics of the inductively coupled plasma mass spectrometry interface. J. Anal. At. Spectrom., **3**, 743-747.

Drake, V.A. (1987) Predicting the behaviour of neptunium during nuclear fuel reprocessing. Nucl. Energy, **26**, 253-258.

Duniec, S., Hallstadius, L. and Holm, E. (1984) A study of the transport of radionuclides in the sea by use of isotope ratios. In: The behaviour of long-lived radionuclides in the marine environment, Cigna, A. and Myttenaere, C. (eds.), CEC, Brussels, 245-254.

Dyer, K.R. (1986) Review of oceanographic processes influencing radioactive waste dispersal in the Irish Sea. DOE/RW/86/094.

Eakins, J.D. and Lally, A.E. (1984) The transfer of actinide bearing sediments from the Irish Sea by spray. Sci. Total Environ., **35**, 23-32.

Eakins, J.D., Morgan, A., Baston, G.M.N., Pratley, F.W., Strange, L.P. and Burton, P.J. (1990) Measurements of α-emitting plutonium and americium in the intertidal sands of West Cumbria, UK. J. Environ. Radioactivity, **11**, 37-54.

Eakins, J.D., Morgan, A., Baston, G.M.N., Pratley, F.A., Yarnold, L.P. and Burton, P.J. (1988) Studies of environmental radioactivity in Cumbria, Part 8: Plutonium and americium in the intertidal sands of north west England. UKAEA, Harwell,

AERE-R12061.

Edgington, D.N. (1981) A review of the persistence of long-lived radionuclides in the marine environment- sediment/water interactions. IAEA-SM-248/148.

Edgington, D.N. and Nelson, D.M. (1984) The chemical behaviour of long-lived radionuclides in the marine environment. In: Int. Symp. on the Behaviour of long-lived Radionuclides in the Marine Environment, Cigna, A. and Myttenaere, C. (eds.), CEC, Luxembourg, Eur 9214EN, 19-66.

Efurd, D.W., Knobeloch, G.W., Perrin, R.E. and Barr, D.W. (1982) Np-237 production from atmospheric testing. Los Alamos Laboratory Report, LA-9585-MS.

Efurd, D.W., Knobeloch, G.W., Perrin, R.E. and Barr, D.W. (1984) An estimate of ^{237}Np production during atmospheric testing. Health Phys., **47**, 786-787.

Efurd, D.W., Drake, J., Roensch, F.R., Cappis, J.H. and Perrin, R.E. (1986) Quantification of neptunium by isotope dilution mass-spectrometry. Los Alamos Nat. Lab. Rep., La-10701-MS.

Ewart, F.T. (1981) Fuel inventories and derived parameters for the reactor systems CDFR, LWR, AGR, and Magnox. AERE-R-10037.

Facer, G. (1980) Quantities of transuranic elements in the environment from operations relating to nuclear weapons. In: Transuranium nuclides in the environment, Hanson, W.C. (ed.), USDoE/TIC-22800, 86-91.

Fahey, J.A. (1986) Neptunium. In: The Chemistry of the Actinide Elements, Katz, J.J., Seaborg, G.T. and Morss, L.R. (eds.), Chapman, New York, 443-498.

Flowers, R.H. (1983) How reactors work. In: Nuclear power and technology, Volume 1 Reactor technology, Marshall, W. (ed.), Clarendon, Oxford, 1-49.

Fulford, J.E. and Douglas, D.J. (1986) Ion kinetic energies in ICP-MS. Appl. Spectrosc., **40**, 971-974.

Furuta, N. (1986) Spatial emission distribution of YO, YI, YII and YIII radiation in an inductively coupled plasma for the elucidation of excitation mechanisms. Spectrochim. Acta, **41B**, 1115-1129.

Furuta, N., Nojiri, Y. and Fuwa, K. (1985) Spatial profile measurement of electron number densities and analyte line intensities in an inductively coupled plasma. Spectrochim. Acta, **40B**, 423-434.

Garland, J.A., McKay, W.A., Cambray, R.S. and Burton, P.J. (1989) Man-made radionuclides in the environment of Dumfries and Galloway. Nucl. Energy, **28**, 369-392.

Germain, P., Guéguéniat, P.M., May,S. and Pinte, G. (1987) Measurement of transuranic elements, chiefly ^{237}Np (by naa) in the physical and biological compartments of the French shore of the English Channel. J. Environ. Radioact.,

5, 319-331.

Gillson, G.R., Douglas, D.J., Fulford, J.E., Halligan, K.W. and Tanner, S.D. (1988) Nonspectroscopic interelement interferences in inductively coupled plasma mass spectrometry. Anal. Chem., **60**, 1472-1474.

Gordon, A.D. (1980) SLOTSEQ: a FORTRAN IV program for comparing two sequences of observations. Comp. and Geosci., **6**, 7-20.

Gordon, A.D. (1982) An investigation of two sequence-comparison statistics. Austral. J. Statist., **24**, 332-342.

Gordon, A.D. and Reyment, R.A. (1979) Slotting of borehole sequences. Math. Geol., **11**, 309-314.

Graham, M. (1994) pers. comm.

Gray, A.L. (1978) Isotope ratio determination on solutions with a plasma ion source. Dynamic Mass Spectrom., **5**, 106-113.

Gray, A.L. (1985) The ICP as an ion source - origins, achievements and prospects. Spectrochim. Acta, **40B**, 1525-1537.

Gray, A.L. (1986) The evolution of the ICP as an ion source for mass spectrometry. J. Anal. Atom. Spectrom., **1**, 403-405.

Gray, A.L. (1989) The origins, realisation and performance of ICP-MS system, in: Applications of inductively coupled plasma mass spectrometry. Date, A.R and Gray, A.L (eds.), Blackie, Glasgow, 1-42.

Gray, A.L. (1992) Origins and development. In: Handbook of inductively coupled plasma mass spectrometry, Jarvis, K.E., Gray, A.L. and Houk, R.S. (eds.), Blackie and sons Ltd, Glasgow, 1-9.

Gray, A.L. and Date, A.R (1983) Inductively coupled plasma source mass spectrometry using continuum flow ion extraction. Analyst, **108**, 1033-1050.

Gray, A.L. and Williams, J.G. (1987) System optimisation and the effect on polyatomic, oxide and doubly charged ion response of a commercial inductively coupled plasma mass spectrometry instrument. J. Anal. Atom. Spectrom., **2**, 599-606.

Greenfield, S., Jones, I. L1. and Berry, C.T. (1964) High pressure plasmas as spectroscopic emission sources. Analyst, **89**, 713-720.

Greenwood, N.N. and Earnshaw, A. (eds.) (1984) The Actinide Elements. In: The Chemistry of the Elements, Pergamon Press, Oxford, 1450-1486.

Gregoire, D.C. (1987) The effect of easily ionizable concomitant elements on non-spectroscopic interferences in inductively coupled plasma-mass spectrometry. Spectrochim. Acta, **42B**, 895-907.

Grindler, J.E. (1962) The radiochemistry of Uranium. NAS-NS-3050.

Guéguéniant, P.M., Auffret, J.P. and Ballada, J. (1981) Sediments as indicators of artificial radionuclide distribution west of La Hague. In: Techniques for identifying transuranic speciation in aquatic environments, STI/PUB/613, IAEA, Vienna, 229-245.

Gurbutt, P.A. and Kershaw, P.J. (1987) Biological mixing of shelf seas sediments with applications for modelling. International Council for the Exploration of the Sea, Copenhagen, CM 1987/C:22.

Hamilton, E.I. (1981) α-particle radioactivity from hot particles in the Esk Estuary. Nature, **290**, 690-693.

Hamilton, E.I. and Clarke, K.R. (1984) The recent sedimentation history of the Esk estuary, Cumbria, UK: the application of radiochronology. Sci. Total Environ., **35**, 325-386.

Hamilton, E.I. and Clifton, R.J. (1980) Concentration and distribution of the transuranium radionuclides 239+240-Pu, 238-Pu and 241-Am in Mytilus edulis, Fucus vesiculosus and surface sediment of Esk estuary. Mar. Ecol. Prog. Ser., **3**, 267-277.

Hamilton, E.I. and Clifton, R.J. (1981) CR-39, a new α-particle sensitive polymeric detector applied to investigations of environmental radioactivity. Int. J. Appl. Radioat. Isotop., **32**, 313-324.

Hamilton-Taylor, J., Kelly, M., Mudge, S. and Bradshaw, K. (1987) Rapid remobilisation of plutonium from estuarine sediments. J. Environ. Radioact., **5**, 409-423.

Hamilton-Taylor, J., Kelly, M., Titley, J.G. and Turner, D.R. (1993) Particle-solution behaviour of plutonium in an estuarine environment, Esk Estuary, UK. Geochim. Cosmochim. Acta, **57**, 3367-3381.

Handyside, I., Hunt, G.J. and Partington, C. (1982) Control of radiocaesium discharges to the Irish Sea: ICRP-26 in practice. In: The Dose Limitation System in the Nuclear Cycle and in Radiation Protection, Proc. Symp. Madrid, 1981, IAEA, Vienna, 325-345.

Hardy, E.P., Krey, P.W. and Volchok, H.L. (1973) Global inventory and distribution of fallout plutonium. Nature, **241**, 444-445.

Harris, J.E. (1983) The development and use of magnesium alloys in UK Magnox reactors. Proc. Int. Symp. Light metals - science and technology, Barnes Hindu University Dimond Jubilee Celebrations, India.

Harvey, B.R. (1981) Potential for post-depositional migration of neptunium in the Irish Sea sediments. In: Impacts of radionuclide releases into the marine environment, IAEA, Vienna, 93-103.

Hasegawa, T. and Haraguchi, H. (1987) Fundamental properties of inductively coupled plasma. In: Inductively coupled plasmas in analytical atomic spectroscopy, Montaser, A. and Golightly, D.W. (eds.), VCH Publishers Inc.

Harvey, B.R. and Kershaw, P.J. (1984) The physico-chemical interaction of long-lived radionuclides in coastal marine sediments and some comparison with the deep-sea environment. In: Int. Symp. on the behaviour of the long-lived radionuclides in the marine environment, Cigna, A. and Myttenaere, C. (eds.), EUR 9214EN, CEC, Brussels, 131-143.

Harvey, B.R. and Thurston, L.M. (1988) Analytical procedures for the determination of neptunium radionuclides in marine waters, sediments and biota. Aquatic Environment Protection: Analytical methods, No. 1, MAFF, Lowestoft.

Hayhurst, A.N. and Sugden, T.M. (1966) Mass spectrometry of flames. Proc. R. Soc. London Ser., **293A**, 36-50.

Hetherington, J.A. (1975) The behaviour of plutonium nuclides in the Irish Sea. In: Environmental toxicity of aquatic radionuclides: models and mechanisms, Miller, M.W. and Stannard, J.N. (eds.), Ann Arbor Science Publish., USA, 81-105.

Hetherington, J.A. (1978) The uptake of plutonium nuclides by marine sediments. Marine Sci. Comm., **4**, 239-274.

Hetherington, J.A., Jefferies, D.F. and Lovett, M.B. (1975) Some investigations into the behaviour of plutonium in the marine environment. In: Impacts of nuclear releases into the aquatic environment, IAEA, Vienna, 193-212.

Hislop, J.S., Long, S.E., Brown, R.M., Morrison, R. and Pickford, C.J. (1987) The use of argon plasma sources for the measurement of long-lived radionuclides. Paper presented at ICRM-low level techniques group meeting, Wurenlingen, June 10-12.

Hoffman, D.C., Lawrence, F.D., Mewherter, J.L. and Rourke, F.M. (1971) Detection of plutonium-244 in nature. Nature, **234**, 132-134.

Hoffman, B.W. and Van Camerik, S.B. (1967) A table method for determining the true time representing a count rate observed in radionuclear counting. Anal. Chem., **39**, 1198-1199.

Holm, E. (1981) Release of ^{237}Np to the environment. In: Impacts of radionuclides released into the marine environment, IAEA, Vienna, 155-160.

Holm, E., Aarkrog, A., Bellesta, S. and Dahlgaard, H. (1986) Origin and isotope ratios of plutonium in the Barents and Greenland Seas. Earth Planet. Sci. Lett., **79**, 27-32.

Holm, E. and Nilsson, M. (1980) Method for the determination of ^{237}Np in low-level environmental samples. In: Techniques for identifying transuranic speciation in aquatic environments, CEC/IAEA, Vienna, 43-47.

Holm, E., Roos, P., Persson, R.B.R., Bojanowski, R., Aarkrog, A., Nielsen, S.P. and Livingston, H.D. (1991) Radiocaesium and plutonium in Atlantic surface waters from 73°N to 72°S. In: Radionuclides in the Study of Marine Processes, Kershaw, P.J. and Woodhead, D.S. (eds.), Elsevier Applied Science, London, 3-11.

Horlick, G., Tan, S.H., Vaughan, M.A. and Rose, C.A. (1985) The effect of plasma operating parameters of analyte signals in inductively coupled plasma mass spectrometry. Spectrochim. Acta, **40B**, 1555-1572.

Horrill, A.D. (1984) Radionuclide levels and distribution in grazed saltmarsh in West Cumbria. Environ. Pollut. Ser. B, **8**, 265-280.

Houk, R.S. (1986) Mass spectrometry of ICPs. Anal. Chem., **58**, 97A-105A.

Houk, R.S., Fassel, V.A., Flesch, G.D., Svec, H.J., Gray, A.L. and Taylor, C.E. (1980) Inductively coupled argon plasma as an ion source for mass spectrometric determination of trace elements. Anal. Chem., **52**, 2283-2289.

Houk, R.S., Fassel, V.A. and Svec, H.J. (1981) Inductively coupled plasma-mass spectrometry: sample introduction, ionisation, ion extraction and analytical results. Dynamic Mass Spectrom., **6**, 231-251.

Houk, R.S. and Thompson, J.J. (1988) Inductively coupled plasma mass spectrometry. Mass Spectro. Reviews, **7**, 425-461.

Howarth, M.J. (1984) Currents in the eastern Irish Sea. Oceanogr. Mar. Biol., Ann. Rev., **22**, 11-53.

Howarth, J.M. and Eggleton, A.E.J. (1988) Studies of environmental radioactivity in Cumbria: Part 12. Modelling of the sea-to-land transfer of radionuclides and an assessment of the radiological consequences. AERE, R-11733, HMSO.

Hunt, G.J. (1985) Timescales for dilution and dispersion of transuranics in the Irish Sea near Sellafield. Sci. Total Environ., **46**, 261-278.

Hunt, G.J. and Kershaw, P.J. (1990) Remobilisation of artificial radionuclides from the sediment of the Irish Sea. J. Radiol. Protect., **10**, 147-151.

Hursthouse, A.S. (1990) Development and application of methods for the assay of neptunium in environmental matrices. Ph.D. Thesis, Glasgow.

Jarvis, K.E., Gray, A.L. and Houk, R.S. (1992) Handbook of inductively coupled plasma mass spectrometry. Blackie, Glasgow.

Jefferies, D.F., Preston, A. and Steele, A.K. (1973) Distribution of caesium-137 in British coastal waters. Mar. poll. Bull., **4**, 118-121.

Jones, P.G. and Folkard, A.R. (1971) Hydrographic observations in the eastern Irish Sea with particular reference to the distribution of nutrient salts. J. Mar. Biol. Ass. U.K., **51**, 159-182.

Jones, D.G., Roberts, P.D. and Miller, J.M. (1988) The distribution of gamma-emitting radionuclides in surface subtidal sediments near the Sellafield plant. Estuar. Coastal Shelf Sci., **27**, 143-161.

Katz, J.J., Morss, L.R. and Seaborg, G.T. (1986b) Summary and comparative aspects of the actinide elements. In: The Chemistry of the Actinide Elements, Katz, J.J., Seaborg, G.T. and Morss, L.R. (eds.), Chapman and Hall Ltd., London, 1121-1195.

Katz, J.J., Seaborg, G.T. and Morss, L.R. (eds.) (1986a) The chemistry of the actinides. Chapman and Hall Ltd., London.

Kautsky, H. and Eicke, H.F. (1982) Distribution of transuranic isotopes in the water of the North sea and adjacent regions. IAEA-TECDOC-265, IAEA, Vienna, 47-54.

Kautsky, H. and Murray, C.N. (1981) Artificial radioactivity in the North Sea. Atom. En. Rev. Suppl., **2**, 63-105.

Kershaw, P.J., Breasley, J.H., Woodhead, D.S. and Lovett, M.B. (1986) Alpha-emitting hot particles in Irish Sea sediments. Sci. Tot. Environ., **53**, 77-87.

Kershaw, P.J., Pentreath, R.J., Woodhead, D.S. and Hunt, G.J. (1992) A review of radioactivity in the Irish Sea A report prepared for the Marine Pollution Monitoring Management Group. MAFF Aquatic Environment Monitoring Report No. 32, MAFF, Lowestoft.

Kershaw, P.J., Swift, D.J. and Denoon, D.C. (1988) Evidence of recent sedimentation in the Eastern Irish Sea. Mar. Geol., **85**, 1-14.

Kershaw, P.J., Swift, D.J., Pentreath, R.J. and Lovett, M.B. (1983) Plutonium redistribution by biological activity in Irish Sea sediments. Nature, **306**, 774-775.

Kershaw, P.J., Swift, D.J., Pentreath, R.J. and Lovett, M.B. (1984) The incorporation of plutonium, americium and curium into the Irish Sea seabed by biological activity. Sci. Total Environ., **40**, 61-81.

Kershaw, P.J., Woodhead, D.S., Malcolm, S.J., Allington, D.J. and Lovett, M.B. (1990) A sediment history of Sellafield discharges. J. Environ, Radioact., **12**, 201-241.

Kershaw, P.J., Woodhouse, D.S., Lovett, M.B. and Leonard, K.S. (1994) Plutonium from European reprocessing operations - its behaviour in the marine environment, In press.

Kim, C.K., Takaku, Y., Yamamoto, M., Kawamura, H., Shiraishi, K., Igarashi, Y., Igarashi, S., Takayama, H. and Ikeda, M. (1989) Determination of ^{237}Np in environmental samples using inductively coupled plasma mass spectrometry. J. Radianal. Nucl. Chem., **132**, 131-137.

Kirby, R., Parker, W.R., Pentreath, R.J. and Lovett, M.B. (1983) Sedimentation studies relevent to low-level radioactive effluent dispersal in the Irish Sea. Part III:

An evaluation of possible mechanisms of the incorporation of radionuclides into marine sediments. Rep. Inst. Ocenogr. Sci., Wormley, **178**, 1-63.

Kirchner, G. (1990) A new hazard index for the determination of risk potentials of disposed radioactive waste. J. Environ. Radioact., **11**, 71-97.

Knoll, G.F. (ed.)(1979) Radiation detection and measurement. John Wiley and Sons, New York.

Koide, M., Bertine, K.K., Chow, T.J. and Goldberg, E.D. (1985) The $^{240}Pu/^{239}Pu$ ratio, a potential geochronometer. Earth Planet. Sci. Lett., **72**, 1-8.

Koppenaal, D.W. (1988) Atomic mass-spectrometry. Anal. Chem., **60**, 113R-131R.

Krey, P.W. and Bogen, D.C. (1987) Determination of acid leachate and total Pu in large soil samples. J. Radioanal. Nuc. Chem., **115**, 335-355.

Krey, P.W., Hardy, E.P., Pachucki, C., Rourke, F., Coluzza, J. and Benson, W.K. (1976) Mass isotopic composition of global fall-out plutonium in soil. In: Transuranium nuclides in the environment, STI/PUB/410, 671-678.

Lally, A.E. and Eakins, J.D. (1978) Some recent advances in environmental analysis at AERE Harwell. In: Symp. on the Detn. of Radionuc. in Environ. Biol. Materials, CEGB, Sudbury House, Paper 12.

Lally, A.E. and Phillips, G. (1984) The development and application of α-particle spectrometry for low-level radioactivity measurements in biological and environmental materials. Intl. J. Appl. Radiat. Isot., **35**, 291-299.

Lam, J.W.H. and Horlick, G. (1990) Effects of sampler-skimmer separation in ICP-MS. Spectrochim. Acta, **45B**, 1327-1338.

Leonard, D.R.P. and Pentreath, R.J. (1981) Further 237-Pu experiments with the plaice Pleuronectes platessa: subcellular distribution of plutonium in the liver. Mar. Biol., **63**, 67-71.

Lim, H.B. and Houk, R.S. (1990) Langmuir probe measurement of electron temperature in a supersonic jet extracted from an ICP. Spectrochim. Acta, **45B**, 453-461.

Livingston, H.D. (1986) Fallout plutonium in western North Pacific sediments. IAEA-TECDOC-368, Vienna, 27-34.

Lovett, M.B., Boggis, S.J. and Blowers, P. (1990) The determination of alpha-emitting nuclides of plutonium, americium and curium in environmental materials: Part 1. Sea water. Aquatic Environment Protection: No. 7, MAFF, Lowestoft.
MacKenzie, A.B. and Scott, R.D. (1984) Some aspects of coastal marine disposal of low level radioactive waste. The Nuclear Engineer, **25**, 110-122.

MacKenzie, A.B., Scott, R.D., Allan, R.L., Ben Shaban, Y.A., Cook, G.T. and

Pulford, I.D. (1994) Sediment radionuclide profiles: Implications for mechanisms of Sellafield waste dispersal in the Irish Sea. J. Environ. Radioactivity, **23**, 39-69.

MacKenzie, A.B., Scott, R.D. and Williams, T.M. (1987) Mechanisms for northwards dispersal of Sellafield waste. Nature, **329**, 42-45.

MAFF (1971-1992) Radioactivity in surface and coastal waters of the British Isles. Aquatic Monitoring Reports. Ministry of Agriculture, Fisheries and Food, Lowestoft, UK.

Malcolm, S.J., Kershaw, P.J., Cromar, N.J. and Botham, L. (1990) Iron and Manganese geochemistry and the distribution of $^{239,240}Pu$ and ^{241}Am in the sediments of the north-east Irish Sea. Sci. Total Environ., **95**, 69-87.

Malcolm, S.J., Kershaw, P.J., Lovett, M.B. and Harvey, B. (1990) The interstitial water chemistry of $^{239,240}Pu$ and ^{241}Am in the sediments of the north-east Irish Sea. Geochem. Cosmochim. Acta, **54**, 29-35.

Mannone, F., Koehly, G. and Lecomte, M. (1984) Actinide partitioning by HDEHP solvent extraction. A verification of the process scheme by counter current experiments in hot cells. Inorg. Chim. Acta, **94**, 148-149.

Mao Huang, Hanselman D.S., Pengyuan Yang, and Hieftje, G.M. (1992) Isocontour maps of electron temperature, electron number density and gas kinetic temperature in the Ar inductively coupled plasma obtained by laser-light Thomson and Rayleigh scattering. Spectrochim. Acta, **47B**, 765-785.

Marks, T.J. (1982) Actinide organometallic chemistry. Science, **217**, 989-997.

Marshall, W. (ed.) (1983) Nuclear power and technology. Volume 1: Reactor technology. Clarendon, Oxford.

Mauchline, J. (1980) Artificial radioisotopes in the marginal seas of north western Europe. In: The North-west European Shelf Sea: the Sea Bed and the Sea in Motion. II Physical and Chemical Oceanography and Physical Resources, Banner, F.T., Collins, M.B. and Massie, K.S. (eds.), Elsevier, Amsterdam, 517-542.

May, S. and Pinte, G. (1988) Neutron activation determination of ^{237}Np in irradiated experimental fuels and in waste solutions and distribution studies in sea water and submarine flora and fauna of disposal areas. In: Modern trends in activation analysis, Risø Nat. Lab. Copenhagen, June 23-27, 1343-1350.

McCarthy, W. (1994) pers. comm.

McCarthy, W. and Nicholls, T.M. (1990) Mass spectrometry analysis of plutonium in soils near Sellafield. J. Environ. Radioact., **12**, 1-12.

McCartney, M., Kershaw, P.J., Woodhead, D.S. and Denoon, D.C. (1994) Artificial radionuclides in the surface sediments of the Irish Sea, 1968-1988. Sci. Total Environ., **141**, 103-138.

McDonald, P., Allan, R.L., MacKenzie, A.B., Cook, G.T. and Pulford, I.D. (1992) Radionuclides in the coastal region of south west Scotland: dispersion, distribution and geochemistry. Analyt. Proceedings.

McDonald, P., Cook, G.T., Baxter, M.S. and Thomson, J.C. (1990) Radionuclide transfer from Sellafield to south-west Scotland. J. Environ. Radioact., **12**, 285-298.

McKay, W.A. and Pattenden, N.J. (1989) Radionuclides in shoreline waters of the northeast Irish Sea. Sci. Total Environ., **84**, 159-167.

McKay, W.A. and Pattenden, N.J. (1990) The transfer of radionuclides from sea to land via the air: a review. J. Environ. Radioactivity, **12**, 49-77.

McKay, W.A. and Pattenden, N.J. (1993) The behaviour of plutonium and americium in the shoreline waters of the Irish Sea: A review of Harwell studies in the 1980s. J. Environ. Radioactivity, **18**, 99-132.

McKay, W.A., Garland, J.A., Livesley, D., Halliwell, C.M. and Walker, M.I. (1993) Studies of environmental radioactivity in Cumbria: Part 26. Transfer of radionuclides from sea-to-air-to-land in sea spray at Cumbria, UK. AEA-EE-0516, AEA, Harwell.

McKay, W.A. and Walker, M.I. (1990) Studies of environmental radioactivity in Cumbria. Part 18: Plutonium and americium behaviour in Cumbrian near-shore waters, AERE-R13441, HMSO, London.

McLaren, J.W., Beauchemin, D. and Berman, S.S. (1987) Application of isotope dilution inductively coupled plasma mass spectrometry to the analysis of marine sediments. Anal. Chem., **59**, 610-613.

Meinhard, J.E. (1976) The concentric glass nebuliser. ICP Inform. Newslett., **2**, 163-165.

Miller, P.E. and Denton, M.B. (1986) The quadrupole mass filter: basic operating concepts. J. Chem. Ed., **63**, 617-622.

Mitchell, P.I., Vives Batelle, J., Ryan, T.P., Schell, W.R., Sanchez-Cabez, J.A. and Vidrac-Quandras, A. (1991) Studies on the speciation of plutonium and americium in the western Irish Sea. In: Radionuclides in the Study of Marine Processes, Kershaw, P.J. and Woodhead, D.S. (eds.). Elsevier, London, 37-51.

Montaser, A. and Golightly, D.W. (1987) Inductively coupled plasmas in analytical atomic spectrometry. VCH Publishers, Weinheim.

Moore, F.L. (1957) Separation and determination of Np by liquid-liquid extraction. Anal. Chem., **29**, 941-944.

Mudge, S., Hamilton-Taylor, J., Kelly, M. and Bradshaw, K. (1988) Laboratory studies of the chemical behaviour of plutonium associated with contaminated estuarine sediments. J. Environ. Radioactivity, **8**, 217-237.

Murray, C.N., Kautsky, H., Hoppenheit, M. and Domain, M. (1978) Actinide activities in water entering the northern North Sea. Nature, Lond., **276**, 225-230.

Musikas, C. (1987) Solvent extraction for the chemical separations of the 5f elements. Inorg. Chim Acta, **140**, 197-206.

Myasoedov, B.F. (1987) Modern methods of separation and determination of radioactive elements. Inorg. Chim Acta, **140**, 231-238.

Myres, W.A. and Lindner, M. (1971) The precise determination of the natural abundance of ^{237}Np and ^{239}Pu in Katanga pitchblende. J. Inorg. Nucl. Chem., **33**, 3233-3238.

Nachtrieb, N.H. and Conway, J.G. (1948a) The extraction of ferric chloride by isopropyl ether, I. J. Am. Chem. Soc., **70**, 3547-3552.

Nachtrieb, N.H. and Conway, J.G. (1948b) The extraction of ferric chloride by isopropyl ether, II. J. Am. Chem. Soc., **70**, 3552-3557.

Nelson, D.M., Carey, A.E. and Bowen, V.T. (1984) Plutonium oxidation state distribution in the Pacific Ocean during 1980-1981. Earth Planet. Sci. Lett., **68**, 422-430.

Nelson, D.M. and Lovett, M.B. (1978) Oxidation states of plutonium in the Irish Sea. Nature, Lond., **276**, 599-601.

Nelson, D.M. and Lovett, M.B. (1981) Measurements of the oxidation state and concentration of plutonium in interstitial waters of the Irish Sea. In: Impacts of radionuclide releases into the marine environment, STI/PUB/565, IAEA, Vienna, 105-118.

Nelson, D.M., Penrose, W.R., Kartunnen, J.O. and Mehlhaff, P. (1985) Effect of dissolved organic carbon on the adsorption properties of plutonium in natural waters. Environ. Sci. Tech., **19**, 127-131.

Nixon, D.E., Fassel, V.A. and Kniseley, R.N. (1974) Inductively coupled plasma-optical emission analytical spectroscopy: tantalum filament vaporisation of microlitre samples. Anal. Chem., **46**, 210-213.

Noshkin, V.E. (1980) Transuranium nuclides as components of the benthic environment of the Enewetak Atoll. In: Transuranium nuclides in the environment, Hanson, W.C. (ed.), USDoE/TIC-22800, 578-601.

Noshkin, V.E. and Wong, K.M. (1980) Plutonium in the North Equatorial Pacific. In: Processes determining the Input, Behaviour and Fate of Radionuclides and Trace Elements in Continental Shelf Environments, US Dep. En. Rep. Conf., 790382, 11-28.

Olivares J.A. and Houk, R.S. (1985a) Ion sampling for inductively coupled plasma mass spectrometry. Anal. Chem., **57**, 2674-2679.

Olivares, J.A. and Houk, R.S. (1985b) Kinetic energy distributions of positive ions in an inductively coupled plasma mass spectrometer. Appl. Spectrosc., **39**, 1070-1077.

Olivares, J.A. and Houk, R.S. (1986) Suppression of analyte signal by various concomitant salts in ICP-MS. Anal. Chem., **58**, 20-25.

Onishi, Y., Serne, R.J., Arnold, E.M., Cowan, C.E. and Thompson, F.L. (1981) Critical review: radionuclide transport, sediment transport and water quality mathematical modelling and radionuclide adsorption/desorption mechanisms. PNL-2901, NUREG/CR-1322.

Orlandini, K.A., Penrose, W.R., Harvey, B.R., Lovett, M.B. and Findlay, M.W. (1990) Colloidal behaviour of actinides in an oligotrophic lake. Environ. Sci. Technol., **24**, 706-712.

Pantin, H.M. (1977) Quaternary sediments of the northern Irish Sea. In: Quaternary history of the Irish Sea, Kidson, C. and Tooley, M. (eds.). Seel House Press, Liverpool, 27-54.

Pantin, H.M. (1978) Quaternary sediments from the northeast Irish Sea: Isle of Man to Cumbria. Bull. Geol. Surv. Gt. Br., **64**, 1-78.

Patil, S.K., Ramakrishna, V.V. and Ramaniah, M.V. (1978) Aqueous coordination complexes of neptunium. Coordn. Chem. Rev., **25**, 133-171.

Pattenden, N.J., Cambray, R.S. and Playford, K. (1989) Studies of environmental radioactivity in Cumbria: Part 16. Trends in radionuclide concentrations in coastal airborne and deposited materials, 1978-1987. AERE R12617, HMSO.

Pentreath, R.J. (1984) Alpha-emitting nuclides in the marine environment. Nucl. Inst. and Methods in Phys. Research, **223**, 493-501.

Pentreath, R.J. (1985) Radioactive discharges from Sellafield (UK). In: Behaviour of radionuclides released into coastal waters, IAEA-TECDOC-329, IAEA, Vienna.

Pentreath, R.J. (1987) The interaction with suspended and settled sedimentary materials of long-lived radionuclides discharged into United Kingdom coastal waters. Contin. Shelf Res., **7**, 1457-1469.

Pentreath, R.J. (1988) Sources of artificial radionuclides in the marine environment. In: A tool for oceanography, Guary, J.C., Guéguéniat, P. and Pentreath, R.J. (eds.). Elsevier Applied Science, London, 12-34.

Pentreath, R.J. and Harvey, B.R. (1981) The presence of ^{237}Np in the Irish Sea. Mar. Ecol. Prog. Ser., **6**, 243-247.

Pentreath, R.J., Harvey, B.R. and Lovett, M.B. (1985) Chemical speciation of transuranium nuclides discharged into the marine environment. In: Speciation of Fission and Activation Products in the Environment, Bulman, R.A. and Cooper, J.R. (eds.), Elsevier, London, 312-325.

Pentreath, R.J., Kershaw, P.J., Harvey, B.R. and Lovett, M.B. (1986a) The behaviour of certain long-lived radionuclides in the marine environment. In: Behaviour of long-lived radionuclides associated with the deep-sea disposal of radioactive wastes, IAEA TECDOC-368, IAEA, Vienna, 101-114.

Pentreath, R.J. and Lovett, M.B. (1976) Occurrence of plutonium and americium in plaice from the northeastern Irish Sea. Nature, **262**, 814-816.

Pentreath, R.J. and Lovett, M.B. (1977) Plutonium and americium in fish. Nature, **265**, 384.

Pentreath, R.J. and Lovett, M.B. (1978) Transuranic nuclides in plaice (pleuronectes platessa L.) in the northeast Irish Sea. Mar. Biol., **48**, 19-26.

Pentreath, R.J., Lovett, M.B., Jefferies, D.F., Woodhead, D.S., Talbot, J.W. and Mitchell, N.T. (1984) Impact on public radiation exposure of transuranium nuclides discharged in liquid wastes from fuel element reprocessing at Sellafield, UK. In: Radioactive Waste Management, Vol **5**, IAEA, Vienna, 315-329.

Pentreath, R.J., Woodhead, D.S., Kershaw, P.J., Jefferies, D.F. and Lovett, M.B. (1986b) The behaviour of plutonium and americium in the Irish Sea. Rapp. R.V. Réun. Cons. Int. Explor. Mer., **186**, 60-69.

Peppard, D.F., Mason, G.W., Gray, P.R. and Mech, J.F. (1952) Occurrence of the (4n + 1) series in nature. J. Am. Chem. Soc., **74**, 6081-6084.

Perkins, R.W. and Thomas, C.W. (1980) World-wide fallout. In: Transuranium nuclides in the environment, Hanson, W.C. (ed.), USDoE/TIC-22800, 53-82.

Perrin, R.E., Knobeloch, G.W., Armijo, V.M. and Efurd, D.W. (1984) High-precision isotopic analysis of nanogram quantities of plutonium. Los Alamos Nat. Lab. Report, LA-10013-MS.

Pierson, D.H. and Cambray, R.S. (1965) Fission product fallout from the nuclear explosions of 1961 and 1962.

Pierson, D.H., Cambray, R.S., Cawse, P.A. and Eakins, J.D. (1982) Environmental radioactivity in Cumbria. Nature, **300**, 27-31.

Popplewell, D.S. and Ham, G.J. (1987) An intercomparison exercise on the determination of ^{237}Np in an environmental material. J. Radioanal. Nuc. Chem., **115**, 191-202.

Poskanser, A.M. and Foreman, B.M. (1961) A summary of TTA extraction coefficients. J. Inorg. Nuc. Chem., **16**, 323-336.

Preston, A. and Jefferies, D.F. (1969) The ICRP critical group concept in relation to the Windscale sea discharges. Health Phys., **16**, 33-46.

Ramamnujan, A., Nadkarni, M.N., Ramakrishna, V.V. and Patil, S.K. (1978) Studies on the TTA extraction of the tetravalent actinides. J. Radioanal. Nuc. Chem., **42**,

349-357.

Reed, T.B. (1961) Induction-coupled plasma torch. J. Appl. Phys., **32**, 821.

Rees, J.H. and Shipp, C.M. (1983) Chemical aspects of the management of neptunium in nuclear wastes: a review. Nucl. Energy, **22**, 423-432.

Riddel, C., Vander Voet, A. and Doherty, W. (1988) Rock analysis using ICP-MS: a review. Geostandards Newsletter, **12**, 203-234.

Rimke, H., Herrmann, G., Mühleck, C., Sattelberger, P., Rehklan, D. and Ruster, W. (1987) Detection of trace amounts of actinides by RIMS. Inorg. Chim. Acta, **140**, 277-278.

Russ, G.P. (1989) Isotope ratio measurements using ICP-MS. In: Applications of inductively coupled plasma mass-spectrometry, Date, A.R. and Gray, A.L. (eds.), Blackie, Glasgow, 91-114.

Saito, N. (1984) Selected data on ion exchange separations in radioanalytical chemistry. Pure Appl. Chem., **56**, 523-529.

Sakanoue, M. (1988) The analysis of transuranic nuclides in the environment. In: Low-level measurements and their application to environmental radioactivity, García-León, M. and Madurga, G. (eds.), World Scientific Pub. Co., Singapore, 382-391.

Sakanoue, M. (1987) Transuranium nuclides in the environment. Radiochim. Acta, **46**, 103-113.

Salbu, B., Bjørnstad, H.E., Svaeren, I., Prosser, S.L., Bulman, R.A., Harvey, B.R. and Lovett, M.B. (1993) Size distribution of radionuclides in nuclear fuel reprocessing liquids after mixing with seawater. Sci. Total Environ., **130**, 51-63.

Santchi, P.H. and Honeyman, B.D. (1989) Radionuclides in the aquatic environment. Radiat. Phys. Chem., **34**, 213-240.

Santchi, P.H. (1988) Factors controlling the biogeochemical cycles of trace elements in fresh and coastal marine waters as revealed by artificial radioisotopes. Limnol. Oceanogr., **33**, 848-866.

Schulz, W.W. and Horwitz, E.P. (1986) Recent progress in the extraction chemistry of actinide ions. J. Less-Common Met., **122**, 125-138.

Schulz, W.W. and Penneman, R.A. (1986) Americium. In: The Chemistry of the Actinides, Katz, J.J., Seaborg, G.T. and Morss, L.R. (eds.), Chapman and Hall Ltd., London, 887-961.

Scott, R.H., Fassel, V.A., Kniseley, R.N. and Nixon, D.E. (1974) Inductively coupled plasma-optical emission analytical spectrometry: a compact facility for trace analysis of solutions. Anal. Chem., **46**, 76-80.

Scott, M.R., Salter, P.F. and Halverson, J.E. (1983) Transport and deposition of plutonium in the ocean: evidence from the Gulf of Mexico sediments. Earth Planet. Sci. Lett., **63**, 202-222.

Shen, G.T., Sholkovitz, E.R. and Mann, D.R. (1983) The coagulation of dissolved $^{239,240}Pu$ in estuaries as determined from a mixing experiment. Earth Planet. Sci. Letts., **64**, 437-444.

Shen, W.L., Caruso, J.A., Fricke, F.L. and Satzger, R.D. (1990) Electrothermal vaporisation interface for sample introduction in inductively coupled plasma mass spectrometry. J. Anal. Atom. Spectrom., **5**, 451-455.

Sholkovitz, E.R. (1983) The geochemistry of plutonium in fresh and marine water environments. Earth Sci. Rev., **19**, 95-161.

Sillen, L.G. and Martell, A.E. (1964) Stability constants of metal-ion complexes. Chem. Soc., London, Special Publication No. 17.

Smith, T.J., Parker, W.R. and Kirby, R. (1980) Sedimentation studies relevent to low-level radioactive effluent dispersal in the Irish Sea. Part 1: Radionuclides in marine sediments. IOS Report No. 110, Institute of Oceanographic Sciences, Godalming, UK, 1-87.

Stanners, D.A. and Aston, S.R. (1981) An improved method of determining sedimentation rates by the use of artificial radionuclides. Estuar. Coastal and Shelf Sci., **13**, 101-106.

Stanners, D.A. and Aston, S.R. (1984) The use of reprocessing effluent radionuclides in the geochronology of recent sediments. Chem. Geol., **44**, 19-32.

Sugden, T.M. (1965) The direct mass spectrometry of ions in flames. In: Mass spectrometry, Reed, R.I. (ed.), Academic press, New York, 347-358.

Swift, D.J. and Kershaw, P.J. (1986) Bioturbation of contaminated sediments in the north-east Irish Sea. International Council for the Exploration of the Sea, Copenhagen, CM 1986/E:18.

Tan, S.H. and Horlick, G. (1986) Background spectral features in inductively coupled plasma mass spectrometry. Appl. Spectrosc., **40**, 445-460.

Tan, S.H. and Horlick, G. (1987) Matrix effect observations in inductively coupled plasma mass spectrometry. J. Anal. Atom. Spectrom., **2**, 745-763.

Tanner, S.D. (1992) Space charge in ICP-MS: calculation and implications. Spectrochim. Acta, **47B**, 809-823.

Thompson, J.J. and Houk, R.S. (1987) A study of internal standardisation in inductively coupled plasma mass spectrometry. Appl. Spectrosc., **1**, 801-806.

Thompson, R.C. (1982) Neptunium - the neglected actinide: a review of the biological and environmental literature. Radiat. Res., **90**, 1-32.

Tyror, J.G. (1971) A series of lectures on the reactor physics of burn-up. AEEW-M999.

UNSCEAR (1982) Ionizing Radiation: Sources and Biological Effects. United Nations, New York.

Vaughan, M.A. and Horlick, G. (1990a) Effect of sampler and skimmer orifice size on analyte and analyte oxide signals in ICP-MS. Spectrochim. Acta, **45B**, 1289-1300.

Vaughan, M.A. and Horlick, G. (1990b) Ion trajectories through the input ion optics of an ICP mass spectrometer. Spectrochim. Acta, **45B**, 1301-1312.

VG Isotopes (1988) PlasmaQuad system manual Ver.2A - March 1988.

Vickers, G.H., Ross, B.S. and Hieftje, G.M. (1989) Reduction of mass-dependent interferences in ICP-MS by using flow injection analysis. Appl. Spectrosc., **43**, 1330-1333.

Weigel, F. (1986) Uranium. In: The Chemistry of the Actinide Elements, Katz, J.J, Seaborg, G.T. and Morss, L.R. (eds.), Chapman and Hall Ltd., London, 169-442.

Weigel, F., Katz, J.J. and Seaborg, G.T. (1986) Plutonium. In: The Chemistry of the Actinide Elements, Katz, J.J., Seaborg, G.T. and Morss, L.R. (eds.), Chapman and Hall Ltd., London, 499-886.

Wendt, R.H. and Fassel, V.A. (1965) Induction-coupled plasma spectrometric excitation source. Anal. Chem., **37**, 920-922.

Williams, J.G. (1992) Sample introduction for liquids and gases. In: Handbook of inductively coupled plasma mass spectrometry, Jarvis, K.E., Gray, A.L. and Houk, R.S. (eds.), Blackie, Glasgow, 81-124.

Woodhead, D.S. (1988) Mixing processes in the near-shore marine sediments as inferred from the distribution of radionuclides discharged into the Irish Sea from BNFL Sellafield. In: Radionuclides: a tool for oceanography, Guary, J.C., Guegueniat, P. and Pentreath, R.J. (eds.), Elselvier Appl. Sci., Oxford, 331-340.

Yamamoto, M., Yamauchi, Y., Komura, K., Ueno, K., and Assinder, D.J. (1991) Chemical leaching behaviour of ^{237}Np from intertidal coastal sediment in the Irish Sea. J. Radioanalytical and Nucl. Chem. Lett., **154**, 299-307.